UMTRI-82-50-2

EXPERIMENTAL DATA FOR USE WITH BIOMECHANICAL MODELS VOLUME 2

Guy S. Nusholtz
Paula Lux
Miles Janicki

INTERIM REPORT
DECEMBER 1982
UMTRI The University of Michigan Transportation Research Institute

EXPERIMENTAL DATA FOR USE WITH BIOMECHANICAL MODELS

INTERIM REPORT

Volume 2

by

Guy S. Nusholtz
Paula Lux
Miles Janicki

Biosciences Department
The University of Michigan
Transportation Research Institute
Ann Arbor, Michigan 48109

December 1982

Technical Report Documentation Page

1. Report No.	2. Government Accession No.	3. Recipient's Catalog No.

4. Title and Subtitle	5. Report Date
EXPERIMENTAL DATA FOR USE WITH BIOMECHANICAL MODELS, Volume 2	December 1982
	6. Performing Organization Code
7. Author(s)	8. Performing Organization Report No.
Guy S. Nusholtz, Paula Lux, Miles Janicki	UMTRI-82-50-2
9. Performing Organization Name and Address	10. Work Unit No. (TRAIS)
The University of Michigan Transportation Research Institute Biosciences Department Ann Arbor, Michigan 48109	015651
	11. Contract or Grant No.
	DOT-HS-7-01636
	13. Type of Report and Period Covered
12. Sponsoring Agency Name and Address	INTERIM
Department of Transportation National Highway Traffic Safety Administration 400 Seventh Street, S.W. Washington, D.C. 20590	14. Sponsoring Agency Code

15. Supplementary Notes

Report is bound in 2 volumes:
1. Technical Report, Appendix A
2. Appendices B, C, D

16. Abstract

The objective of the work presented in this report was to provide biomechanical data on the impact response of the human head, thorax, and pelvis for a variety of current modeling and impact tolerance studies. Human cadavers were used as test subjects with multiple impacts being performed on each subject.

In a typical test series a single cadaver was subjected to two frontal head impacts, a series of three to six low-velocity thorax impacts with the subject in various positions, a high-velocity lateral thorax impact, and a lateral pelvis impact. In addition to kinematic response and injury tolerance data, information concerning the repeatability of impacts to the head of a single subject was obtained.

17. Key Words	18. Distribution Statement
	Unlimited

19. Security Classif. (of this report)	20. Security Classif. (of this page)	21. No. of Pages	22. Price
Unclassified	Unclassified	166	

TABLE OF CONTENTS

VOLUME 1

VOLUME 2

APPENDIX B: Impact Response and Injury of the Pelvis

Impact Response and Injury of the Pelvis

Guy S. Nusholtz, Nabih M. Alem, and John W. Melvin

Proceedings of the 26th Stapp Car Crash Conference, Paper No. 821160
SAE, Inc., 1982.

ABSTRACT

Multiple axial knee impacts and/or a single lateral pelvis impact were performed on a total of 19 cadavers. The impacting surface was padded with various materials to produce different force-time and load distribution characteristics. Impact load and skeletal acceleration data are presented as functions of both time and frequency in the form of mechanical impedance. Injury descriptions based on gross autopsy are given.

The kinematic response of the pelvis during and after impact is presented to indicate the similarities and differences in response of the pelvis for various load levels. While the impact response data cannot prescribe a specific tolerance level for the pelvis, they do indicate variables which must be considered and some potential problems in developing an accurate injury criterion.

INTRODUCTION

Pelvis injuries of varying type and severity have been found to occur in a significant number of automotive accidents (1-5). Investigations of trauma of the pelvis resulting from impact in an automotive environment have been documented primarily through accident investigation methods. There have only been a limited number of biomechanical studies attempting to research pelvis impact trauma under laboratory conditions. One of the earliest of these studies was conducted by Evans and Lissner in 1955 (6), and consisted of impacts to the denuded pelvis in the inferior-superior direction. Although no fracture tolerance data were obtained, it was concluded from this study that the pelvis exhibited elastic behavior and failed due to tensile stresses in various structural members. Ten years later a study of the behavior of the knee-femur-pelvis complex in an automotive impact environment was reported by Patrick et al. (7) In this series of tests, an impact sled was used to apply femoral-axis impacts to the knee of embalmed cadavers. The lowest applied load found to cause pelvis injury was 7.1 kN, and loads ranging from 8.5 kN to 17 kN were found to cause multiple fractures of the pelvis. It was suggested that a maximum force criterion (of about 6.2 kN) should be the threshold level for injury for the patella/femur/pelvis complex. A similar study using unembalmed cadavers was reported by Melvin and Nusholtz in 1980. A single pelvis fracture was found to occur at an applied load of about 20 kN, however loads up to 26 kN were applied with no resulting pelvis injury.

A recent biomechanical study of pelvis impact in an automotive environment was documented first in 1979 (9) and more completely in 1980 (10) by Cesari and Ramet. The goal of this research was to supply data for design of side door padding by impacting cadavers laterally in the pelvis and recording the force/injury relationships observed. It was suggested from this study that the response to impact is characterized by velocity of impacts, maximum force, and impulse. Admissible force tolerance for females was documented as 5-7 kN (1100-1600 lb) and for males as 7-13 kN (1600-2900 lb). These studies essentially characterize pelvis injury tolerance using maximum force and impulse indicators.

To further investigate the kinematic and injury response of the pelvis in automotive-environment impacts, a series of tests involving indirect impacts to the pelvis have been

conducted by the Biomechanics Deprtment at HSRI. The tests were conducted using unembalmed cadavers and two types of impact facilities: a pendulum impactor and a pneumatic impactor. Indirect loads were delivered to the acetabulum of the pelvis by impacting the femur either axially or laterally. This allowed loads to be delivered to the acetabulum in either anterior-to-posterior or right-to-left directions. The cadavers were instrumented to measure pelvic triaxial accelerations in all tests, while in some tests three-dimensional motion of the pelvis was recorded with nine accelerometers. Additionally, triaxial accelerations of the femur and the thoracic vertebrae (T8) were measured. Photographic targets on the pelvis and femur were used for photokinemetric analysis of motion due to the impact.

ANATOMICAL OVERVIEW

The bony pelvis (Figure 1) consists of two large, flat irregular shaped hip (coxal) bones that join one another at the pubic symphysis on the anterior midline. Posteriorly the wedge shaped sacrum completes the pelvic ring forming a relatively rigid structure.

In the adult, each hip bone is formed by the fusion of three separate bones, the ilium, ischium, and pubis, which join at the acetabulum. The ilium forms the broad upper lateral part of the hip bone and the upper portion of the acetabulum. Its upper curved edge is the iliac crest. The most commonly refered to prominence on this crest is the anterior-superior iliac spine. Posteriorly the crest ends in the posterior iliac spine, adjacent to its articulation with the sacrum, the sacroiliac joint. The ischium forms part of the acetabulum and has a superior ramus that ends below in the ischial tuberosity. From there the inferior ramus ascends to join with the inferior ramus of the pubic bone. Together this bar of bone is frequently referred to as the ischio-pubic ramus or inferior pubic ramus. The body of the pubic bone forms the anterior part of the acetabulum. From here the superior pubic ramus passes to the midline where it joins its fellow of the opposite side through the pubic symphysis. Below the inferior pubic ramus joins the inferior ischial ramus. The posterior-lateral bony pelvis is covered by multiple muscle layers, buttock fat and skin. The iliac crest is relatively free of heavy musculature. The rounded head of the femur articulates wih the acetabulum and is held within the socket by ligaments. Laterally, on the upper femur is a large bony prominence, the greater trochanter, for the attachment of muscles.

METHODOLOGY

SUBJECT PREPARATION

Following transfer to HSRI, the cadaveric subjects were stored at 4° C until subsequent use. The cadavers were sanitarily prepared and were examined radiologically prior to the installation of accelerometer hardware and after the test.

IMPACT TESTING

Impact tests were conducted using HSRI's pendulum and pneumatic impacting devices. A total of 19 cadavers were used in three series of tests. Multiple left knee impacts (described below) and a single lateral impact were performed on a group of eight cadavers, instrumented with triaxial accelerometer clusters on the pelvis and right trochanter of the femur. A second group of eight cadavers was subjected to knee impacts along the direction of the femoral axis of each side. Of these eight subjects, four had triaxial accelerometer clusters on both trochanters, one was instrumented with a nine-accelerometer plate on the pelvis, and three had no instrumentation. Finally, three cadavers were subject to left-side lateral impacts, each instrumented with a pelvic nine-accelerometer plate.

Acceleration Measurement -- Accelerations were measured in three orthogonal directions at two different sites (trochanter and pelvis) with Endevco 2264-2000 piezoresistive accelerometers by securing a triaxial accelerometer cluster to a mounting platform at each site. Three-dimensional motion determination was made possible by affixing three triaxial clusters of accelerometers to a lightweight magnesium plate which was in turn rigidly attached to the pelvis. The location of the center of gravity, the coordinate system of the triaxial clusters, and the nine accelerometer array are shown in Figure 2. The figure is divided into four sections. The top half of the figure shows the location of the instrumentation for those tests in which the response of both trochanters were obtained. The lower left hand corner shows the location of triaxial clusters in those tests in which both trochanter and pelvis response were measured. The lower right hand corner shows the location of the triaxial cluster or nine accelerometer array for those tests in which only pelvis response was measured. The location and mounting of the accelerometer platforms were as follows:

Trochanter: An incision was made below the greater trochanter and several short self-

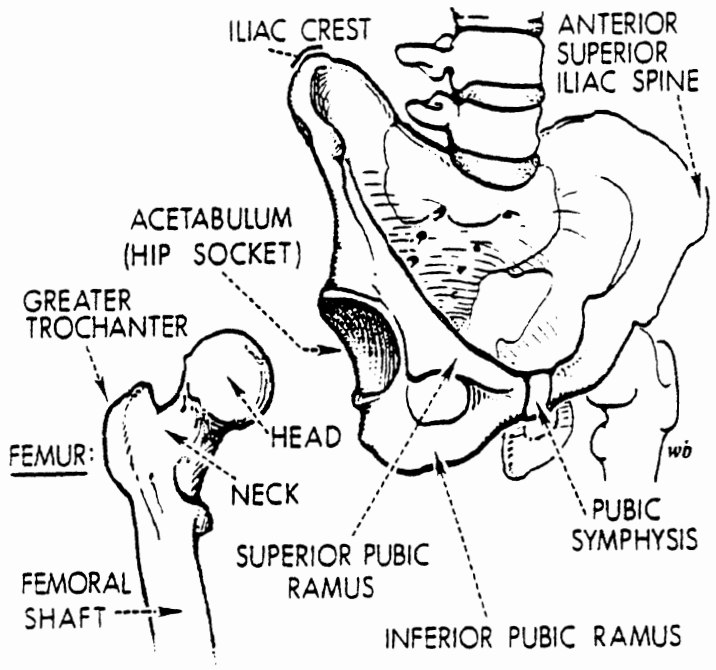

Fig. 1 - Anatomical overview of pelvis (5)

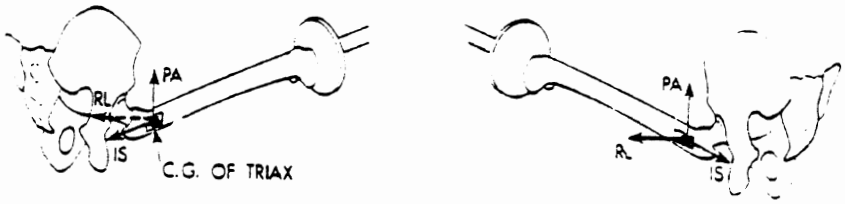

BI-TROCHANTERION RESPONSE

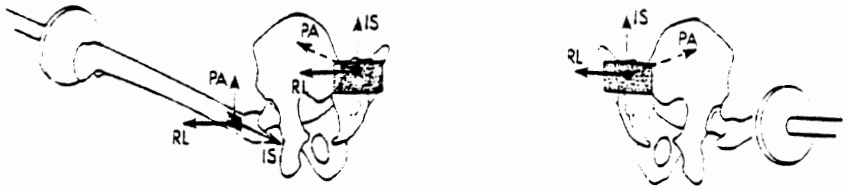

LEFT TROCHANTER AND/OR PELVIC RESPONSE

Fig. 2 - Instrumentation and phototarget location

tapping screws using a multi-point attachment scheme secured the mounting platform to the femur. The platform was then anchored with acrylic to insure rigidity.

Pelvis 9-Accelerometer: Four lag bolts were screwed into the pelvis near the posterior-superior iliac spines. Acrylic was applied, encasing both the bolts and the mounting plate, with the CG of the instrumentation plate midway between the posterior-superior iliac spines.

Pelvis Triax: Two lag bolts with tapped heads were screwed into the posterior-superior iliac spines. A lightweight magnesium plate spanned the bolts and was secured by two screws anchored into the tapped heads of the lag bolts.

Pendulum Impacts -- The pendulum impact device consists of a free-falling pendulum as an energy source which strikes either a 25 kg or a 56 kg impact piston. The impactor, guided by a set of Thompson linear ball bushings, was brought to impact velocity prior to impact and traveled up to 25 cm before being arrested. Axial loads were measured with either a GSE biaxial load cell or a Setra model 111 accelerometer. Shear loads were measured (when relevant) with the GSE biaxial load cell. Impact conditions between tests were controlled by varying impact velocity (up to 8.5 m/s), and the type and depth of padding on the impact piston surface. The piston excursion and the distance the piston traveled from the point of contact to the point of arrest ranged from 3 to 20 cm. The velocity of the piston was measured by timing the pulses from a magnetic probe which sensed the motion of targets on the piston at 0.89 cm intervals. A specially designed timer box was used to control and synchronize the events of a test, such as the release of the pendulum and activation and deactivation of lights and high speed cameras.

For tests conducted with this device, the subject was placed in a restraint harness and suspended in a seated position. Indirect impacts to the acetabulum in the anterior-to-posterior direction were delivered by impacting the knee along the direction of the femoral shaft axis ("axial knee impacts"). Indirect lateral impacts to the acetabulum were delivered by impacting the trochanteric region of the femur, along the axis of the neck of the femur.

Pneumatic Impacts -- The pneumatic impact device consists of an air reservoir which is connected to a honed steel cylinder. A driver piston is propelled down the cylinder by the pressurized air in the reservoir. The driver piston contacts a striker piston which is fitted with a piezoelectric accelerometer (Kistler 904A) and a piezoelectric load washer (Kistler 805A) to allow the determination of acceleration-compensated contact loads applied to the test subject. The mass, velocity, and stroke of the striker piston can be controlled to provide the desired impact conditions for a particular test. The velocity of the impactor is measured by timing the pulses from a magnetic probe which senses the motion of targets on the impactor at 1.3 cm intervals.

For the pneumatic impactor tests, the subject was suspended by a body harness and an overhead pulley system and in addition was seated on a block of balsa wood. Impacts were delivered indirectly to the pelvis through loading of the femur at the knee, as described above.

THREE-DIMENSIONAL MOTION DETERMINATION

The HSRI method used for measuring the three-dimensional motion of the pelvis is based on a technique used to measure the general motion of a vehicle in a simulated crash (11). In the current application, three triaxial clusters of Endevco 2264-2000 accelerometers are affixed to a light-weight magnesium plate which is then rigidly attached to the pelvis. With this method it is possible to take advantage of the physical and geometrical properties of the test subject as well as the site of impact in the design of a system for measurements of 3-D motion.

The nine acceleration signals obtained from the three triaxial clusters are used for the computation of the pelvis motion using a least-squares technique, the details of which are described elsewhere (12,13). The method takes advantage of the redundancy of nine independent acceleration measurements to minimize the effect of experimental error.

PHOTOKINEMETRICS

Each subject underwent two radiologic examinations, one prior to and one following the test. High-speed photographic coverage of the test consisted of two lateral views. A Hycam camera operating at 3000 frames per second provided a close-up view of the pelvis, while a Photosonics 1B camera operating at 1000 frames per second was used to obtain an overall view of the test subject. The motion of the subject was determined from the film by following the motions of five-point phototargets. The targets were affixed to the rigid accelerometer mounts located on the pelvis, trochanter, and spine. Since the resulting film provided a lateral view of the test, the motion observed was two-dimensional and restricted to the plane of the film.

INITIAL CONDITIONS AND POSITIONING

For all tests, the subject was placed in a restraint harness which was in turn suspended from the ceiling. For the axial knee impacts, the subject was positioned as in Figure 3 with the impactor initially 8 to 10 cm from the knee. These tests used as padding either 2.5 cm of Ensolite, 2.5 cm of styrofoam, or a combination of 2.5 cm Ensolite and 2.5 cm styrofoam. The lateral pelvis impacts required that the subject be positioned as in Figure 4, with the impactor initially centered 8 cm anterior to the greater trochanter. For these tests, the impactor was either rigid, padded with 2.5 cm Ensolite, or a combination of 2.5 cm Ensolite and 2.5 cm styrofoam.

PELVIS IMPACT RESPONSE

One method for analyzing the motion of a material body is to analyze the motion of a point on that body. In the case of the tests performed in this study, the point chosen is midway between posterior-superior iliac spines (PSIS). The motion is then analyzed using the concept of a moving frame discussed elsewhere (13) and briefly summarized here.

A vector field is a function which assigns a uniquely defined vector to each point along the path generated by the moving point. Similarly, any collection of three mutually orthogonal unit vectors emanating from each point on the path is a frame field. Thus any vector defined on the path (for example, acceleration) may be resolved into three orthogonal components of any well defined frame field.

In biomechanics research, frame fields which are frequently used are defined based on anatomical reference frames. The anatomical reference frames used here are shown in Figure 2. The frames are based on the anatomical orientation of a standing test subject. Therefore, the I-S direction of the trochanter is roughly equivalent to the minus A-P direction of the pelvis for a seated subject. Other frame fields such as the Principal Direction Triad (14) or Frenet-Serret frame (13), which contain information about the motion embedded in the frame field, have also been used to describe motion resulting from impact.

The Frenet-Serret frame consists of three mutually orthogonal vectors T, N, B. At any point in time a unit vector can be constructed that is co-directional with the velocity vector. This normalized velocity vector defines the tangent direction T. A second unit vector N is constructed by forming a unit vector co-directional with the time derivative of the tangent vector T (the derivative of a unit vector is normal to the vector). To complete the orthogonal frame, a third unit vector B (the unit binormal) can be defined as the cross product T x N. This then defines a frame at each point along the path and resolves the acceleration into two distinct types. The tangent acceleration (Tan(T)) is always the rate of change of speed (absolute velocity) and the normal acceleration (Nor(N)) contains acceleration information about the change in direction of the velocity vector. The binormal direction contains no acceleration.

In the case of a single triaxial accelerometer, the use of the Frenet-Serret frame is impractical but it has been found (14) that in many cases during direct impacts it is possible to find the most significant component of acceleration, therefore the principal direction of motion can be obtained.

One method of determining the principal direction of motion and constructing the Principal Direction Triad is to determine the direction of the acceleration vector in the moving frame of the triaxial accelerometer cluster and then prescribe the transformation necessary to obtain a new moving frame that would have one of its axes in the principal direction. A single point in time at which the acceleration is a maximum was chosen to define the directional cosines for transforming from the triax frame to a new frame in such a way that the resultant acceleration vector (AR) and "principal" unit vector (A1) were co-directional. This then can be used to construct a new frame rigidly fixed to the triax, but differing from the original one by an initial rotation. After completing the necessary transformation, a comparison between the magnitude of the principal direction and the resultant acceleration is performed. In the case of the impacts presented here, there was only a slight difference between the two quantities during the most significant part of the impact. However, for responses occurring after impact this was not always the case.

FORCE-TIME DURATION DETERMINATION

In order to define the pulse duration, a standard procedure was adopted which determines the beginning and end of the pulse. The procedure is to determine first the peak and the time at which it occurs. Next, the left half of the pulse, defined from the point where the pulse starts to rise to the time of the peak, is

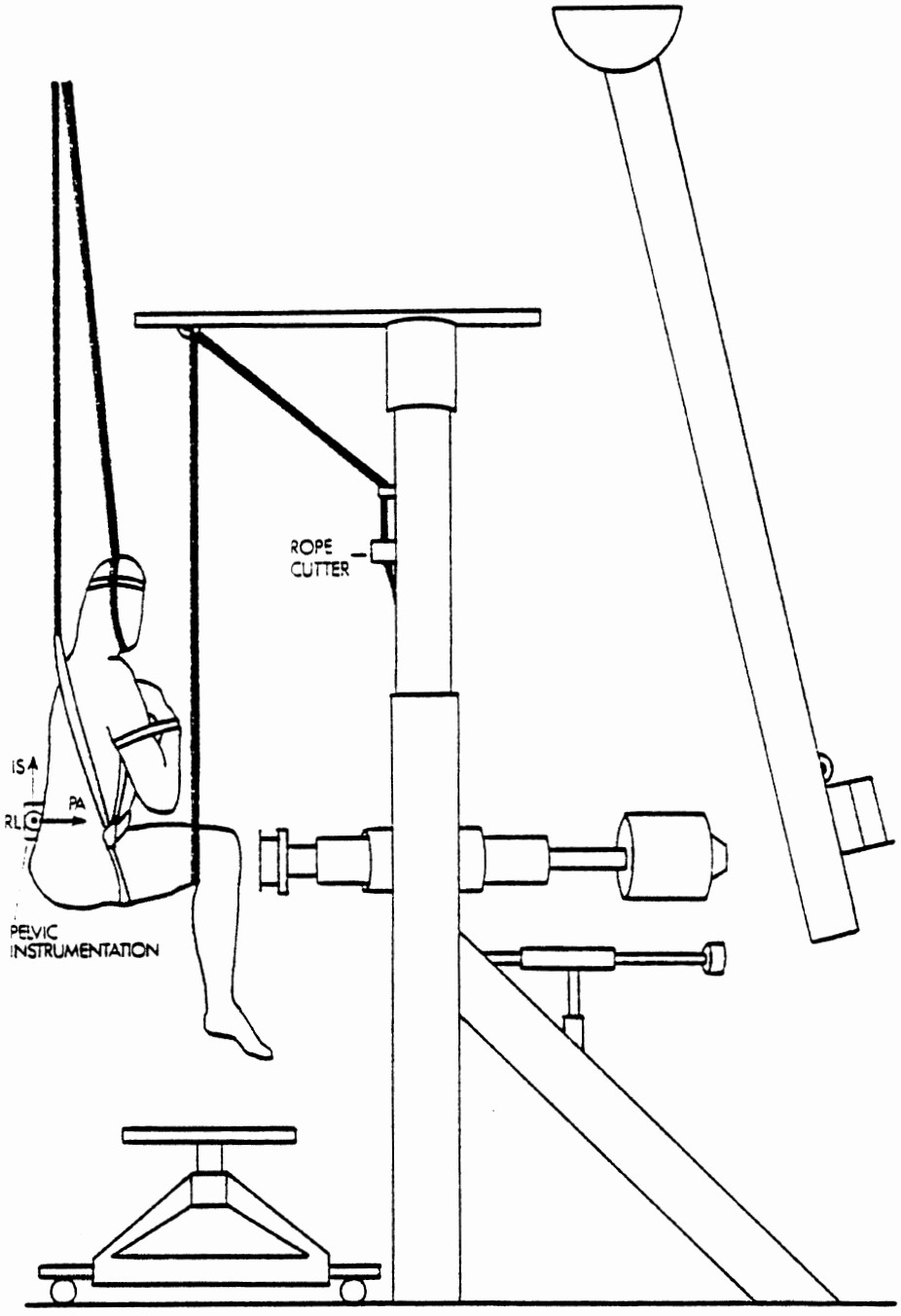

Fig. 3 - Schematic pendulum test setup — right leg impact

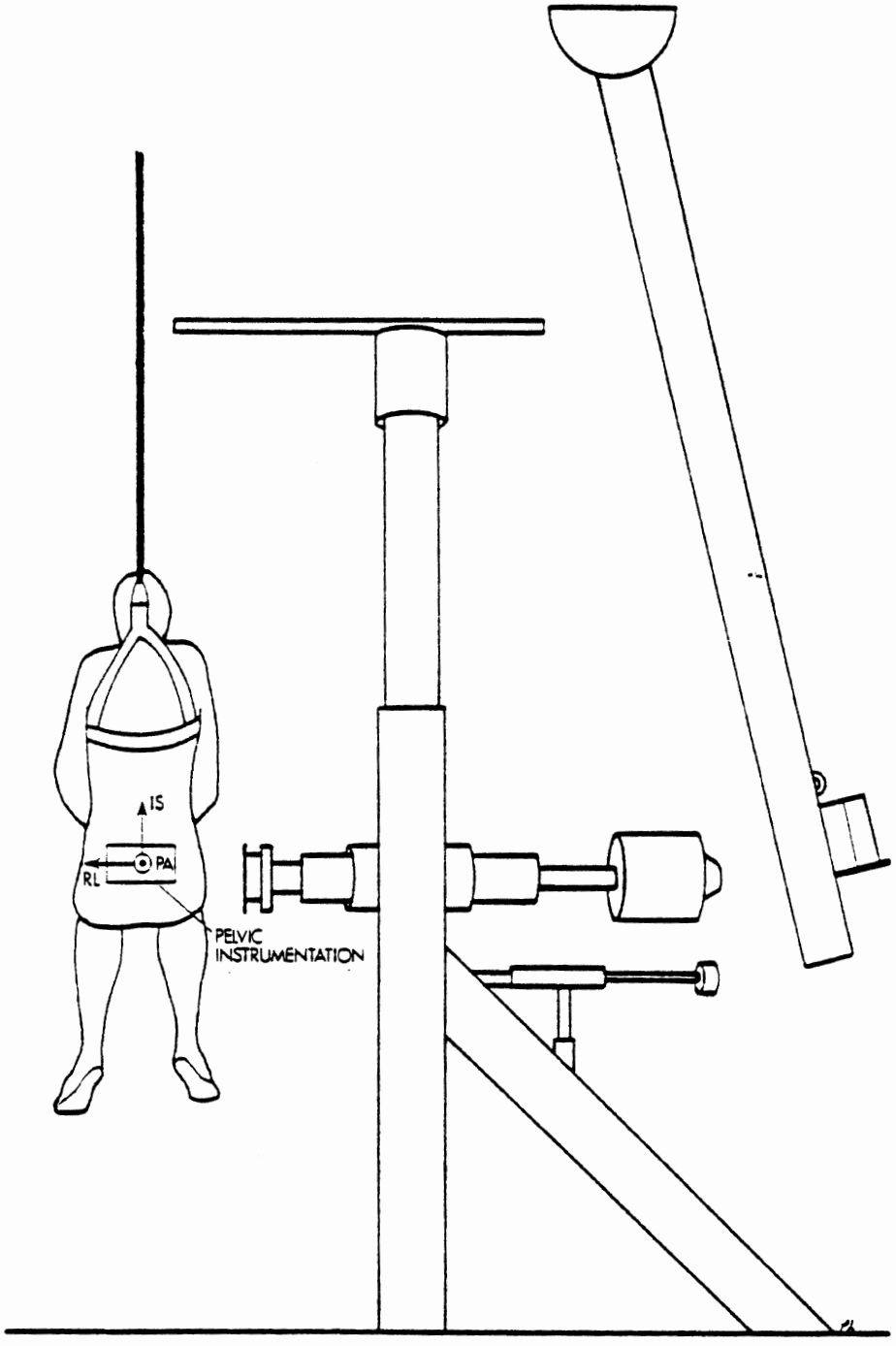

Fig. 4 - Schematic pendulum test setup — pelvis impact

least-squares fitted with a straight line. This rise line intersects the time axis at a point which is taken as the formal beginning of the pulse. For those tests which exhibit multimodal signals, the least-squares line is fitted from where the pulse starts to the time of the first significant peak. A similar procedure is followed for the right half of the pulse, i.e., a least squares line is fitted to the fall section of the pulse which is defined from the peak to the point where the first pulse minimum occurs. The formal end of the pulse is defined then as the point where the fall line intersects the time axis. In many cases, however, the formal end of the pulse (as defined above) is not the end of contact between the impactor and the subject. In these instances, two durations are used; one to indicate the end of the most significant aspect of the force-time history and one to indicate the end of the contact.

IMPACT TRANSFER FUNCTION ANALYSIS

With blunt impacts, the relationship between impact force and the motion resulting at various points of the impacted system can be expressed in the frequency domain through the use of a transfer function. A fast Fourier transformation of simultaneously monitored transducer time histories can be used to obtain the frequency response functions of impact force and accelerations of remote points. Once obtained a transfer function of the form

$$Z(i\omega) = \omega \cdot \frac{\mathcal{F}(F(t))}{\mathcal{F}(A(t))}$$

can be calculated from the transformed quantities where ω is the given frequency, and $\mathcal{F}(F(t))$ and $\mathcal{F}(A(t))$ are the Fourier transforms of the impact forces and acceleration of the point of interest, at the given frequency. This particular transfer function is closely related to mechanial transfer impedance which is defined as the ratio between simple harmonic driving force and corresponding velocity of the point of interest. Mechanical transfer impedance (15) is a complex valued function which for the purpose of presentation will be described by its magnitude and its phase angle.

RESULTS

The tables and graphs presented on the following pages represent the data considered most pertinent in discussing the test results. Table 1 contains biometric data of all test subjects, as well as the test numbers corresponding to each subject (since most subjects received multiple knee impacts as well as a lateral pelvis impact, one subject will have several corresponding test numbers). The initial conditions for all knee impact tests and all lateral impact tests are presented in Tables 2 and 3, respectively.

A summary of gross autopsy results for the lateral impact tests is presented in Table 4. The series of knee impacts produced only one injury. All pelvic injuries were sustained on the impacted side of the pelvis.

Impact test summaries containing force and three-dimensional motion information for axial knee impacts to each cadaver appear in Table 5, and in Table 6 for lateral pelvis impacts. Summaries for force and triaxial acceleration are presented in Tables 7 and 8 for the axial knee impacts, and in Table 9 for the lateral impacts.

DISCUSSION

The results presented in this paper have been obtained from a series of pelvis injury research programs conducted during the past five years. The data is presented in abbreviated form to represent the trends which are felt to be important factors in pelvis impact response.

PELVIS RESPONSE FROM AXIAL KNEE IMPACTS

The response of the pelvis as characterized by the time history of various accelerations and velocities (both angular and linear) in addition to the force time history, is dependent on the impactor surface padding, mass and initial velocity as well as variations between individual test subjects. This is arrived at from analysis of three dimensional motion obtained from nine accelerometers, triaxial accelerometer clusters (affixed to the pelvis, the impacted femur and the femur opposite the impactor), as well as high speed photokinemetric documentation.

Three-Dimensional Motion -- Tests 79A243-79A248 represent six impacts to a single test subject. The six tests are divided into three groups with similar impacts on each knee. The three groups are: low velocity (3.5 m/s and 2.5 cm Ensolite impactor surface padding), medium velocity (5.0 m/s with 2.5 cm Ensolite impactor surface padding), and high velocity (8.5 m/s with rigid impactor surfaces). The time history of the three dimensional motion of the pelvis obtained from the nine accelerometer array is summarized in Table 5. The maximum impact force ranged from 4kN to 20kN with the duration of impact ranging from 12 ms to 30 ms.

Table 1. Biometrics

Cadaver No.	Height (cm)	Weight (Kg)	Age	Cause of Death
1	173	29.0	64	Differentiated lymphoma
2	160	57.2	73	Pneumonia
3	175	99.5	76	Cardiac arrest
4	178	106	63	Myocardial infarction
5	176	35.3	67	Cardiac resp. arrest intractible congestion
6	169	65.9	89	Cardiac arrest
7	176	68.1	76	Coronary occlusion
8	174	91.7	76	Myocardial infarction
9	179	41.6	66	Amyotrophic lateral sclerosis
10	174	61.9	73	Terminal pneumonia
11	180	91.2	56	Cardiac arrest
12	175	100	62	Cardiac arrest
13	--	88.0	61	Cardiac arrest
14	--	--	52	Cardiac arrest
15	184	52.0	60	Cardiac arrest
16	180	76.9	67	Cardiac arrest
17	169	86.5	65	Myocardial infarction
18	--	--	--	Cardiac arrest
19	174	68.3	40	Cardiac arrest

Table 2: Summary of Initial Conditions for Knee Impacts

Test No.	Cadaver No.	Impactor Velocity (m/s)	Impactor Mass (Kg)	Padding
77A204	18	15.2	10	10 cm Ensolite
77A205	13	12.2	10	10 cm Ensolite
77A206	13	15.2	10	10 cm Ensolite
77A207	12	18.3	10	10 cm Ensolite
77A208	12	21.3	10	10 cm Ensolite
79A243	14	3.4	25	2.5 cm Ensolite
79A244	14	3.4	25	2.5 cm Ensolite
79A245	14	5.0	25	2.5 cm Ensolite
79A246	14	5.0	25	2.5 cm Ensolite
79A247	14	8.6	25	Rigid
79A248	14	8.5	25	Rigid
79L081	1	5.5	56	2.5 cm Ensolite+ 2.5 cm Styrofoam
79L082	1	5.5	56	2.5 cm Ensolite+ 2.5 cm Styrofoam
79L085	2	5.5	56	2.5 cm Ensolite+ 2.5 cm Styrofoam
79L086	2	5.5	56	2.5 cm Ensolite+ 2.5 cm Styrofoam
79L089	3	5.5	56	2.5 cm Ensolite+ 2.5 cm Styrofoam
79L090	3	5.5	56	2.5 cm Ensolite+ 2.5 cm Styrofoam
80L094	4	5.9	56	2.5 cm Ensolite
80L097	5	5.5	56	2.5 cm Ensolite
80L098	5	5.9	56	Rigid

Table 2: Summary of Initial Conditions for Knee Impacts (continued)

Test No.	Cadaver No.	Impactor Velocity (m/s)	Impactor Mass (Kg)	Padding
80L102	6	5.5	56	2.5 cm Ensolite
80L103	6	5.8	56	Rigid
80L109	7	5.5	56	2.5 cm Ensolite
80L110	7	5.9	56	Rigid
80L114	8	5.9	56	2.5 cm Ensolite
80L115	8	5.8	56	Rigid
80L118	9	4.1	56	Rigid
80L119	9	4.2	56	Rigid
80L120	9	5.9	56	Rigid
80L124	10	4.1	56	Rigid
80L125	10	5.9	56	Rigid
80L129	11	4.0	56	Rigid
80L130	11	5.9	56	Rigid
80L135	19	4.0	56	Rigid
80L135	19	6.0	56	Rigid
80L135	19	4.0	56	Rigid
80L136	19	6.0	56	Rigid

Table 3. Summary of Initial Conditions for Lateral Impacts

Test No.	Cadaver No.	Impactor Velocity (m/s)	Impactor Mass (Kg)	Padding
80L095	4	5.1	56	2.5 cm Ensolite
80L099	5	5.7	56	2.5 cm Ensolite
80L104	6	5.8	56	Rigid
80L111	7	5.8	56	Rigid
80L116	8	5.7	56	Rigid
80L121	9	5.9	56	Rigid
80L126	10	5.8	56	Rigid
80L131	11	5.5	56	Rigid
80L137	19	5.9	56	Rigid
82E008	15	8.4	25	2.5 cm Ensolite+ 1.3 cm Styrofoam
82E028	16	8.4	25	0.5 cm Ensolite
82E049	17	8.6	25	2.5 cm Ensolite+ 2.5 cm Styrofoam

Table 4. Summary of Autopsy Results

Test No.	Results
80L095	No observed injuries.
80L099	No observed injuries.
80L104	Vertical separation fracture of superior public ramus approximately one inch from public symphysis.
80L111	Horizontal separation fracture of illo-public ramus, connected to a horizontal fracture of the acetabulum.
80L116	No observed injuries.
80L121	Vertical stellar fracture on outer aspect of ilium extending from iliac crest to anterior-inferior iliac spine.
80L126	Non-separational fractures of superior and ischio-public ramus.
80L131	Horizontal fracture of illo-public ramus.
80L137	No observed injuries.
82E008	No observed injuries.
82E028	Vertical Separation fracture of ischio-public ramus. Horizontal fracture of acetabulum extending two inches into superior public ramus.
82E049	No observed injuries.

Table 5. 3-D Motion Knee Impact Test Summary

Test No.	Peak Force (N)	Impulse (N.s)	Duration (m/s)	Peak Linear Acceleration (m/s/s)				Peak Angular Acceleration (rad/s/s)			
				P-A	R-L	I-S	TAN	P-A	R-L	I-S	RES
79A243 @ ms=	3750 11	58	30	-95 7	-150 6	70 6	160 6	-150 4	-670 5	1200 5	1180 6
79A244 @ ms=	3750 11	59	30	-90 5	200 5	75 5	250 5	430 3	-380 5	-1130 5	1050 5
79A245 @ ms=	5750 12	80	30	-120 7	+300 7	115 6	320 6	530 4	-800 5	-1750 5	2000 6
9A246 @ ms=	6000 11	75	32	-150 4	-260 4	160	340 8	-600 3	-1440 8	2000 5	2200 4
79A247 @ ms=	20000 3	120	12	-1750 2	-2600 2	100 3	3200 2	-1700 3	-30000 3	20000 2	31000 3
79A248 @ ms=	21000 2	135	12	-1050 2	2750 2	1600 2	3200 2	19000 1	-20000 2	-17500 1	25000 1

Table 6: Padded Knee Impacts

Test No.	Force				Acceleration		Velocity	
	Maximum (N)	Duration (ms)	Impulse (N-s)	Energy (N-M)	Troch. Maximum (m/s)	Opposite Troch. Maximum (m/s)	Troch. Maximum (m/s)	Opposite Troch. Maximum (m/s)
79L081- @ ms-	1550 11	25 (35)	22	5	43 4	16 35	4.9 22	2.8 60
79L082- @ ms-	1750 13	26 (31)	25	6	34 12	19 27	5.0 22	2.8 56
79L085- @ ms-	900	30	10	1	21 12	8 25	4.0	2.4 60
79L086- @ ms-	1100	30	12	1 +	7.5 15	10 20	4.3	2.5 65
79L089- @ ms-	5200 17	31 (43)	65		48 13	9 23	4.5 30	2.5 65
79L090- @ ms-	4600 17	34 (44)	60	32	33 (13)	13 27	4.0 30	2.2 65

Table 7: Knee Impacts

Test No.	Force					Acceleration		Velocity	
	1st Peak (N)	Maximum (N)	Duration (ms)	Impulse (N-s)	Energy (N-m)	Troch. Maximum (g's)	Pelvis Maximum (g's)	Troch. Maximum (m/s)	Pelvis Maximum (m/s)
80L094 @ ms=		5850 8	27 (73)	88	69	80 8	60 12	3.7 22	3.4 15
80L097 @ ms=		3950 9	20 (5)	45	18	115 9	80 8	6.2 16	5.2 1
80L098 @ ms=		2475 2	12 (36)	21	3.9	450 1	250 2	5.5 4	6.2 6
80L102 @ ms=		7000 8	24 (46)	100	88.8	140 7	95 8	4.8 11	4.0 10
80L103 @ ms=		7550 3	15 (40)	56	28.4	400 2	120 4	5.9 3	3.2 5
80L109 @ ms=		8100 9	25 (61)	98	85.2	200 9	70 8	5.3 8	3.4 9
80L110 @ ms=		9500 3	20 (44)	89	0.9	700 2	190 3	5.7 6	3.7 5
80L114 @ ms=		10000 7	35 (55)	107	102	230 6		6.2 7	3.1 28
80L115 @ ms=		12000 2	24 (34)	100	92	675 2		5.9 3	3.4 16
80L118 @ ms=	5200 1	6000 2	12 (66)	36	11.6	220 1	115 1.5	3.9 8	3.2 7
80L119 @ ms=	4500 1	5750 2	13 (70)	45.7	18.7	300 2	155 3	4.2 4	3.2 8
80L120 @ ms=	5250 1	8900 3	15 (55)			500 3	150 (3.5)	4.9 3	4.0 10
80L124 @ ms=	1	7500 2	20 (77)	46.9	19.6	390 2	115 4	4.4 4	3.0 7
80L125 @ ms=	5600 1	9700 3	20 (57)	88	70	400 2	175 4	5.2 3	3.5 6
80L129 @ ms=		8750 3	20 (27)	74.4	49.5	205 1	140 2	4.1 6	3.5 15
80L130 @ ms=	8900 2	9750 3	16 (29)	105	100	650 2	185 2	5.6 6	5.1 14
80L135 @ ms=	5000 2	8700 4	17 (28)	75	51	1750 1	135 2	3.9 7	3.4 10
80L136 @ ms=	9700 6	11800 6	16 (58)	105	101	900 2	240 3	5.4 8	4.1 9

Table 8. Lateral Pelvis Impact

Test Number	Force		Acceleration		Velocity
	Maximum (N)	Duration (ms)	1st Peak	Maximum (g's)	Maximum (m/s)
80L095 @ ms=	10700 10	44		38 10	4.4 44
80L099 @ ms=	3200	42	23 5	50 11	4.6 38
80L104 @ ms=	5900 9	49		40 11	4.7 42
80L111 @ ms=	7600	50		100 4	4.7 40
80L116 @ ms=	7700 9	51		57 11	4.3 48
80L121 @ ms=	3300 15	30	105 2	110 4	4.3 56
80L126 @ ms=	7400 5	44	50 4	135 11	4.3 40
80L131 @ ms=	8500 7	40	50 6	135 11	4.3 52
80L137 @ ms=	9200 5	22	40 3	48 6	4.8 50

Table 9. Lateral Impacts

Test No.	Peak Force (N)	Impulse (N-s)	Duration (ms)	Peak Linear Acceleration (m/s/s)				Peak Angular Acceleration (rad/s/s)			
				P-A	R-L	I-S	Tan	P-A	R-L	I-S	Res
82E008 @ ms=	14000 13	190	29	300 18	840 11	-340 14	831 14	-2270 14	-6910 14	-4600 16	6010 11
82E028 @ ms=	13000 7	190	21	350 6	710 6	550 11	650 6	3620 4	10100 8	8190 5	10250 8
82E049 @ ms=	14000 14	206	26	127 15	360 14	-100 14	370 14	2700 13	-3480 13	-1990 16	3750 16

Several distinct events occurred in all the force time histories and could be used as event markers. They are: the beginning of impact noted as E1, the peak force noted as E2, and the end of impact noted as E3. Both angular and linear accelerations begin at the E1 event and reach maximums at or before the E2 event. Even though there is significant angular acceleration during this interval, the primary acceleration is in the tangent direction (with a smaller component in the normal direction) indicating that the direction of motion changes slowly with time. In addition, the angular acceleration during this interval differs in magnitude and direction for each of the three sets of tests. For tests 79A243 and 79A244 (Figures 5 and 6) the angular acceleration was found to be primarily in the I-S direction (although lesser components occurred in the R-L and P-A directions). In tests 79A245 and 79A246, the magnitude of the angular acceleration is greater and is to a greater degree in the R-L and P-A direction. In tests 79A247 and 79A248 (Figures 7 and 8), the magnitude of the angular acceleration in the R-L and P-A direction is similar in magnitude to that of the I-S direction. Along with the changes in magnitude and direction of the angular acceleration with changing impact velocity, there is an increasing ratio of angular acceleration to peak force as well as a change in the relative phasing of the angular acceleration time history to force time history during the E1-E2 interval. In addition to changes in angular acceleration with increasing impactor velocity, there were also changes in the linear acceleration; its magnitude, direction, and phasing with respect to the E2 events. For tests 79A243 and 79A244, the linear acceleration was primarily in the RL-PA plane during the E1-E2 event interval. As the magnitude of the loading increased (as in tests 79A245 through 79A248), a significant component of linear acceleration in the I-S direction developed.

Physically, this implies that the response of the pelvis can be interpreted as the response of one material body (the pelvis) in contact with other material bodies (the femur, spine, abdominal organs, and soft tissue). The degree to which each of the material bodies interacts with the pelvis is dependent upon the amount of available impactor energy and how it is transmitted to the pelvis.

Triaxial Bitrochanteric Response -- Although the padding on the impactor surface was different, the loading in tests 79L081 through 79L090 (Table 7) is similar to that of the the previous tests. The response is measured with two triaxial accelerometer clusters located near each trochanter. Using the same event markers on the force time history as in the previous tests, some information about the response of the pelvis from the trochanteric response may be obtained. Near the E1 event the acceleration of the trochanter of the impacted side begins, however the accelerometer of the opposite trochanter displays little or no motion until near or after the E2 event. Acceleration of the impacted side peaks before the E2 event, whereas the acceleration response of the other trochanter reaches a maximum near the E3 event. The motion indicated by this type of response is somewhat similar to test 79A243 and 79A244 (for the pelvis) with the greatest rotation in the I-S direction. However, it is clear from the accelerometer data and high-speed movies that although the pelvis seems to behave as it were rotating about a fixed point near the trochanter of the opposite femur during the E1-E2 interval, motion after the E2 event is considerably more complex, with the peak velocity of the opposite femur more than half of that of the impacted femur.

Pelvis and Trochanteric Response -- Tests 80L094 to 80L136 (Table 8) represent similar loading to that of the previously mentioned tests (79A243-248 and 79L081-090). The response is measured by the use of triaxial accelerometers located on the pelvis and trochanter on the side of impact, as well as photokinemetric documentation. The peak forces range from 6 to 12 kN.

In some of these tests, the force time history is similar to that of 79L081 through 79L090 with one peak and a well defined beginning and end, however a few of the tests have a more complex force time history. They exhibit several local maxima and/or continuing impactor contact after the initial part of the pulse occurs. Although the response of the trochanter as interpreted by the principal direction acceleration and resulting acceleration time-history waveforms is similar to some of the previous heavily-padded tests, others display damped oscillatory motion (Figure 9). This response is generally observed during the first section of the pulse and unobservable shortly after the E2 event. In addition the peak acceleration generally occurs around the time of the first significant maximum of the force time history. Other researchers using finite element modeling of the femur (16) have shown that various modes of bending and torsion can occur. Potentially both the oscillatory nature of the trochanteric response and the multimodal nature of the force time histories for these tests are a result of the bending of the femur.

Although in these tests only triaxial acceleration is measured and the force time history varies from test to test in a very

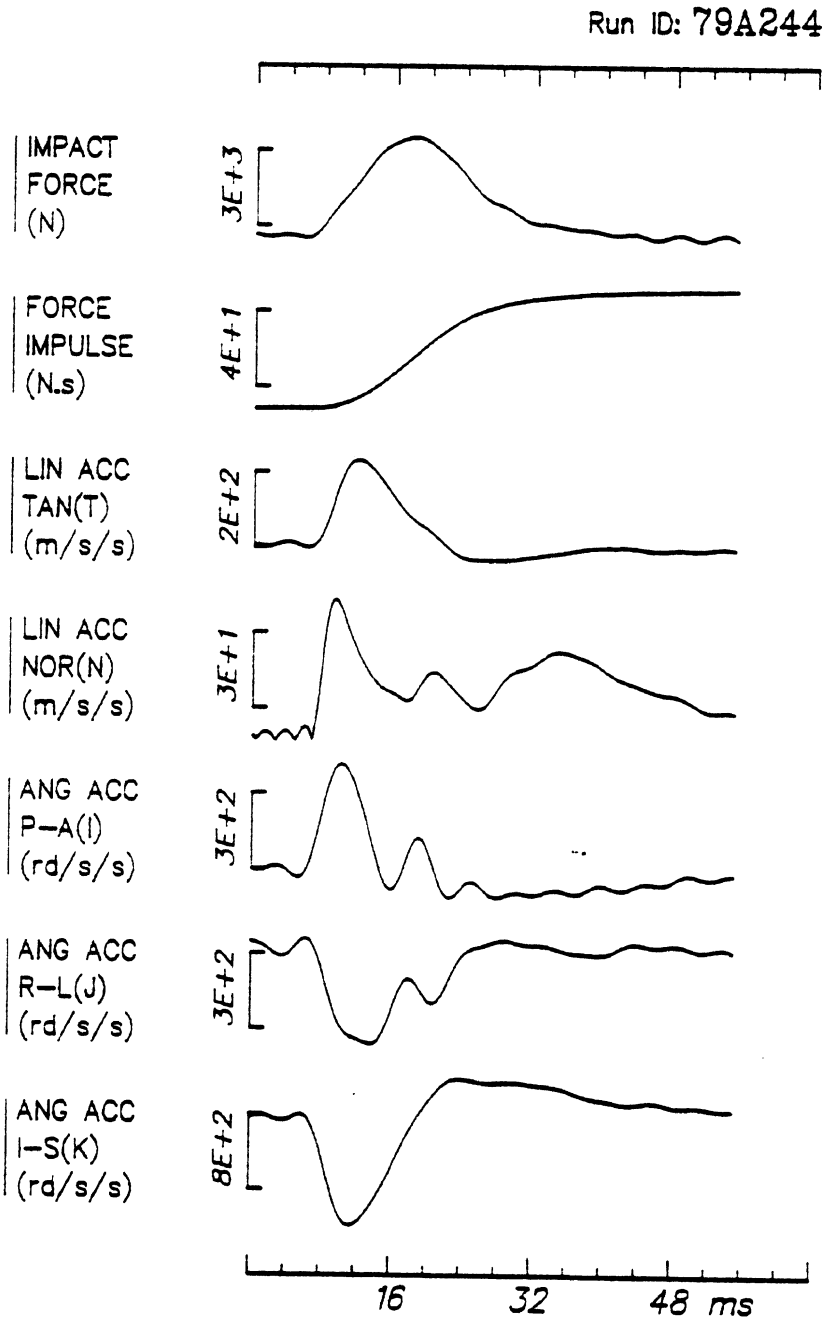

Fig. 5 - Test 79A244

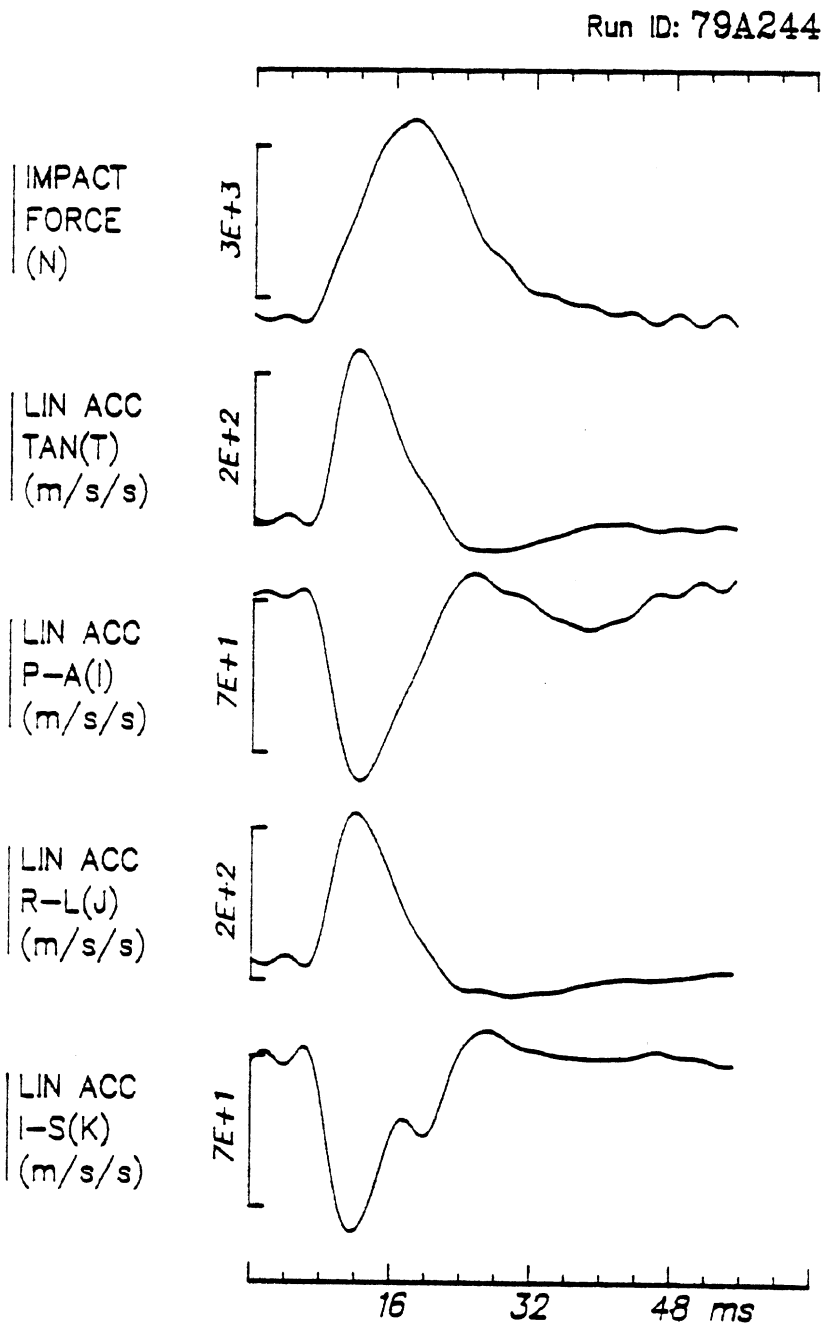

Fig. 6 - Test 79A244

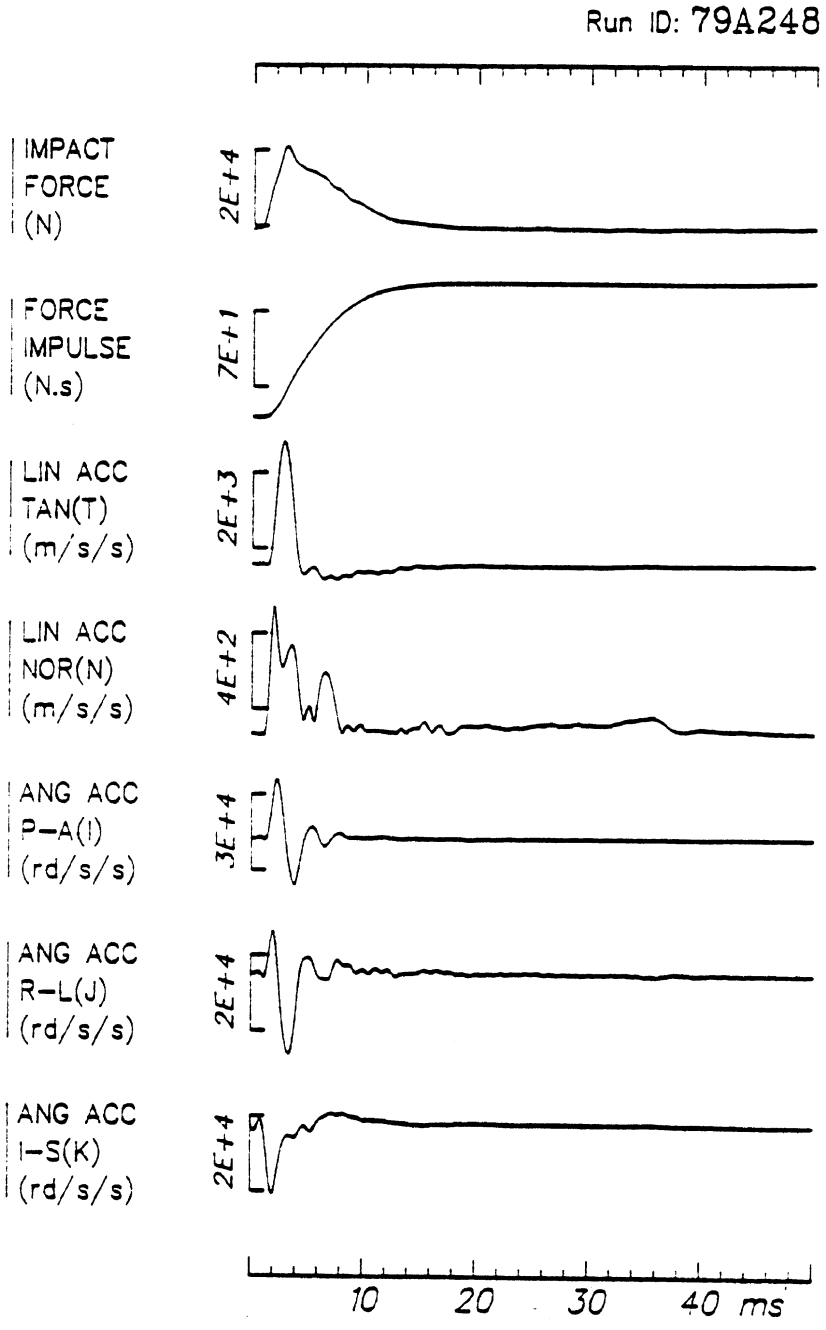

Fig. 7 - Test 79A248

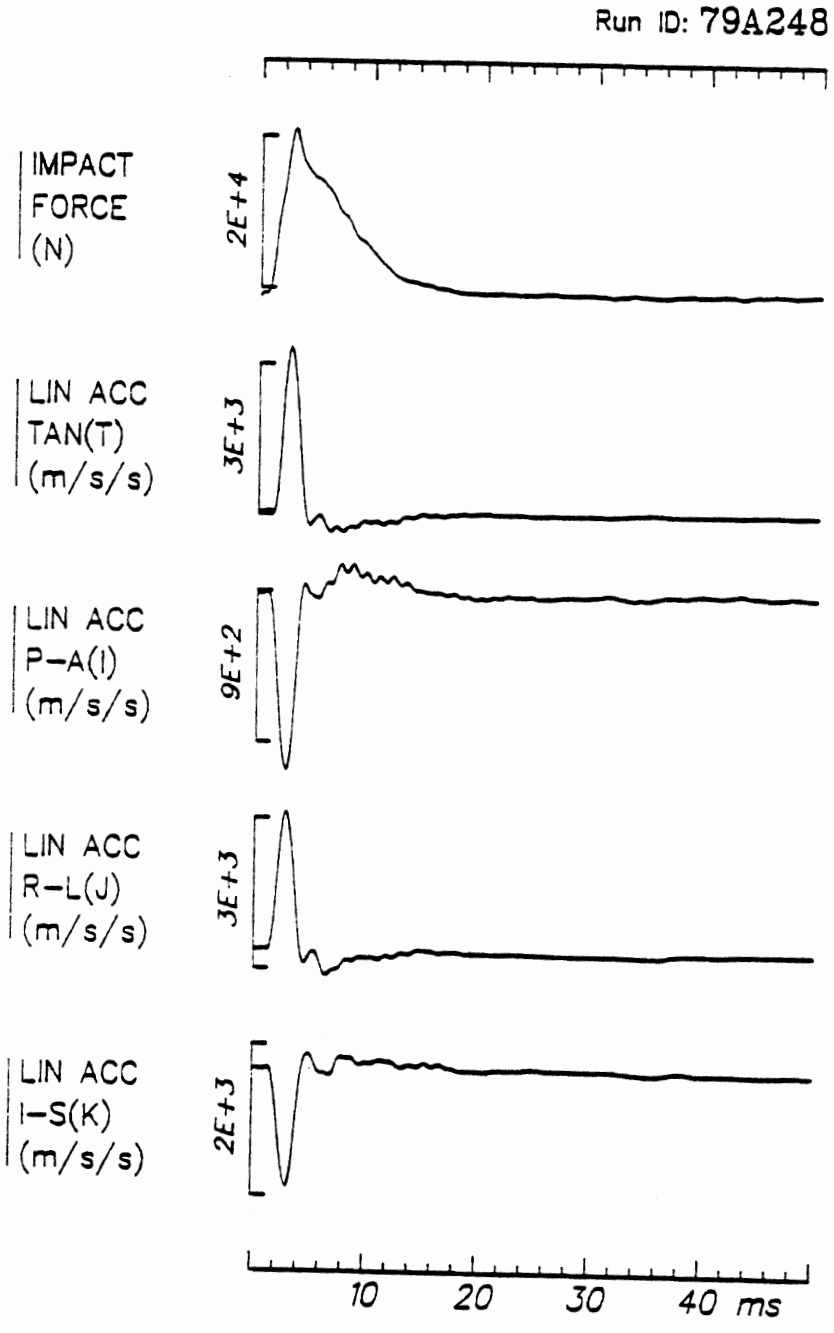

Fig. 8 - Test 79A248

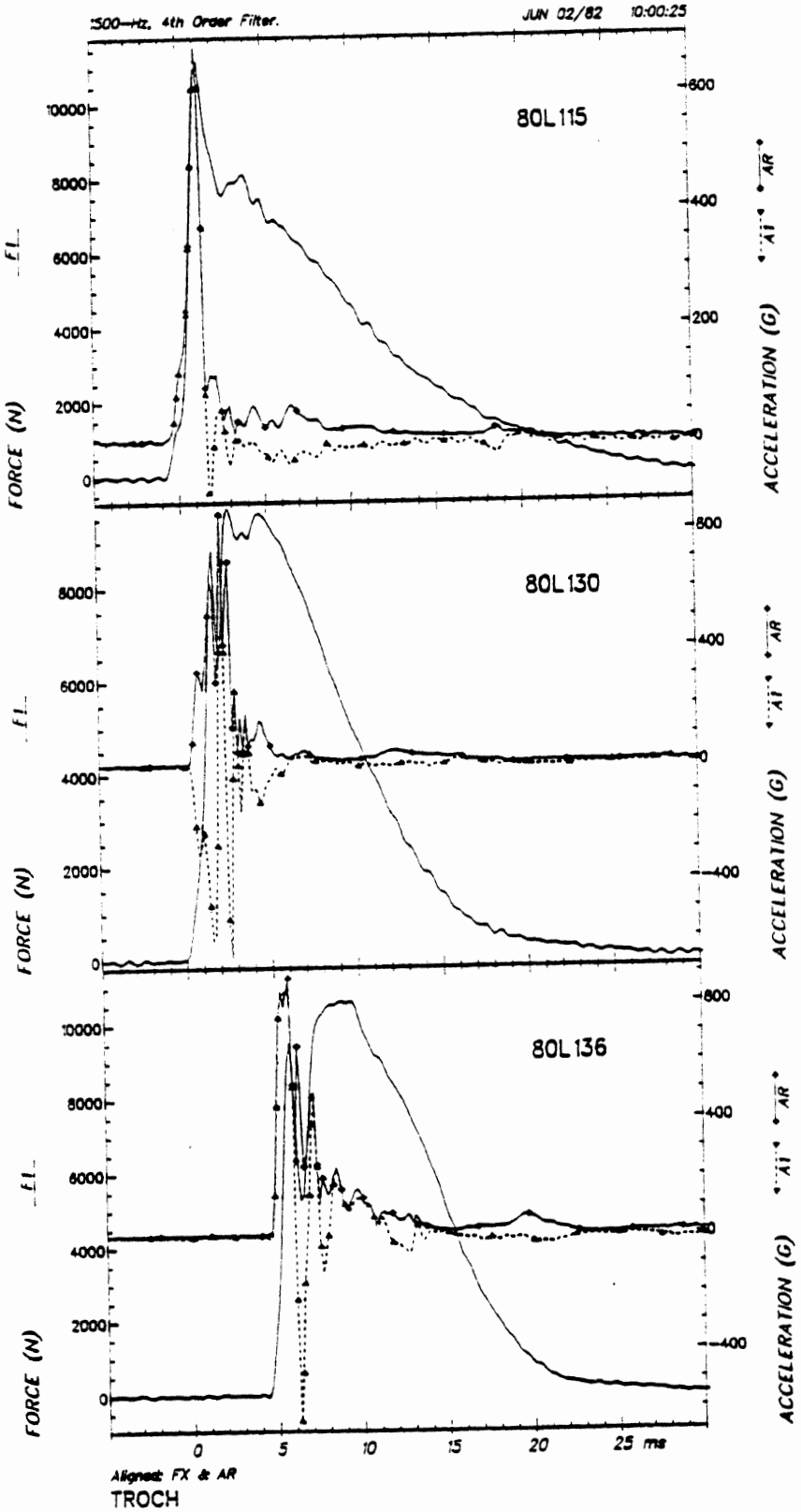

Fig. 9 - Trochanter impact response

general way the response of the pelvis, as interpreted by the principal direction accelerations, is similar in these tests to that of the response interpreted by tangential acceleration in tests 79A247 and 79A248. Table 8 compares the acceleration time history of the pelvis to that of the force time history and acceleration time history of the trochanter. In general, the peak acceleration of the pelvis is less than and lags behind that of peak trochanteric accelerations. In addition, the resultant peak velocity of the trochanter is greater than and precedes the pelvis peak velocity, and is primarily in the I-S direction (of the femur).

Transfer Functions -- The transfer function formed from the impact force and acceleration includes the effects of padding and subject response. A corridor for transfer functions formed from the impact force and tangent acceleration for tests 79A243-79A248 is shown in Figure 10.

For tests 79A243 and 79A244 the transfer function is included in the corridor to 100 Hz. For test 79A245 and 79A246 the transfer function is included to 150 Hz, and for tests 79A247 and 79A248, it is included from 10 to 400 Hz. The corridor representing pelvis response (interpreted by mechanical impedance for force and resulting velocity) shows that all six tests are similar to 100 Hz. Four tests are similar to 150 Hz and two are similar to 400 Hz. This seems to be true despite the different impact conditions (different padding, different initial velocity, opposite side impacts), and different time history responses. This would seem to indicate that the responses for this subject are repeatable, symmetric (same response for opposite sides) and linear to at least 100 Hz.

The mechanical impedance for tests 79A081 - 79A090 (Figure 11) is generated from force and principal direction acceleration, and is considered valid between 10 and 100 Hz. In the frequency range between 10 and 30 Hz it is somewhat similar to the impedance of tests 79A243 through 79A248. Above this range, however, there is a continual decline in the value of the impedance. This is believed to be a result of the styrofoam padding used in these tests.

For pelvis tests 80L094 - 80L136, the mechanical impedance obtained from the principal direction acceleration was significantly less than those calculated from the accelerations in the two directions normal to it above 25 Hz in all tests. For the trochanter, the mechanical impedance was valid for regions below this range however for comparison purposes it is presented down to 25 Hz. The upper limit for the validity of the pelvis impedance was 400 Hz and therefore the trochanteric upper limit is chosen as 400 Hz. To obtain information about the repeatability of the response of different test subjects, multiple impacts (at a subinjurious level) were performed on each subject (Table 8) with each subject in the same initial postural configuration while the impactor surface padding and velocity were varied. The transfer function formed from the principal direction acceleration and force-time history for both the pelvis and trochanter are shown in Figures 12 and 13 for tests 80L114 and 80L115, respectively, and in Figures 14 and 15 for tests 80L135 and 80L136, respectively.

It was observed that the acceleration response of the trochanter is primarily in the same direction as that of the force while the acceleration of the pelvis is not. Despite this and the fact that impact conditions varied between impacts to the same side, observation of these transfer function waveforms (and others not presented) show that the transfer functions for repeated tests on the same side are similar for both the pelvis and trochanter. The transfer function for the pelvis and the trochanter of the same subject are similar in waveform up to 200 Hz, although they differ in magnitude -- values for the mechanical impedance of the pelvis are generally two to four times that of those for the trochanter. The amount of scatter between subjects is addressed in Figures 16 and 17, which represent the corridor for impacts that did not result in injury for both the pelvis and trochanter, respectively. Although the two corridors look similar (differing only in magnitude below 100 Hz), they cover a wide range of possible responses, particularly above 200 Hz. This magnitude indicates that although the response of a single subject is similar for repeated impacts, there is wide scatter between subjects.

In addition to the above observations on the transfer functions, in some of the tests (e.g., 80L135 and 80L136) a resonance was observed between 180 and 280 Hz, which is within the band in which others have observed a resonance (16,17). This resonance (which is observed in both the pelvis and trochanter, although it is more pronounced in the trochanter transfer function) is potentially related to the oscillatory behavior mentioned above and also to the predicted first mode bending (16). Although most of the test subjects did not display this resonance, it does occur in a few of the tests which may help to explain some of the scatter observed.

Damage to the Pelvis and Femur -- Many of the tests involved loads above 10 kN, with only one resulting injury (test 80L103 resulted in a

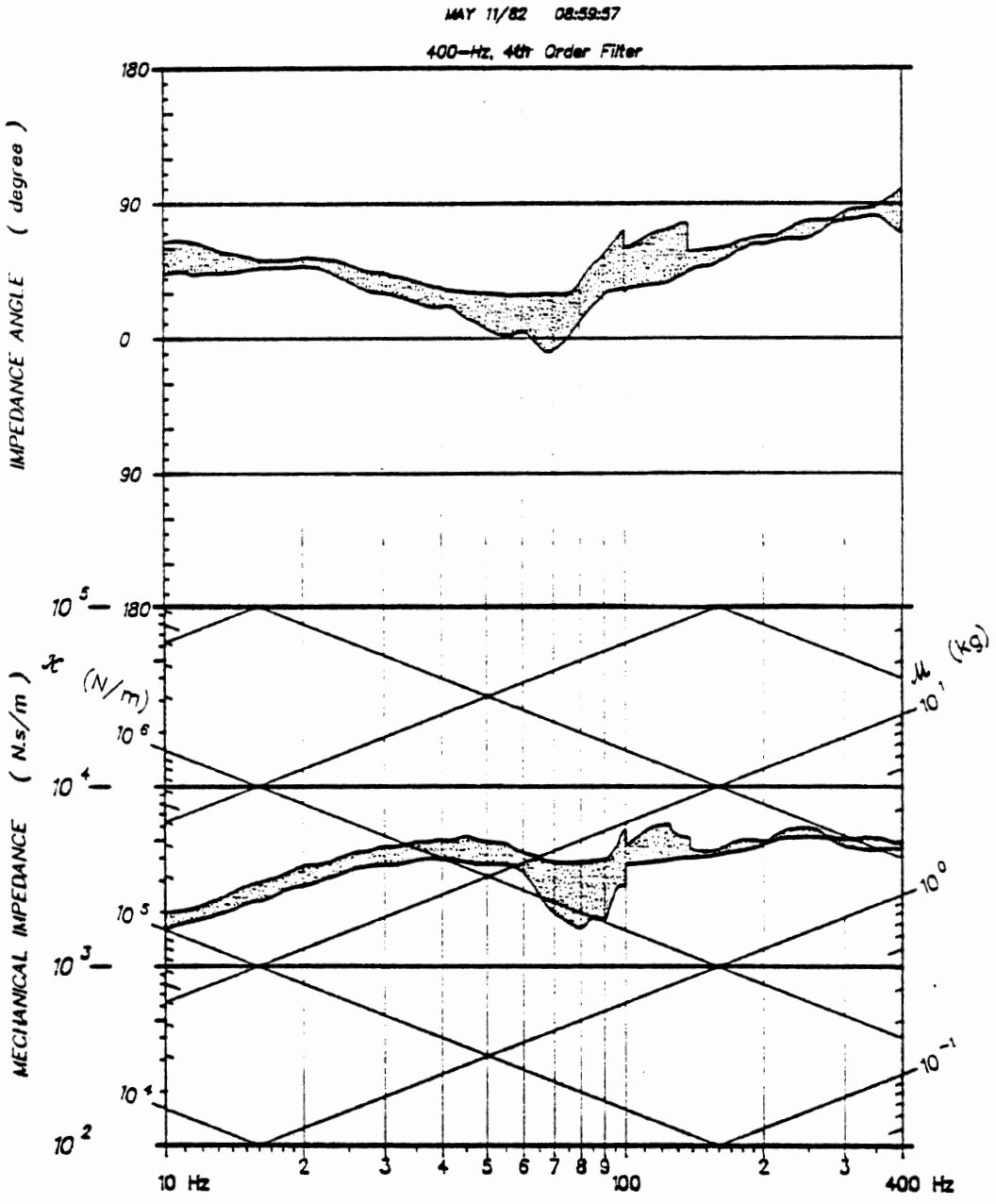

Fig. 10 - Corridor for pelvis impacts, 79A243-79A248

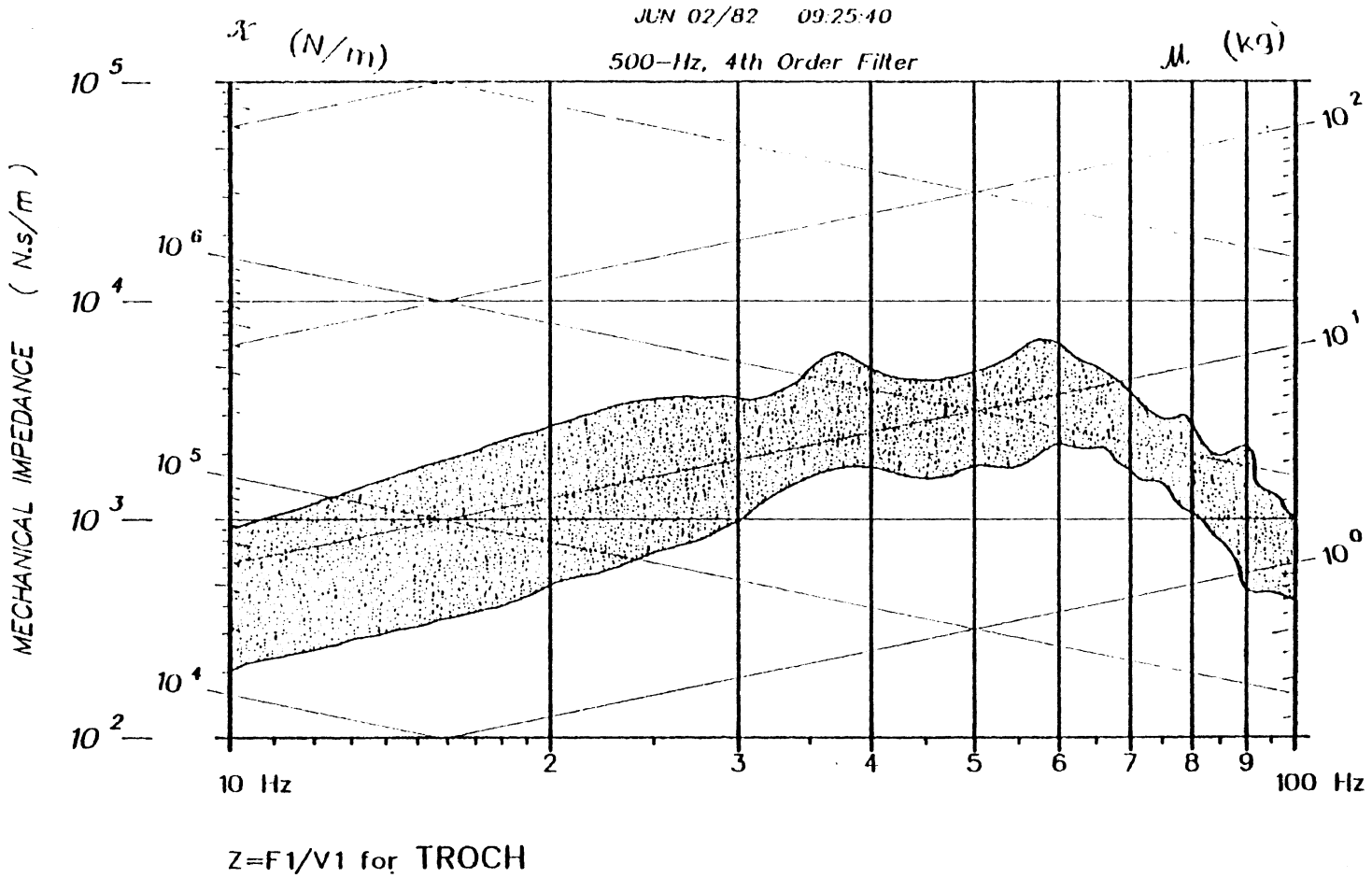

Fig. 11 - Trochanter corridor for axial knee impacts, 79L081-79L092

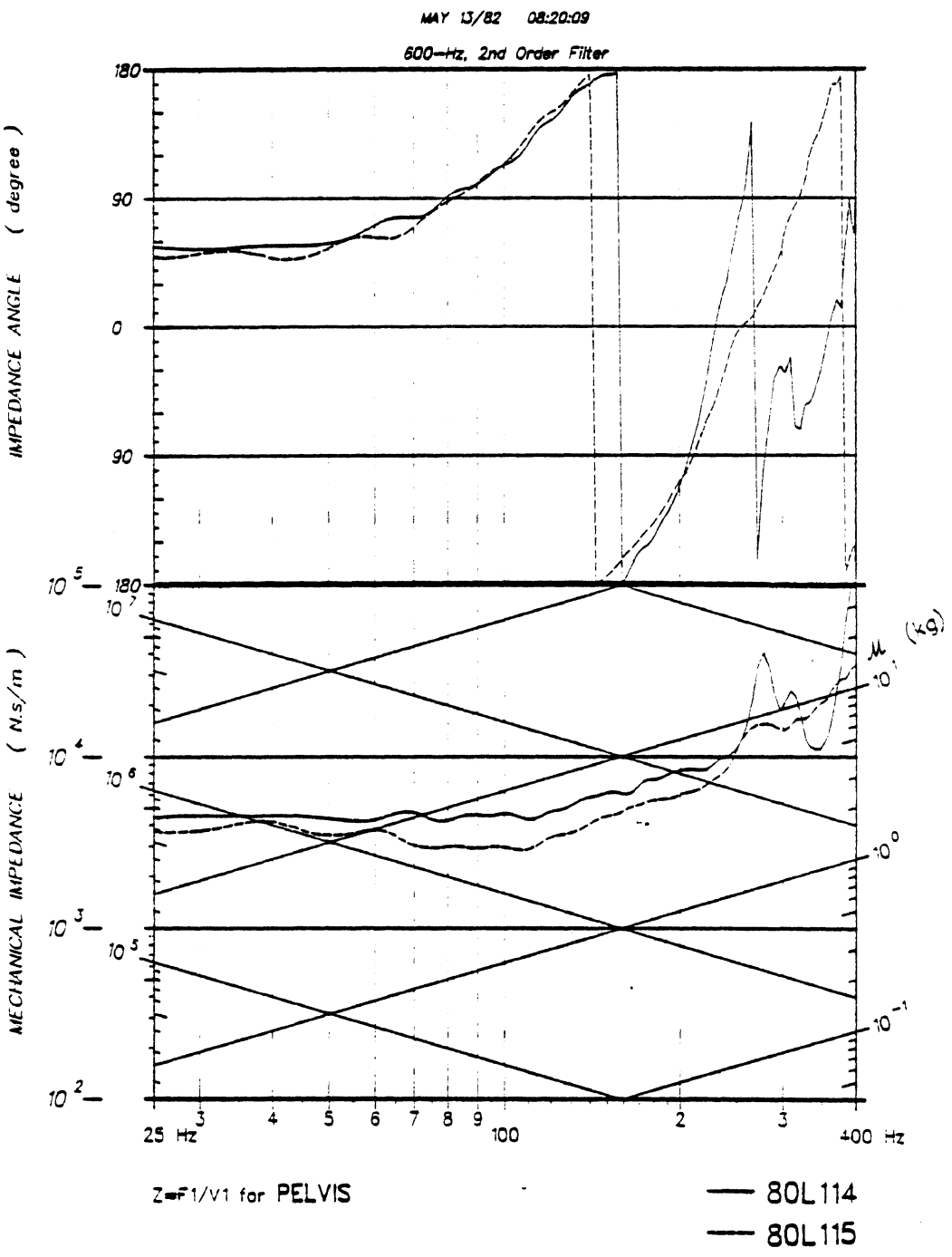
MAY 13/82 08:20:09
600-Hz, 2nd Order Filter
IMPEDANCE ANGLE (degree)
180
90
0
90
180
MECHANICAL IMPEDANCE (N.s/m)
10^6
10^5
10^4
10^3
10^2
10^7
10^6
10^5
M (kg)
10^1
10^0
10^{-1}
25 Hz
3
4
5
6
7
8
9
100
2
3
400 Hz
Z=F1/V1 for PELVIS
80L114
80L115

Fig. 12

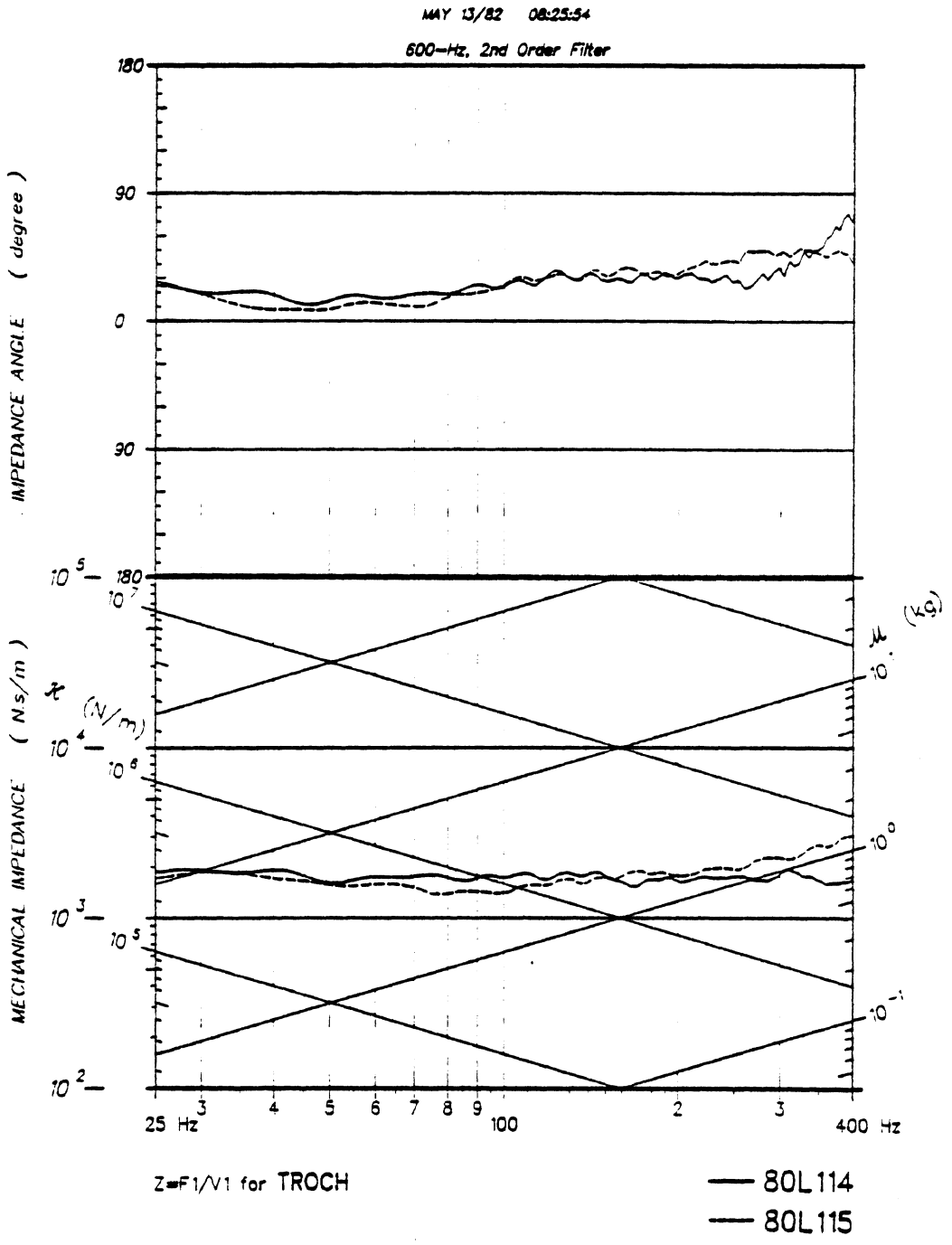
MAY 13/82 08:25:54
600-Hz, 2nd Order Filter
IMPEDANCE ANGLE (degree)
180
90
0
90
180
MECHANICAL IMPEDANCE (N s/m)
10^5
10^4
10^3
10^2
10^7
10^6
10^5
$\mathcal{K}$ (N/m)
$\mathcal{M}$ (kg)
10^0
25 Hz
3
4
5
6
7
8
9
100
2
3
400 Hz
Z=F1/V1 for TROCH
80L114
80L115

Fig. 13

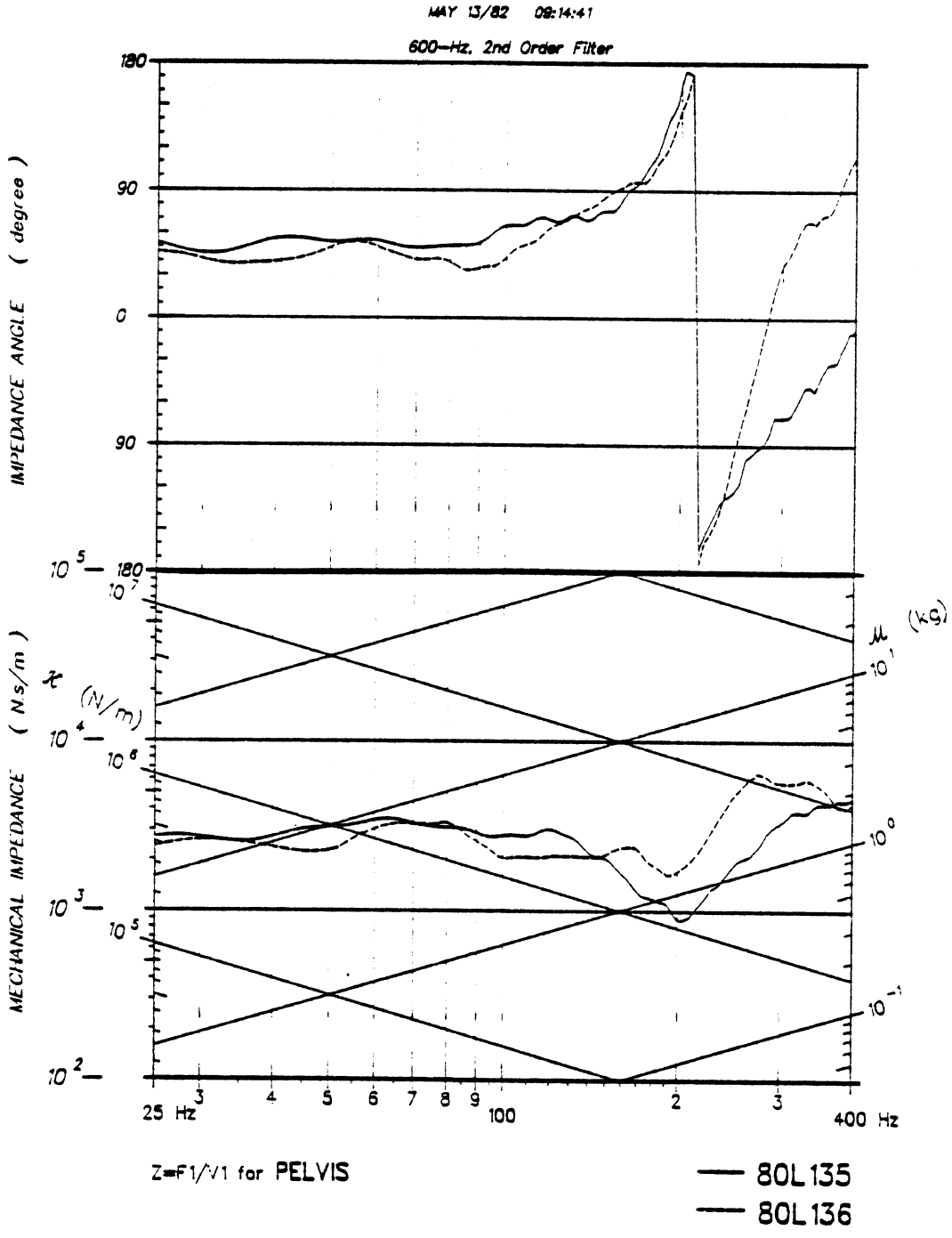
MAY 13/82 09:14:41
600-Hz, 2nd Order Filter
IMPEDANCE ANGLE (degree)
180
90
0
90
180
MECHANICAL IMPEDANCE (Ns/m)
k (N/m)
10^5
10^4
10^3
10^2
10^7
10^6
10^5
M (kg)
10^1
10^0
10^{-1}
25 Hz
3
4
5
6
7
8
9
100
2
3
400 Hz
Z=F1/V1 for PELVIS
80L135
80L136

Fig. 14

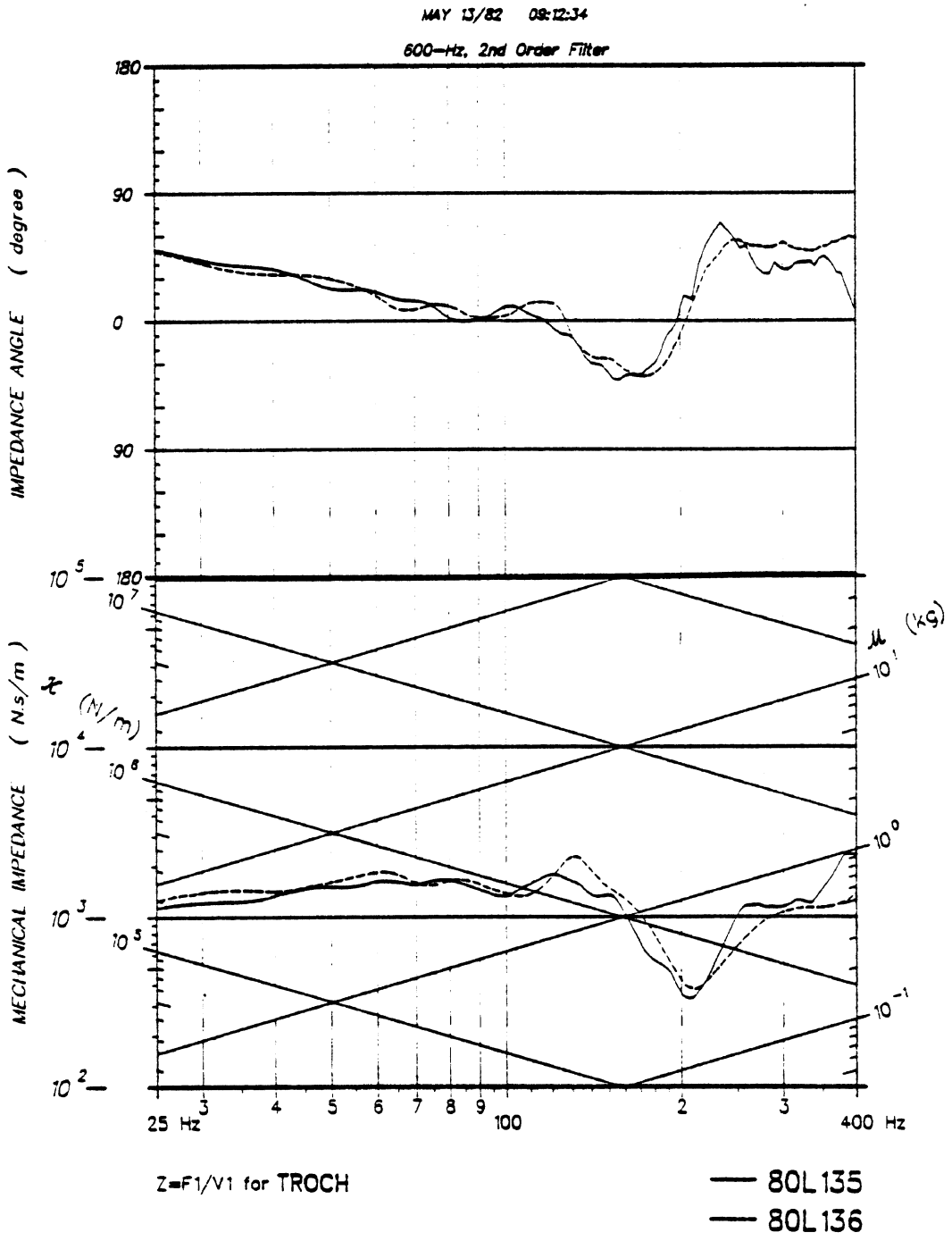
MAY 13/82 09:12:34
600-Hz, 2nd Order Filter
IMPEDANCE ANGLE (degree)
180
90
0
90
180
MECHANICAL IMPEDANCE (N.s/m)
10^5
10^4
10^3
10^2
10^7
10^6
10^5
(N/m)
M (kg)
10^1
10^0
10^-1
25 Hz
3
4
5
6
7
8
9
100
2
3
400 Hz
Z=F1/V1 for TROCH
80L135
80L136

Fig. 15

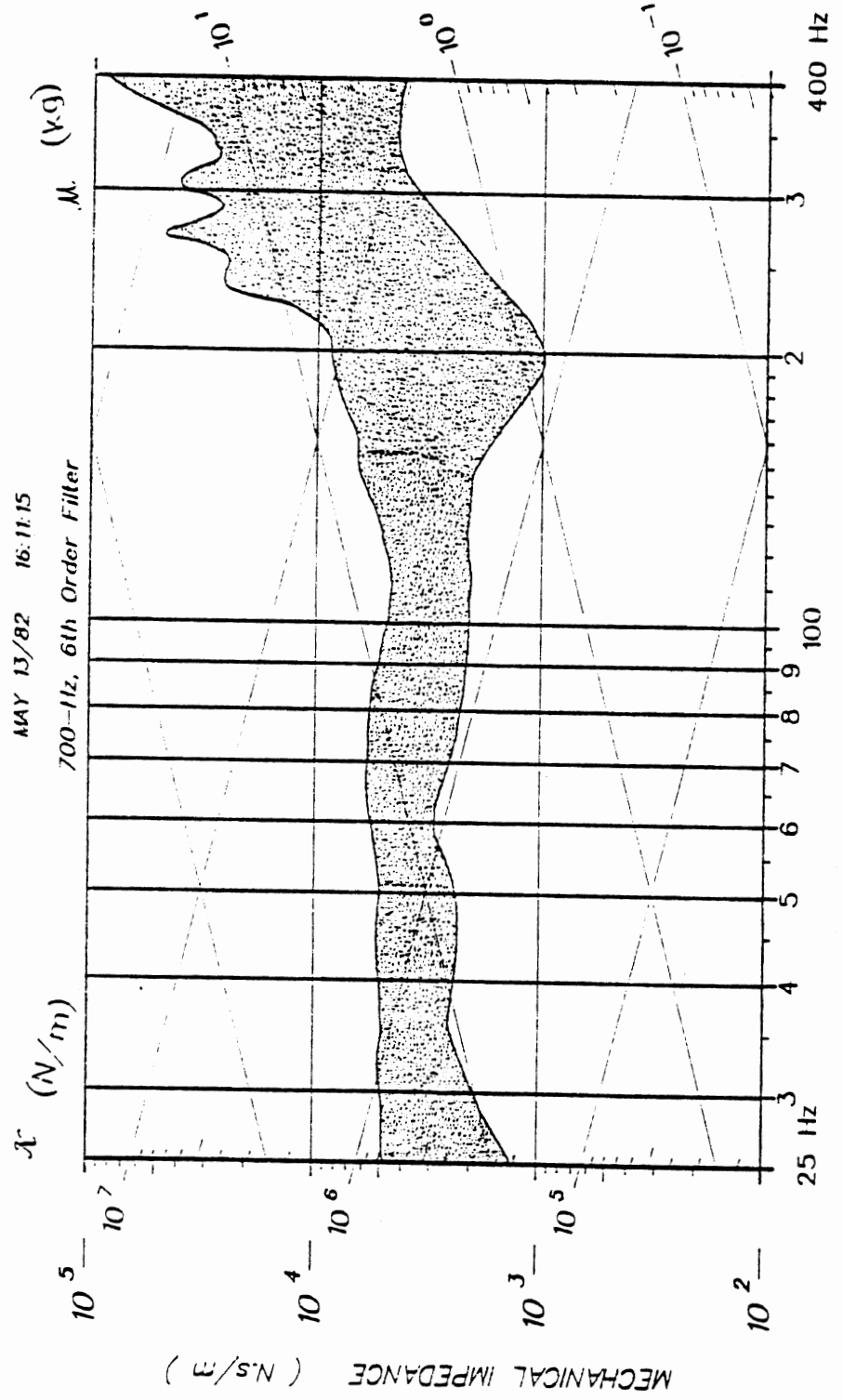

Fig. 16 – Pelvis corridor

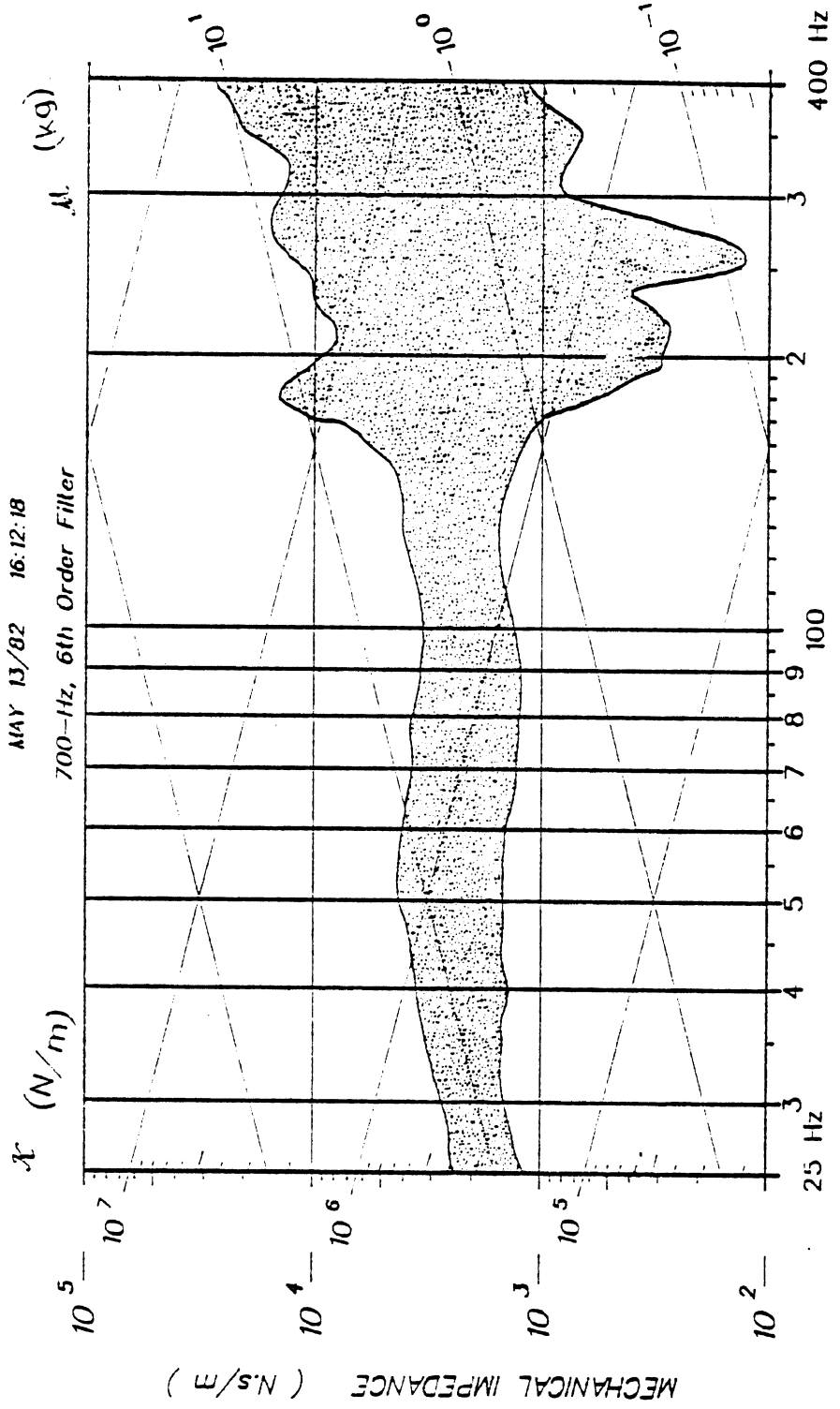

Fig. 17 – Trochanter corridor

commuted fracture of the femoral condyles). In this regard, tests 79A204 to 79A208, with loads from 20 to 37 kN, resulted in no injury to the femur or pelvis. Therefore, with respect to setting tolerance levels, the indication is that either much higher impact velocities (for a given mass) than have been used in these tests must be considered, or else other factors not addressed in this study influence the injury response of the pelvis. In these tests, the subject's initial configuration was held constant and the impactor padding, mass, and initial contact velocity were varied. Possibly, the tolerance level could be influenced by the orientation of the pelvis and/or femur before contact. In addition, no consideration was given to the interaction of the pelvis with a seat, which could be an important factor given the complexity of the pelvis response shown in this study. Therefore, the information generated in these knee impact tests cannot be used to set tolerance levels in and of themselves. The complex nature of the response and the scatter between test subjects emphasize the difficulty of this task.

LATERAL IMPACTS

The response of the pelvis under dynamic lateral loads requires the description of several material bodies: the impactor, the femur, the soft tissue and the pelvis. The ball and socket nature of the interface of the acetabulum and the head of the femur as well as the difficulty of impacting through the effective center of mass of the pelvis-femur complex suggest that in general an instability will result as asymmetric loading of the acetabulum occurs during impact. This type of interaction as well as the effects of damage produced during loading can lead to a wide range of responses. In this regard the accelerometer mounting platform, which is anchored to the pelvis through the use of lag bolts, may add to the lateral stiffness of the pelvis by reducing the differential movement between the two coxal bones during impact, and consequently simplifying the gross whole body motion of the pelvis. However, although the degree to which the acceleromter plate stiffens the pelvis is undetermined. No damage was observed as a result of the lag bolts indicating that the accelerometer platform was not a significant load path. The tests represented in Tables 6 and 9 describe the results of lateral acetabulum loadings through the trochanteric area. Only in test 80L121 was the pelvis loaded directly near the iliac crest. The force time-history from these tests can be described in a manner similar to that of tests 79A243 through 79A248 (Table 5) and 79L081 through 79L090 (Table 7) using the same event markers. The peak forces for the tests ranged from 3 to 19 kN with durations from 30 to 50 ms.

Table 6 summarizes the three-dimensional motion for the pelvis of 82E008, 82E028, and 82E049. In these tests the direction, magnitude, phasing, and waveform of the motion descriptors obtained from the nine accelerometer analysis did not follow a consistent pattern. These differences occur primarily in both angular acceleration and linear accelerations in those directions perpendicular to the impactor motion. Examples are Figures 18 and 19 for 82E049, and Figures 20 and 21 for 82E028. Both the linear and angular variables differ significantly during the E1 to E2 interval even though the gross overall motion as obtained from both the nine accelerometer analysis and the high-speed movies are the same. Variables representing this trend are the relative magnitude and phasing of the resultant and principal direction acceleration for tests 80L095 to 80L137 (depicted in Table 9), with no clear relation between peak force and acceleration as well as when it will occur in the force time history. This is consistent with the results from the acceleration data presented in (10). Figure 22 depicts some of the waveforms observed in these tests.

The response of the pelvis to impact is complicated not only by dynamic instabilities of the femur-pelvis complex, but also by the variability between subjects. Since load is distributed to the pelvis through both soft tissue and the femur, variations in these physical aspects between subjects can lead to varied stress levels on the acetabulum for a given impact force. For those subjects with large amounts of soft tissue, a longer E1 to E2 interval was observed.

Because of the complex nature of the response of the pelvis to lateral impacts, it becomes difficult to generate a transfer function for these experiments. However, for some tests in which a triax was used a transfer function could be obtained that generated mechanical impedance values significantly less than those calculated for the two directions normal to the principal direction above 10 Hz. In addition a transfer function was generated from the tangental acceleration for those tests in which the nine accelerometer plate was used (Figure 23). The transfer function shows that in these tests for low frequencies (from 10 to 40 Hz) the pelvis behaves as a mass of about 25 kg indicating that the gross overall motion of the pelvis may be simply modeled.

Damage -- The pelvic bone damages observed in these tests are similar to those observed in the automotive environment as reported in (1-5):

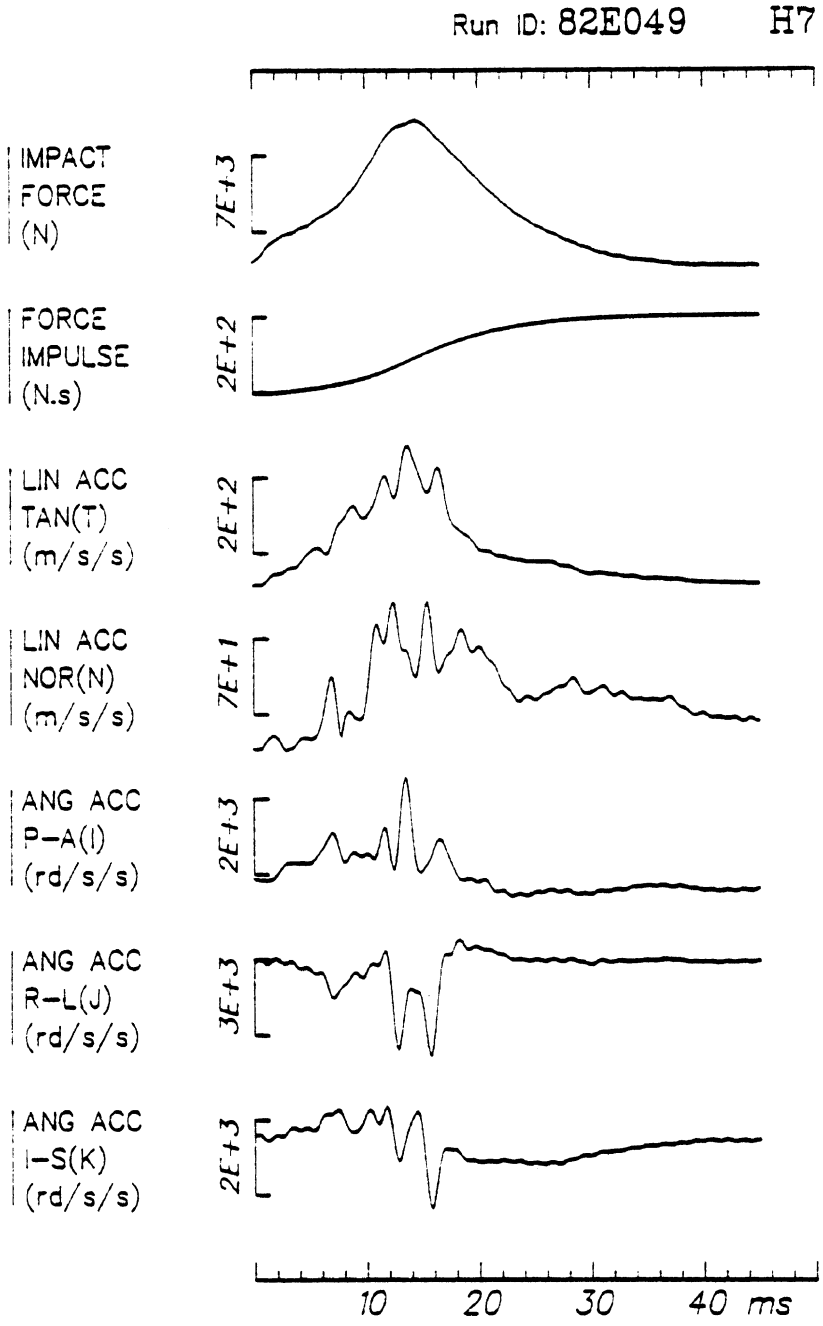

Fig. 18 - Test 82E049

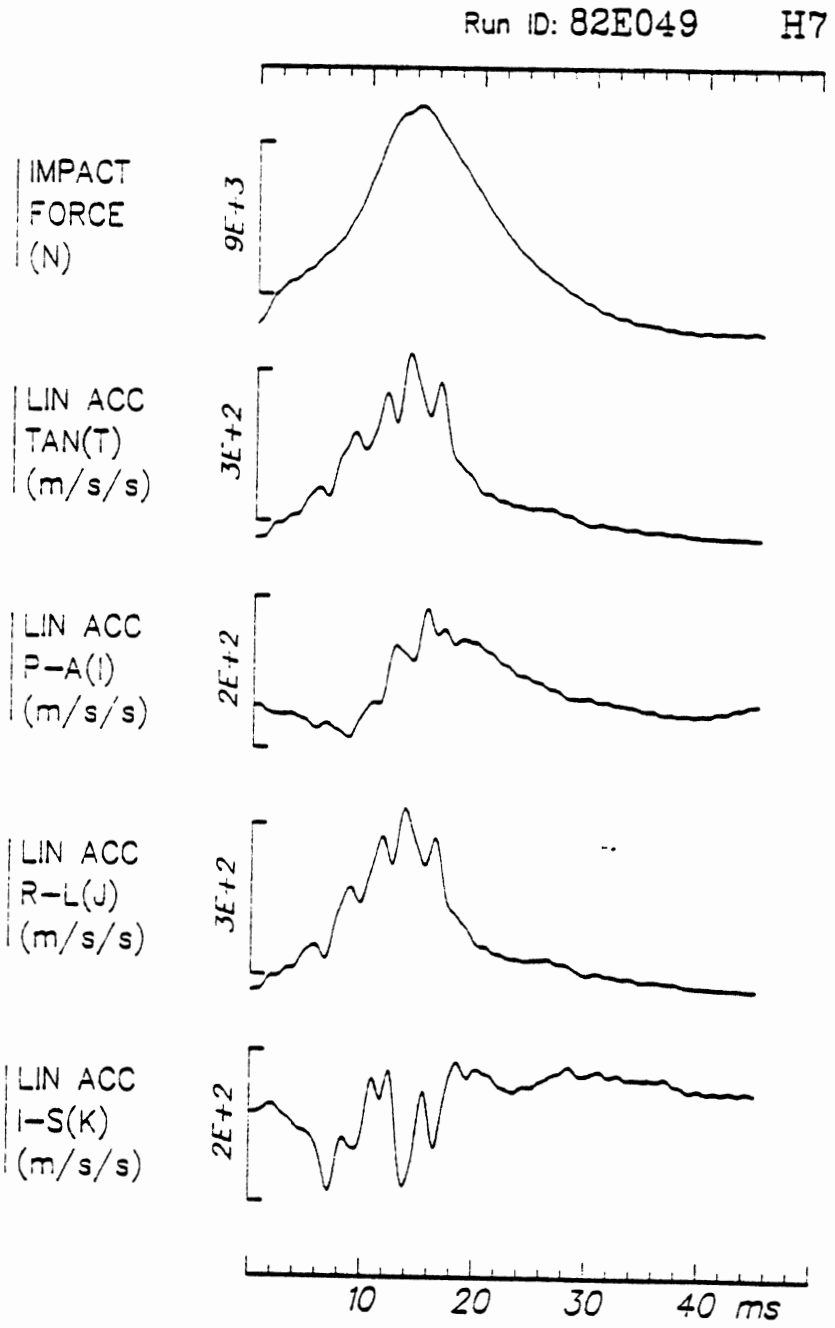

Fig. 19 - Test 82E049

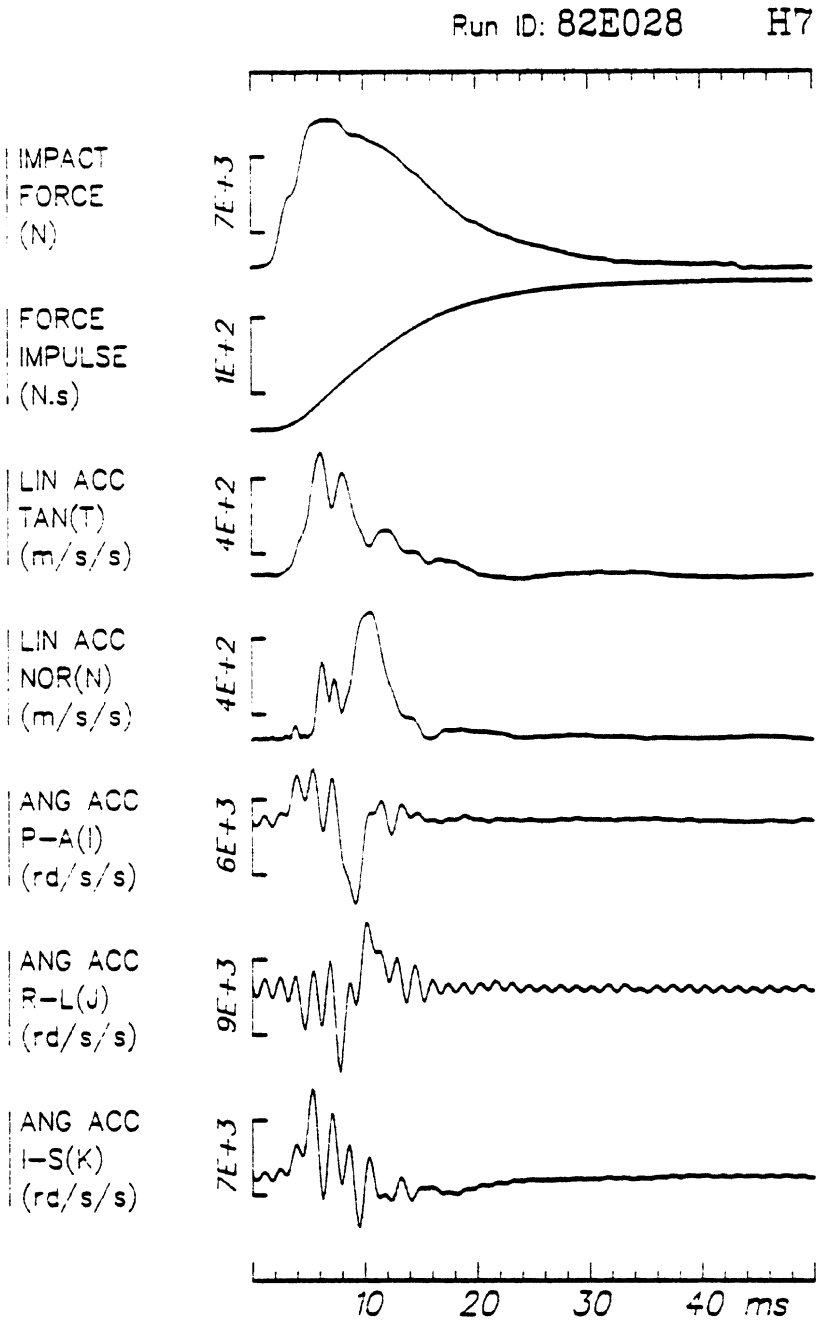

Fig. 20 - Test 82E028

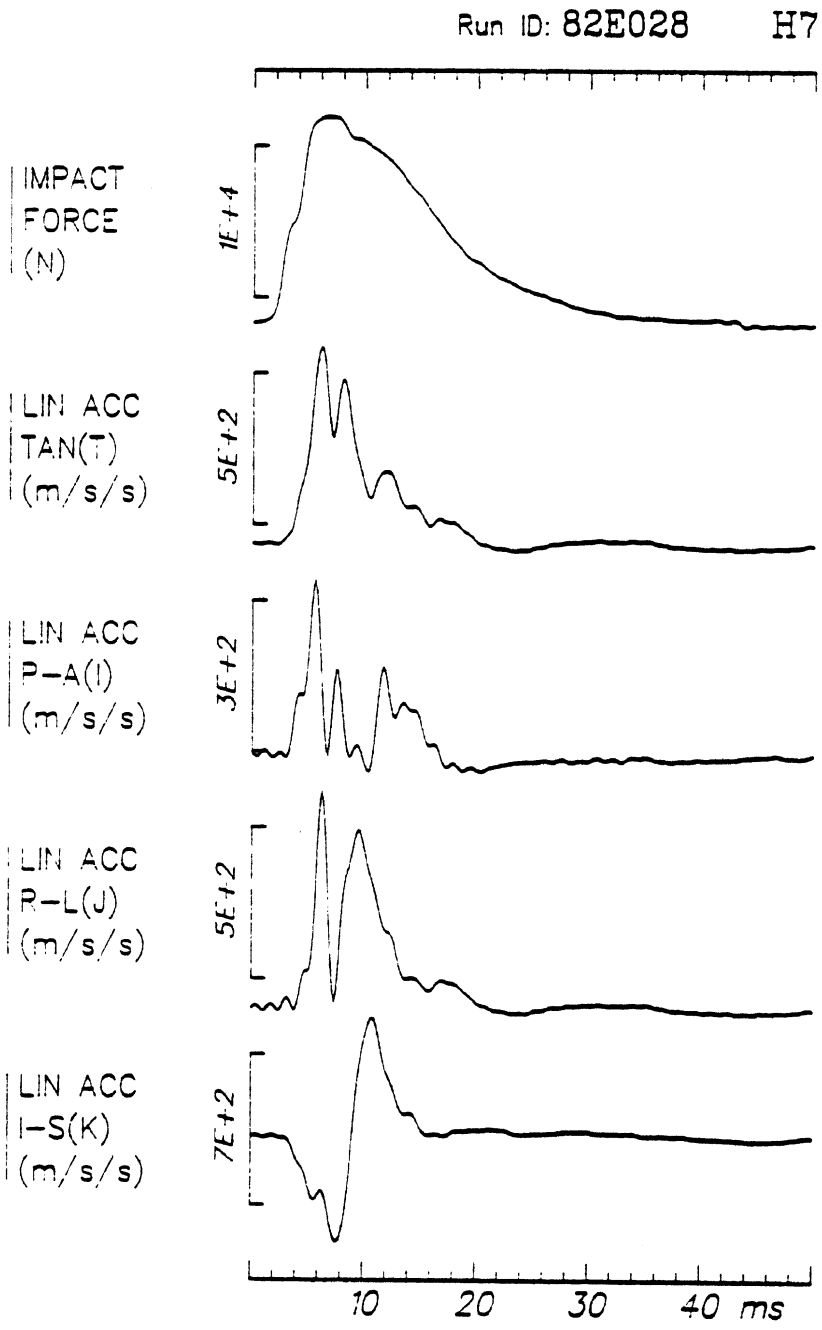

Fig. 21 - Test 82E028

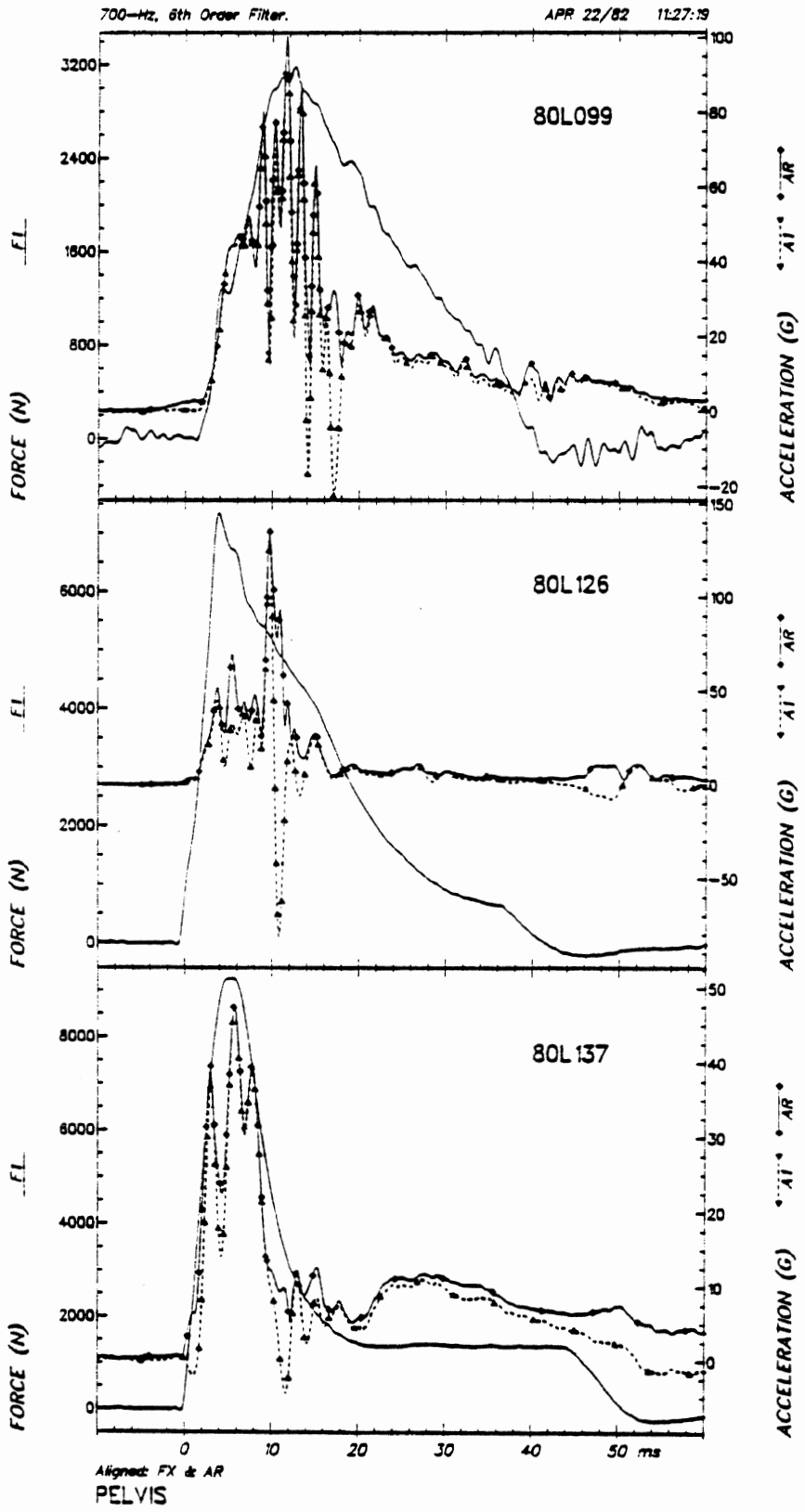

Fig. 22 - Pelvis impact response

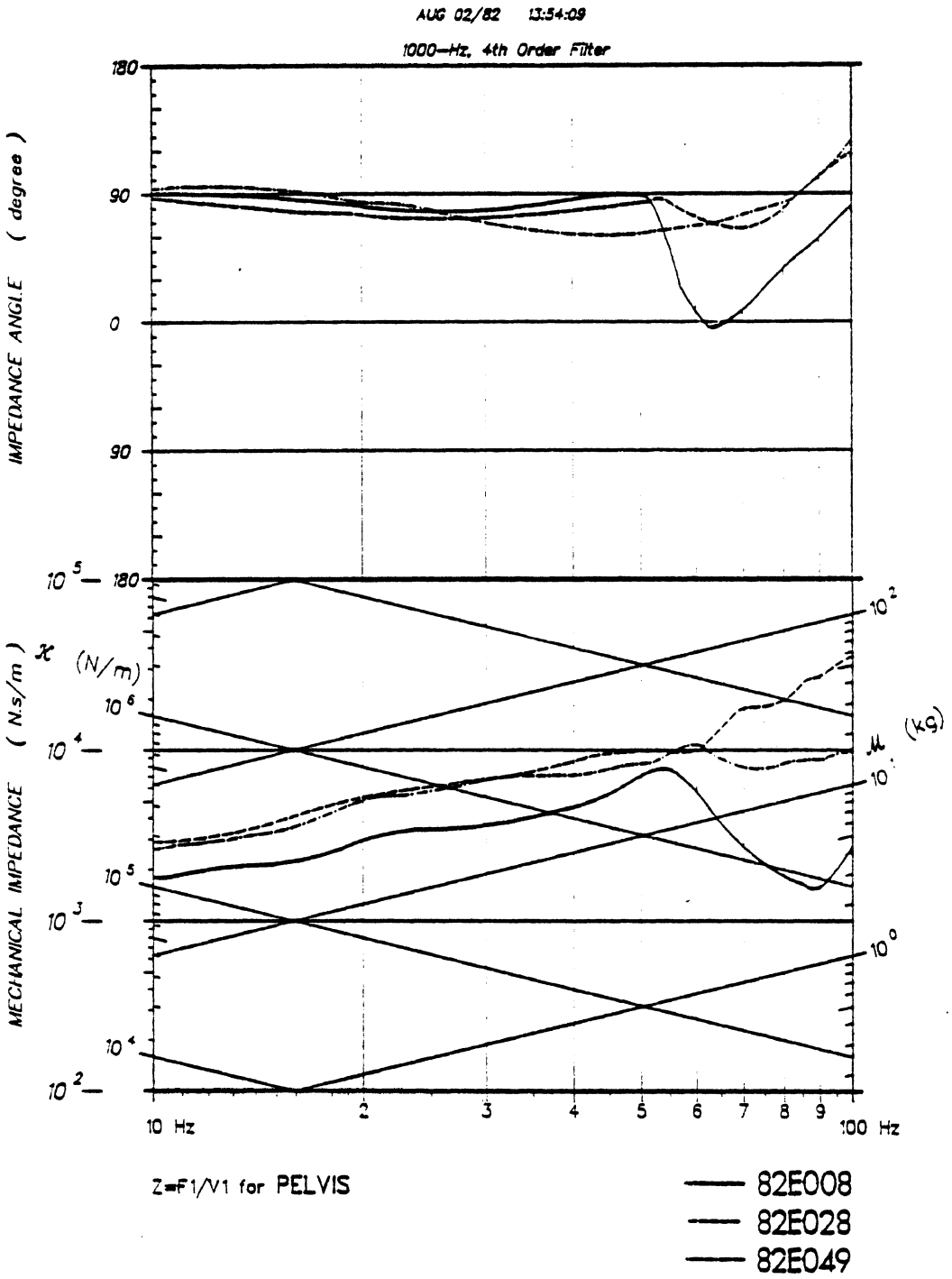
AUG 02/82 13:54:09
1000—Hz, 4th Order Filter
IMPEDANCE ANGLE (degree)
180
90
0
90
180
MECHANICAL IMPEDANCE (N.s/m)
10^5
10^4
10^3
10^2
$\mathcal{K}$ (N/m)
10^6
10^5
10^4
10^2
M (kg)
10^1
10^0
10 Hz
2
3
4
5
6
7
8
9
100 Hz
Z=F1/V1 for PELVIS
82E008
82E028
82E049

Fig. 23

however, no bilateral fractures occurred. The complex nature of the response of the pelvis to lateral loads may preclude the determination of a single tolerance criterion. This is arrived at by comparing the results in Tables 4 and 9 as well as the above discussion. In this regard, peak force does not relate to the damage produced. This is believed to be a result of the interactions of the padding, impactor surface shape, and/or the soft tissue between the impactor and the pelvis. With additional padding and soft tissue the load can be distributed over a larger area of the pelvis, and therefore less of the available impact energy is concentrated on the acetabulum. The maximum force tolerable seems to increase with an increase in load-distributing padding for similar available impact energy.

Based on differences in the initial conditions of the tests performed at HSRI and those described in (10), it is not readily verifiable that peak force and impulse are accurate pelvis injury criteria. The test methods described in (10) employed a subject seated in an upright position and impacted by an unpadded 17.3 kg impactor with a hemispherical surface. It was found in this series of tests performed at HSRI (which employed an unconstrained subject and flat impactor surface) that variations in impactor padding, mass, and load path may result in large differences in the peak force and impulse of the impact which do not necessarily correspond to the injuries produced. Additional test parameters, such as subject configuration, also affect comparisons between test series results in an unknown manner. For example, the fact that in one research program the subject is seated in a fixed position may result in subject-seat interactions thus producing different injuries for an otherwise similar impact.

CONCLUSIONS

This has been a limited preliminary study of some important kinematic factors and damage modes associated with indirect loading of the pelvis through the femur.

Because of the complex nature of the pelvis-femur interaction during an impact event, more work is necessary before these kinematic factors can be generalized to describe pelvis response. However, the following conclusions can be drawn:

(1) The complete description of three-dimensional motion is invaluable to the understanding of pelvis response.

(2) The response of the pelvis of a single test subject to axial knee impacts as given by mechanical impedance is linear from 10 to 100 Hz, repeatable, and symmetric (the same for each side).

(3) The complex nature of the response of the femur/pelvis/soft tissue system, between-subjects variability, and damage patterns produced may preclude the determination of a single tolerance criterion such as maximum force or peak acceleration response.

(4) Energy-absorbing and load-distributing materials are effective methods of transmitting greater amounts of energy to the pelvis without damage being produced in lateral impacts.

(5) The nature of the impactor/femur/pelvis interaction as well as the biometrics of the population at large are critical factors in understanding the response of the pelvis to impact and subsequent damage patterns.

ACKNOWLEDGEMENTS

The results presented in this paper have been obtained from a series of independently funded research programs conducted during the past five years. The funding agencies were: The Biomedical Science Department of General Motors, the Motor Vehicle Manufacturer's Association, and the United States Department of Transportation, National Highway Traffic Safety Administration.

The authors wish to acknowledge the contributions of Jean Brindamour, Don Huelke, Marv Dunlap, Jodi Blank, Valerie Moses, Paula Lux, Miles Janicki, Jeff Pinsky, and Carol Sobecki in completion of this work.

REFERENCES

1) States, J., and States, D., "The Pathology and Pathogenesis of Injuries Caused by Lateral Impact Accidents", Proceedings of the Twelfth Stapp Car Crash Conference, Society of Automotive Engineers, Inc., 1968.

2) Ryan, F., "Traffic Injuries of the Pelvis at St. Vincent's Hospital, Melbourne", Medical Journal of Australia, Vol. 1, 27 Feb. 1971.

3) Knudsen, P., "Pelvis Fraktur Ved Sidekollision" Ugeskrift for Lager, Vol. 143, No. 16, 13 April 1981.

4) Huelke, D., and Lawson, T., "Lower Torso Injuries and Automobile Seatbelts", SAE Paper 760370, 1976.

5) Huelke, D.F., O'Day, J., States, J.D., and Lawson, T.E. "Lower extremity injuries in automobile crashes." HSRI, Jan. 1980, 65 p. Report No. UM-HSRI-80-10. Sponsored by the National Highway Traffic Safety Administration.

6) Evans, F., and Lissner, H., "Studies on Pelvic Deformations and Fractures", Anatomical Record, Vol. 121, No. 2, Feb. 1955.

7) Patrick, L., Kroell, C., and Mertz, H., "Forces on the Human Body in Simulated Crashes", Proceedings of the Ninth Stapp Car Crash Conference, 1965.

8) Melvin, J., and Nusholtz, G., "Tolerance and Response of the Knee-Femur-Pelvis Complex to Axial Impacts", Final Report to the Motor Vehicle Manufacturer's Association, UM-HSRI-80-27, June 1980.

9) Ramet, M., and Cesari, D., "Experimental Study of Pelvis Tolerance in Lateral Impact", International IRCOBI Conference on the Biomechanics of Trauma, 4th Proceedings, Bron, 1979.

10) Cesari, D., Ramet, M., and Clair, P., "Evaluation of Pelvic Fracture Tolerance in Side Impact", Proceedings of the Twenty-Fourth Stapp Car Crash Conference, Paper No. 801306, Society of Automotive Engineers, Inc., 1980.

11) Bartz, J., and Butler, F., "Passenger Compartment With Six Degrees of Freedom", Auxiliary Programs to "Three Dimensional Computer Simulation of a Motor Vehicle Crash Victim", Final Technical Report on DOT Contract No. FH-11-7592, 1972.

12) Alem, N., et al., "Whole-Body Human Surrogate Response to Three-Point Harness Restraint", Proceedings of the Twenty-Second Stapp Car Crash Conference, Paper No. 780895, Society of Automotive Engineers, Inc., 1978.

13) Nusholtz, G., Melvin, J., and Alem, N., "Head Impact Response Comparisons of Human Surrogates", Proceedings of the Twenty-Third Stapp Car Crash Conference, Paper No. 780895, Society of Automotive Engineers, Inc., 1979.

14) Nusholtz, G., et al., "Response of the Cervical Spine to Superior-Inferior Head Impact", Proceedings of the Twenty-Fifth Stapp Car Crash Conference, Paper No. 811005, Society of Automotive Engineers, Inc., 1981.

15) Hixson, E., "Mechanical Impedance", Shock and Vibration Handbook, ed. C. M. Harris and C. E. Crede, McGraw-Hill Book Co., New York, 1976.

16) Khalil, T., Viano, D., and Taber, L., "Vibrational Characteristics of the Embalmed Human Femur", General Motors Research Laboratories, Publication #GMR-3270 29 Apr., 1980.

17) Melvin, J., et al., "Impact Response and Tolerance of the Lower Extremities", Proceedings of the Nineteenth Stapp Car Crash Conference, Society of Automotive Engineers, Inc., 1975.

APPENDIX C: Reference Frames and Head Impact Motion

REFERENCE FRAMES AND HEAD IMPACT MOTION

Guy S. Nusholtz
Nabih M. Alem
John W. Melvin
Richard L. Stalnaker

Biomechanics Department
Highway Safety Research Institute
University of Michigan

INTRODUCTION

The description of the impact response of the human body and its surrogates requires that the kinematic quantities measured experimentally be described in reference frames which vary from one instrumentation method to another.

In order to assure precise comparison of mechanical responses between subjects, it is necessary to refer all results to a "standard" anatomical frame which may be easily identified. On the other hand, it is impractical to require that transducers be aligned with this anatomical frame, since this would create problems which may not be satisfactorily solved.

An alternative is to mount transducers in an arbitrary and convenient reference frame, then describe the transformation necessary to convert the data from this frame to the desired anatomical one (1)*.

We now have three reference frames in which to describe the kinematic quantities: the instrumentation frame, the anatomical frame and the inertial (or laboratory) frame. An additional method for describing the kinematic quantities of a test is that of frame fields. One such frame field, introduced by Frenet in 1847 and independently by Serret in 1851, has been adopted for use in head motion analysis at HSRI.

INSTRUMENTATION REFERENCE FRAME

The method used at HSRI to measure the 3-D motion of the head employs nine accelerometers mounted on the head in three clusters. Each cluster is a triaxial unit which measures the components of the acceleration vector at its center in three orthogonal directions, which are the same for the other two clusters. These orthogonal instrumentation directions are arbitrarily chosen for convenience of mounting and are such that the centers Q1, Q2 and Q3 of the three triaxial clusters will lie on the axes $\hat{E}1$, $\hat{E}2$, and $\hat{E}3$ of the instrumentation frame, at known distances, R1, R2 and R3 from the origin P, as shown in Figure 1.

Given the coordinates of the origin P, and those of two points

* Number in parentheses indicate reference at end of paper.

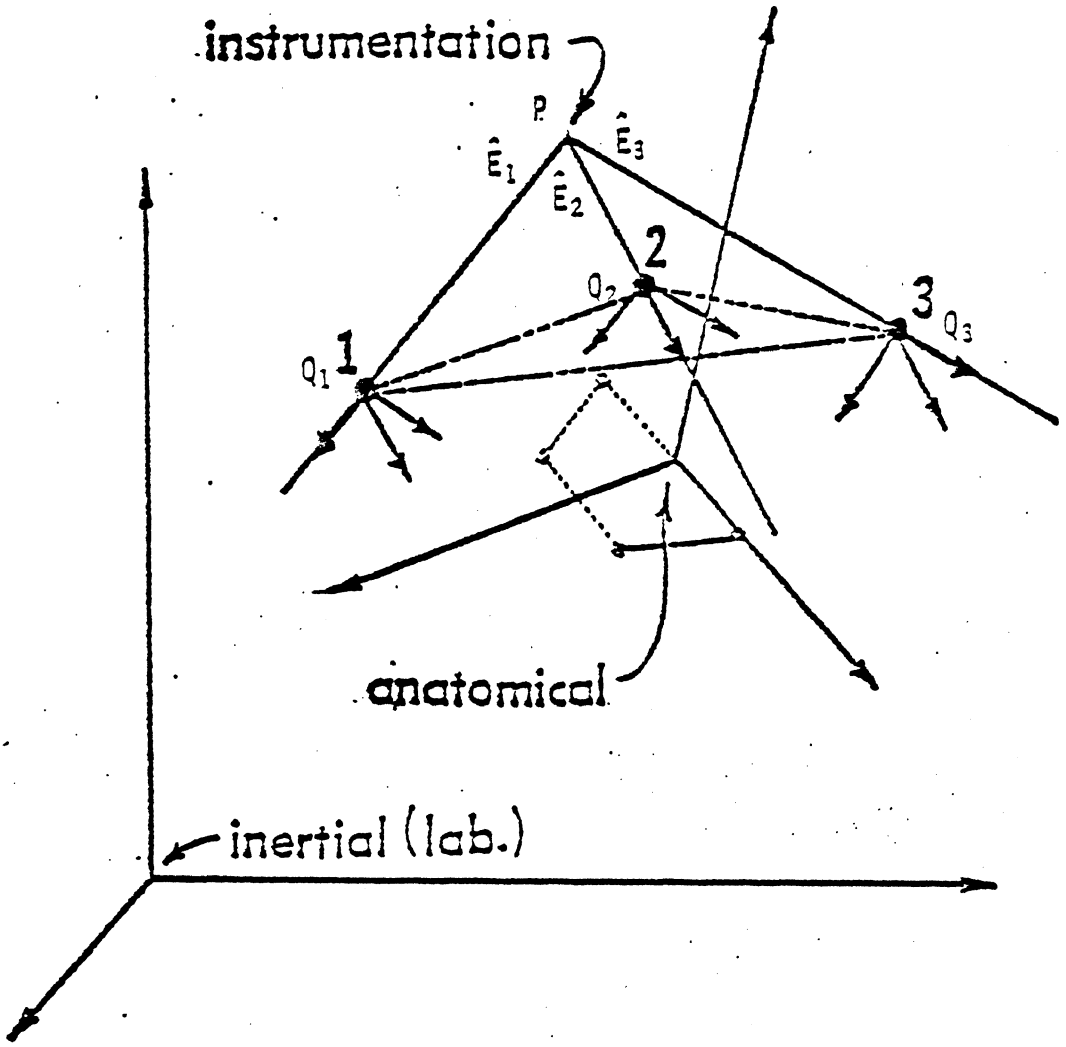

FIGURE 1. INSTRUMENTATION REFERENCE FRAME, AND THE LOCATION OF THE THREE TRIAXIAL ACCELEROMETERS FOR THE ESRI 3-D MOTION MEASUREMENT.

Q1 and Q2, the unit vectors $\hat{E}1$ and $\hat{E}2$ are determined by normalizing the distances PQ1 and PQ2. The third unit vector $\hat{E}3$ is then obtained by cross-multiplying $\hat{E}1$ by $\hat{E}2$. However, it is experimentally more practical to supply the coordinates of all three points Q1, Q2 and Q3, as well as the distances from them to the origin P, then compute the coordinates of other points necessary to define the instrumentation frame completely in the 3-D space.

The anatomical $\hat{i}$-axis is defined along the intersection of the Frankfort and midsagittal planes in the posterior-to-anterior (P-A) direction. The $\hat{j}$-axis is defined along the line joining the two superior edges of the auditory meati, in the right-to-left (R-L) direction. This $\hat{j}$-axis, which lies in the Frankfort plane, is perpendicular to the midsagittal plane at the "anatomical center," which is taken as the origin of the anatomical frame (Figure 2). Finally, the $\hat{k}$-axis is defined as the cross-product of the unit vectors of $\hat{i}$- and $\hat{j}$-axes, and therefore, will lie in the midsagittal plane perpendicular to the Frankfort plane, and will be in the inferior-to-superior (I-S) direction.

Thus, the anatomical reference frame ($\hat{i}$, $\hat{j}$, $\hat{k}$) can be completely defined once the four anatomical landmarks are specified.

LABORATORY REFERENCE FRAME

It is desired to describe the instrumentation ($\hat{E}1$, $\hat{E}2$, $\hat{E}3$) in terms of the anatomical ($\hat{i}$, $\hat{j}$, $\hat{k}$) unit vectors:

$$\begin{pmatrix} \hat{E}1 \\ \hat{E}2 \\ \hat{E}3 \end{pmatrix} = [E] \begin{pmatrix} \hat{i} \\ \hat{j} \\ \hat{k} \end{pmatrix} \qquad (1)$$

where [E] is an orthogonal transformation matrix made up with the nine unknown direction cosines. This matrix may be determined by first expressing each of the ($\hat{E}1$, $\hat{E}2$, $\hat{E}3$) and ($\hat{i}$, $\hat{j}$, $\hat{k}$) in terms of an arbitrary frame ($\hat{I}$, $\hat{J}$, $\hat{K}$):

$$\begin{pmatrix} \hat{E}1 \\ \hat{E}2 \\ \hat{E}3 \end{pmatrix} = [U] \begin{pmatrix} \hat{I} \\ \hat{J} \\ \hat{K} \end{pmatrix} \quad \text{and} \quad \begin{pmatrix} \hat{i} \\ \hat{j} \\ \hat{k} \end{pmatrix} = (V) \begin{pmatrix} \hat{I} \\ \hat{J} \\ \hat{K} \end{pmatrix} \qquad (2)$$

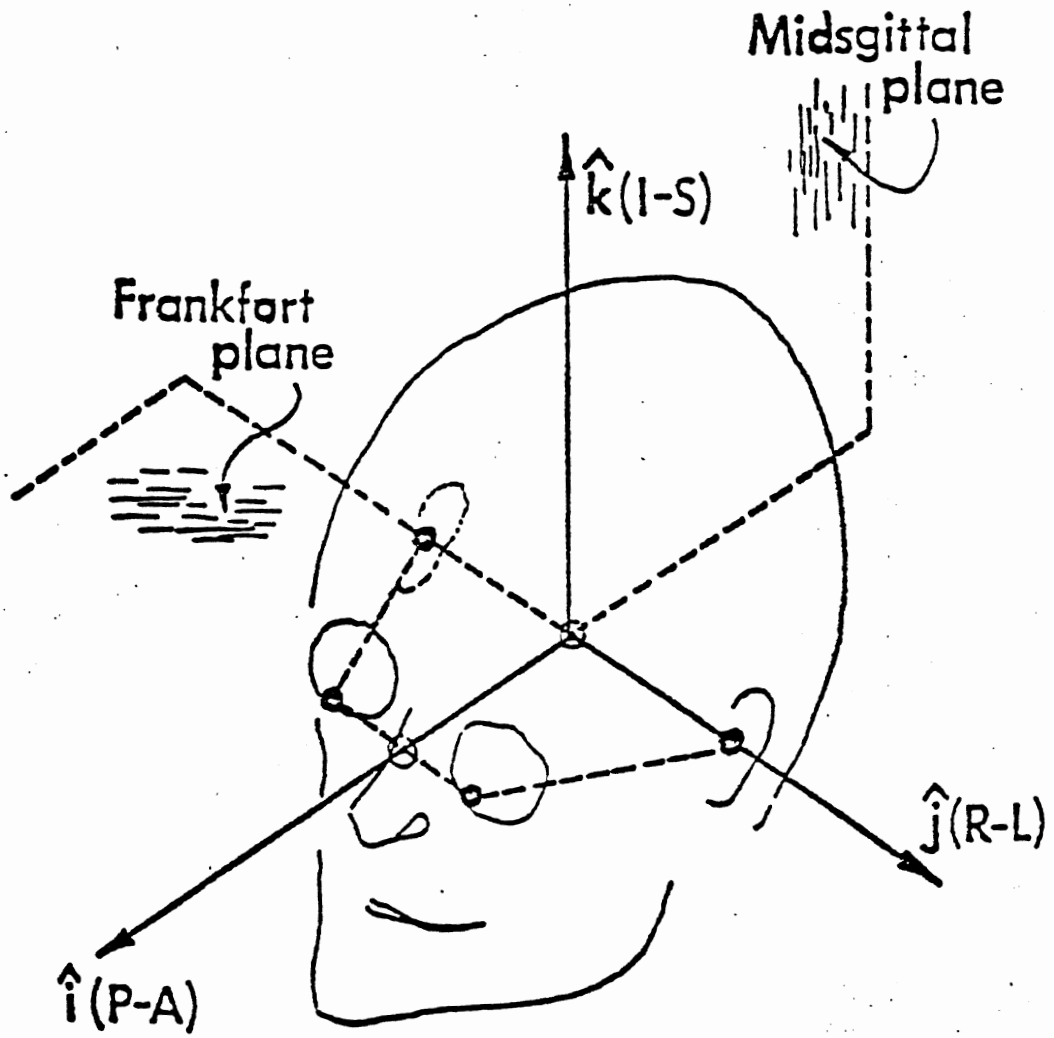

FIGURE 2. HEAD ANATOMICAL REFERENCE SYSTEM, BASED ON THE SKULL'S FRANKFORT AND MIDSAGITTAL PLANES.

then eliminating the ($\hat{I}$, $\hat{J}$, $\hat{K}$) between the two expressions to obtain the matrix [E]:

$$[E] = [U] \quad [V]^{-1} \tag{3}$$

Since [U] and [V] are determined from coordinates of several points, the arbitrary frame ($\hat{I}$, $\hat{J}$, $\hat{K}$) will simply be the laboratory frame in which these coordinates are measured. The x-ray method used at HSRI to measure these points automatically defines the laboratory frame.

FRENET SERRET TRIAD

For any moving point, such as the anatomical center of the head, the absolute position, velocity and acceleration vectors are given in the laboratory reference frame as:

$$\vec{R} = x(t)\,\hat{I} + y(t)\,\hat{J} + z(t)\,\hat{K}$$

$$\dot{\vec{R}} = \dot{x}(t)\,\hat{I} + \dot{y}(t)\,\hat{J} + \dot{z}(t)\,\hat{K} \tag{4}$$

$$\ddot{\vec{R}} = \ddot{x}(t)\,\hat{I} + \ddot{y}(t)\,\hat{J} + \ddot{z}(t)\,\hat{K}$$

As the point moves in space, it travels along a curve defined by x(t), y(t) and z(t). This curve may be thought of as a skewed "one-way track" which is fixed in the laboratory ($\hat{I}$, $\hat{J}$, $\hat{K}$) reference frame.

The distance traveled along the curve is a function of time, s(t). This function determines the position of any point on the curve, and the tangent to the curve at this point is defined as a unit vector:

$$\hat{T} = \frac{d\vec{R}}{ds} \tag{5}$$

but since $\dot{\vec{R}} = \frac{d\vec{R}}{dt}$

then

$$\dot{\vec{R}} = \frac{d\vec{R}}{ds} \cdot \frac{ds}{dt} = \frac{ds}{dt}\,\hat{T} = v(t)\,\hat{T} \qquad (6)$$

The quantity $v(t)$ is called the speed of the point, and is equal to the derivative of $s(t)$ with respect to time. It is clear that $v(t)$ is precisely the resultant of the velocity vector, i.e.,

$$v(t) = \sqrt{\dot{x}^2 + \dot{y}^2 + \dot{z}^2} \qquad (7)$$

Since the derivative of a vector is normal to the vector, the principle normal of the curve is defined as:

$$\hat{N} = \frac{1}{\kappa}\frac{d\hat{T}}{ds}, \quad \kappa \geq 0 \qquad (8)$$

where $\hat{N}$ is perpendicular to $\hat{T}$ and κ chosen so that $\hat{N}$ is a unit vector. Finally,, the cross product $\hat{T} \times \hat{N}$ defines a third vector, perpendicular to both the tangent and principal normal, and is called the binormal:

$$\hat{B} = \hat{T} \times \hat{N}. \qquad (9)$$

Any line perpendicular to the tangent $\hat{T}$ is called a normal line and the plane containing all the normal lines is called the normal plane. The plane containing both the tangent $\hat{T}$ and principle normal $\hat{N}$ is called the osculating plane.

The three orthogonal unit vectors ($\hat{T}$, $\hat{N}$, $\hat{B}$) shown in figure 3 form a right-hand triad, called the Frenet triad. As the rigid body moves in 3-D space, each body point moves along a space curve; ; therefore, each point of the rigid body leaves behind a unique track characterized by individual Frenet triads attached to that curve. For a given curve the collection of its triads is often called a "field," which is stationary in 3-D space.

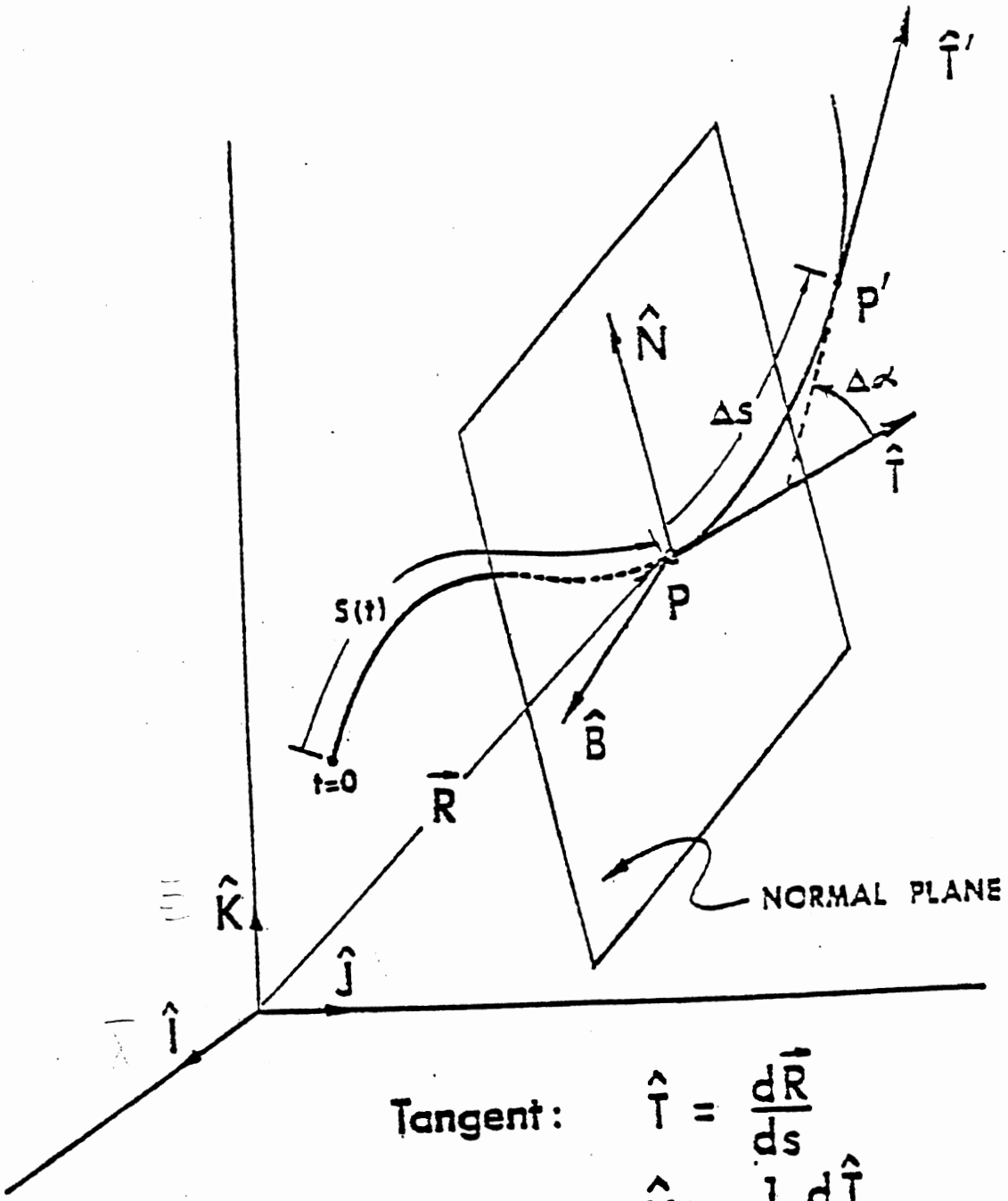

$$\text{Tangent:} \quad \hat{T} = \frac{d\vec{R}}{ds}$$

$$\text{Normal:} \quad \hat{N} = \frac{1}{K}\frac{d\hat{T}}{ds}$$

$$\text{Binormal:} \quad \hat{B} = \hat{T} \times \hat{N}$$

FIGURE 3. FRENET SERRET TRIAD

CURVATURE AND TORSION OF A CURVE

It is often useful to study, in 3-D space, the turning and twisting of the curve of a point on a rigid body. For head motion, one such point is the anatomical center. The Frenet formulas provide mathematical measurements of the turning and twisting, when the inertial components of the position, velocity and acceleration vectors of the point of interest are given.

Let P be a point on a given curve and P' a neighboring point shown in Figure 3, such that:

$$\text{arc}\,(P, P') = \Delta S \tag{10}$$

and let $\vec{T}$ and $\vec{T}'$ be the tangent vectors to the curve at P and P', respectively, such that the angle between $\vec{T}$ and $\vec{T}'$ is:

$$(\vec{T}, \vec{T}') = \Delta\alpha \tag{11}$$

The definition of a derivative of $\vec{T}$ is given by:

$$\frac{d\vec{T}}{ds} = \lim_{\Delta S \to 0} \frac{\Delta\alpha}{\Delta S} \tag{12}$$

and that of the normal unit vector $\hat{N}$ is given by

$$\hat{N} = \frac{1}{\kappa}\frac{d\hat{T}}{ds} \ . \tag{13}$$

But $\hat{N}$ is a unit vector, κ must be the resultant (absolute value) of the tangent, so that

$$\kappa = \left| \frac{d\vec{T}}{ds} \right| \cdot \lim_{\Delta S \to 0} \frac{\Delta\alpha}{\Delta S} \ . \tag{14}$$

Therefore, as P approaches P', the above limit is defined as the <u>curvature</u> of the curve at point P . The <u>radius of curvature</u> ρ is defined as the inverse of κ:

$$\rho = \frac{1}{\kappa} = \left| \frac{ds}{d\theta} \right| \tag{15}$$

$$\frac{d^2R}{ds^2} = \frac{d\hat{T}}{ds} = \kappa\hat{N} = \frac{1}{\rho}\hat{N} \tag{16}$$

A slow turn of the curve is characterized by a small curvature

(or large radiuso), while large curvature (small ρ) indicates a sharp turn of the curve. A numerical value of the curvature κ is therefore extremely useful in quantitatively describing the sharpness of the turns in the curve of interest.

In order to calculate the curvature κ, consider the velocity vector of a point along the curve,

$$\dot{\vec{R}} = \frac{d\vec{R}}{dt} = \frac{ds}{dt}\,\hat{T} \tag{17}$$

The acceleration vector may be obtained by differentiating $\dot{\vec{R}}$:

$$\ddot{\vec{R}} = \frac{d\dot{\vec{R}}}{dt} = \frac{ds}{dt}\cdot\frac{d\hat{T}}{dt} + \frac{d^2s}{dt}\,\hat{T} \tag{18}$$

but

$$\frac{d\hat{T}}{dt} = \frac{d\hat{T}}{ds}\cdot\frac{ds}{dt} = \kappa\hat{N}\cdot\frac{ds}{dT} = \kappa v\hat{N} \tag{19}$$

so that

$$\ddot{\vec{R}} = \kappa\left(\frac{ds}{dt}\right)^2\hat{N} + \frac{d^2s}{dt}\,\hat{T} = \kappa v^2\hat{N} + (\ddot{\vec{R}}\cdot\hat{T})\hat{T} \tag{20}$$

Thus, the acceleration vector may be resolved into two orthogonal components, one along the tangent (called tangential acceleration) and one along the principal normal (called the normal acceleration). By cross multiplying the above equation by the unit $\hat{T}$ vector, we have:

$$\hat{T}\times\ddot{\vec{R}} = \kappa\left(\frac{ds}{dt}\right)^2\hat{T}\times\hat{N} \tag{21}$$

but since $\hat{T}$ and $\ddot{\vec{R}}$ are defined by the components of the absolute velocity and acceleration vector, it is possible to express all terms in the above equation as functions of $(\dot{x}, \dot{y}, \dot{z})$ and $(\ddot{x}, \ddot{y}, \ddot{z})$ to obtain the curvature κ:

$$\kappa = \frac{\|\hat{T}\times\ddot{\vec{R}}\|}{v^2} = \frac{\|\dot{\vec{R}}\times\ddot{\vec{R}}\|}{v^3} \tag{22}$$

Next, we turn our attention to the binormal vector $\hat{B}$ defined earlier. The derivative of $\hat{B}$ with respect to s may be shown to be:

$$\frac{d\hat{B}}{ds} = \frac{d}{ds}(\hat{T} \times \hat{N}) = \hat{T} \times \frac{d\hat{N}}{ds} \tag{23}$$

Thus, in addition to being perpendicular to $\hat{B}$, the derivative is also perpendicular to $\hat{T}$ and, subsequently, must be along the normal direction $\hat{N}$, i.e.,

$$\frac{d\hat{B}}{ds} = -\tau\hat{N} \tag{24}$$

where τ is called the <u>torsion</u> of the curve, and may be either positive or negative. The radius of torsion λ is defined as the inverse of the torsion τ, and, in a manner similar to the curvature, may be shown to be

$$\lambda = \frac{1}{\tau} = \frac{ds}{d\beta} = \lim_{\Delta s \to 0} \frac{\Delta s}{\Delta\beta} \tag{25}$$

where $\Delta\beta$ is the angle between two adjacent binormals to the curve at two points separated by Δs.

It is possible to show that the torsion τ may be calculated from the velocity $\dot{\vec{R}}(\dot{x}, \dot{y}, \dot{z})$ accelaration $\ddot{\vec{R}}(\ddot{x}, \ddot{y}, \ddot{z})$ and jerk $\dddot{\vec{R}}(\dddot{x}, \dddot{y}, \dddot{z})$ vectors first by forming the mixed (triple) product

$$m = (\dot{\vec{R}}, \ddot{\vec{R}}) \cdot \dddot{\vec{R}} = -\frac{1}{e^2}\left(\frac{ds}{d\tau}\right)^6 \tau \tag{26}$$

so that τ is calculated by

$$\tau = \frac{(\dot{\vec{R}} \times \ddot{\vec{R}}) \cdot \dddot{\vec{R}}}{||\dot{\vec{R}} \times \ddot{\vec{R}}||^2} \tag{27}$$

Finally, we turn our attention to the normal vector, the derivative of $\hat{N}$ with respect to s may be shown to be

$$\frac{d\hat{N}}{ds} = -\frac{d\hat{B} \times \hat{T}}{ds} = \frac{d\hat{B}}{ds} \times \hat{T} + \hat{B} \times \frac{d\hat{T}}{ds} = -\kappa\hat{T} + \tau\hat{B} \tag{28}$$

Collecting the three formulas for $\frac{d\hat{T}}{ds}$, $\frac{d\hat{N}}{ds}$, $\frac{d\hat{B}}{ds}$ we obtain the following equations (Frenet equations):

$$\begin{pmatrix} \frac{d\hat{T}}{ds} \\ \frac{d\hat{N}}{ds} \\ \frac{d\hat{B}}{ds} \end{pmatrix} = \begin{bmatrix} 0 & \kappa & 0 \\ -\kappa & 0 & \tau \\ 0 & -\tau & 0 \end{bmatrix} \begin{pmatrix} \hat{T} \\ \hat{N} \\ \hat{B} \end{pmatrix} \tag{29}$$

and

$$\begin{pmatrix} \frac{d\hat{T}}{dt} = \frac{d\hat{T}}{ds}\frac{ds}{dt} \\ \frac{d\hat{N}}{dt} = \frac{d\hat{N}}{ds}\frac{ds}{dt} \\ \frac{d\hat{B}}{dt} = \frac{d\hat{B}}{ds}\frac{ds}{dt} \end{pmatrix} = \begin{bmatrix} 0 & \kappa v & 0 \\ -\kappa v & 0 & \tau v \\ 0 & -\tau v & 0 \end{bmatrix} \begin{pmatrix} \hat{T} \\ \hat{N} \\ \hat{B} \end{pmatrix} \tag{30}$$

Examination of equation (30) shows that κv and τv can be interpreted as components of the angular velocity (ω) of the triad as it moves along the curve; in fact setting

$$\omega = \tau v \hat{T} + \kappa v \hat{B} \tag{31}$$

the frenet equation becomes:

$$\begin{aligned} \frac{d\hat{T}}{dt} &= \omega \times \hat{T} \\ \frac{d\hat{N}}{dt} &= \omega \times \hat{N} \\ \frac{d\hat{B}}{dt} &= \omega \times \hat{B} \end{aligned} \tag{32}$$

The vector ω is sometimes called the Darboux vector after the inventor of this interpretation of the meaning of curvature and torsion. The equation (32) states that the torsion measures the rate at which the osculating plane turns about the tangent vector to the curve while the curvature measures the rate at which the normal plane turns about the binormal vector.

EXAMPLES OF HEAD RIGID BODY MOTION DUE TO DIRECT IMPACT

In principle, every geometric problem involving motion along a curved path can be solved by means of the Frenet formulas. For simple cases, it may be sufficient to record the acceleration data and express it in a convenient form.

For example, the following can be shown to be true:

Geometrical Quantity	Motion of a Point
$\kappa = 0$	straight line
$\kappa > 0, \tau = 0$	planar
$\kappa > 0, \kappa = \text{constant } \tau = 0$	circular

The use of the Frenet frame field can be an important tool in understanding the curve of the head as a rigid body as it moves through space. Some examples of the way this frame field can be used follow. These examples come from a series of direct head impacts in which the subject was positioned in front of the HSRI pneumatic cannon with the head surface to be impacted approximately normal to the cannon impacting surface, and the centerline of the impact approximately through the head center of gravity (2).

Padded rear impact

Examination of the tangential and normal component in Figure 4 shows that during impact the anatomical center's motion is essentially a straight line until near the end of impact. At this point not only does it move off the line of impact (normal acceleration) but there is also a negative acceleration along the tangent, indicating a force acting on the skull other than that caused by the impactor.

Rigid impact

Figure 5 shows a rigid impact in which the skull was fractured (depression under the impactor). The skull is loaded very rapidly. The force then drops, during which the tangent acceleration drops to zero; the normal acceleration increases rapidly, indicating that the large unfractured portion of the skull is not in complete contact with the impactor and that the only acceleration is from the change in $\hat{T}$. This short-lived change of $\hat{T}$ (rotation) ends when the impactor comes in complete contact with the skull, as evidenced by a rapid increase of the angular velocity. Once the unfractured portion of the skull is back in complete contact with the impactor, the angular velocity drops and the tangential acceleration increases.

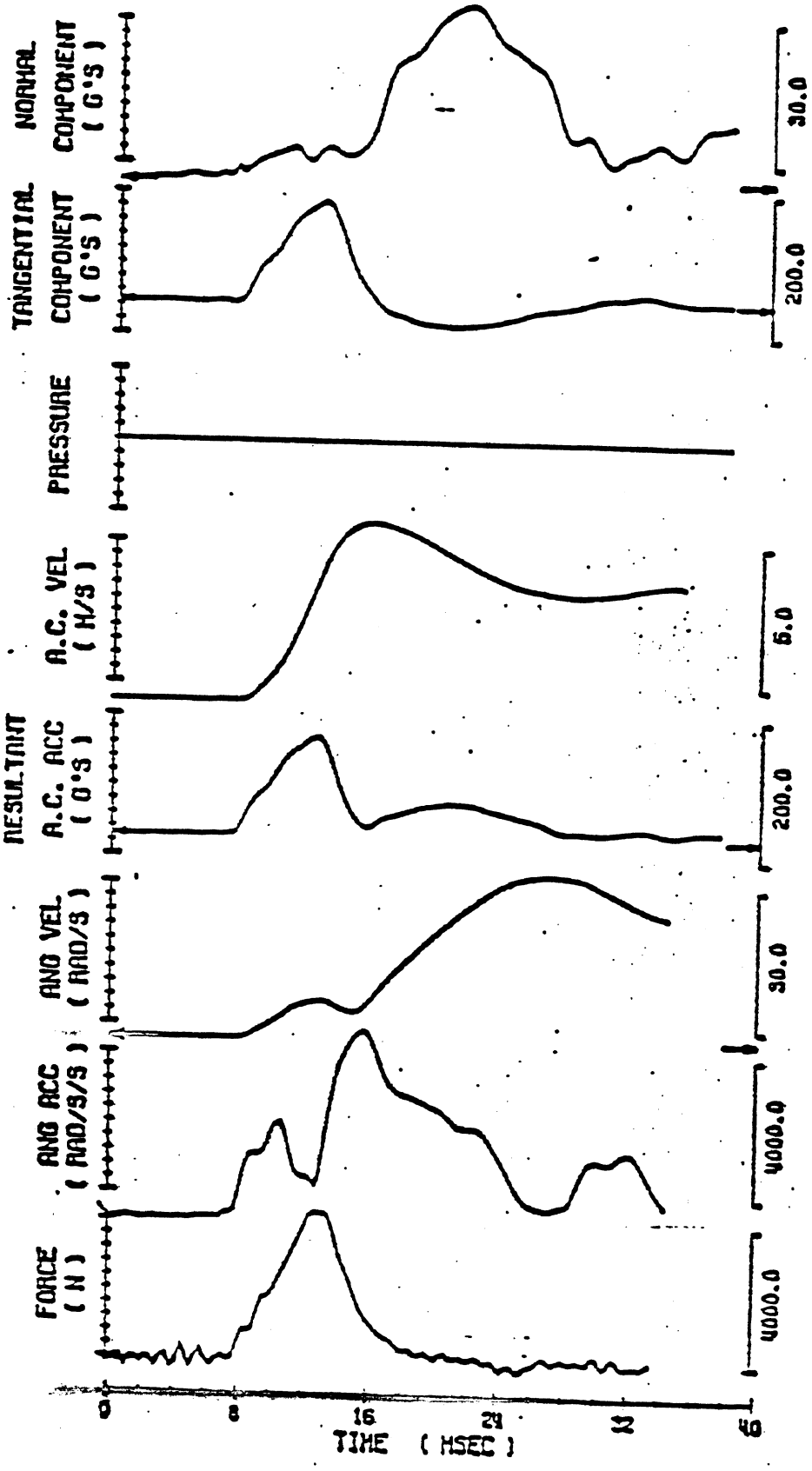

Figure 4 DATA SUMMARY SHEET OF 76A135

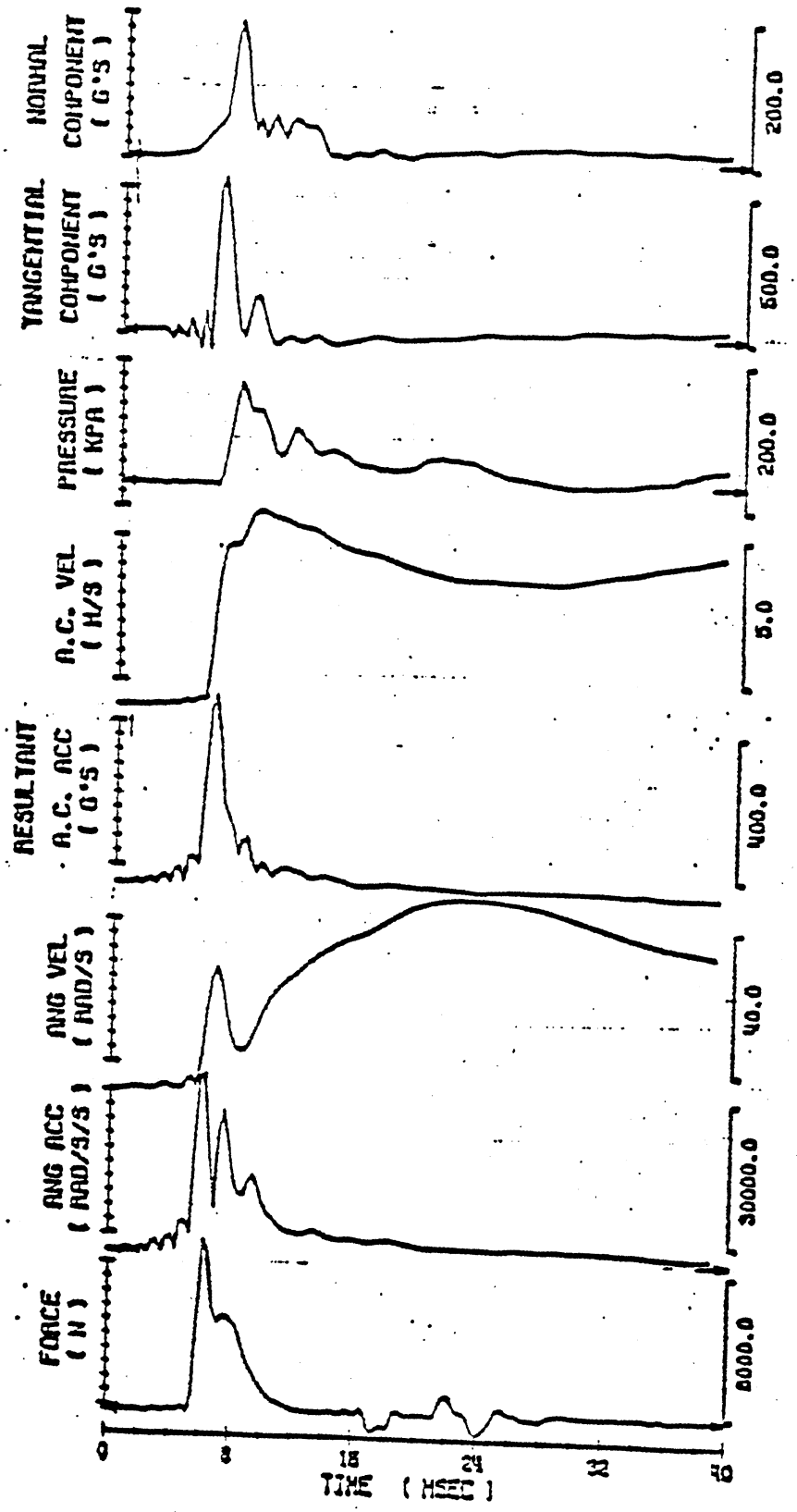

Figure 5 DATA SUMMARY SHEET OF 76A145

REFERENCES

1. Thomas, D. J., Robbins, D. H., Eppinger, R. H., King, A. I., and Hubbard, R. P., "Guidelines for the comparison of human and human analogue biomechanical data," A report of an ad hoc committee, Ann Arbor, Michigan, December 6, 1974.

2. R. L. Stalnaker, J. W. Melvin, G. S. Nusholtz, N. M. Alem, J. B. Benson, "Head Impact Response." Proceedings of the 21st Stapp Car Crash Conference, 1977.

APPENDIX D: Force Time Histories

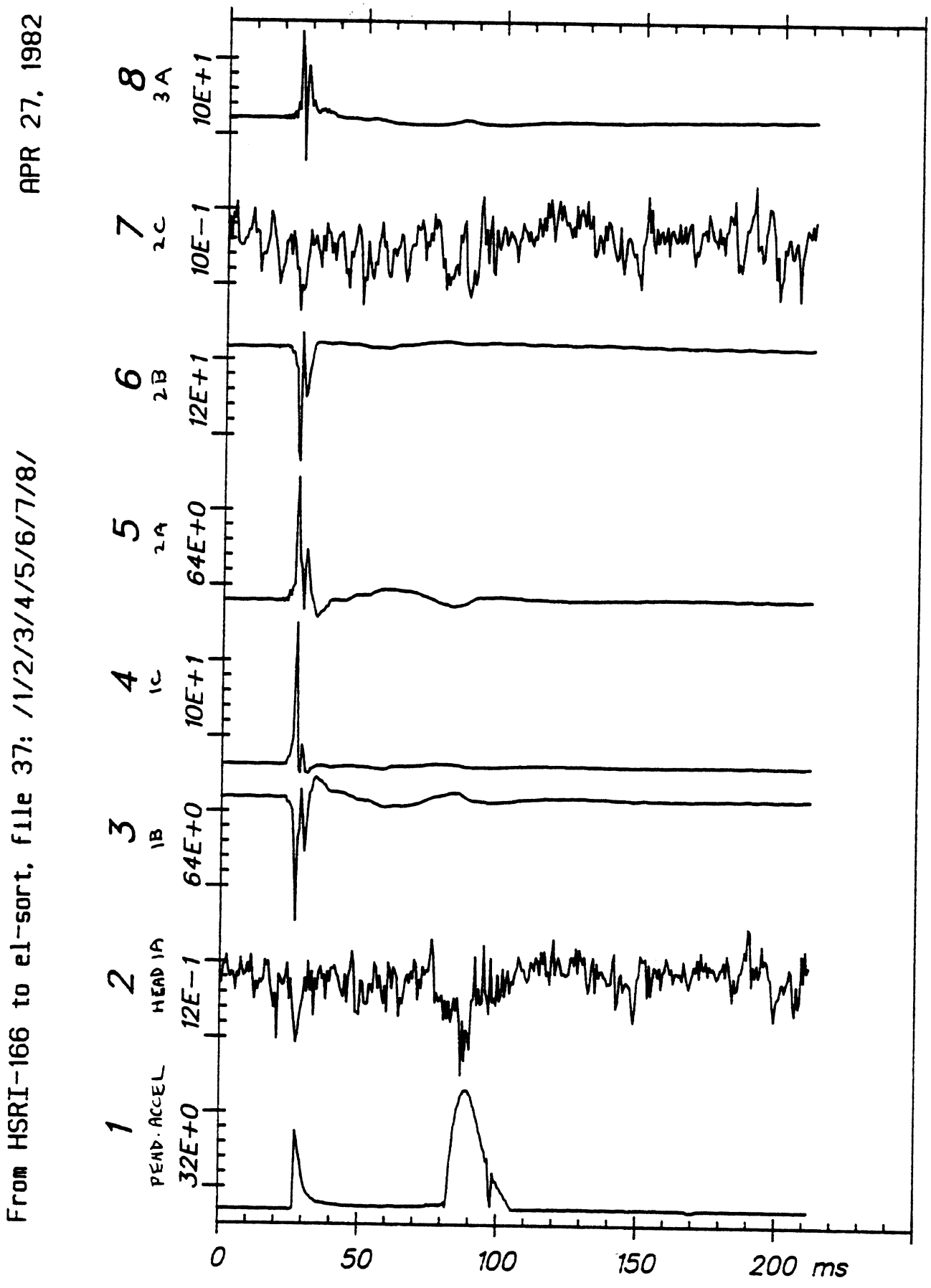

Time Histories 82E001 H7

From HSRI-166 to el-sort, file 37: /9/10/11/12/13/14/-/-/

APR 27, 1982

Time Histories 82E001 H7

APR 27, 1982

From HSRI-167 to el-sort, file 44: /1/2/3/4/5/6/7/8/

Time Histories 823001 C3

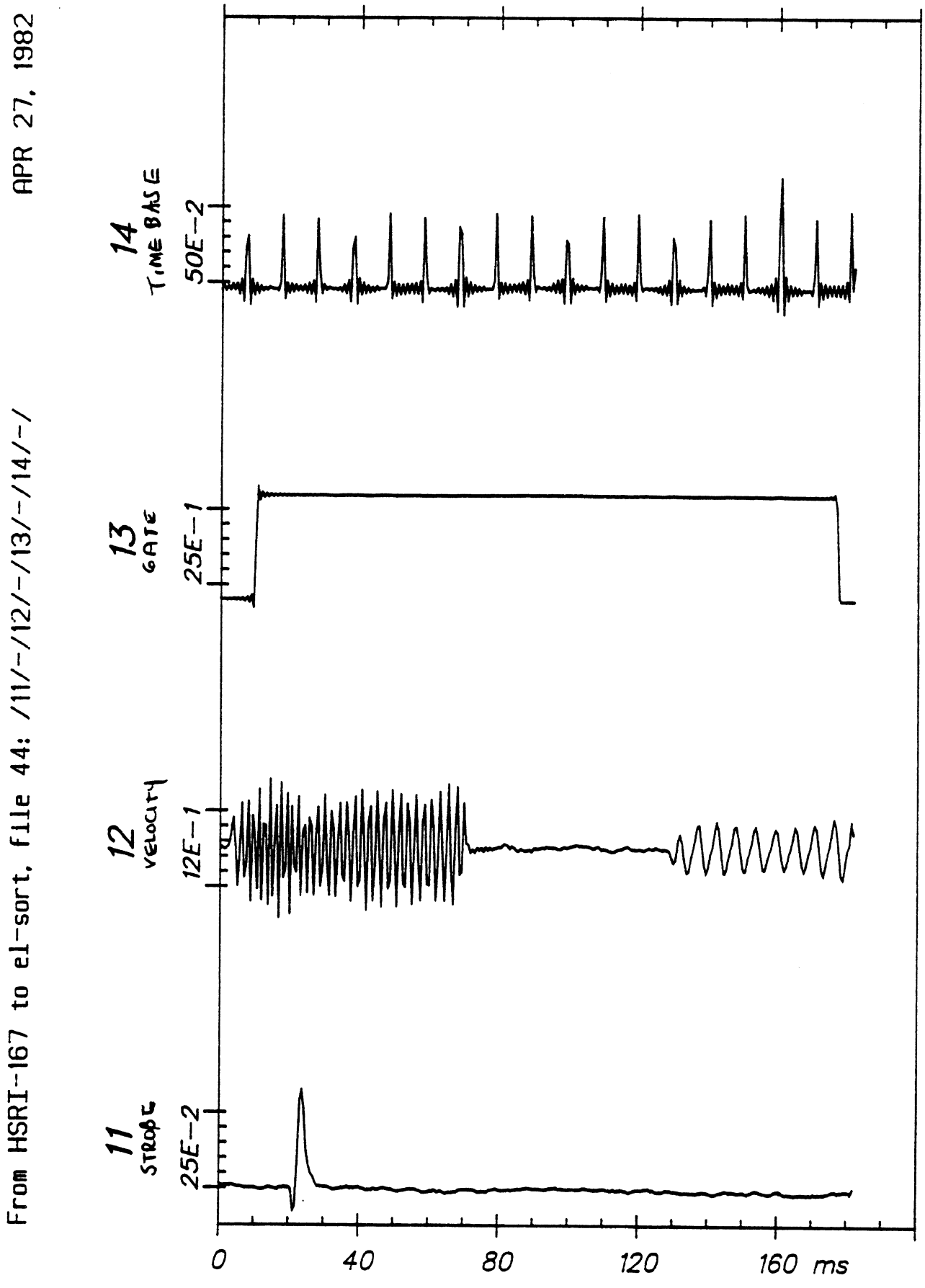

Time Histories 823001 C3

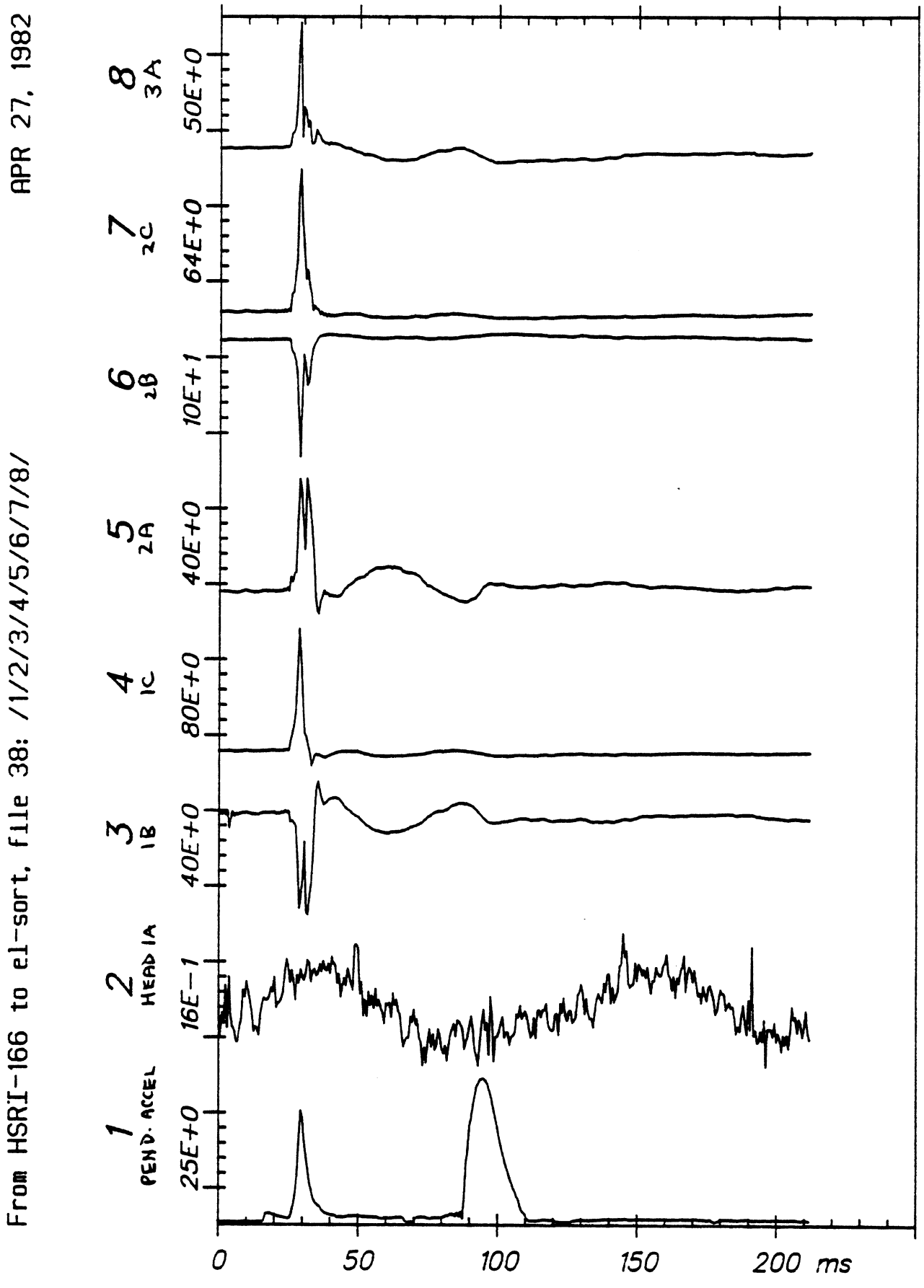
From HSRI-166 to el-sort, file 38: /1/2/3/4/5/6/7/8/
APR 27, 1982
8 3A 50E+0
7 2C 64E+0
6 2B 10E+1
5 2A 40E+0
4 1C 80E+0
3 1B 40E+0
2 HEAD 1A 16E-1
1 PEND. ACCEL 25E+0
0
50
100
150
200 ms
Time Histories
82E002
H7

From HSRI-166 to el-sort, file 38: /9/10/11/12/13/14/-/-/

APR 27, 1982

Time Histories 82E002 H7

Time Histories 82E002 C.

From HSRI-166 to el-sort, file 39: /1/2/3/4/5/6/7/8/ APR 27, 1982

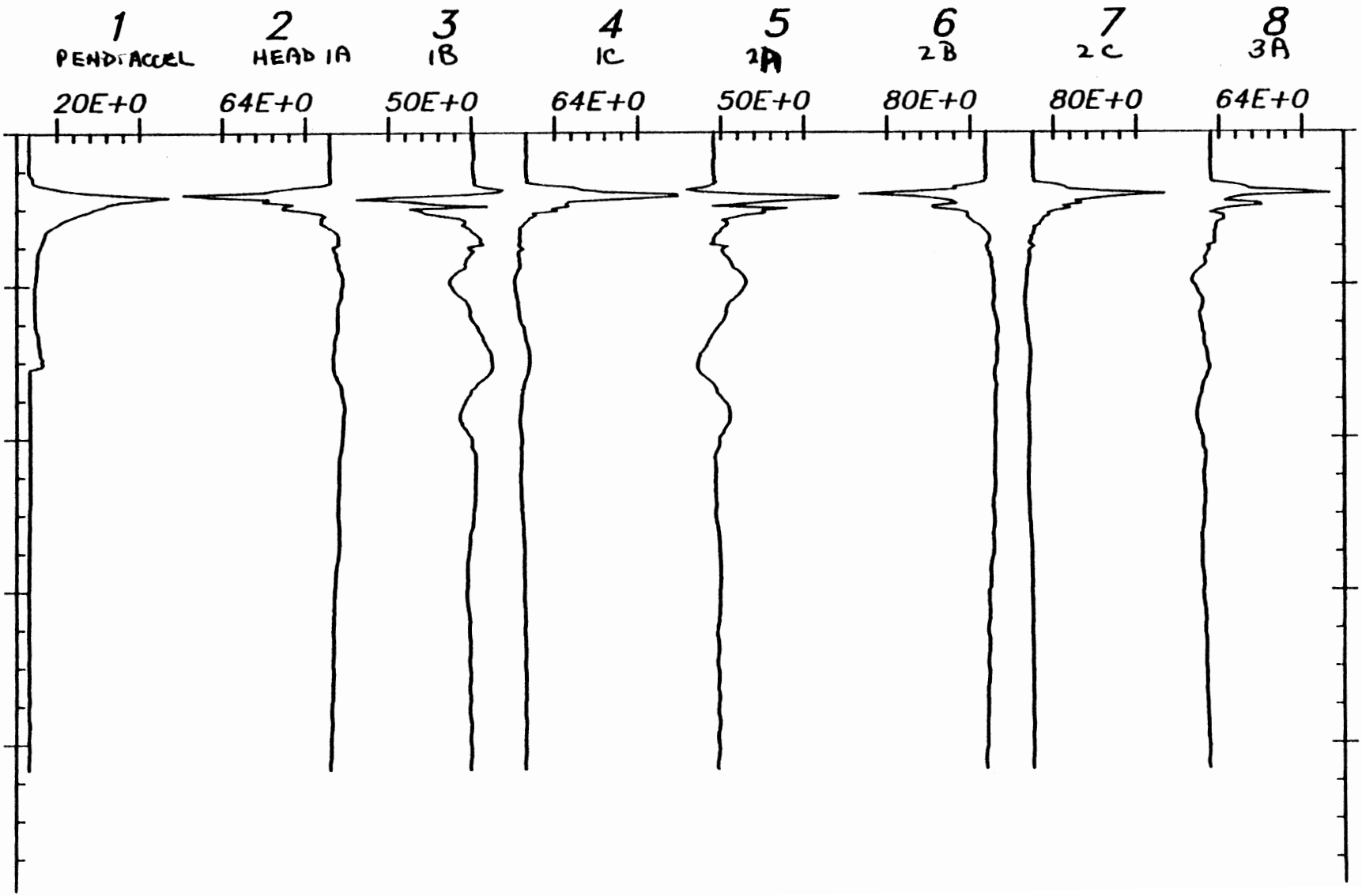

Time Histories

82E003 H7

From HSRI-167 to el-sort, file 46: /1/2/3/4/5/6/7/8/ APR 27, 1982

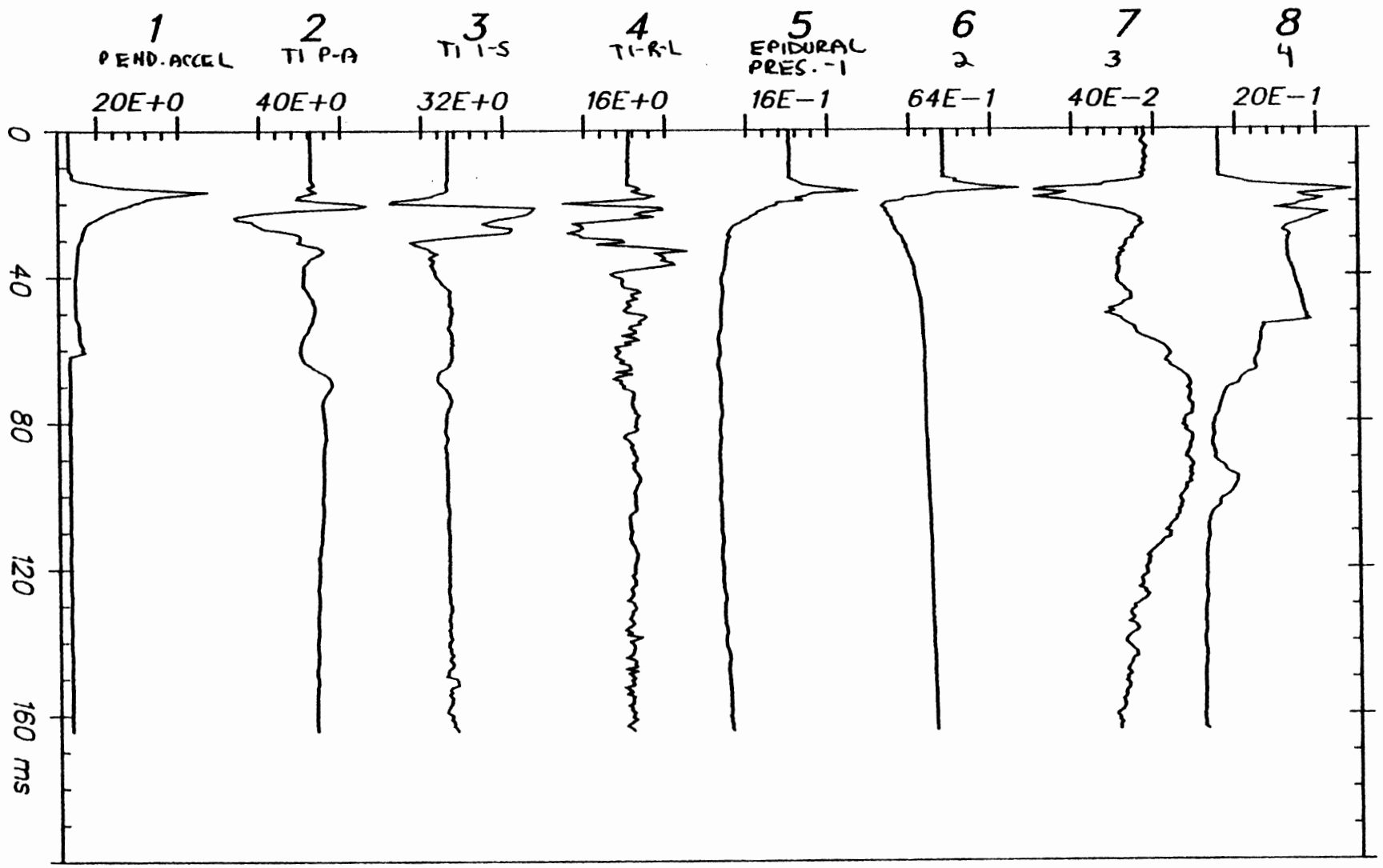

Time Histories 82E003 C3

From HSRI-167 to el-sort, file 46: /11/-/12/-/13/-/14/-/

APR 27, 1982

Time Histories 82E003 C3

From HSRI-166 to EL-SORT, file 10: /1/2/3/4/5/6/7/8/

APR 28, 1982

Time Histories 82E004 H7

From HSRI-166 to EL-SORT, File 10: /9/10/-/11/-/12/13/14/

APR 28, 1982

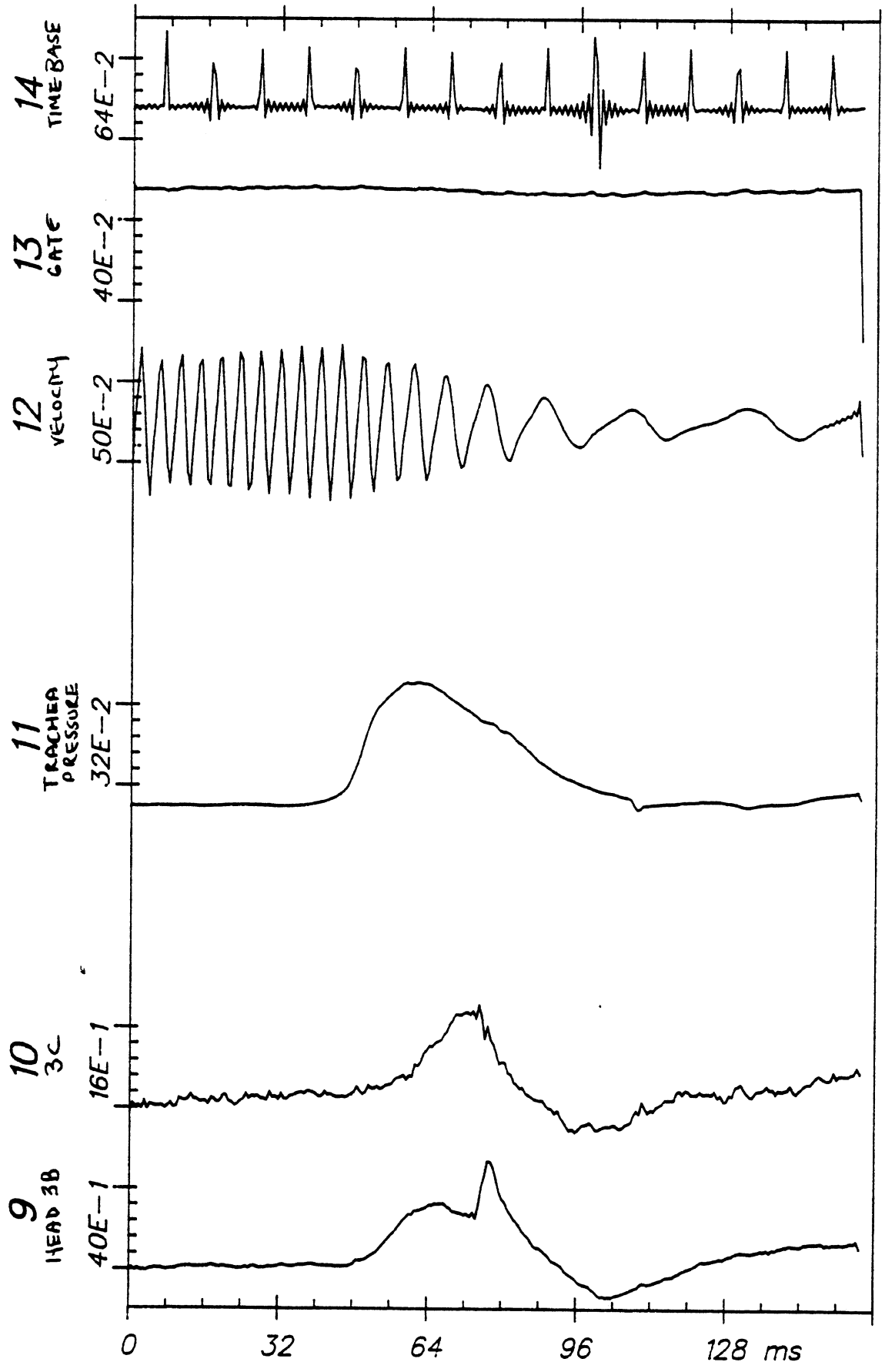

Time Histories 82E004 H7

From HSRI-167 to EL-SORT, file 22: /1/2/3/4/5/6/7/8/ APR 28, 1982

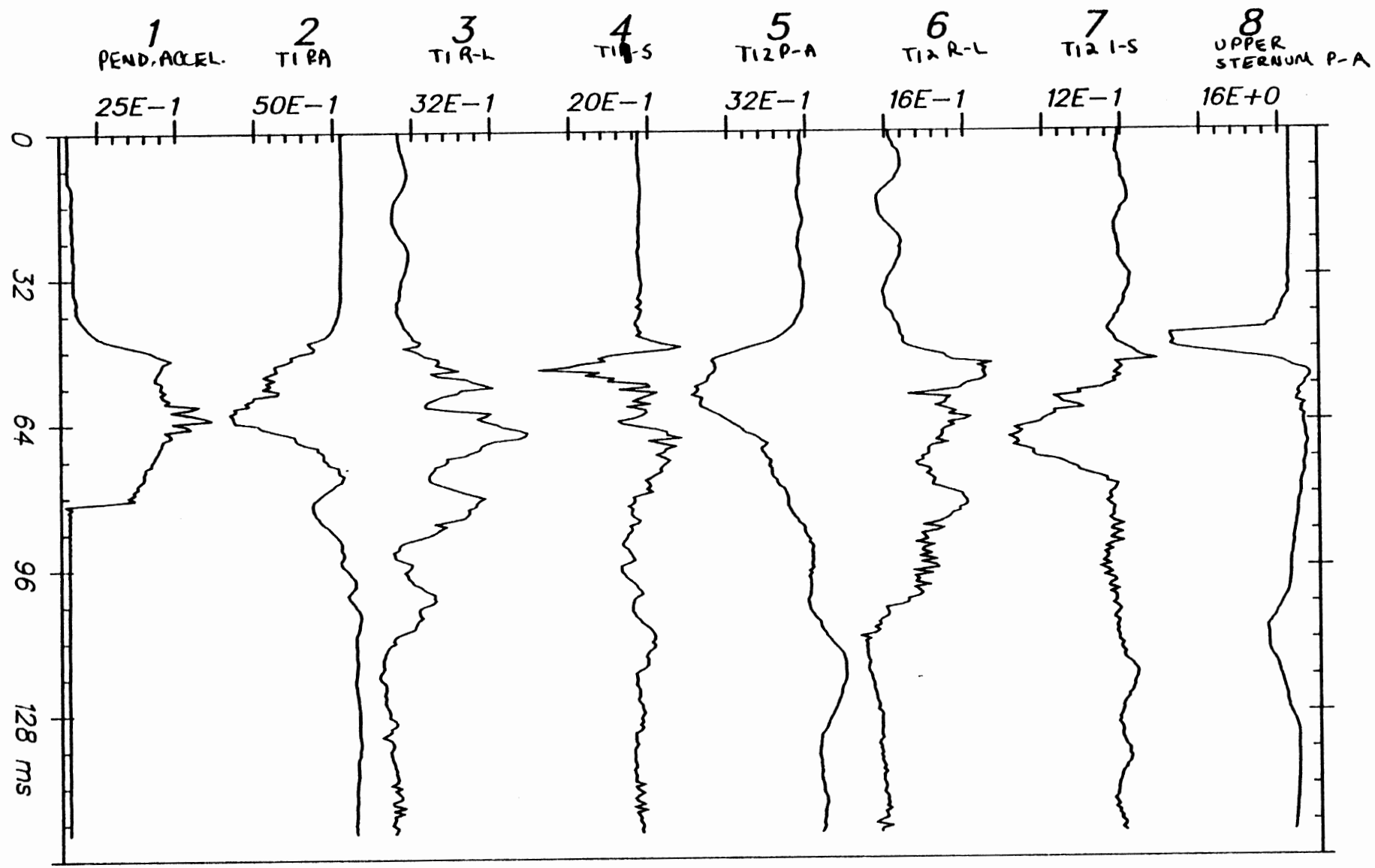

Time Histories

D13

82E004 C3

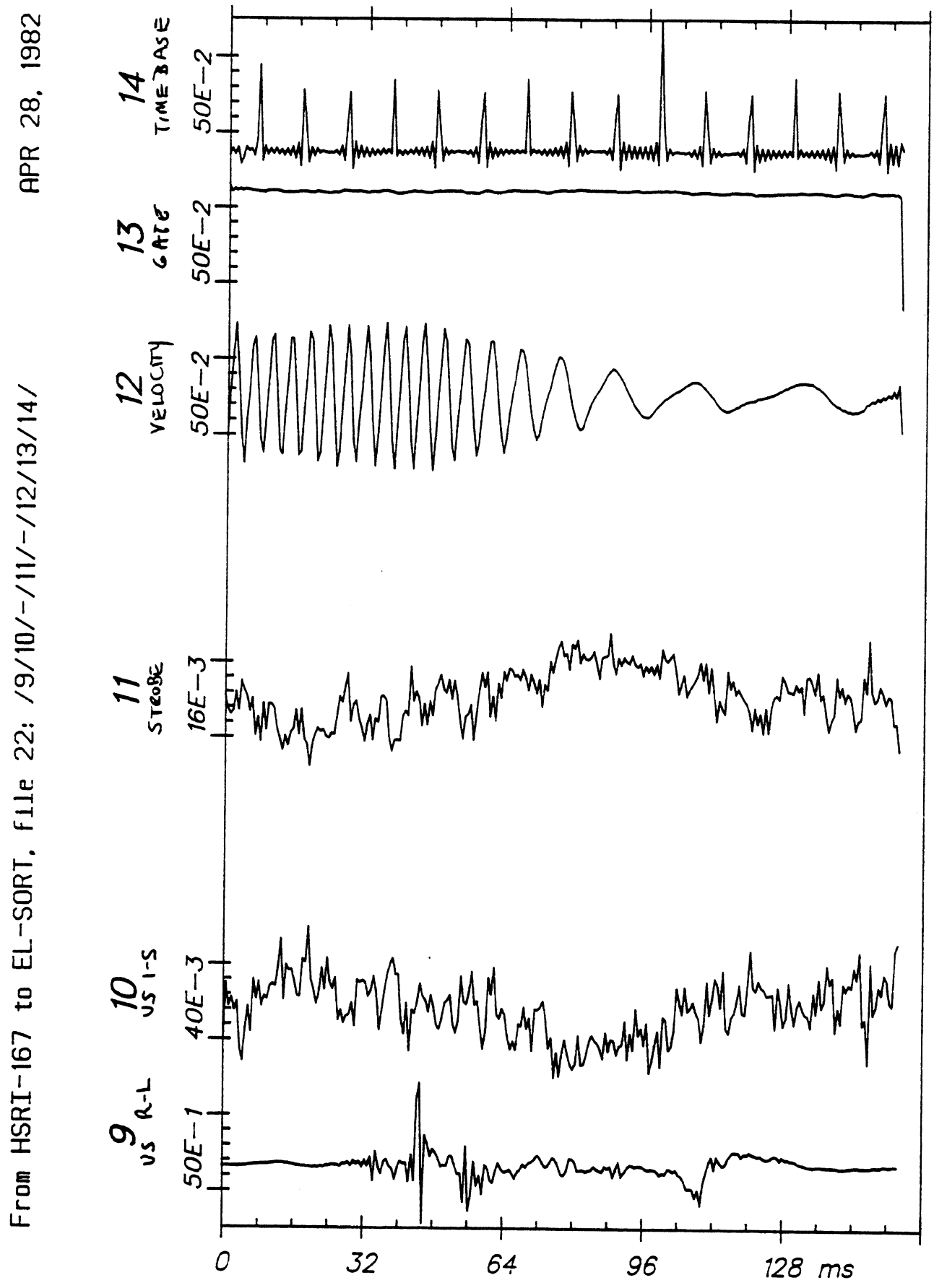

Time Histories 82E004 C3

From HSRI-177 to EL-SORT, file 34: /1/2/3/4/5/6/7/8/ APR 30, 1982

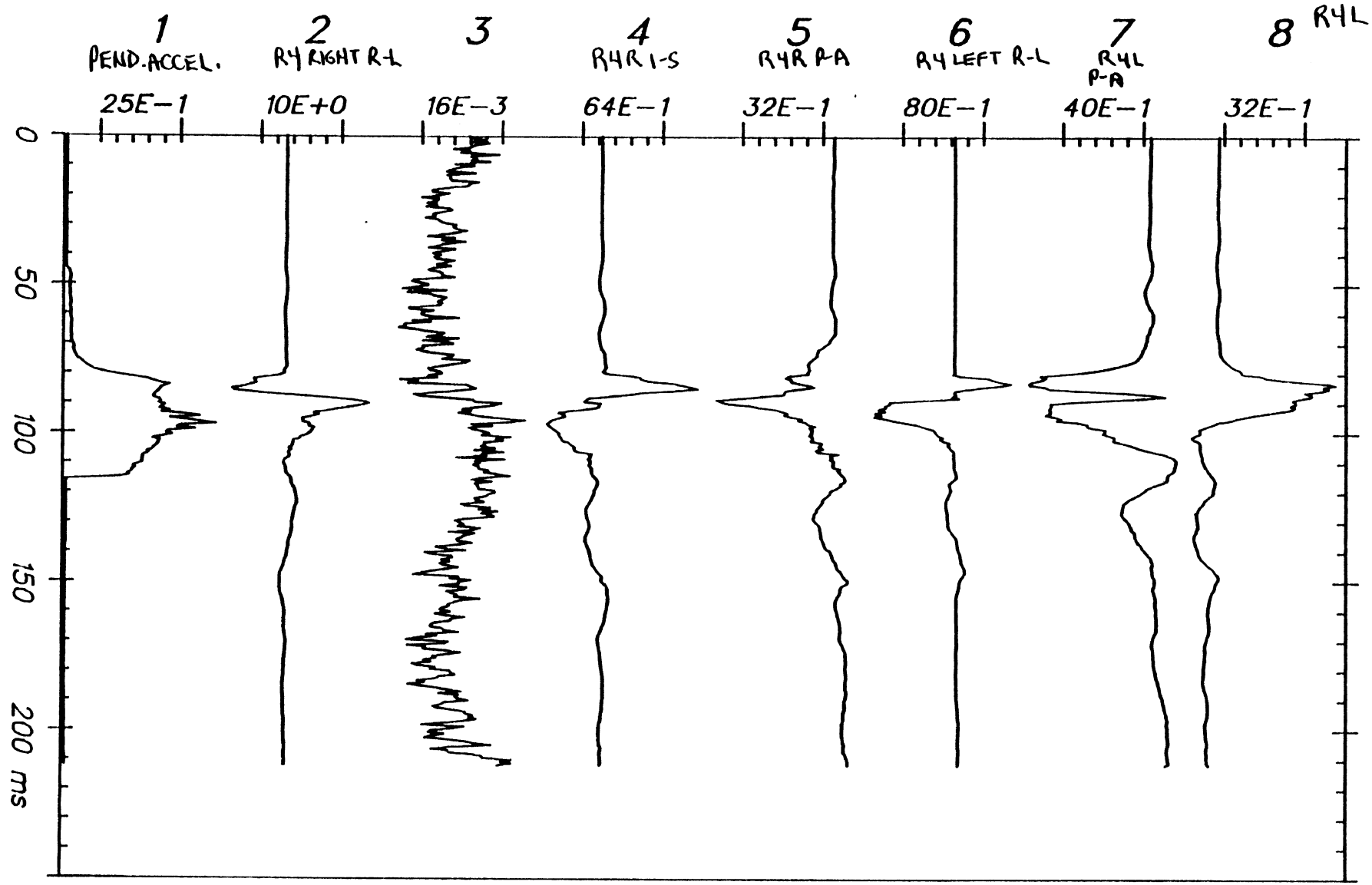

Time Histories 82E004 C4

From HSRI-177 to EL-SORT, file 34: /9/11/12/-/-/13/14/-/

APR 28, 1982

Time Histories 82E004 C4

From HSRI-166 to EL-SORT, file 11: /1/2/3/4/5/6/7/8/
APR 28, 1982
1 PEND. ACCEL
12E-1
2 HEAD IA
12E-1
3 IB
16E-1
4 IC
16E-1
5 aA
12E-1
6 aB
25E-2
7 aC
12E-1
8 aA
12E-1
0
32
64
96
128 ms
Time Histories
82E005
H7

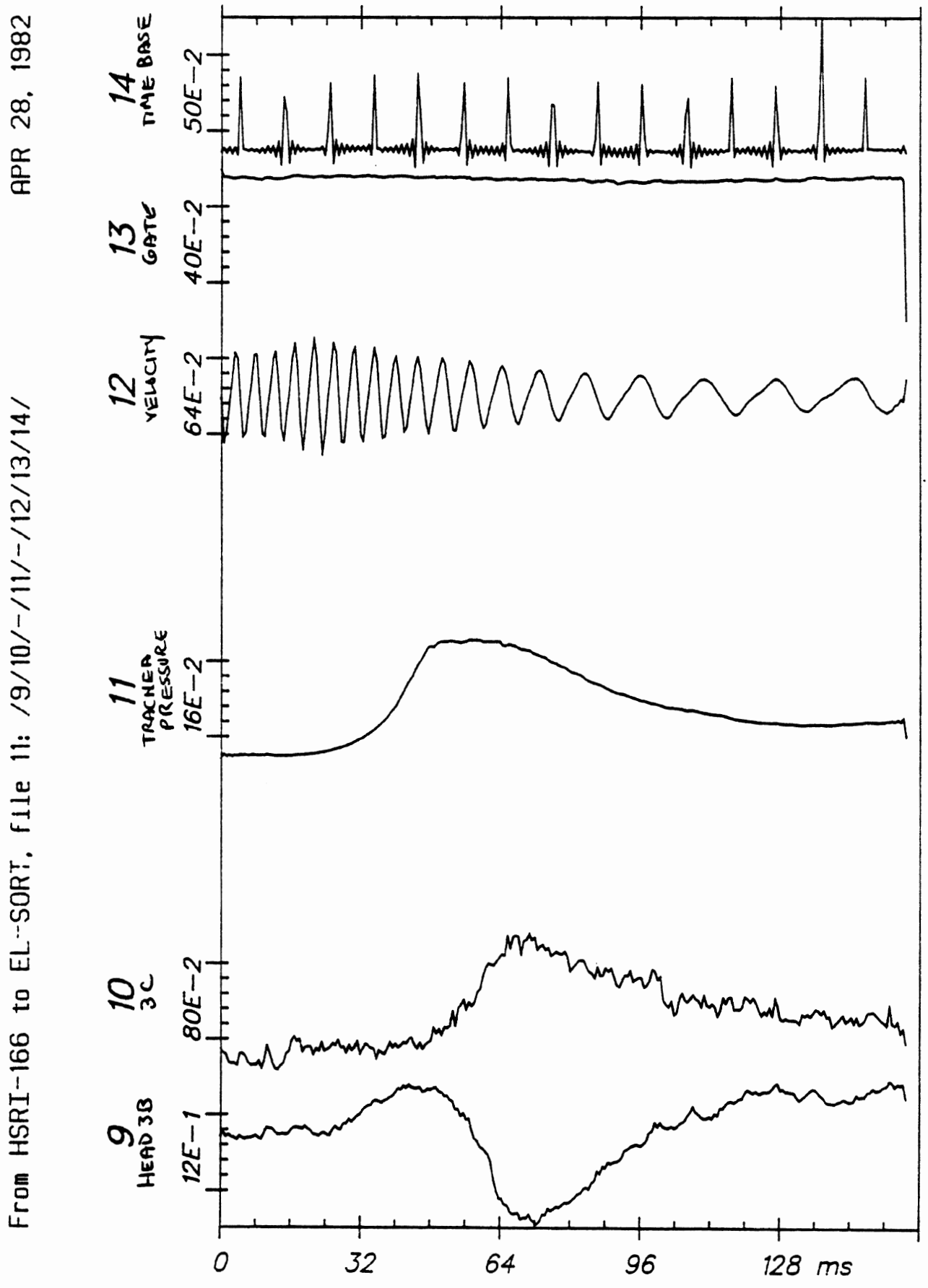
From HSRI-166 to EL--SORT, file 11: /9/10/-/11/-/12/13/14/
APR 28, 1982
14 TIME BASE
50E-2
13 GATE
40E-2
12 VELOCITY
64E-2
11 TRACHEA PRESSURE
16E-2
10 3C
80E-2
9 HEAD 3B
12E-1
0
32
64
96
128 ms
Time Histories
82E005
H7

From HSRI-167 to EL-SORT, file 23: /1/2/3/4/5/6/7/8/

APR 28, 1982

Time Histories 82E005 C3

From HSRI-167 to EL-SORT, file 23: /9/10/-/11/-/12/13/14/

APR 28, 1982

Time Histories 82E005 C3

APR 30, 1982

From HSRI-177 to EL-SORT, File 35: /1/2/3/4/5/6/7/8/

Time Histories 82E005 C4

From HSRI-177 to EL-SORT, file 35: /9/11/12/-/-/13/14/-/

APR 28, 1982

Time Histories 82E005 C4

From HSRI-166 to EL-SORT, File 12: /1/2/3/4/5/6/7/8/

APR 28, 1982

Time Histories 82E006 H7

From HSRI-166 to EL-SORT, file 12: /9/10/-/11/-/12/13/14/

APR 28, 1982

Time Histories 82E006 H7

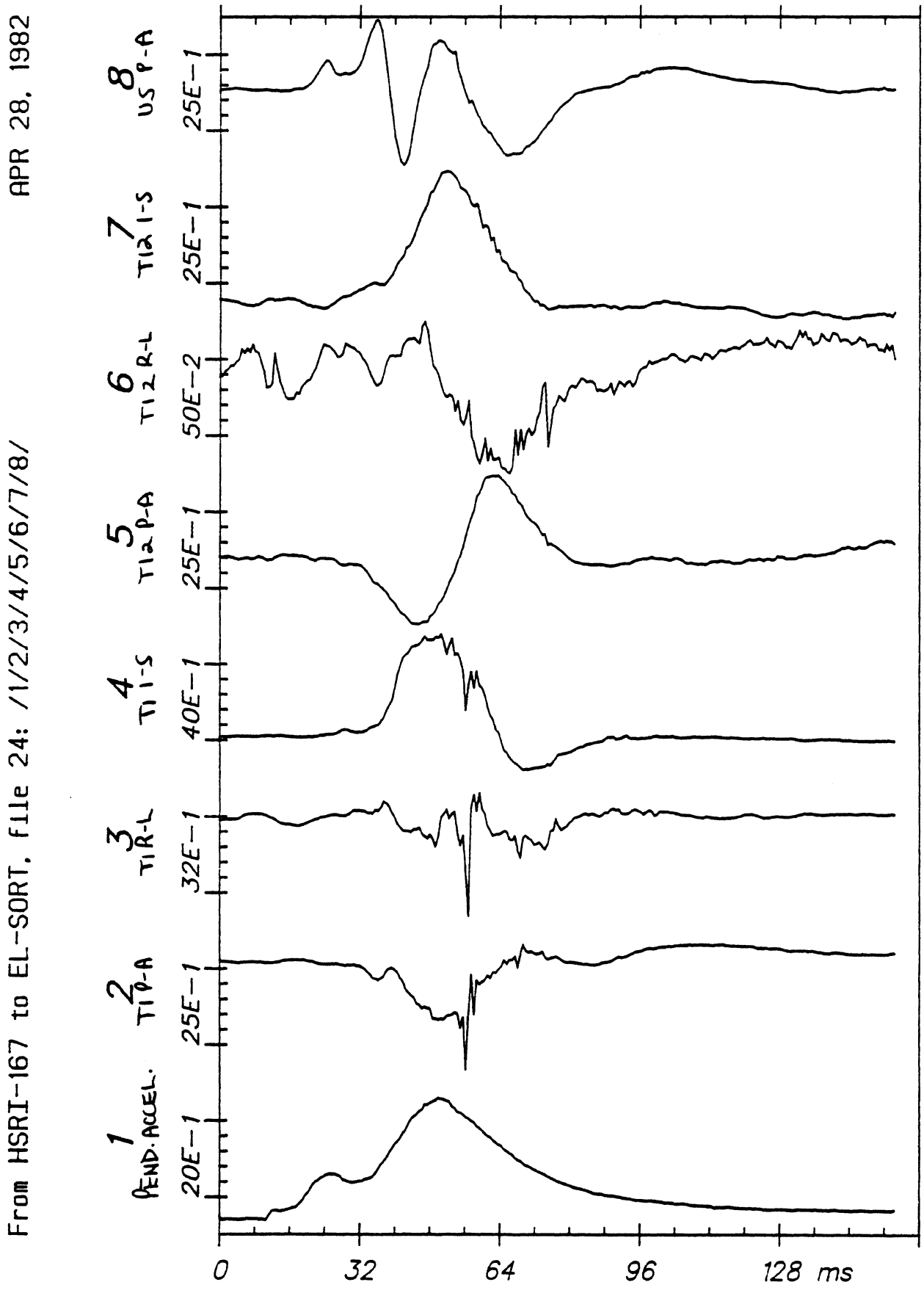

Time Histories 82E006 C3

From HSRI-167 to EL-SORT, file 24: /9/10/-/11/-/12/13/14/

APR 28, 1982

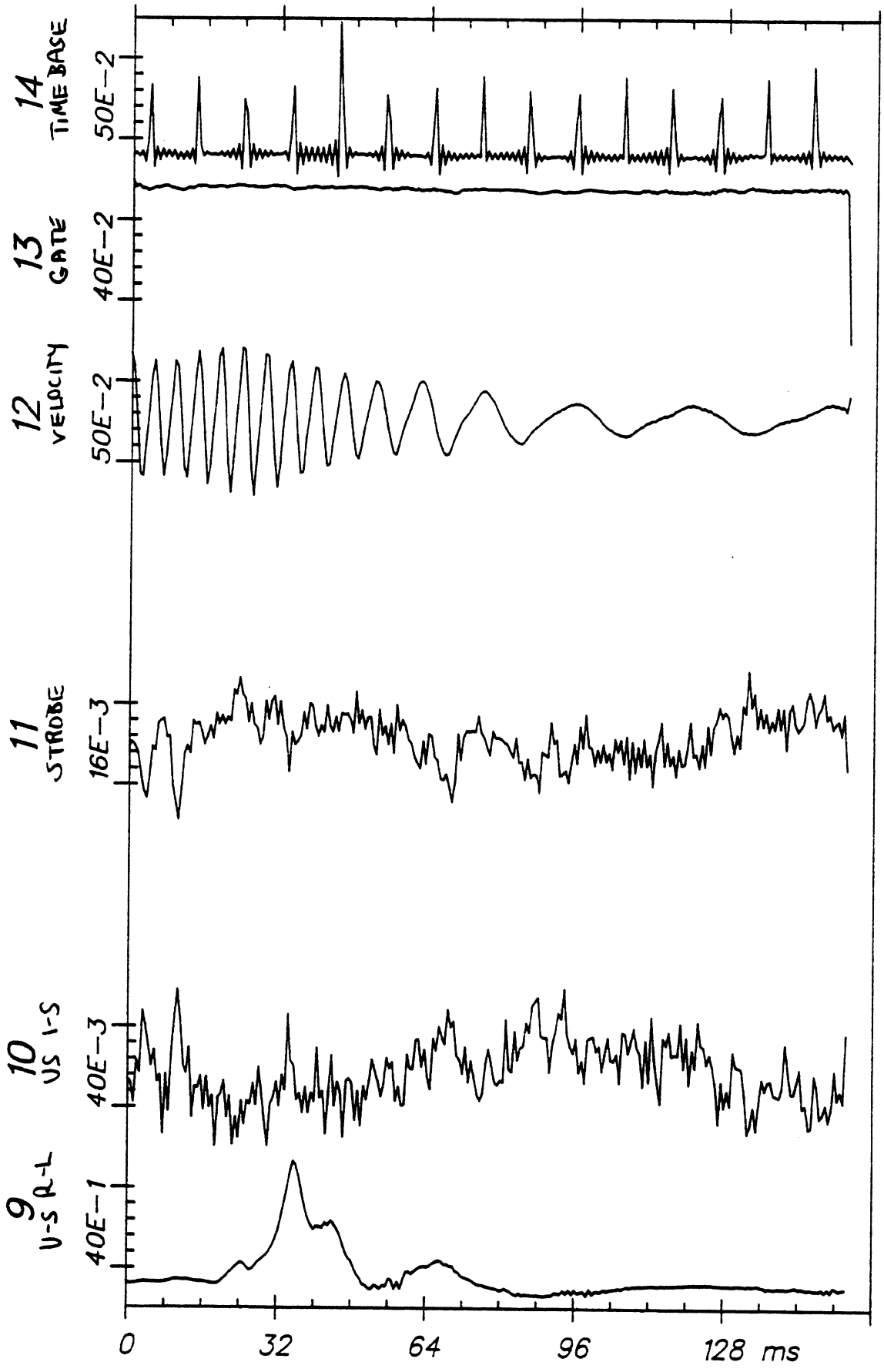

Time Histories 82E006 C3

From HSRI-177 to EL-SORT, File 36: /1/2/3/4/5/6/7/8/

APR 30, 1982

Time Histories 82E006 C4

From HSRI-177 to EL-SORT, file 36: /9/11/12/-/-/13/14/-/ APR 28, 1982

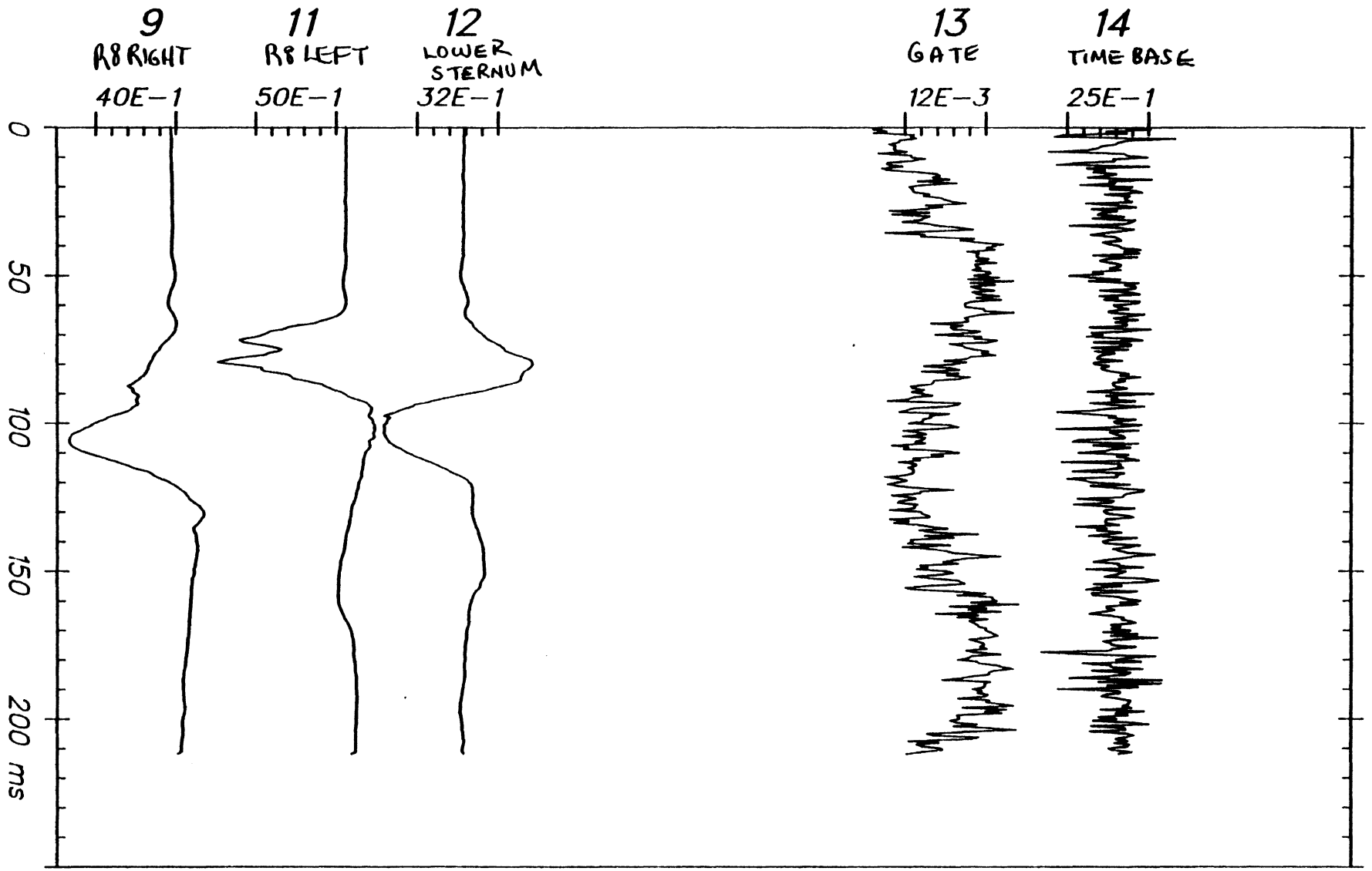

Time Histories 82E006 C4

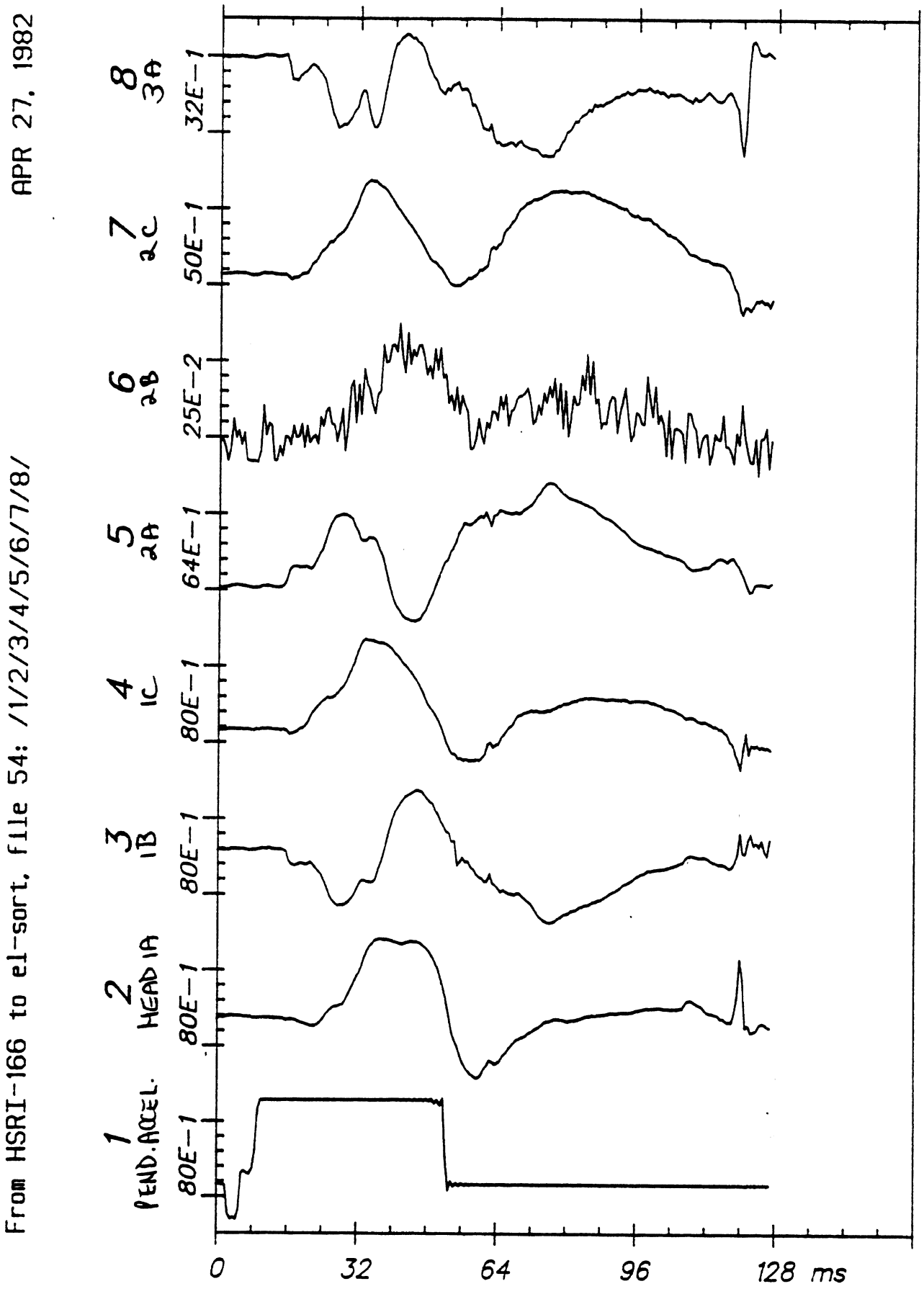
APR 27, 1982
From HSRI-166 to el-sort, file 54: /1/2/3/4/5/6/7/8/
8 3A 32E-1
7 2C 50E-1
6 2B 25E-2
5 2A 64E-1
4 1C 80E-1
3 1B 80E-1
2 HEAD 1A 80E-1
1 PEND. ACCEL. 80E-1
0
32
64
96
128 ms
Time Histories
82E007
H7

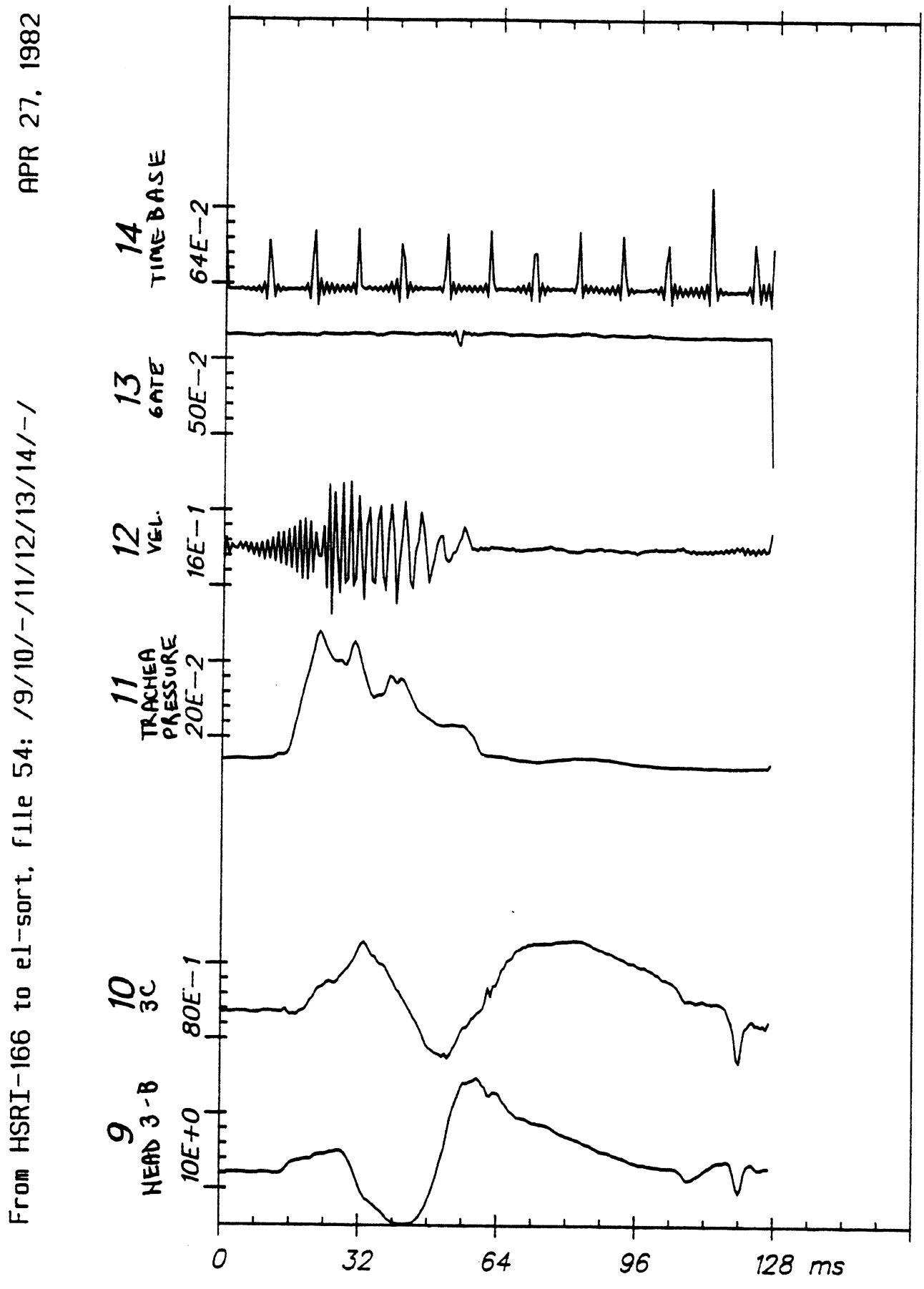
From HSRI-166 to el-sort, file 54: /9/10/-/11/12/13/14/-/
APR 27, 1982
14 TIME BASE
64E-2
13 GATE
50E-2
12 VEL.
16E-1
11 TRACHEA PRESSURE
20E-2
10 3C
80E-1
9 HEAD 3-B
10E+0
0
32
64
96
128 ms
Time Histories
82E007
H7

From HSRI-167 to el-sort, file 57: /1/2/3/4/5/6/7/8/

APR 27, 1982

Time Histories 82E007 C3

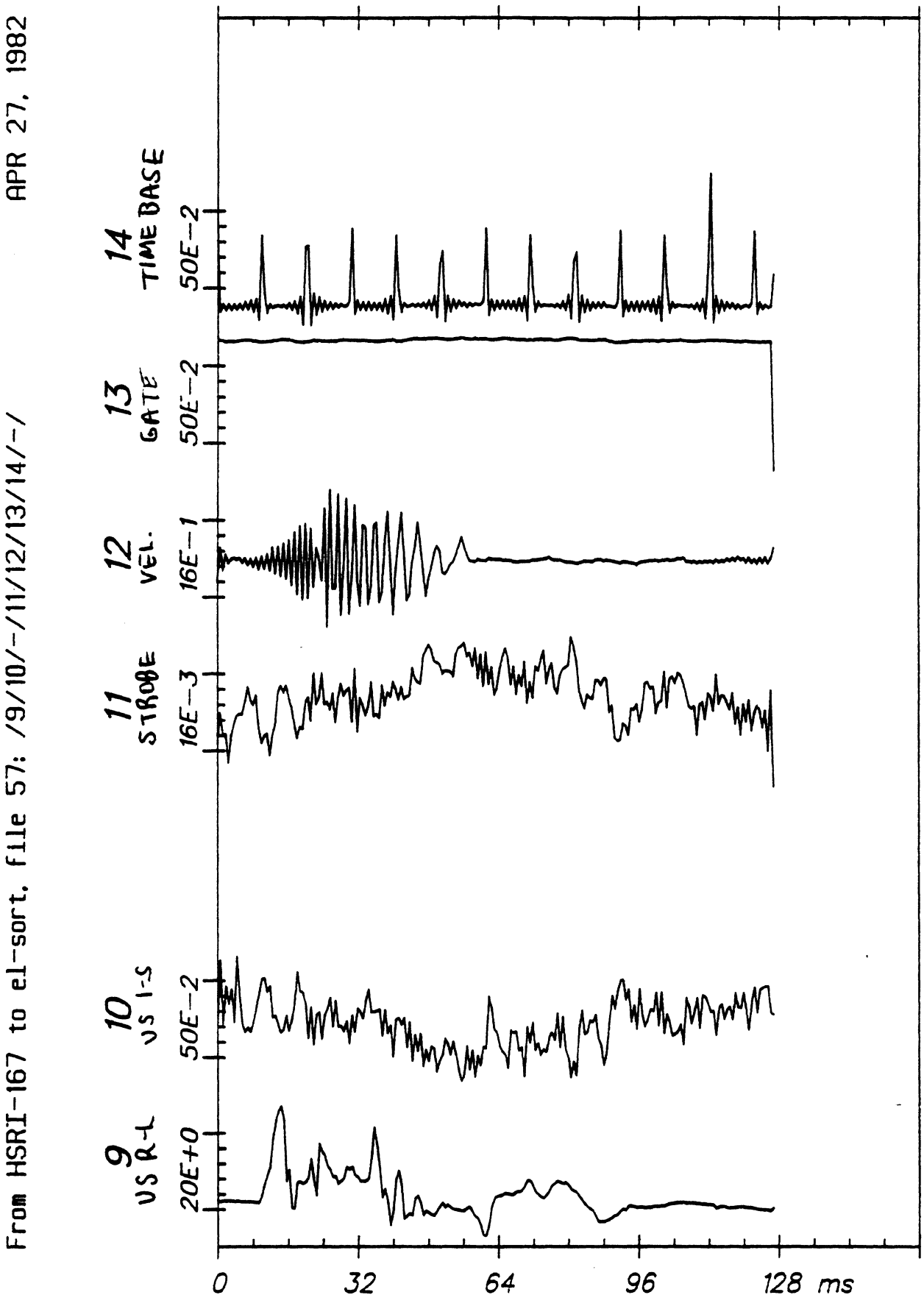

Time Histories 82E007 C3

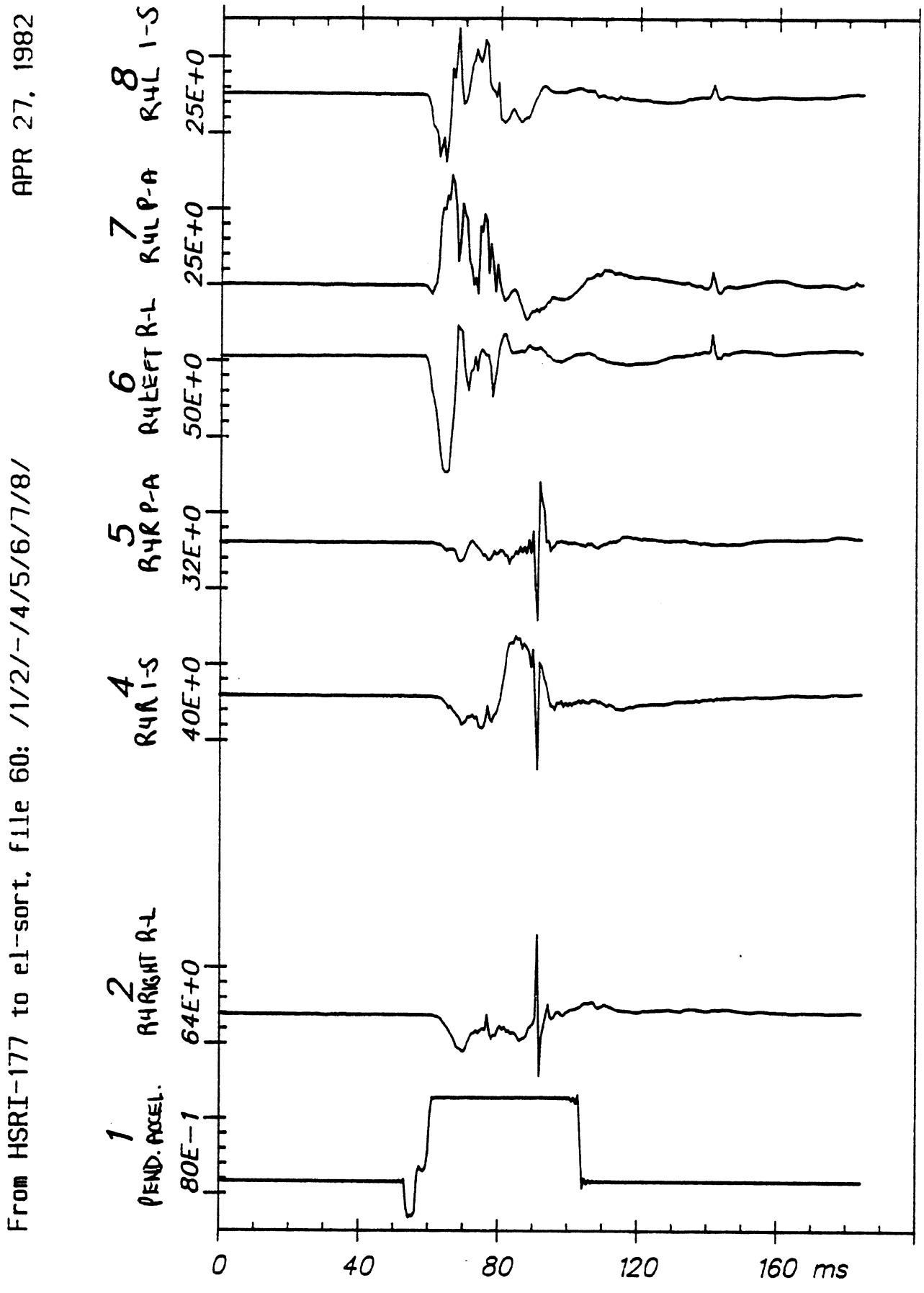
From HSRI-177 to el-sort, file 60: /1/2/-/4/5/6/7/8/
APR 27, 1982
8 R4L 1-S 25E+0
7 R4L P-A 25E+0
6 R4LEFT R-L 50E+0
5 R4R P-A 32E+0
4 R4R 1-S 40E+0
2 R4RIGHT R-L 64E+0
1 PEND. ACCEL. 80E-1
0
40
80
120
160 ms
Time Histories
82E007
C4

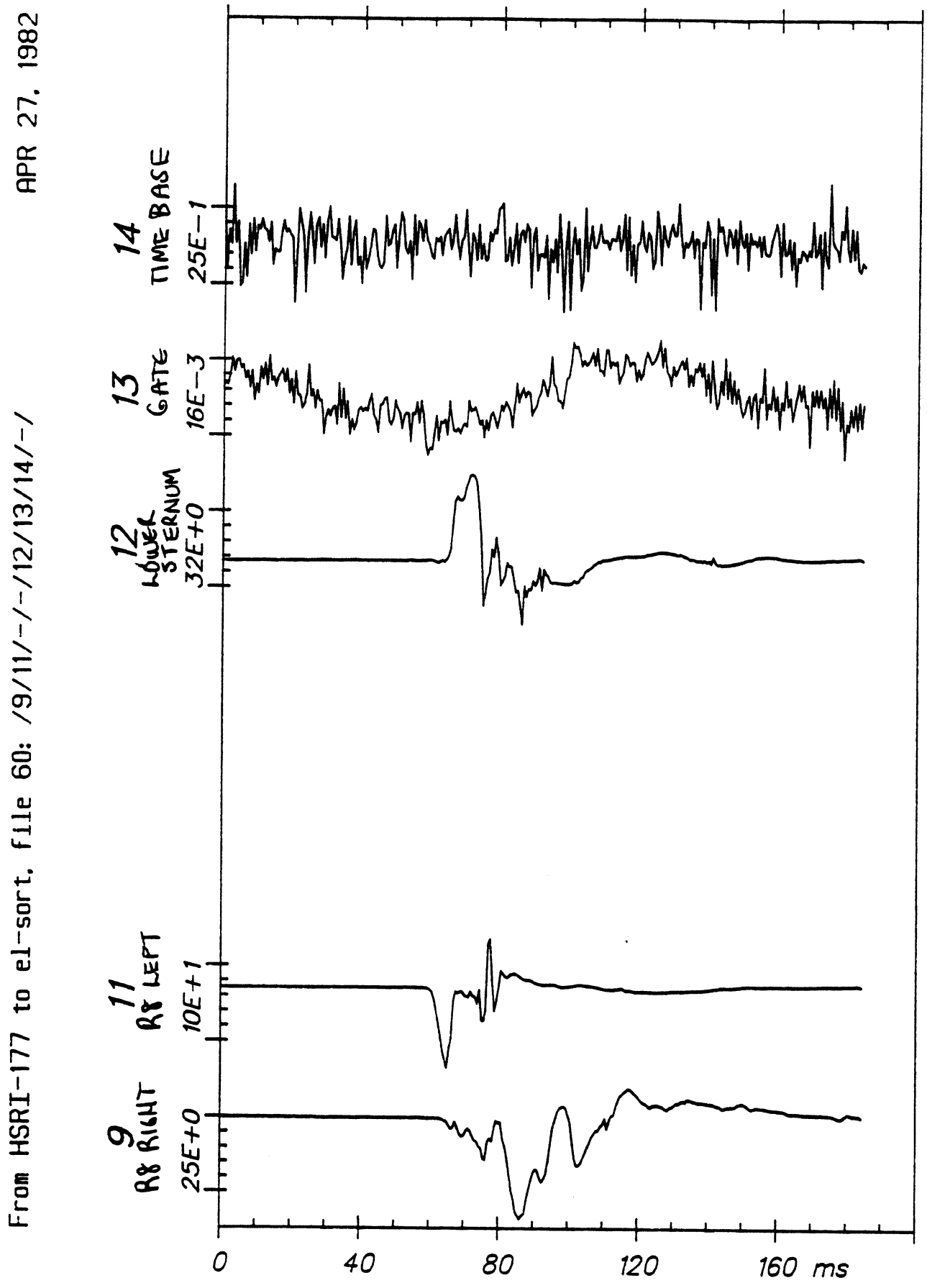

Time Histories 82E007 C4

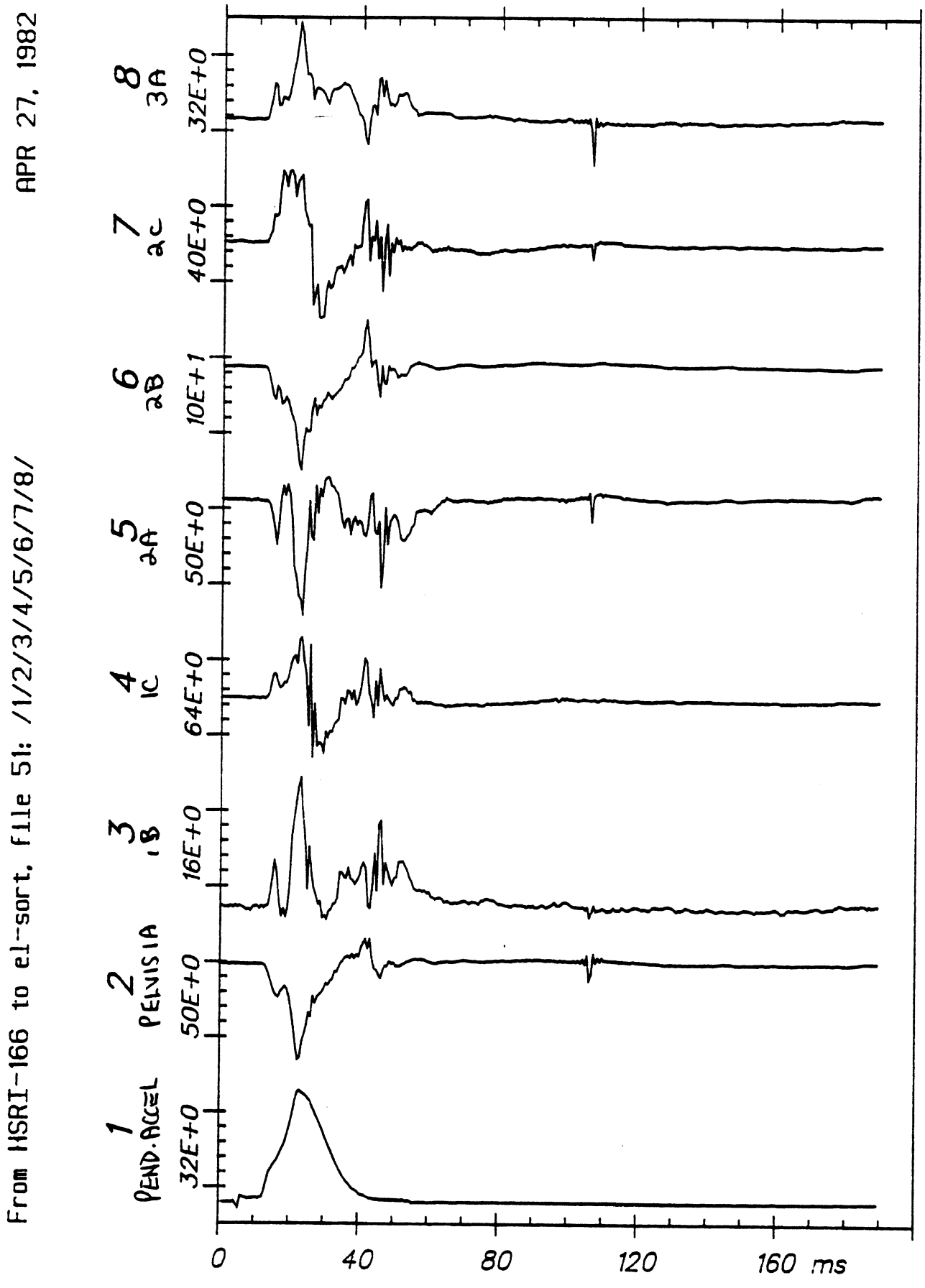
From HSRI-166 to el-sort, file 51: /1/2/3/4/5/6/7/8/
APR 27, 1982
8 3A 32E+0
7 2C 40E+0
6 2B 10E+1
5 2A 50E+0
4 1C 64E+0
3 1B 16E+0
2 PELVIS A 50E+0
1 PEND. ACCEL 32E+0
0
40
80
120
160 ms
Time Histories
82E008
H7

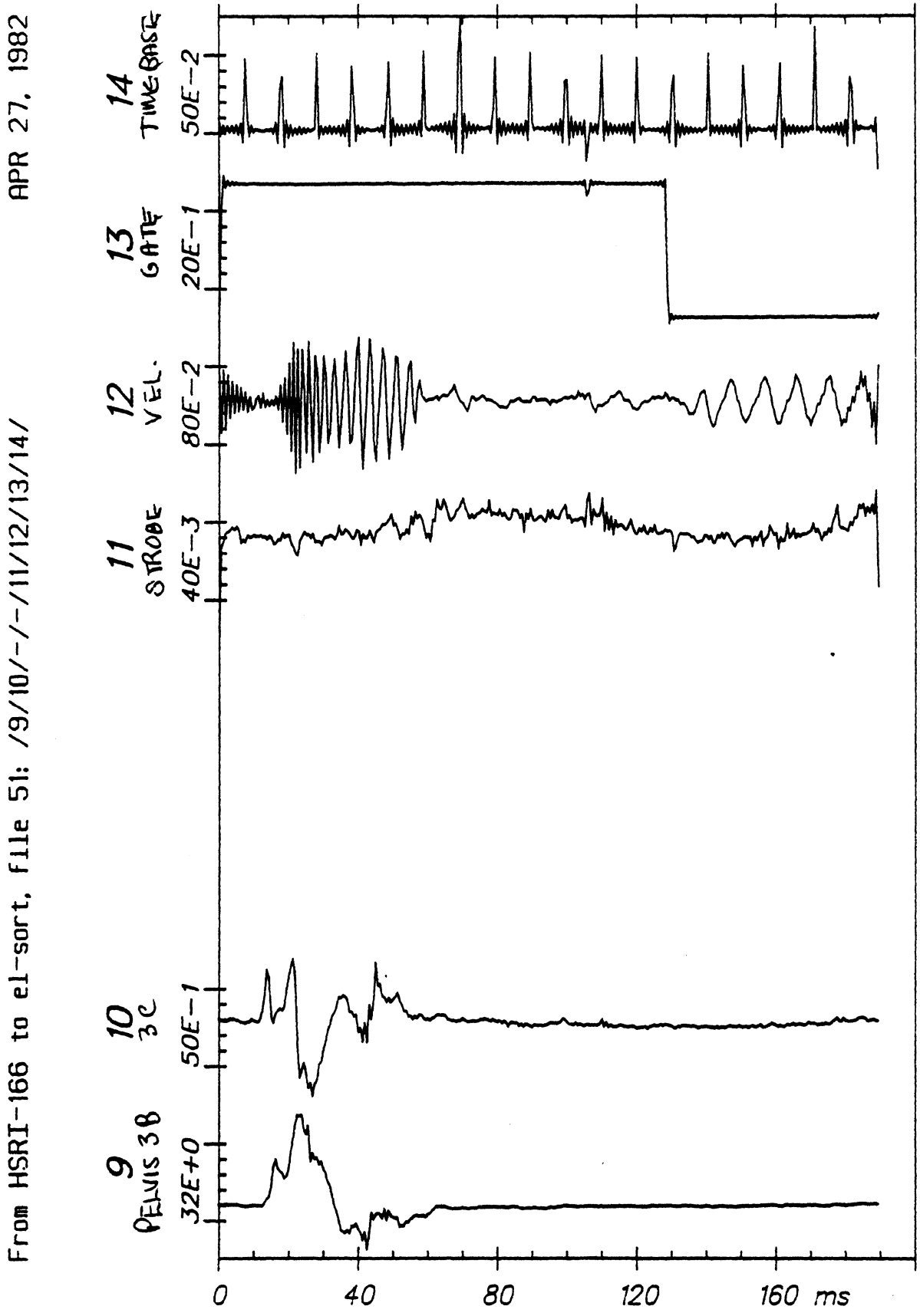

Time Histories 82E008 H7

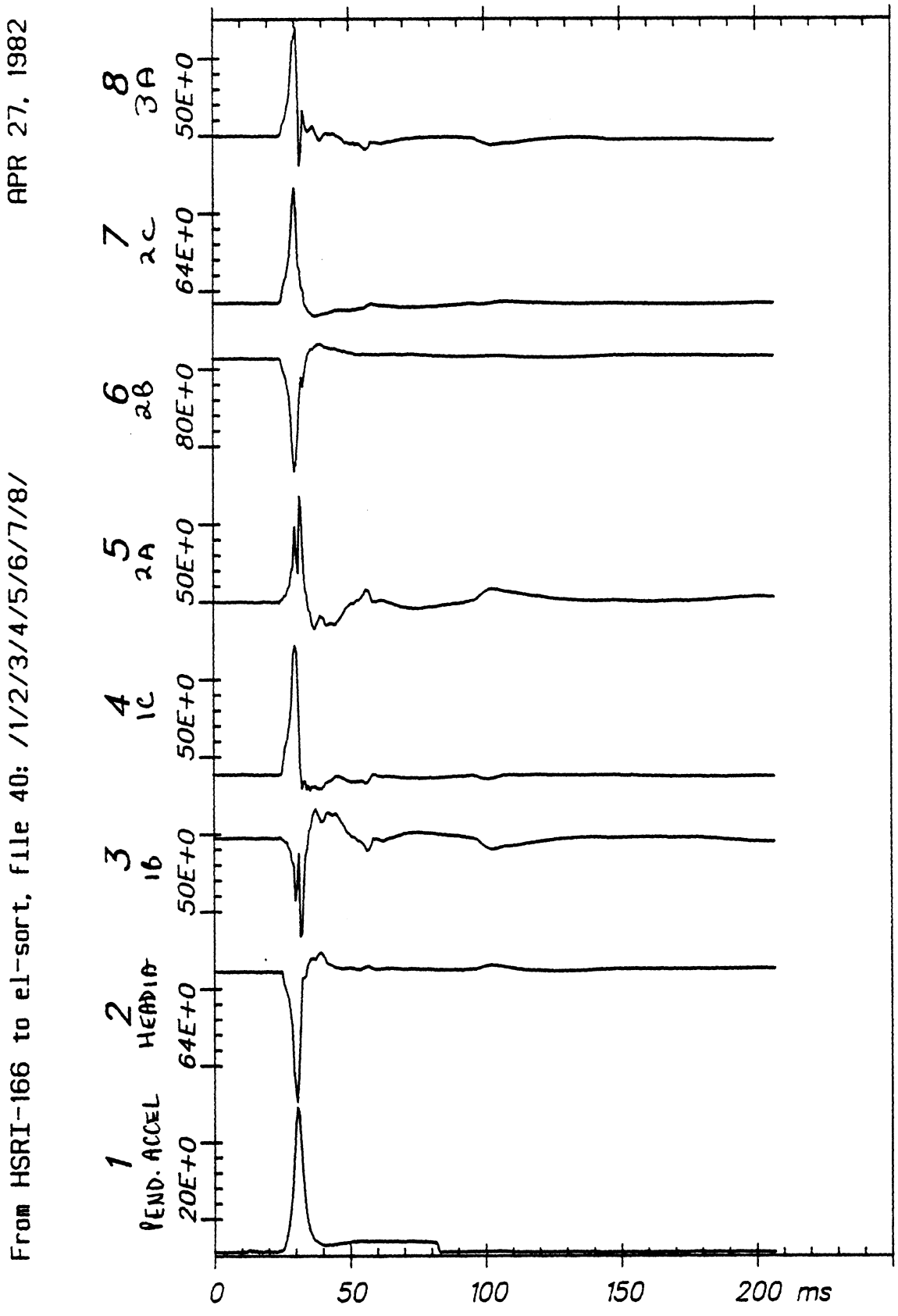

Time Histories 82E021 H7

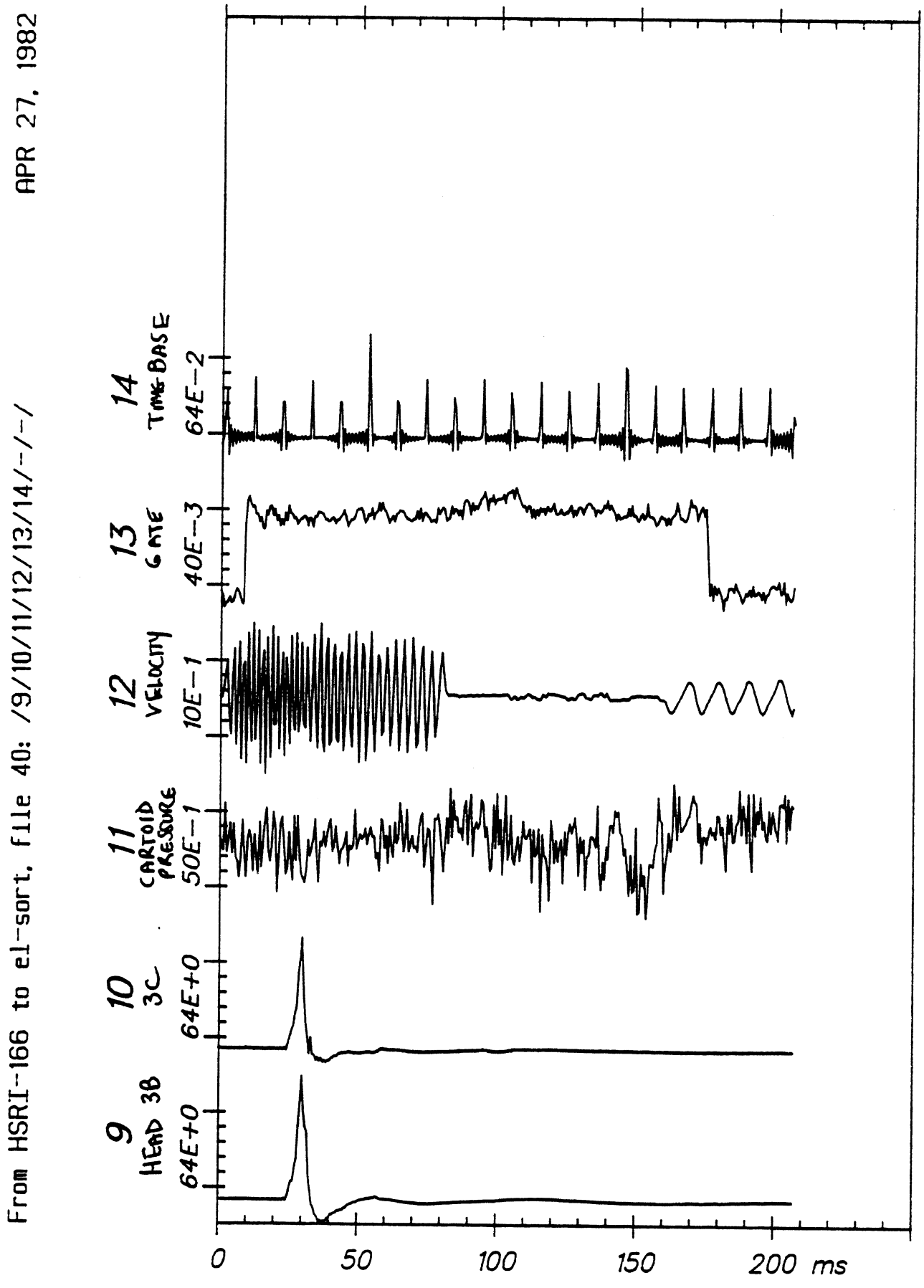
From HSRI-166 to el-sort, file 40: /9/10/11/12/13/14/-/-/
APR 27, 1982
14 TIME BASE 64E-2
13 GATE 40E-3
12 VELOCITY 10E-1
11 CAROTID PRESSURE 50E-1
10 3C 64E+0
9 HEAD 3B 64E+0
0
50
100
150
200 ms
Time Histories
82E021
H7

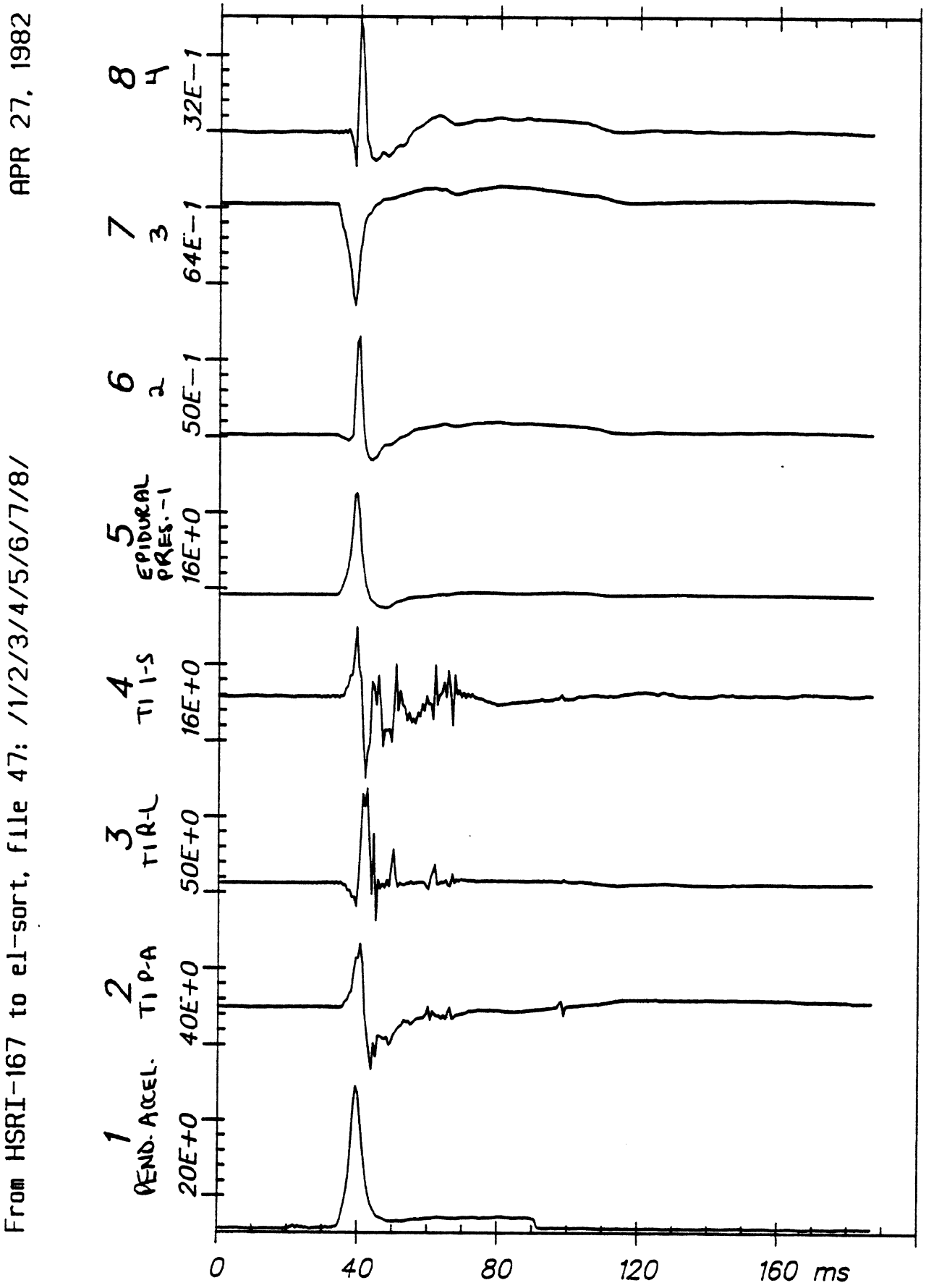

Time Histories 82E021 C3

From HSRI-167 to el-sort, file 47: /11/-/12/-/13/-/14/-/

APR 27, 1982

Time Histories 82E021 C3

From HSRI-166 to el-sort, file 41: /1/2/3/4/5/6/7/8/ APR 27, 1982

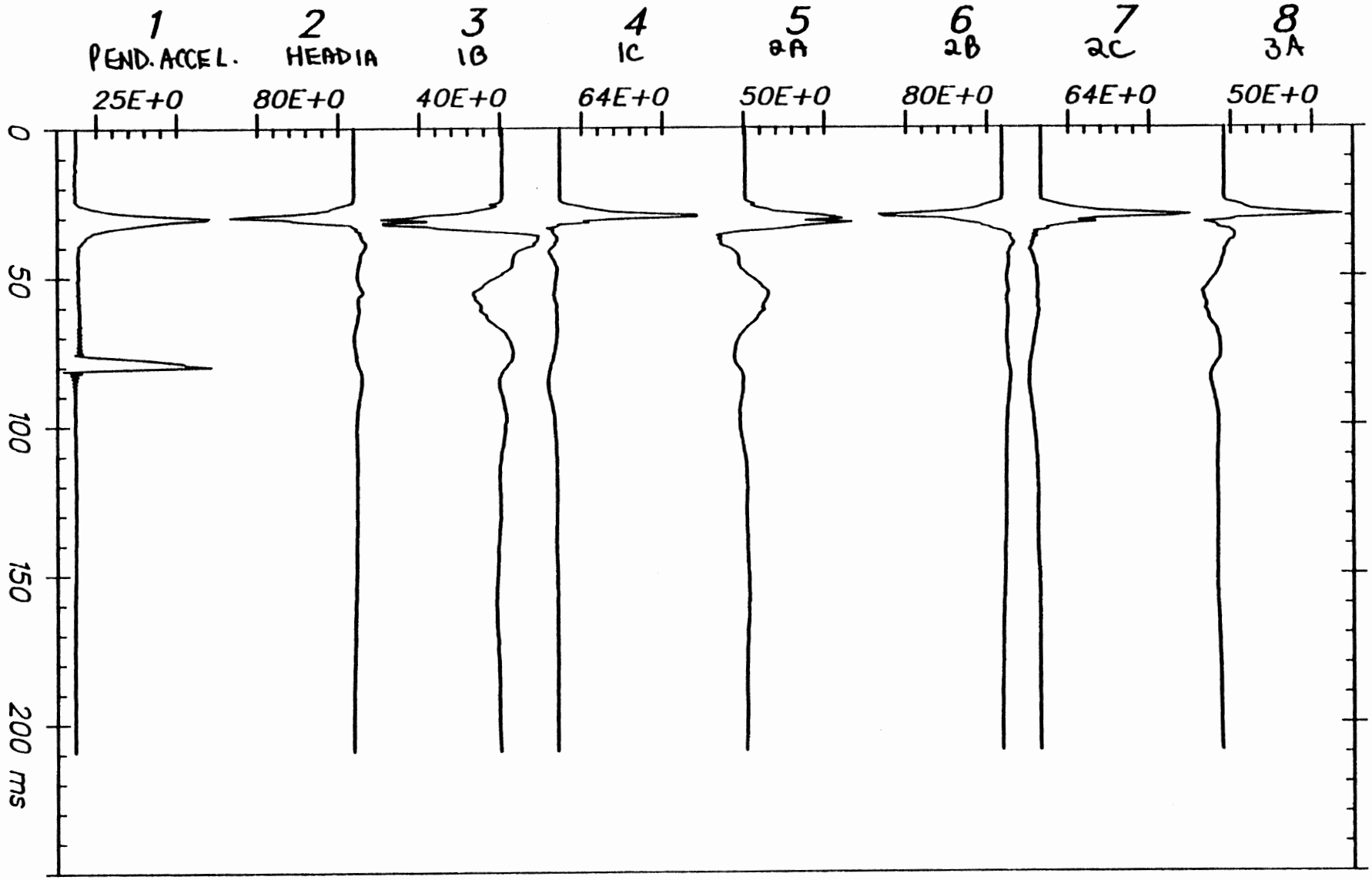

Time Histories 82E022 H7

D41

From HSRI-166 to el-sort, file 41: /9/10/11/12/13/14/-/-/

APR 27, 1982

Time Histories 82E022 H7

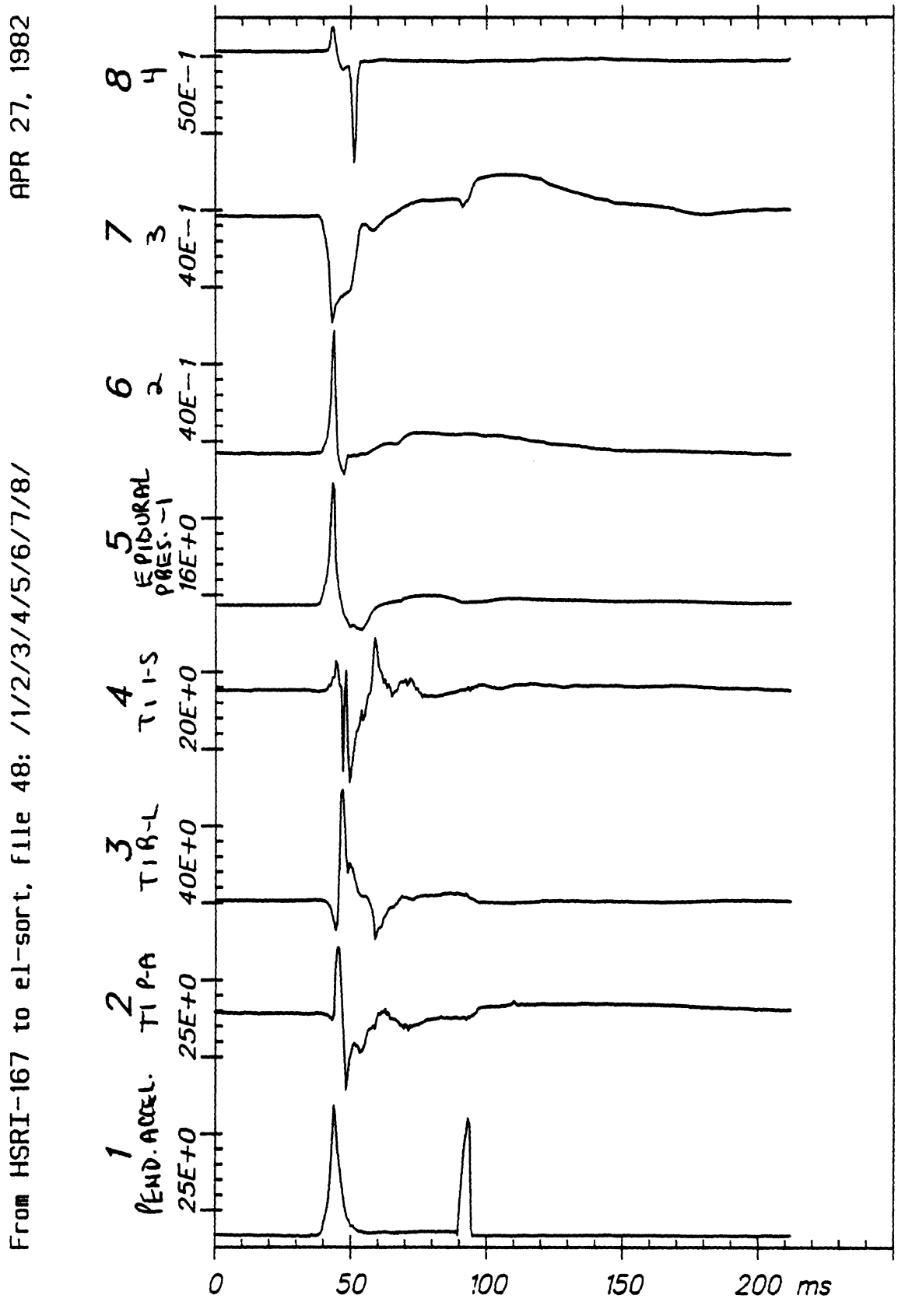

Time Histories 82E022 C3

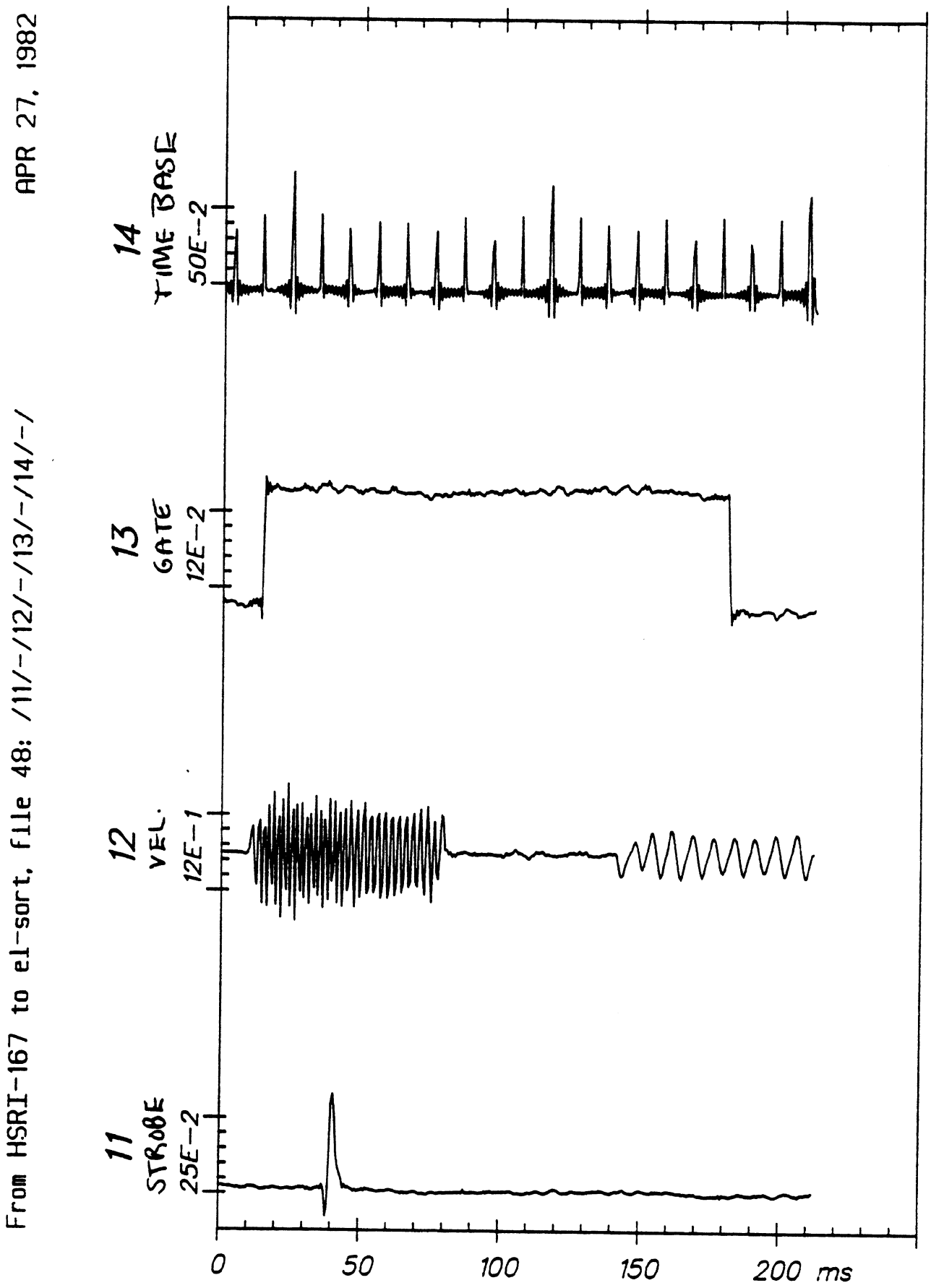

Time Histories 82E022 C3

Time Histories 82E023 H7

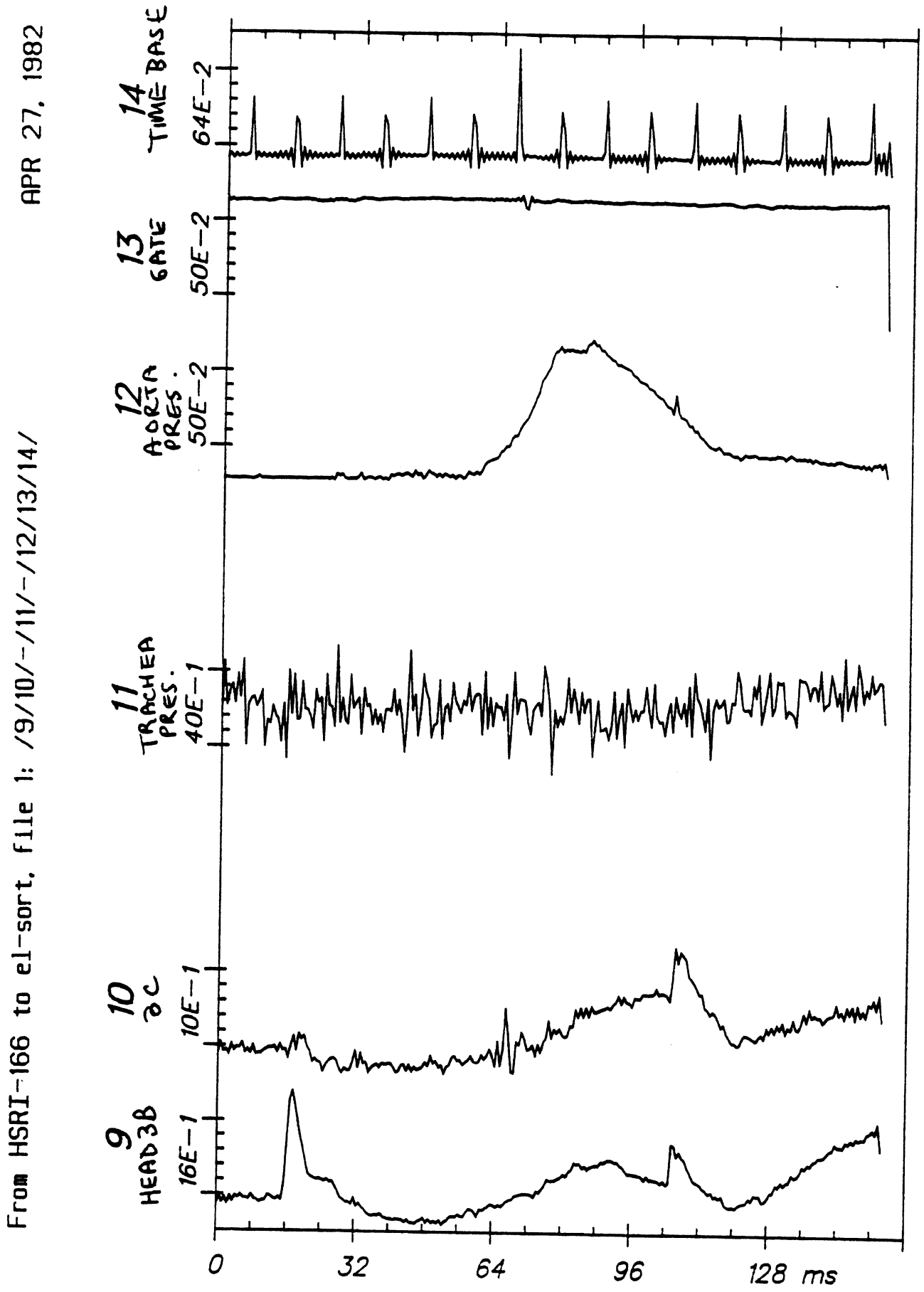

Time Histories 82E023 H7

From HSRI-167 to EL-SORT, File 13: /1/2/3/4/5/6/7/8/ APR 28, 1982

Time Histories 82E023 C3

From HSRI-167 to EL-SORT, File 13: /9/10/-/11/-/12/13/14/

APR 28, 1982

Time Histories 82E023 C3

From HSRI-177 to EL-SORT, file 25: /1/2/3/4/5/6/7/8/ APR 30, 1982

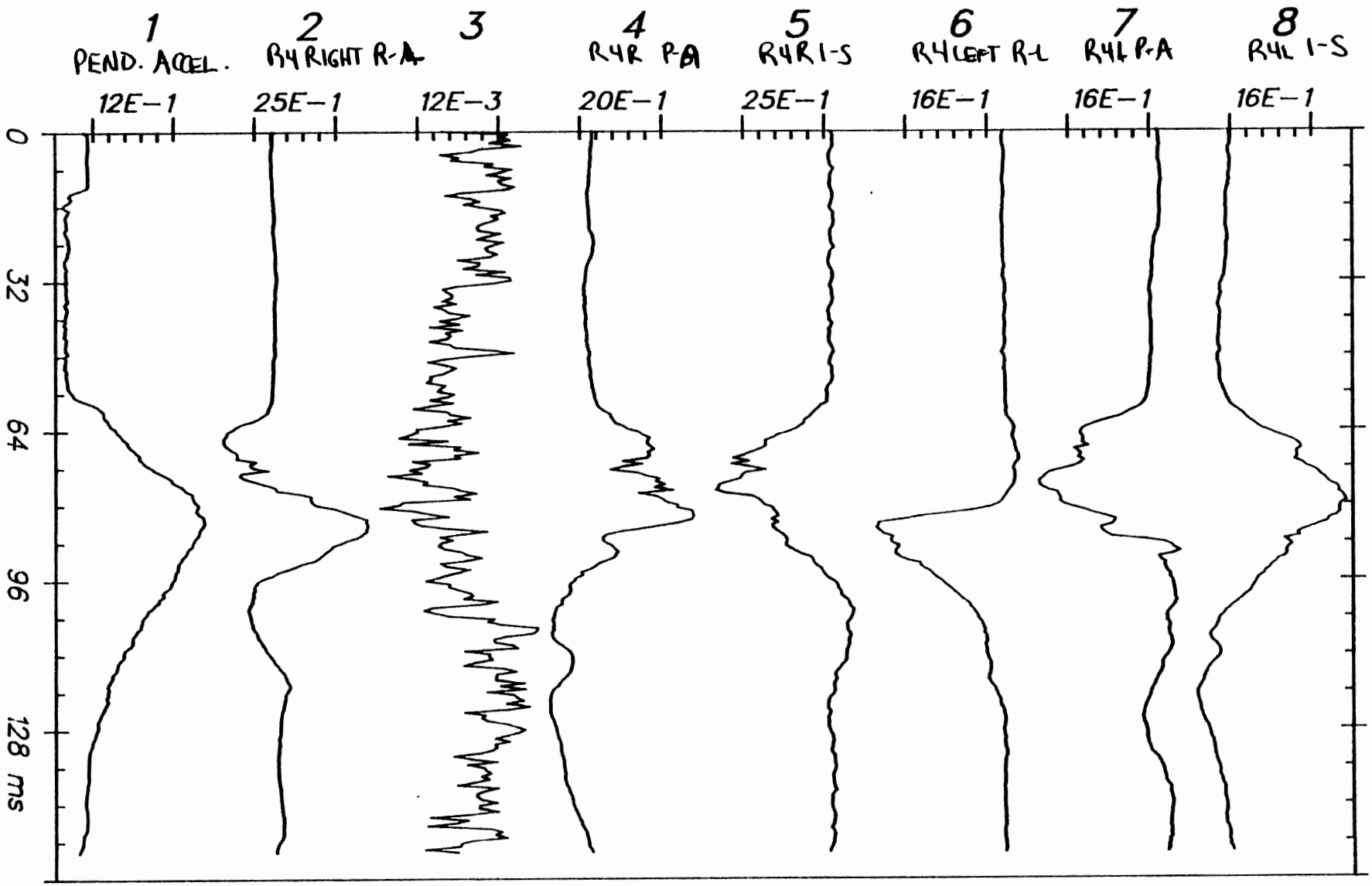

Time Histories 82E023 C4

From HSRI-177 to EL-SORT, file 25: /9/11/12/-/-/13/14/-/

APR 28, 1982

Time Histories 82E023 C4

Time Histories 82E024 H7

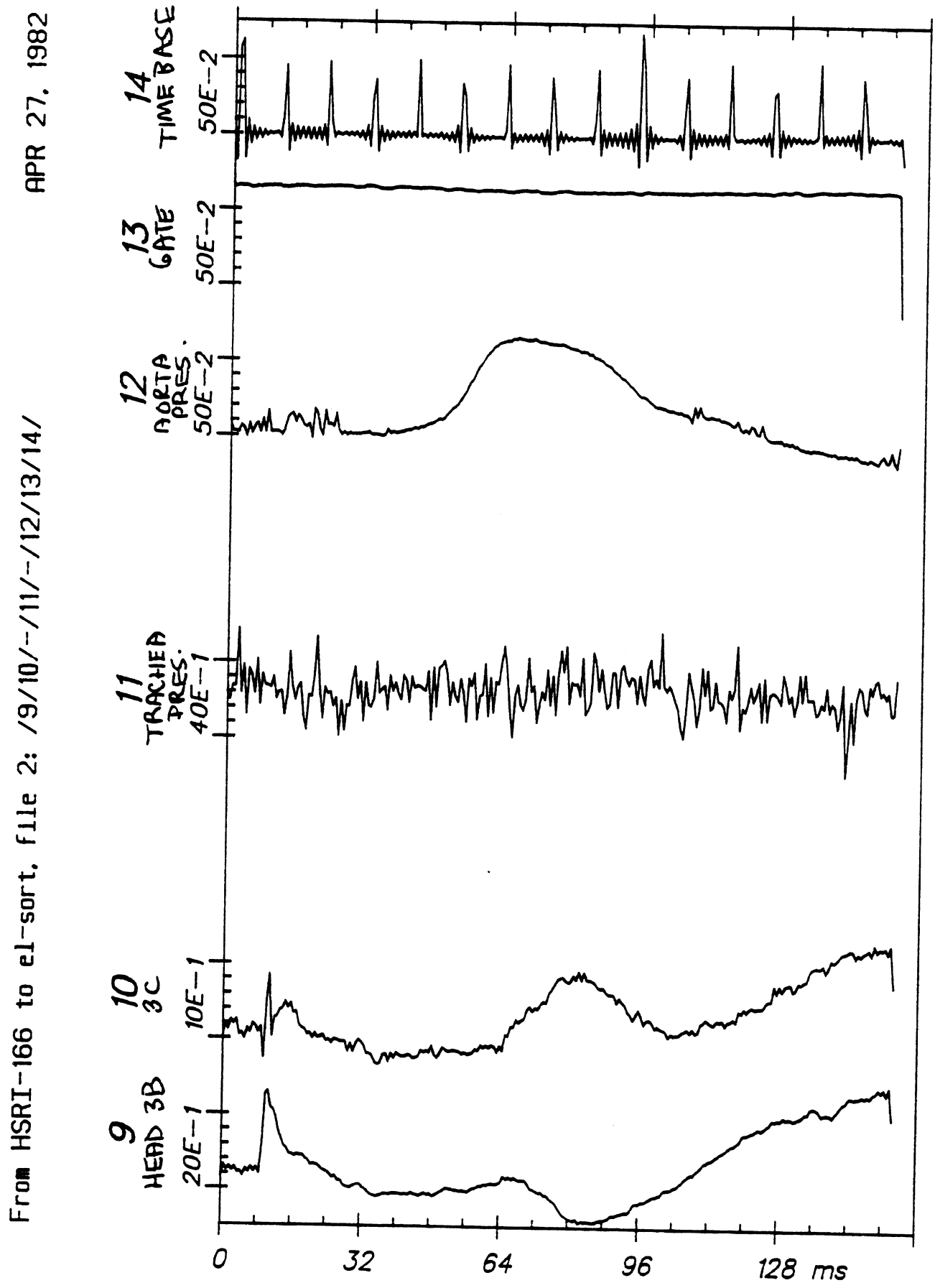

Time Histories 82E024 H7

Time Histories 82E024 C3

From HSRI-167 to EL-SORT, file 14: /9/10/-/11/-/12/13/14/

APR 28, 1982

Time Histories 82E024 C3

From HSRI-177 to EL-SORT, File 26: /1/2/3/4/5/6/7/8/

APR 30, 1982

Time Histories 82E024 C4

From HSRI-177 to EL-SORT, file 26: /9/11/12/-/-/13/14/-/

APR 28, 1982

Time Histories 82E024 C4

From HSRI-166 to el-sort, file 3: /1/2/3/4/5/6/7/8/

APR 27, 1982

Time Histories 82E025 H7

Time Histories 82E025 H7

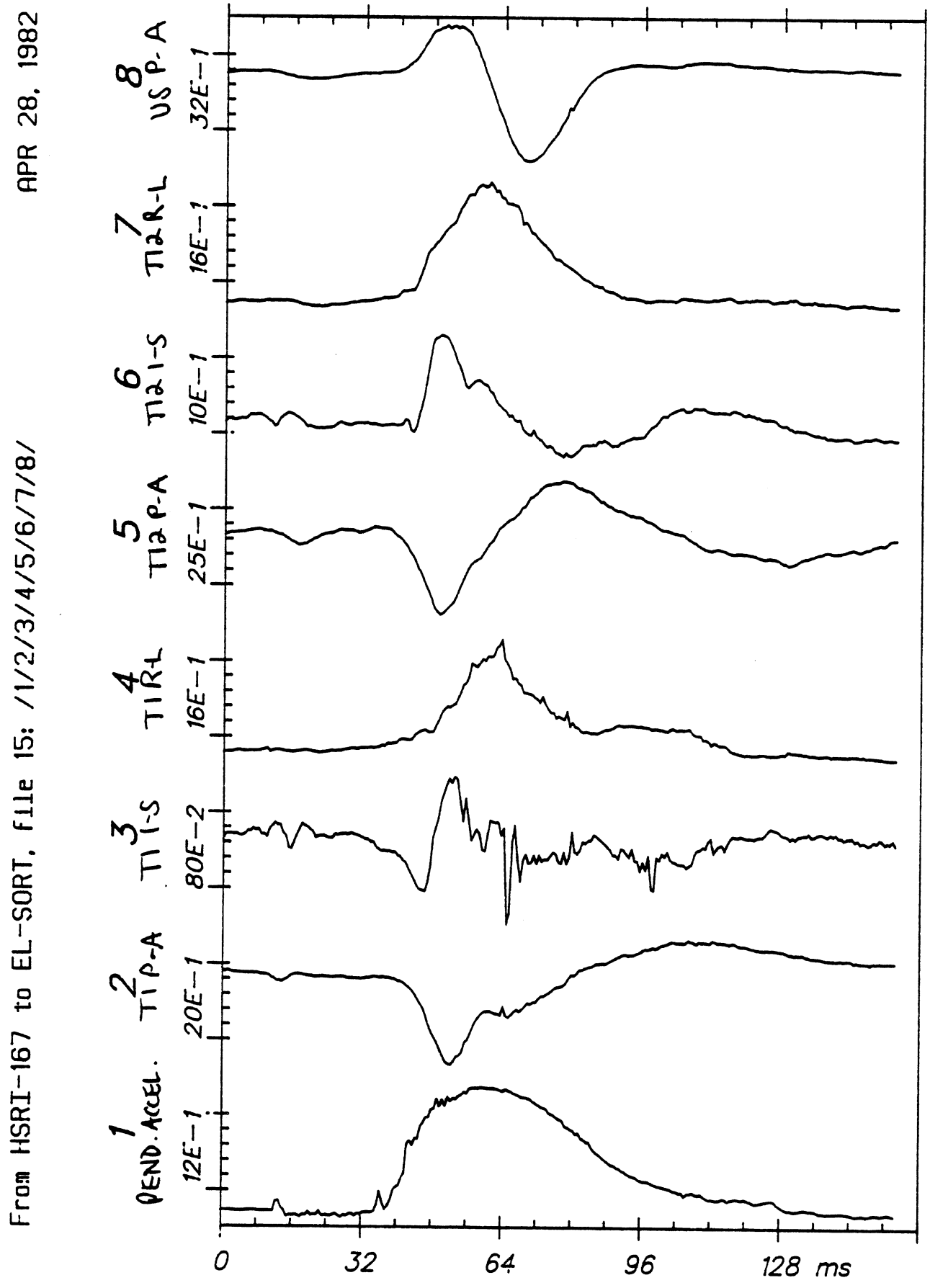

Time Histories 82E025 C3

From HSRI-167 to EL-SORT, file 15: /9/10/-/11/-/12/13/14/ APR 28, 1982

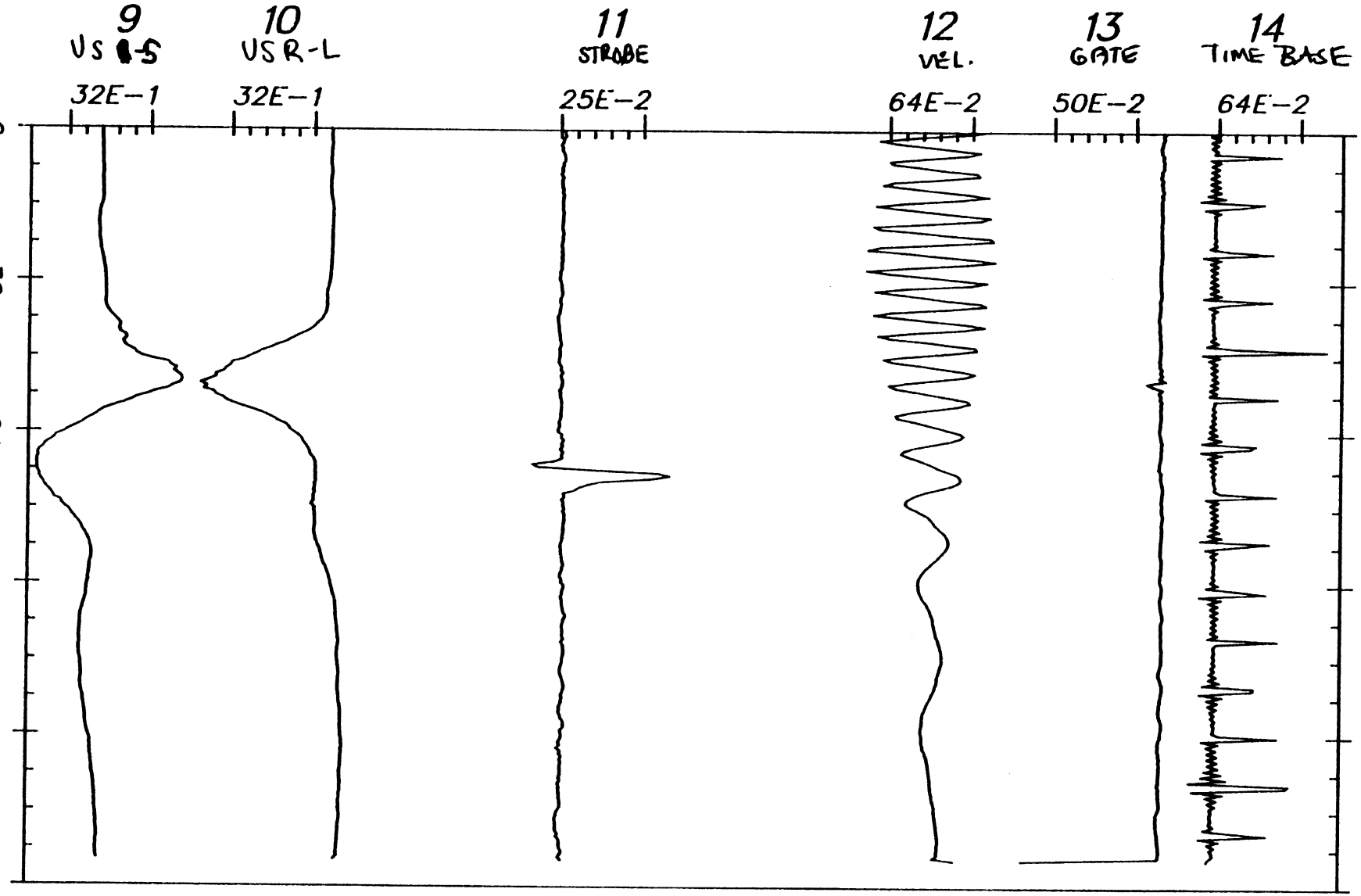

Time Histories 82E025 C3

D60

From HSRI-177 to EL-SORT, file 27: /1/2/3/4/5/6/7/8/

APR 30, 1982

Time Histories 82E025 C4

From HSRI-177 to EL-SORT, file 27: /9/11/12/-/-/13/14/-/

APR 28, 1982

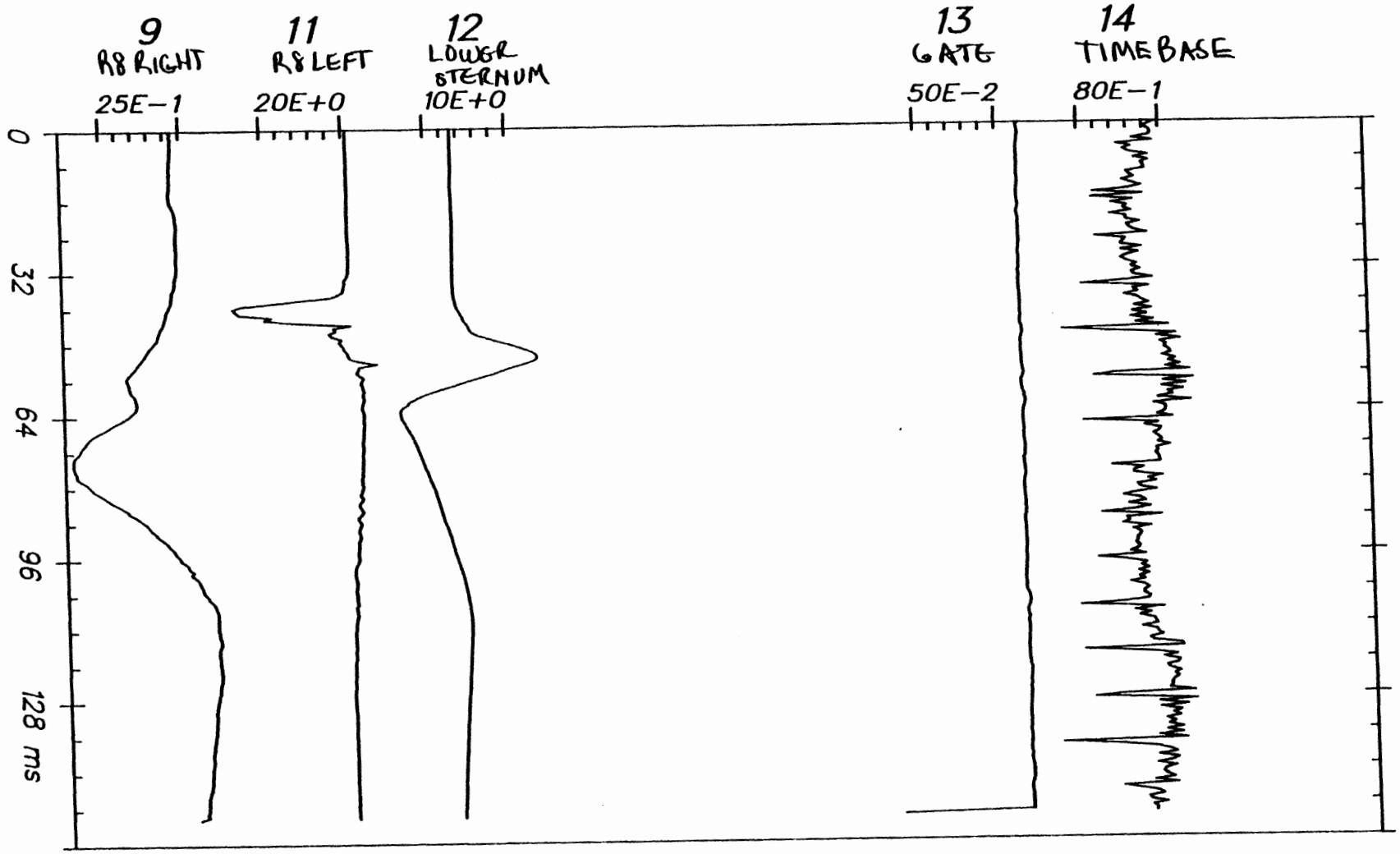

Time Histories

82E025 C4

D62

From HSRI-166 to EL-SORT, File 4: /1/2/3/4/5/6/7/8/
APR 28, 1982
1 PEND. ACCEL. 12E-1
2 HEAD1A 16E-1
3 1B 40E-1
4 1C 16E-1
5 2A 40E-1
6 2B 12E-1
7 2C 10E-1
8 3A 25E-1
0
32
64
96
128 ms
Time Histories
82E026
H7

From HSRI-166 to EL--SORT, File 4: /9/10/-/11/-/12/13/14/

APR 28, 1982

Time Histories 82E026 H7

From HSRI-167 to EL-SORT, File 16: /1/2/3/4/5/6/7/8/

APR 28, 1982

Time Histories 82E026 C3

From HSRI-167 to EL--SORT, file 16: /9/10/-/11/-/12/13/14/

APR 28, 1982

Time Histories 82E026 C3

From HSRI-177 to EL-SORT, file 28: /1/2/3/4/5/6/7/8/

APR 30, 1982

Time Histories 82E026 C4

APR 28, 1982

From HSRI-177 to EL-SORT, file 28: /9/11/12/-/-/13/14/-/

Time Histories 82E026 C4

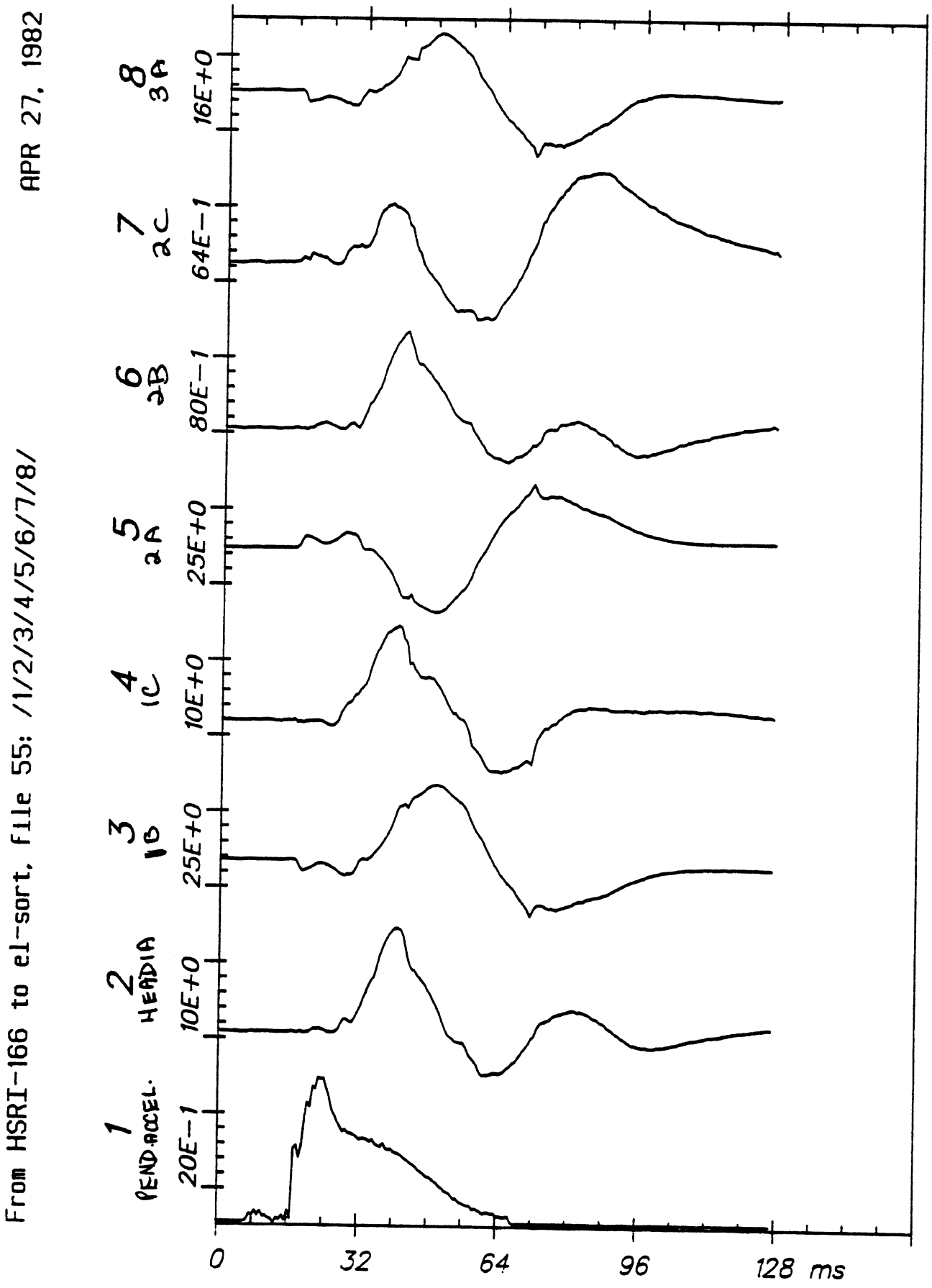

Time Histories 82E027 H7

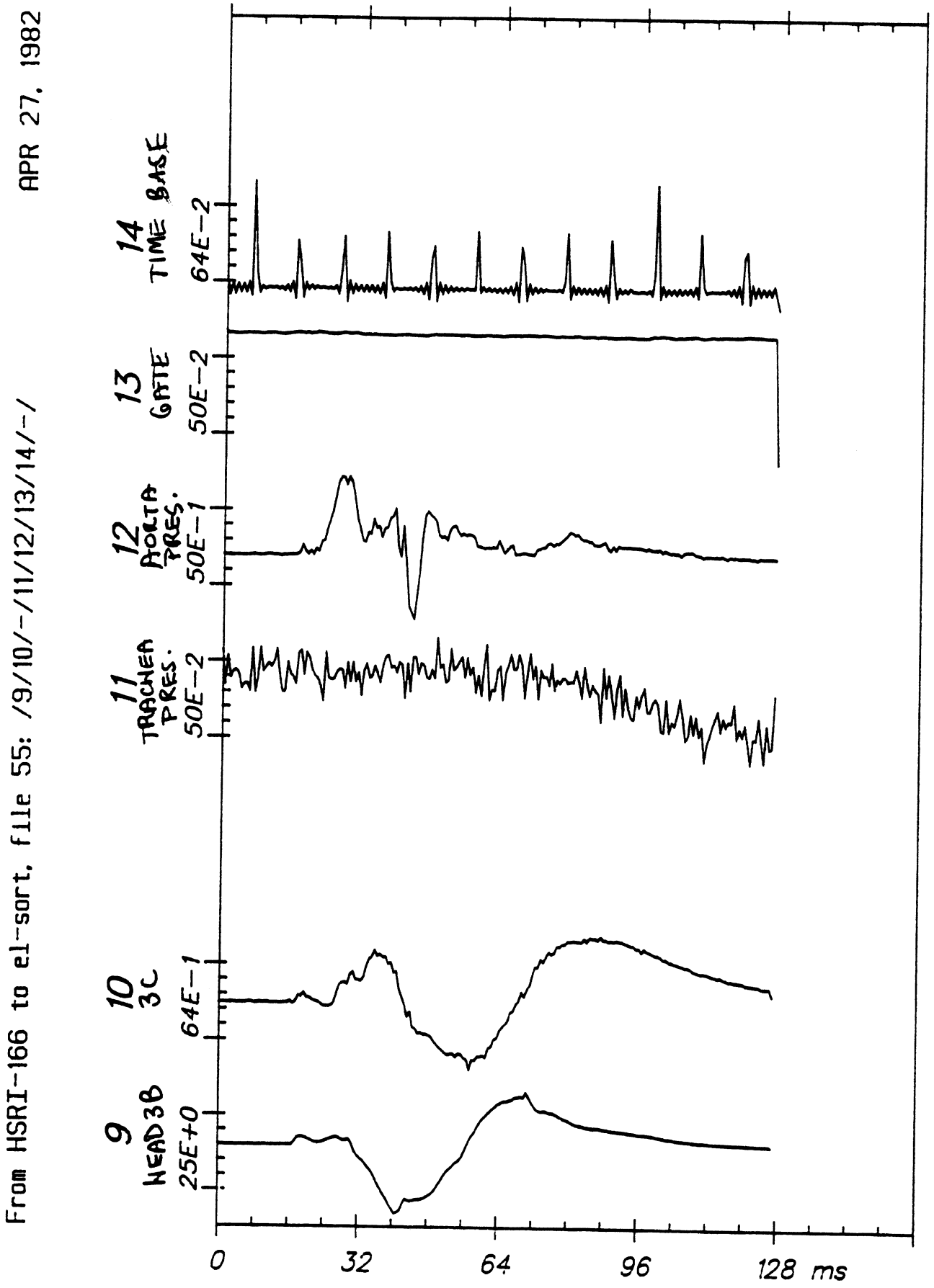
From HSRI-166 to el-sort, file 55: /9/10/-/11/12/13/14/-/
APR 27, 1982
14 TIME BASE 64E-2
13 GATE 50E-2
12 AORTA PRES. 50E-1
11 TRACHEA PRES. 50E-2
10 3C 64E-1
9 HEAD3B 25E+0
0
32
64
96
128 ms
Time Histories
82E027
H7

From HSRI-167 to el-sort, file 58: /1/2/3/4/5/6/7/8/ APR 27, 1982

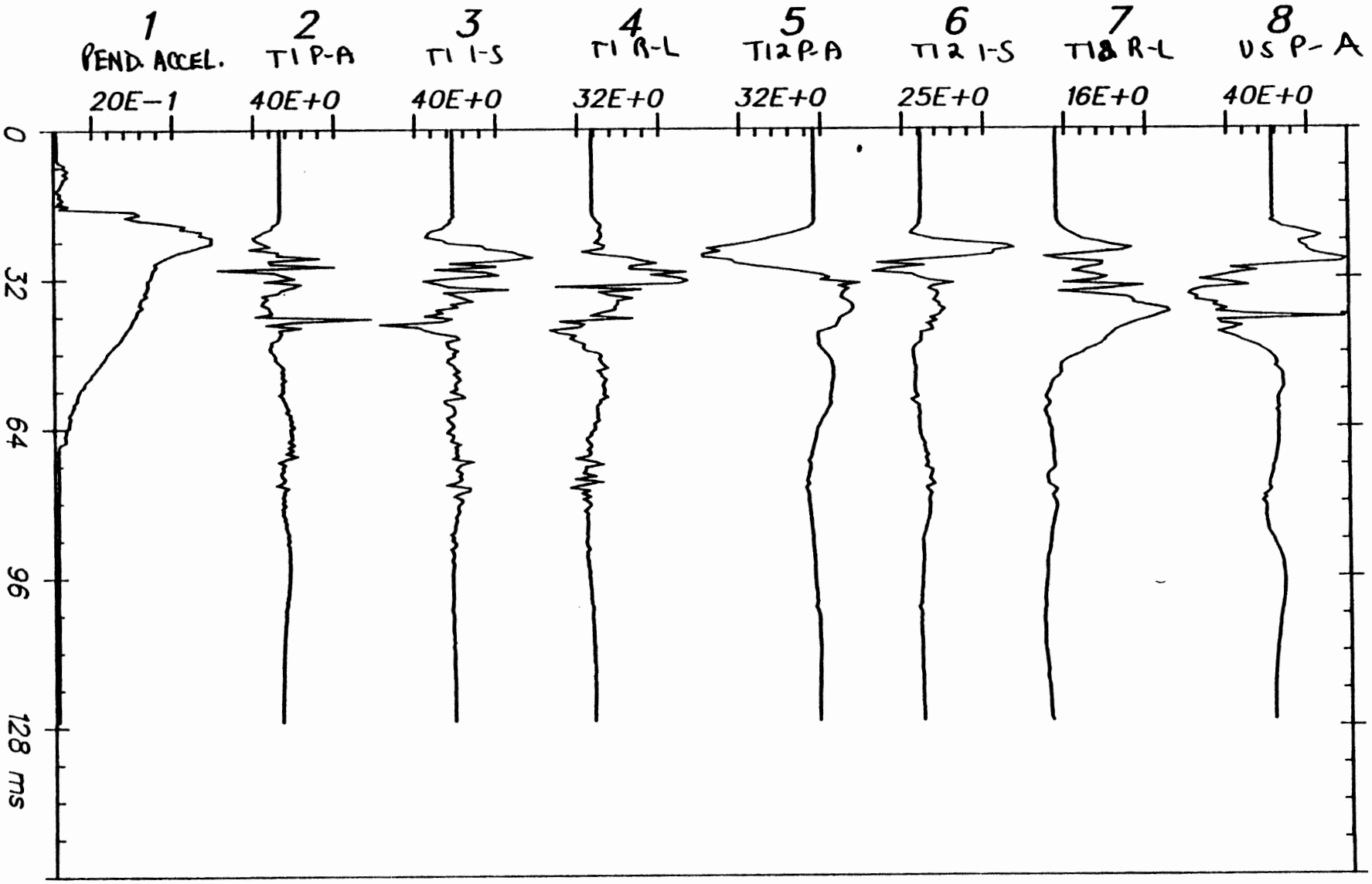

Time Histories

82E027 C3

D71

Time Histories 82E027 C3

From HSRI-~~167~~ 177 to el-sort, file 61: /1/2/-/4/5/6/7/8/ APR 27, 1982

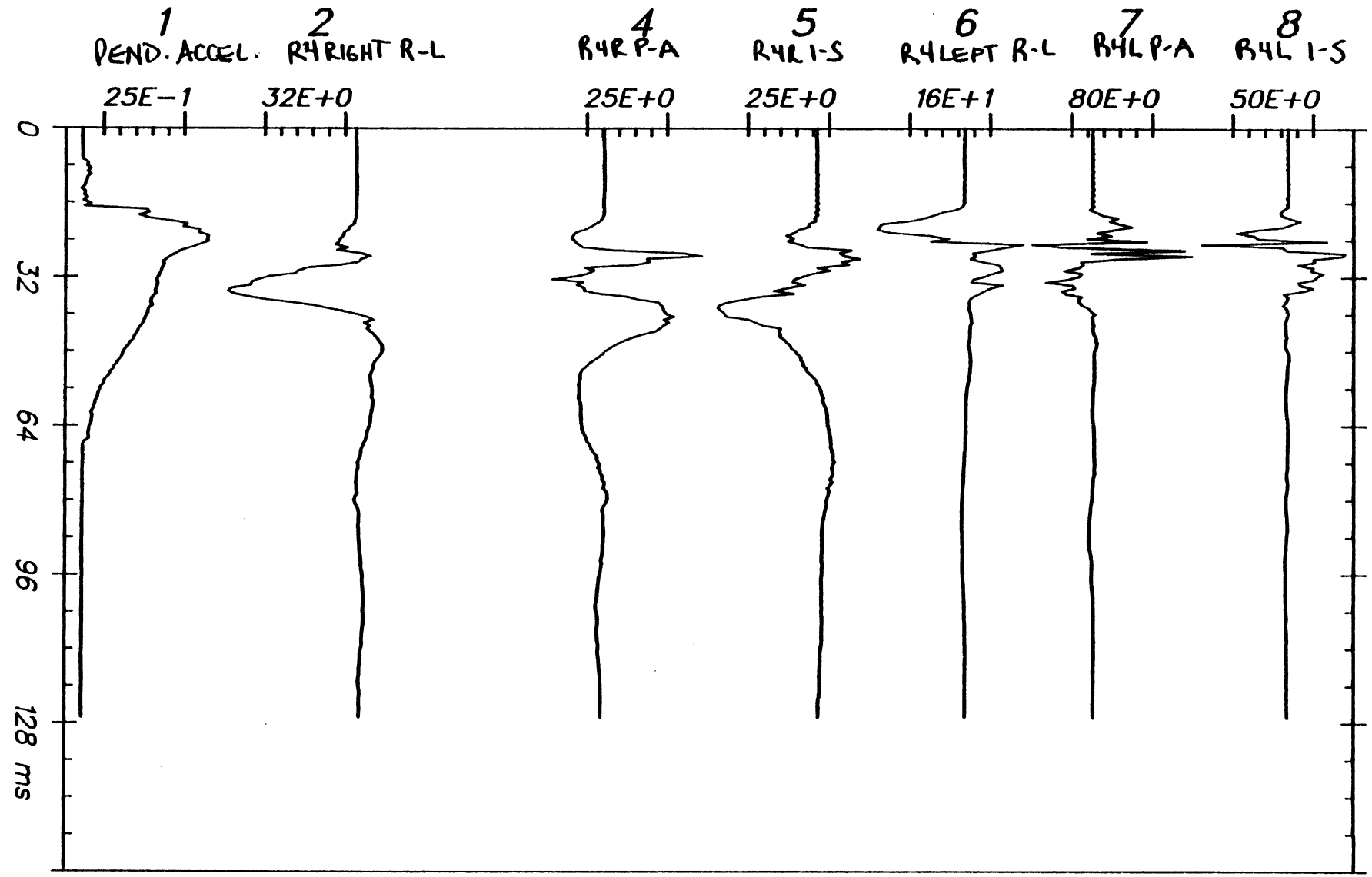

Time Histories 82E027 C4

D73

From HSRI-~~167~~ 171 to el-sort, file 61: /9/11/-/-/12/13/14/-/

APR 27, 1982

Time Histories 82E027 C4

From HSRI-166 to el-sort, file 52: /1/2/3/4/5/6/7/8/ APR 27, 1982

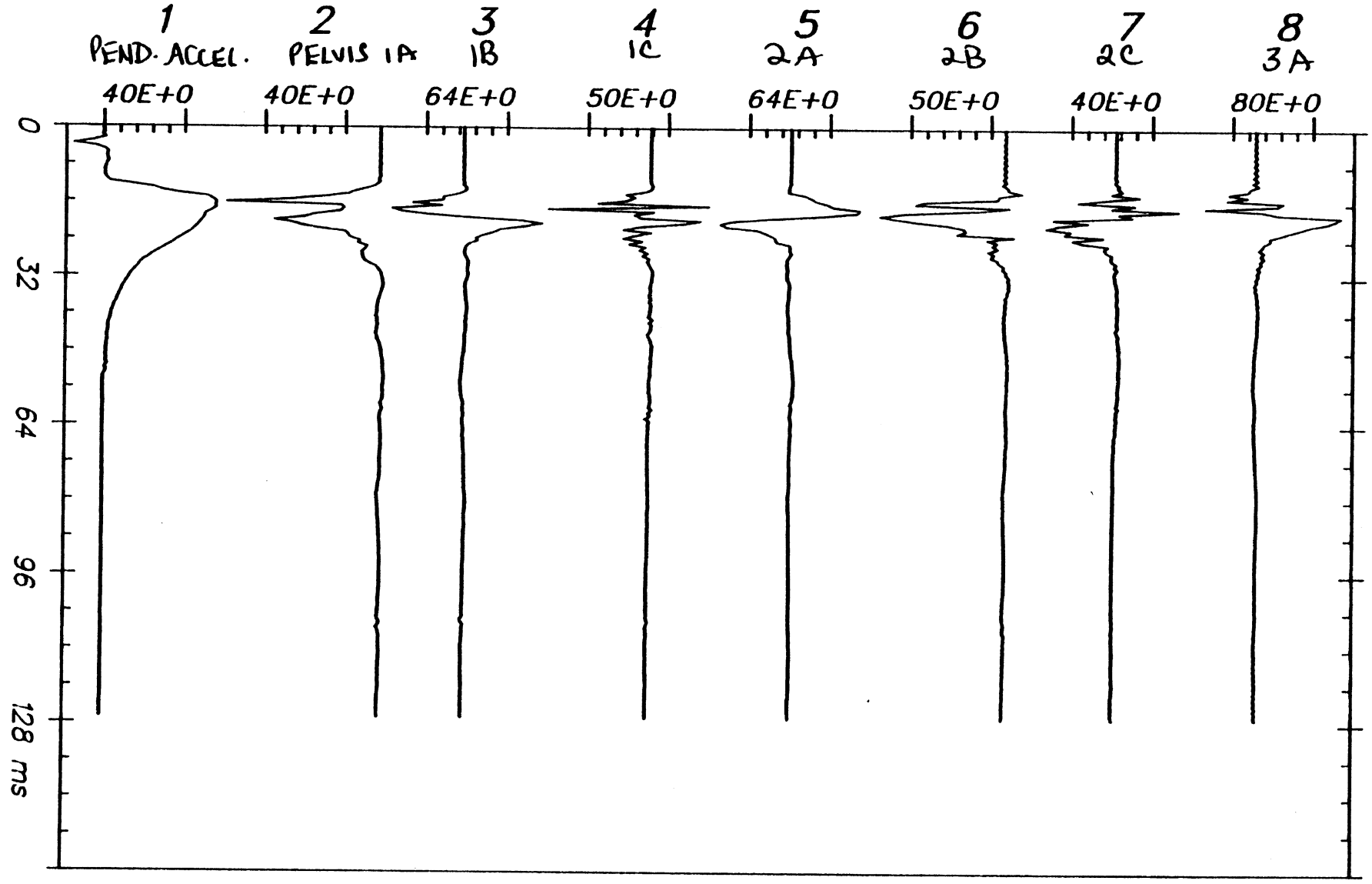

Time Histories 82E028 H7

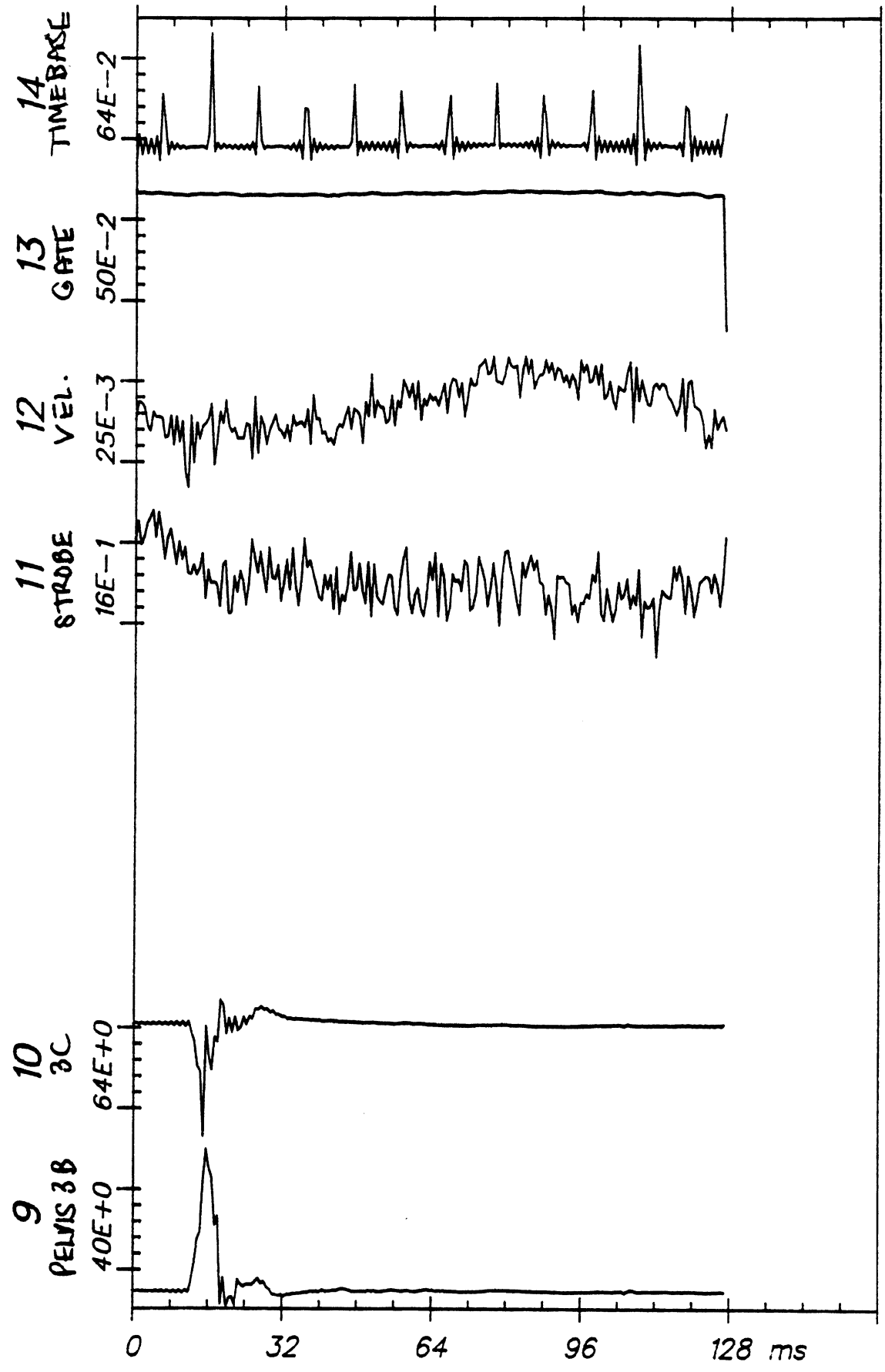

Time Histories 82E028 H7

From HSRI-166 to el-sort, file 42: /1/2/3/4/5/6/7/8/ APR 27, 1982

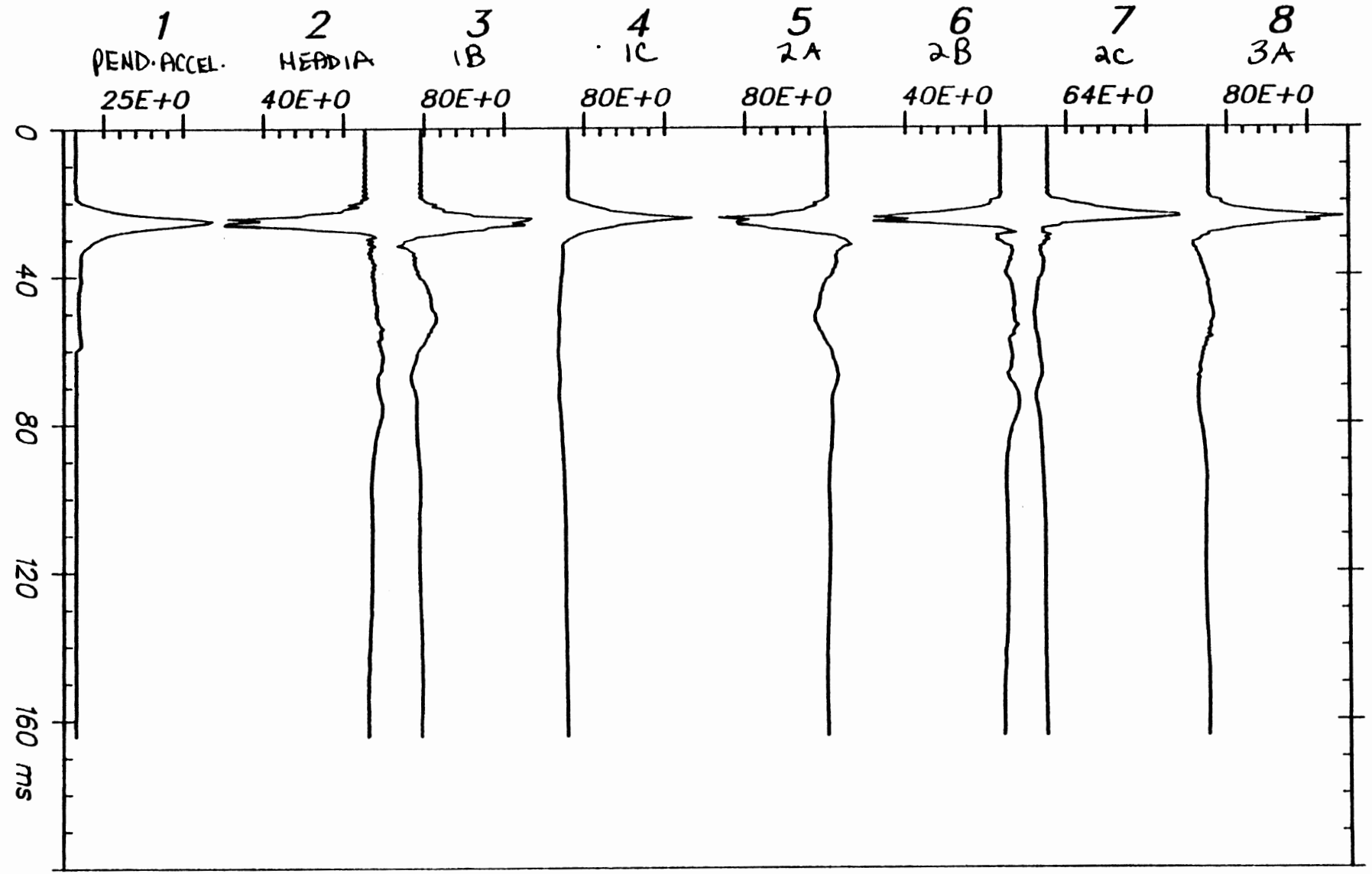

Time Histories 82E041 H7

D77

From HSRI-166 to el-sort, file 42: /9/10/11/12/13/14/-/-/

APR 27, 1982

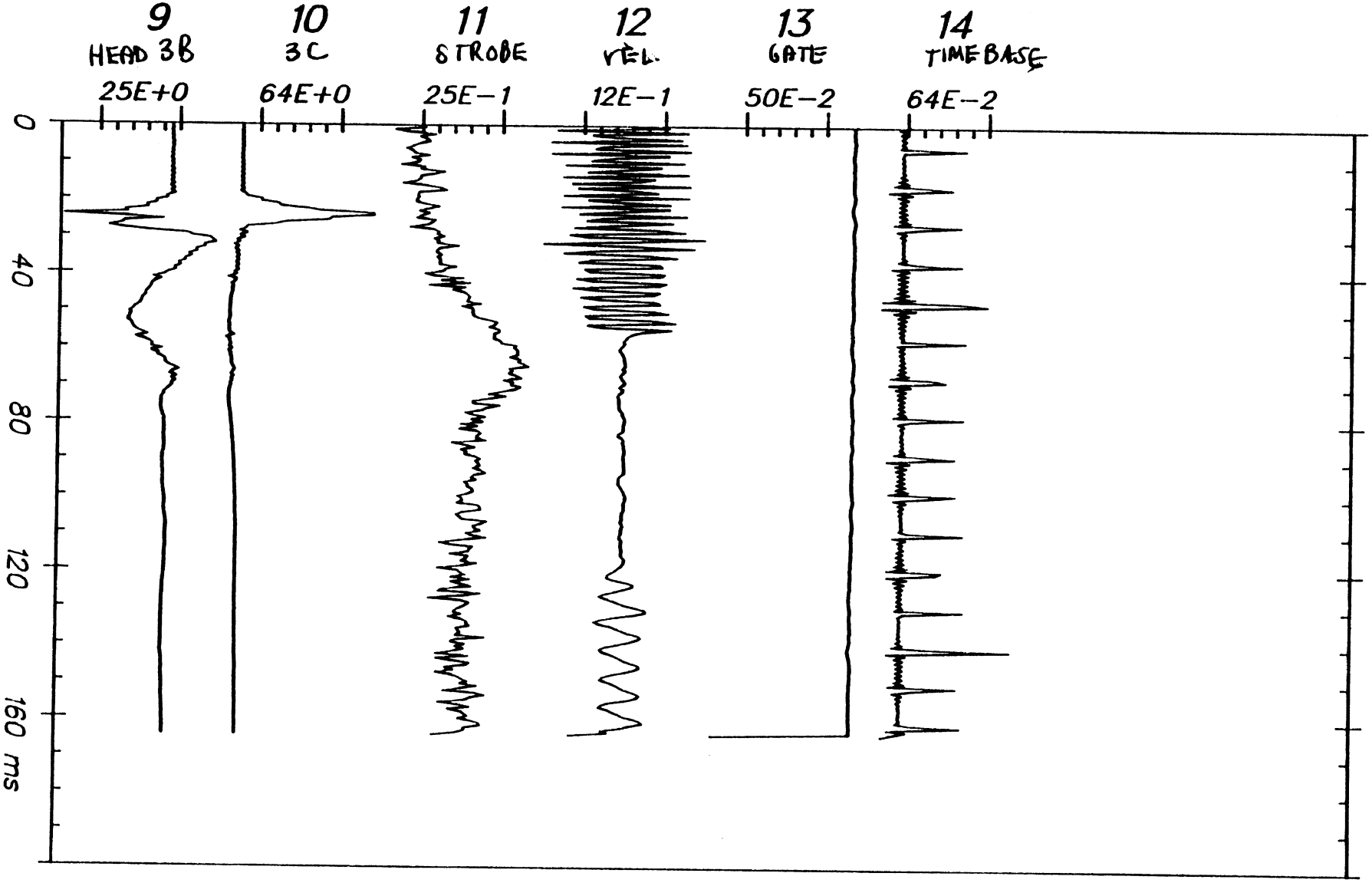

Time Histories

82E041

H7

D78

From HSRI-167 to el-sort, file 49: /1/2/3/4/5/6/7/8/ APR 27, 1982

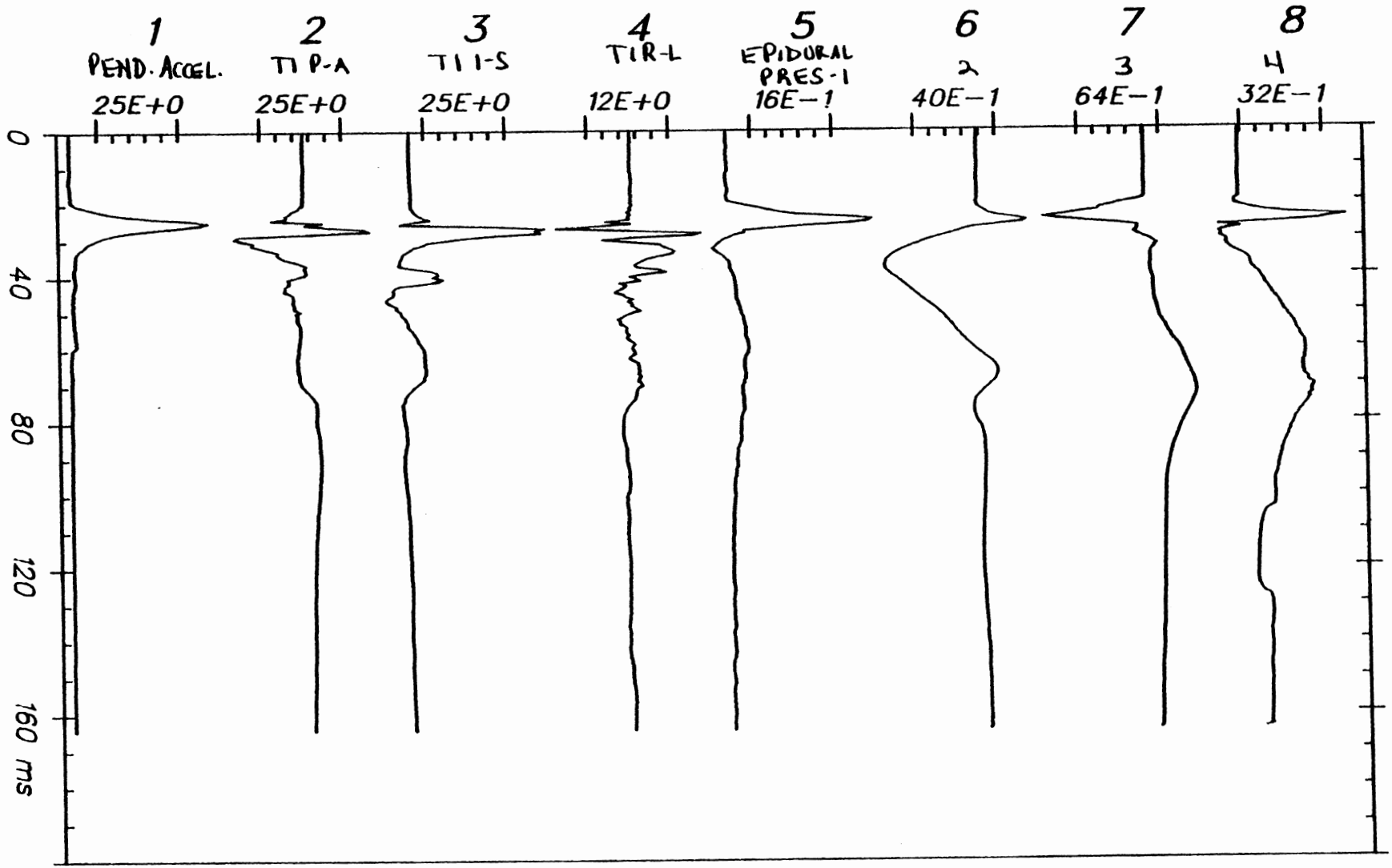

Time Histories 82E041 C3

From HSRI-167 to el-sort, file 49: /9/-/-/11/12/13/14/-/

APR 27, 1982

Time Histories 82E041 C3

From HSRI-166 to el-sort, file 43: /1/2/3/4/5/6/7/8/ APR 27, 1982

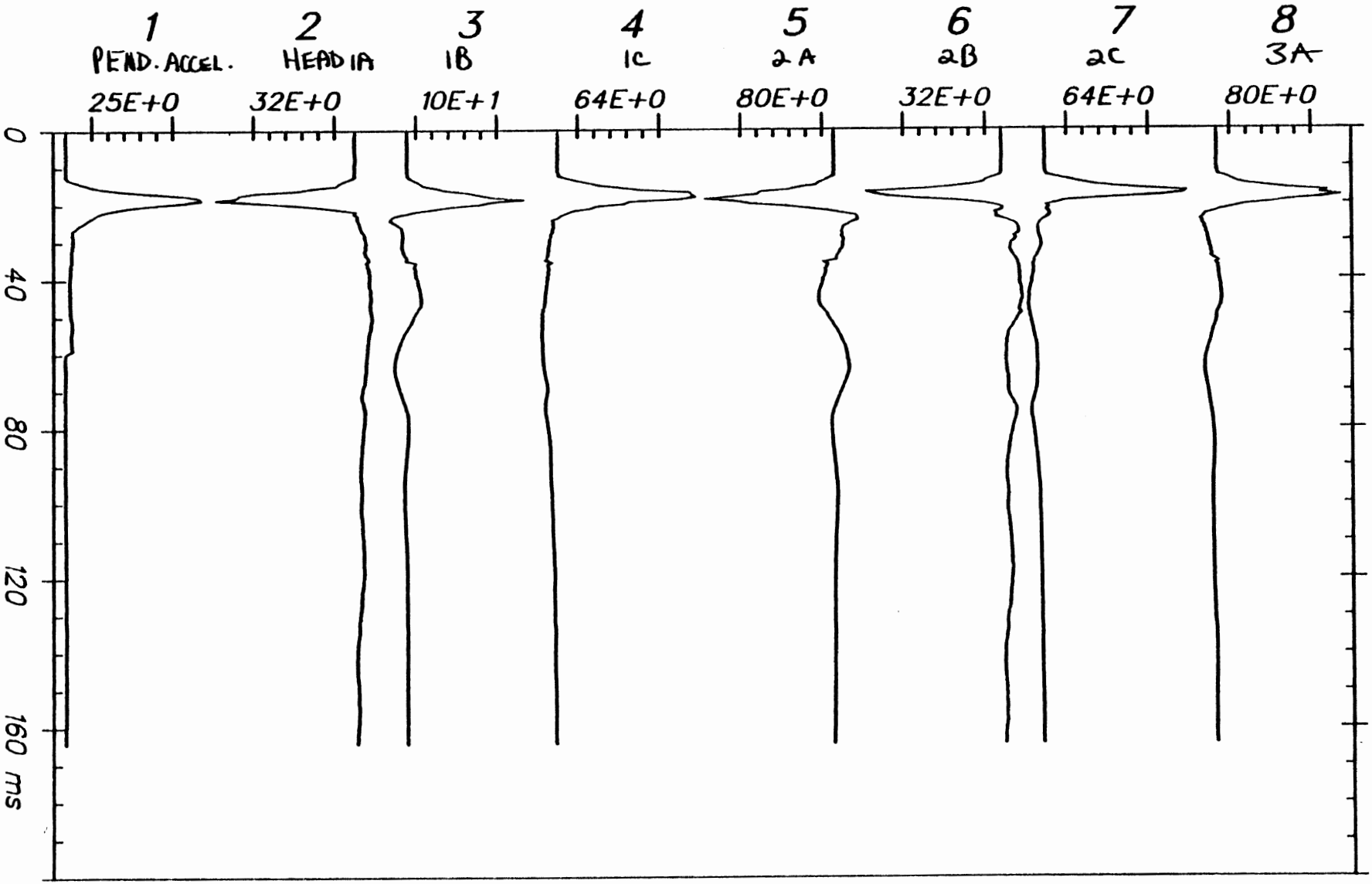

Time Histories 82E042 H7

D81

From HSRI-166 to el-sort, file 43: /9/10/11/12/13/14/-/-/

APR 27, 1982

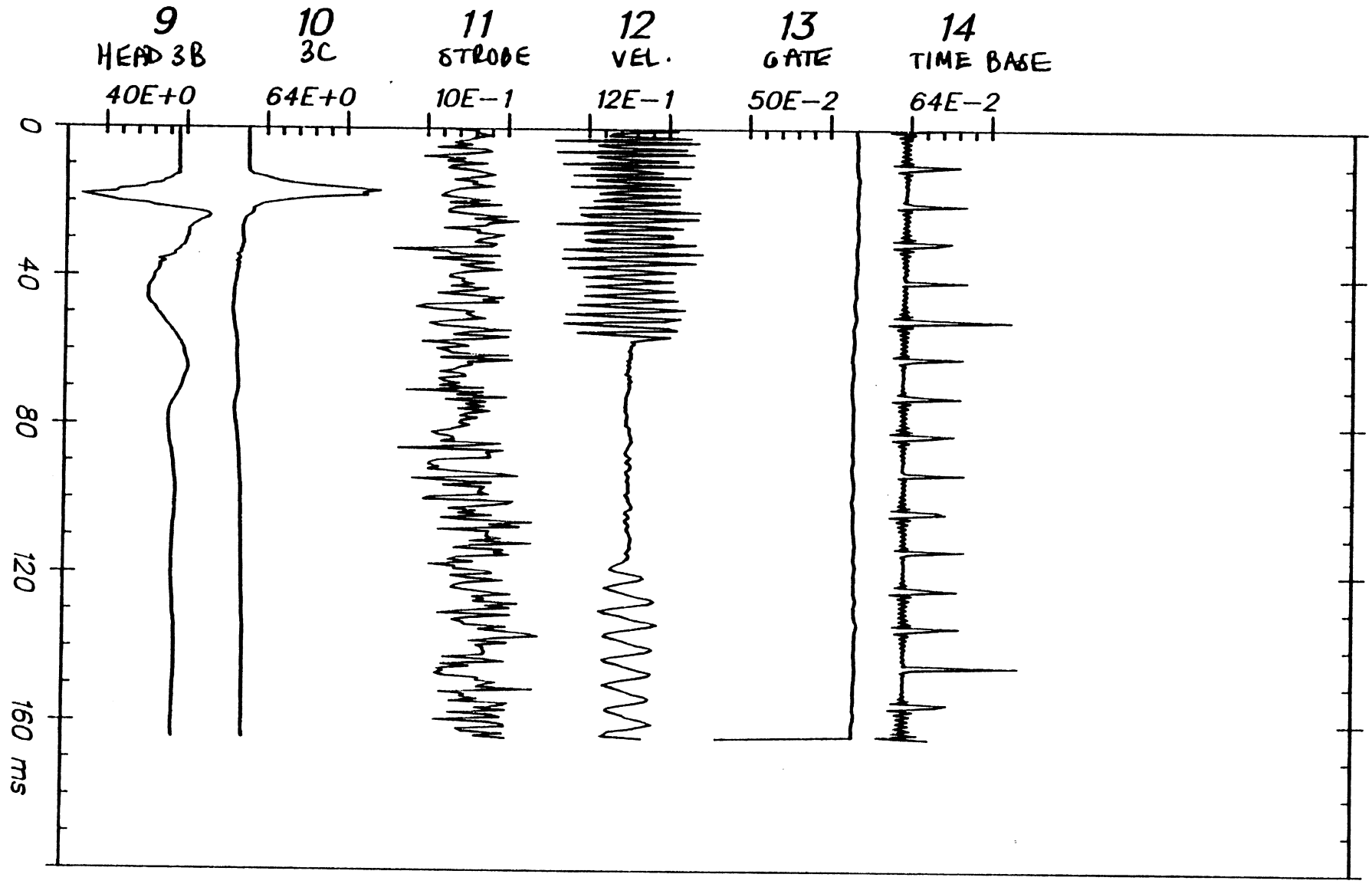

Time Histories

82E042

H7

D82

From HSRI-167 to el-sort, file 50: /1/2/3/4/5/6/7/8/ APR 27, 1982

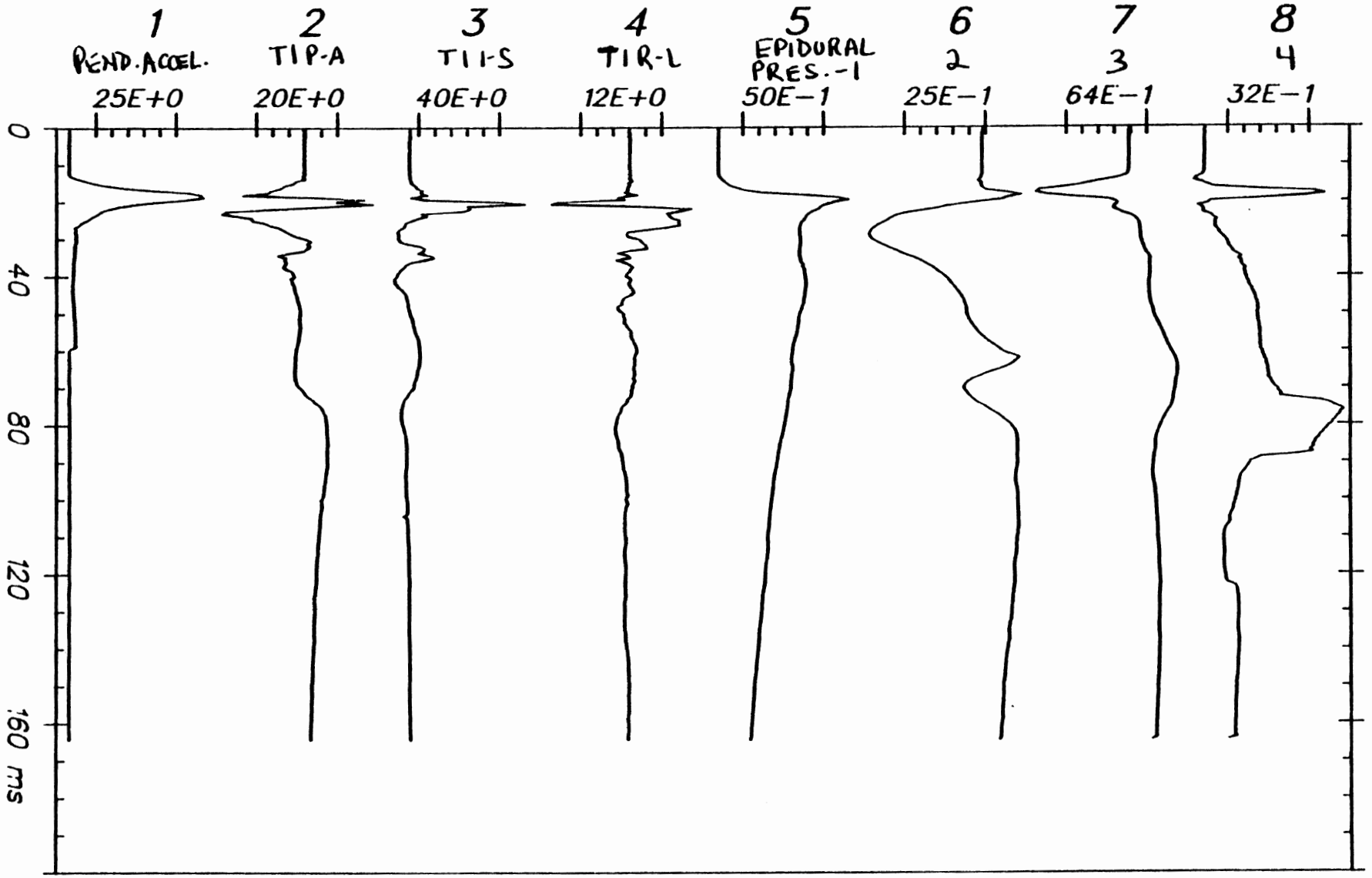

Time Histories 82E042 C3

From HSRI-167 to el-sort, file 50: /9/-/-/11/12/13/14/-/ APR 27, 1982

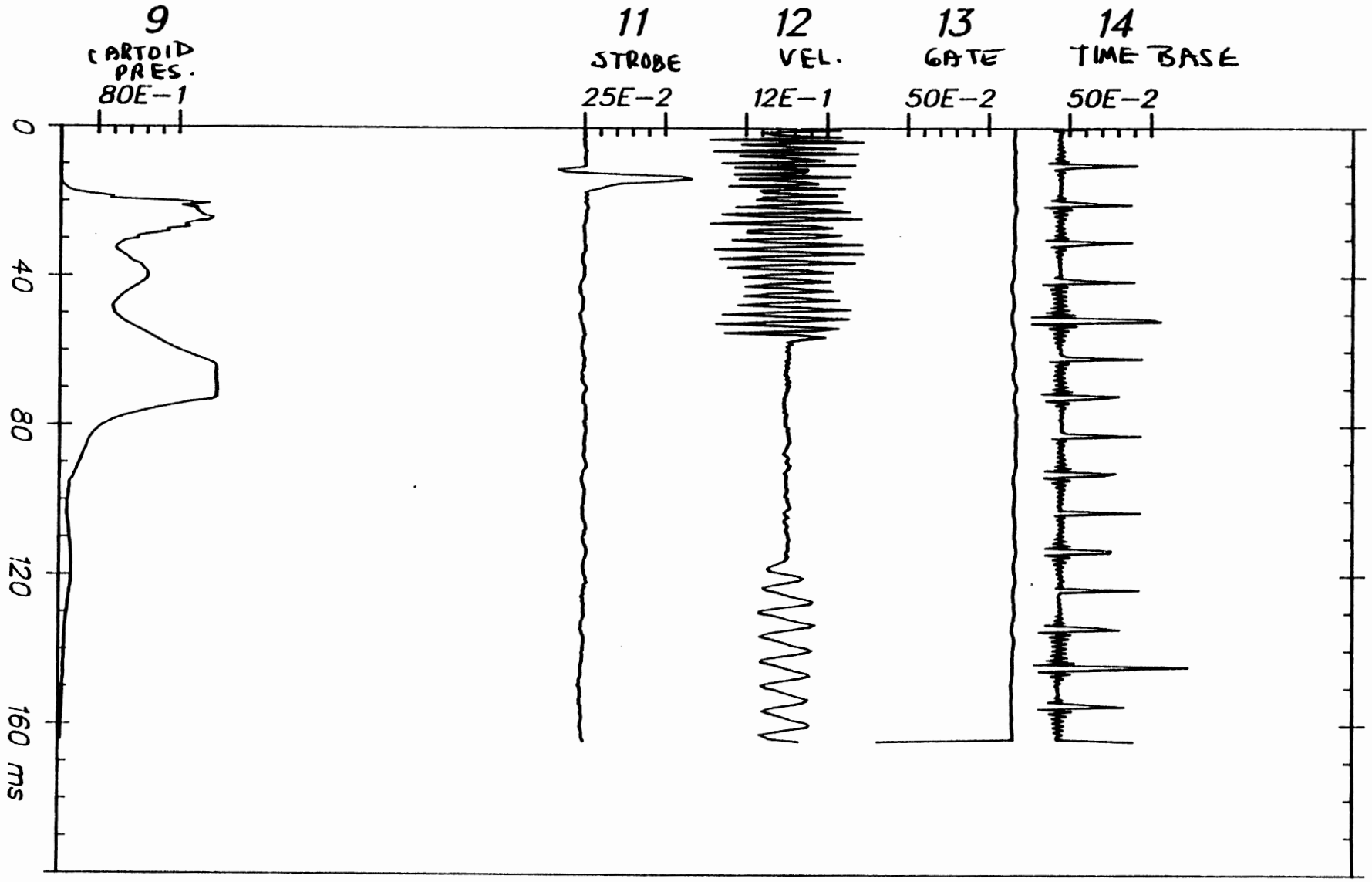

Time Histories 82E042 C3

From HSRI-166 to EL-SORT, file 5: /1/2/3/4/5/6/7/8/ APR 28, 1982

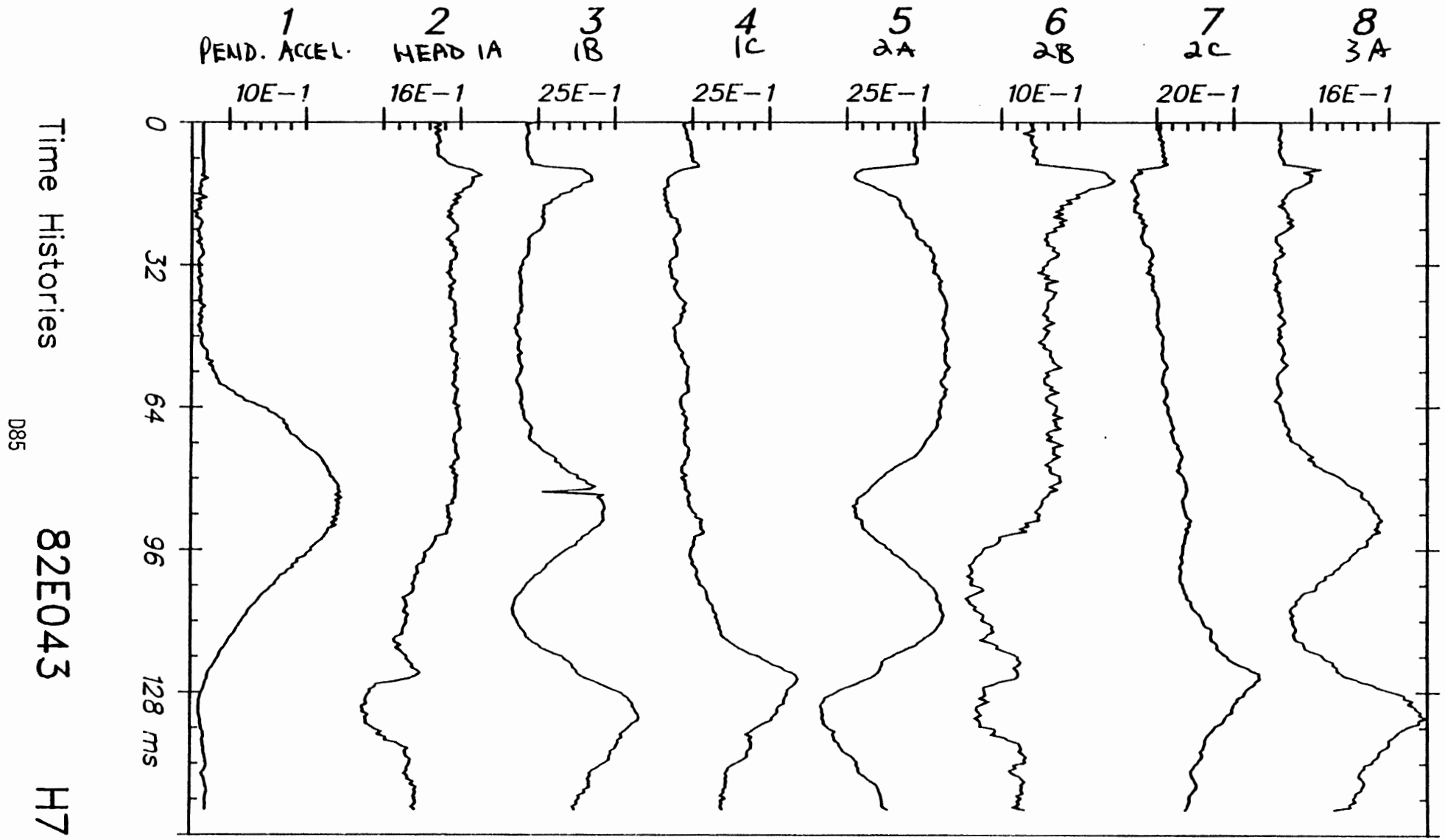

Time Histories

D85

82E043 H7

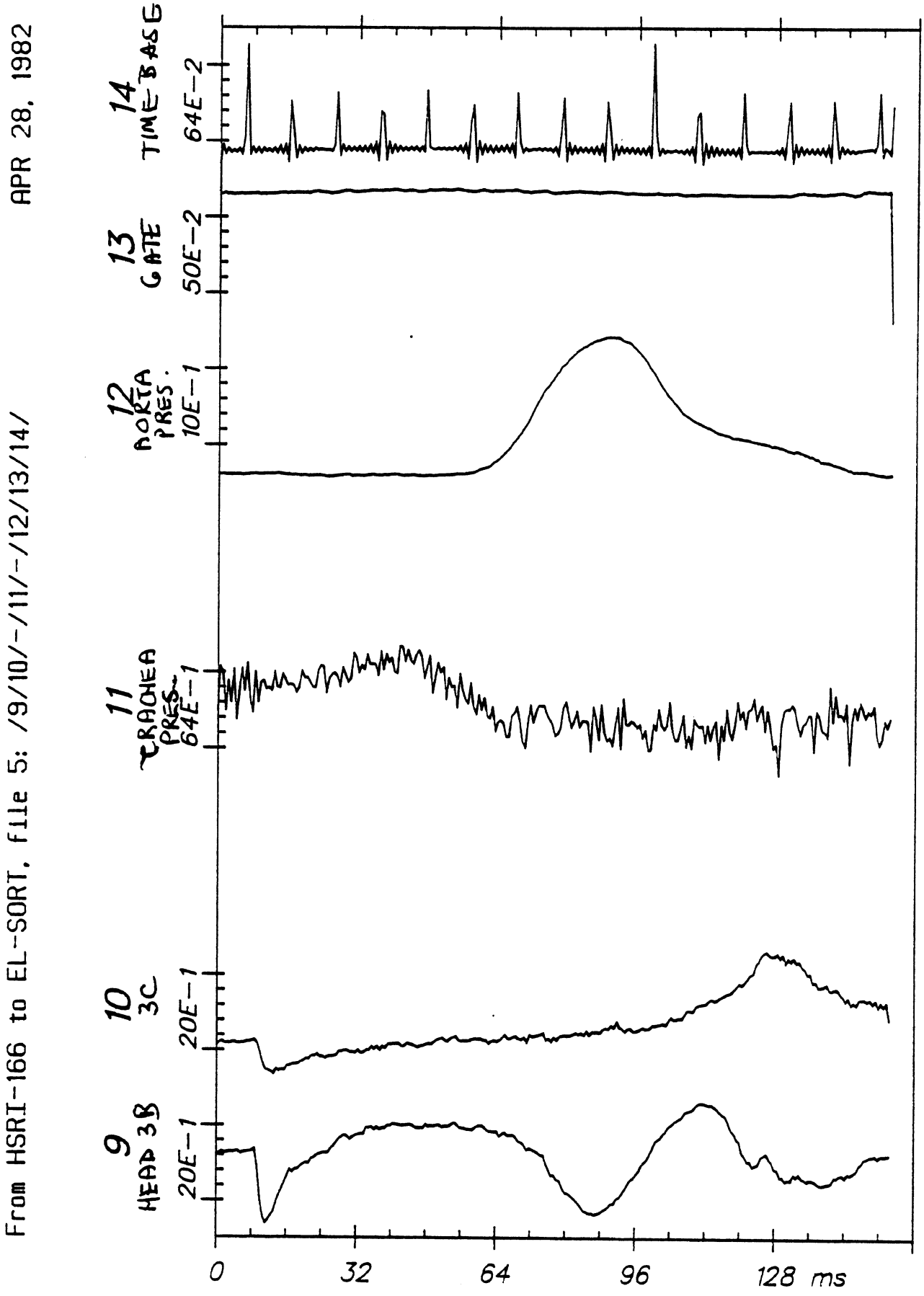

Time Histories 82E043 H7

From HSRI-167 to EL-SORT, file 17: /1/2/3/4/5/6/7/8/ APR 28, 1982

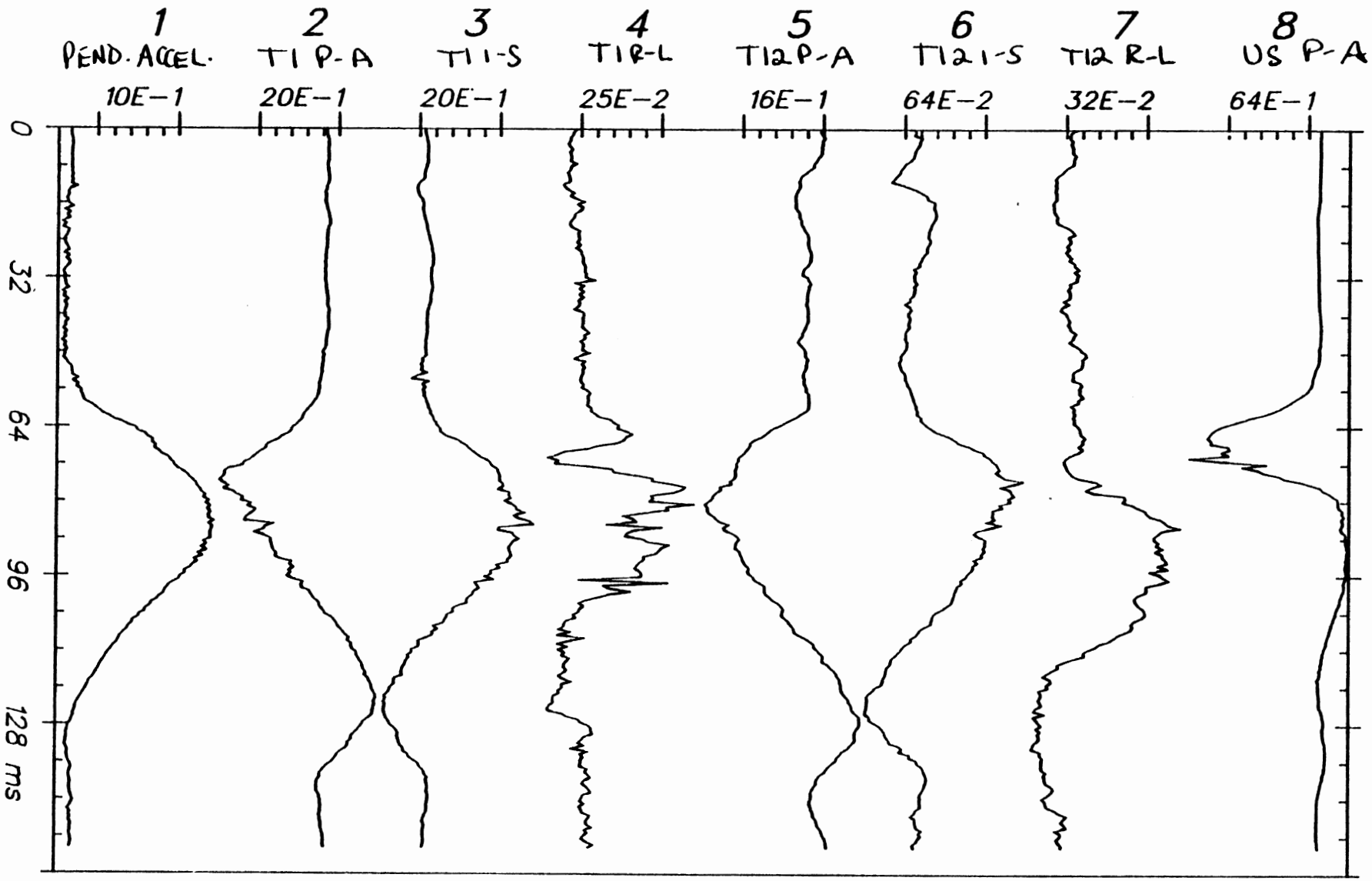

Time Histories

D87

82E043 C3

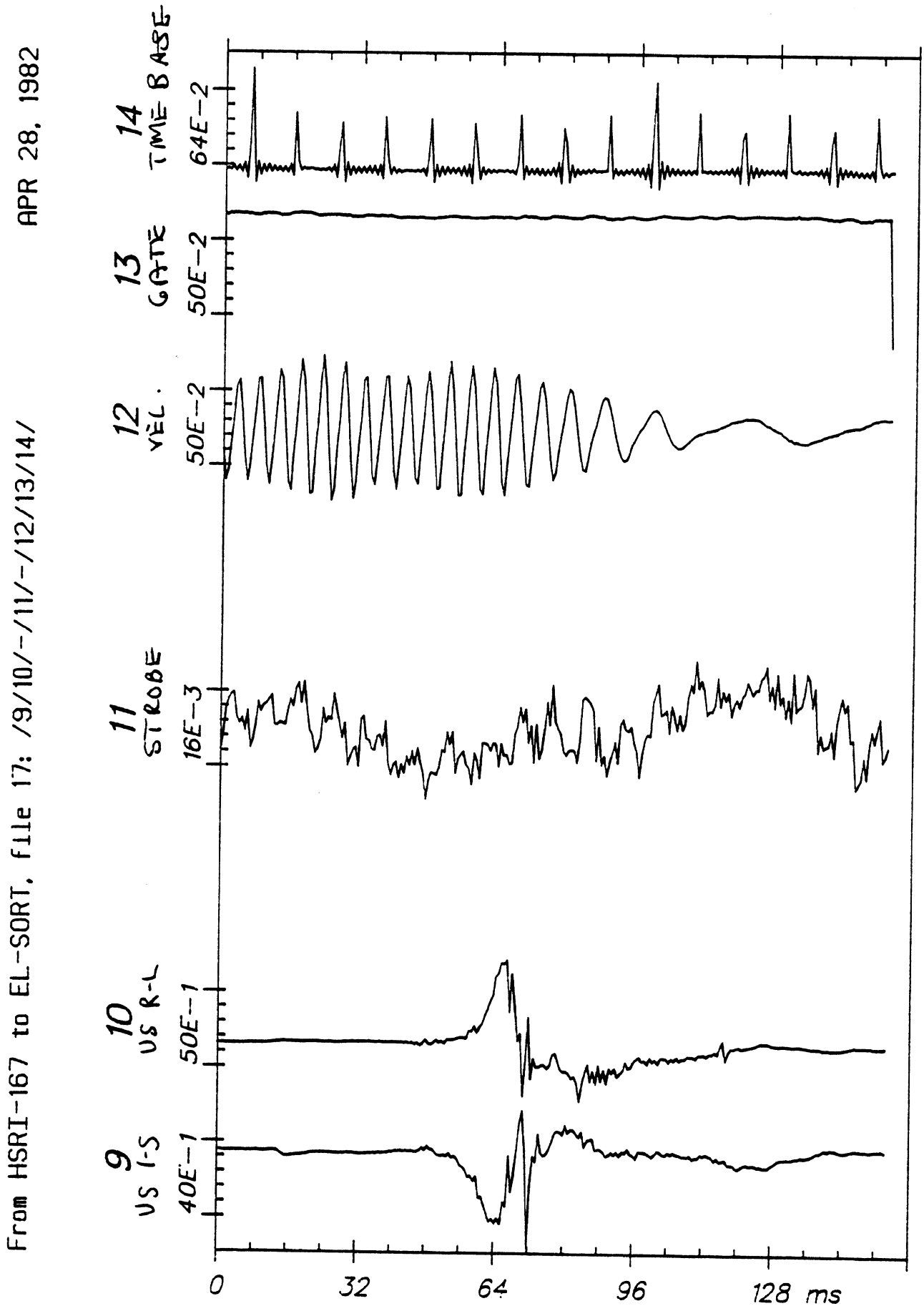
From HSRI-167 to EL-SORT, File 17: /9/10/-/11/-/12/13/14/
APR 28, 1982
14 TIME BASE
64E-2
13 GATE
50E-2
12 VEL.
50E-2
11 STROBE
16E-3
10 US R-L
50E-1
9 US I-S
40E-1
0
32
64
96
128 ms
Time Histories
82E043
C3

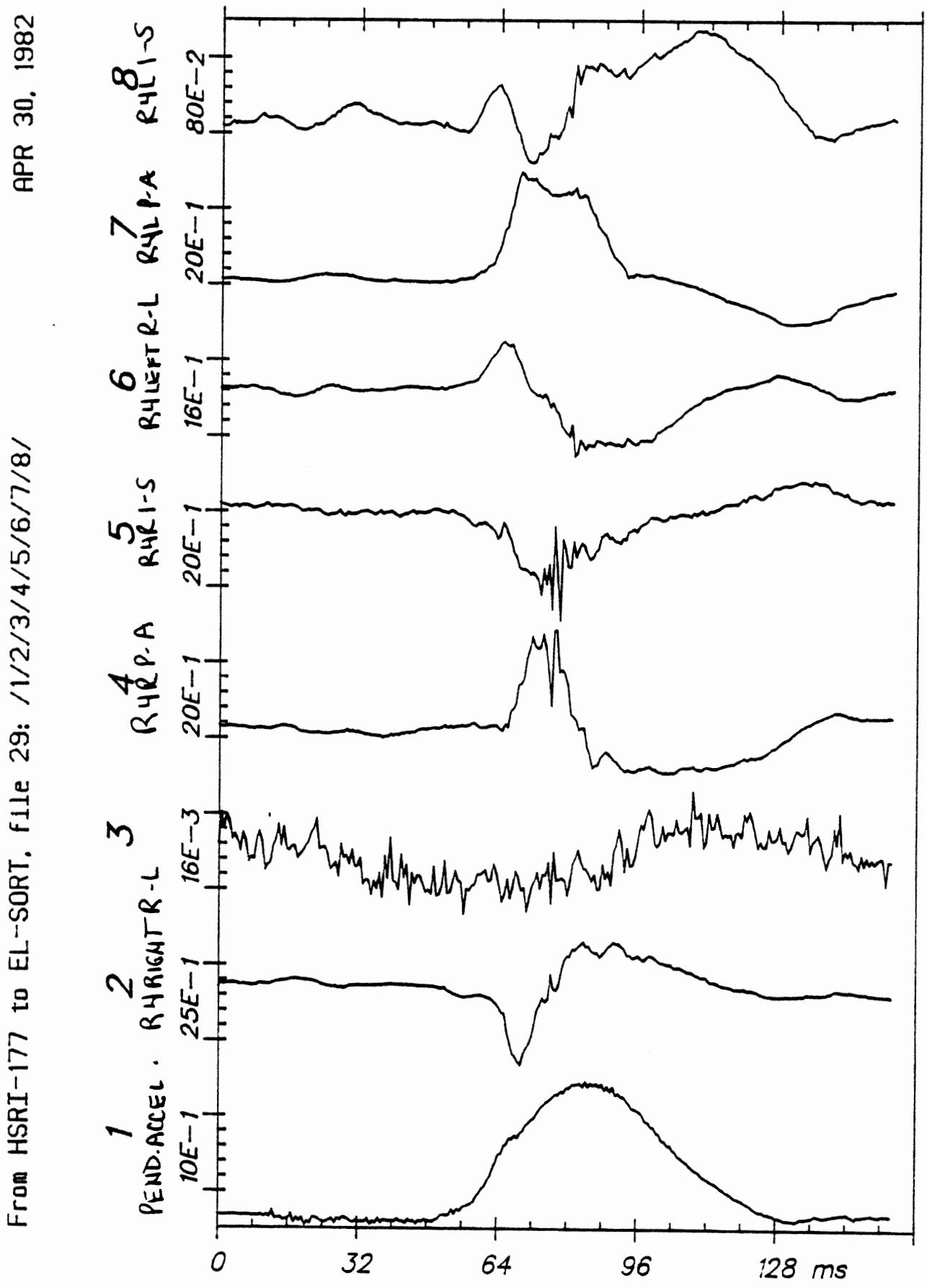
From HSRI-177 to EL-SORT, file 29: /1/2/3/4/5/6/7/8/
APR 30, 1982
1 PEND. ACCEL.
10E-1
2 R4 RIGHT R-L
25E-1
3
16E-3
4 R4R P.A
20E-1
5 R4R I-S
20E-1
6 R4 LEFT R-L
16E-1
7 R4L P-A
20E-1
8 R4L I-S
80E-2
0
32
64
96
128 ms
Time Histories
82E043
C4

From HSRI-177 to EL-SORT, file 29: /9/11/12/-/-/13/14/-/ APR 28, 1982

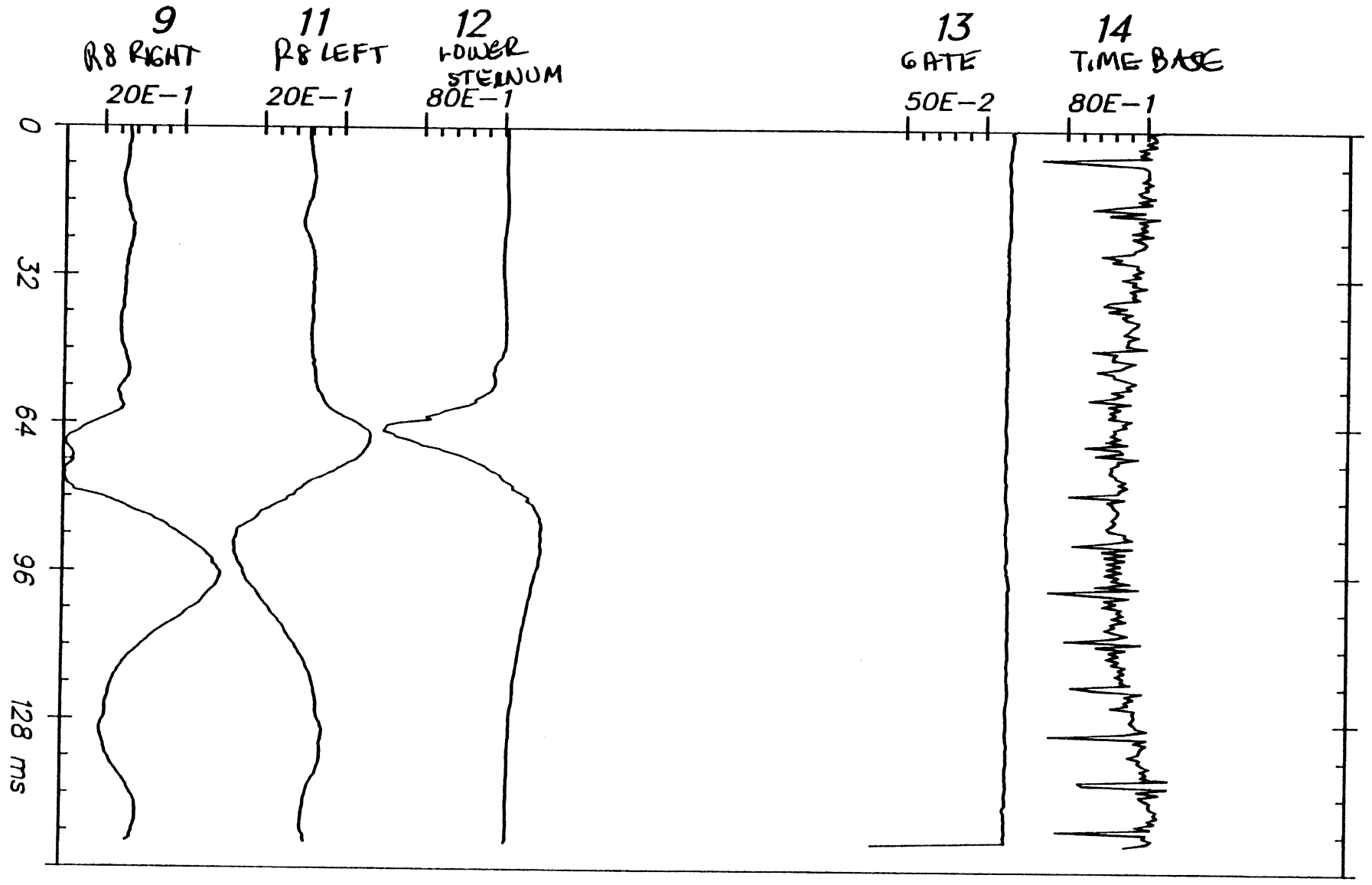

Time Histories

D90

82E043 C4

From HSRI-166 to EL--SORT, file 6: /1/2/3/4/5/6/7/8/

APR 28, 1982

Time Histories 82E044 H7

From HSRI-166 to EL-SORT, File 6: /9/10/-/11/-/12/13/14/
APR 28, 1982
14 TIME BASE
64E-2
13 GATE
50E-2
12 AORTA PRES.
25E-2
11 TRACHEA PRES.
64E-1
10 3C
12E-1
9 HEAD 3B
25E-1
0
32
64
96
128 ms
Time Histories
82E044
H7

From HSRI-167 to EL-SORT, File 18: /1/2/3/4/5/6/7/8/

APR 28, 1982

Time Histories 82E044 C3

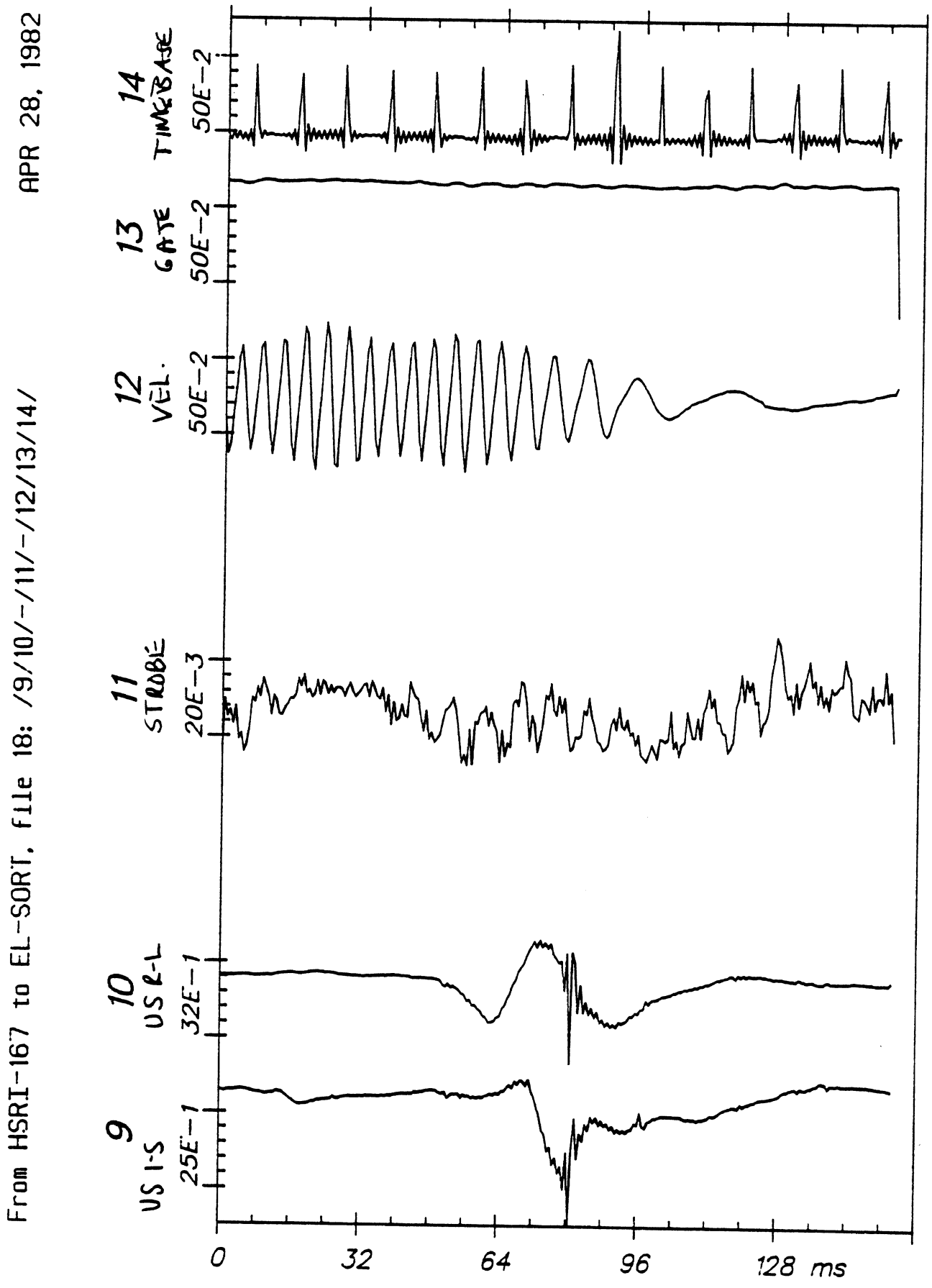

Time Histories 82E044 C3

From HSRI-177 to EL-SORT, File 30: /1/2/3/4/5/6/7/8/

APR 30, 1982

Time Histories 82E044 C4

From HSRI-177 to EL-SORT, file 30: /9/11/12/-/-/13/14/-/

APR 28, 1982

Time Histories 82E044 C4

From HSRI-166 to EL-SORT, File 7: /1/2/3/4/5/6/7/8/

APR 28, 1982

Time Histories 82E045 H7

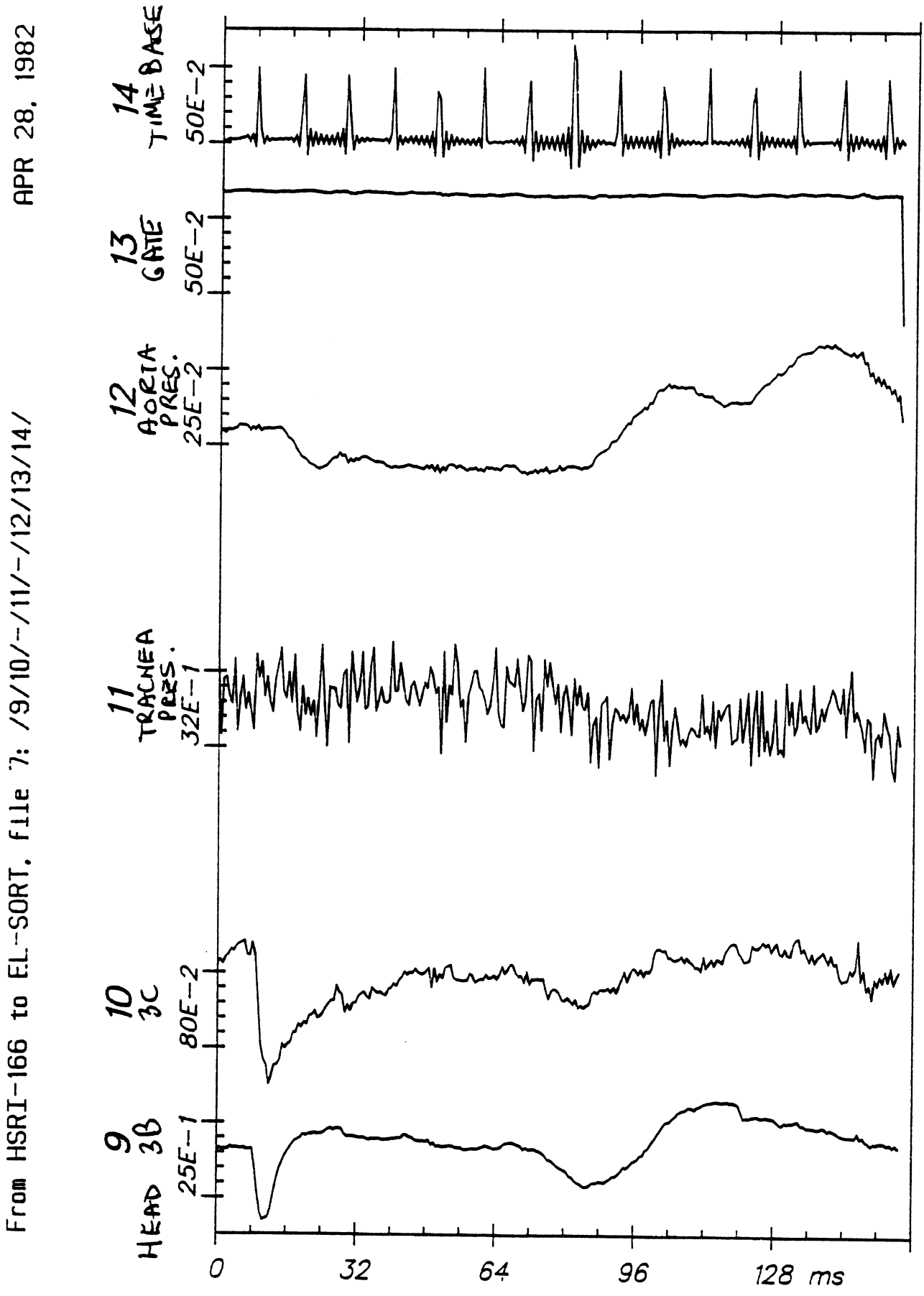

Time Histories 82E045 H7

From HSRI-167 to EL-SORT, file 19: /1/2/3/4/5/6/7/8/ APR 28, 1982

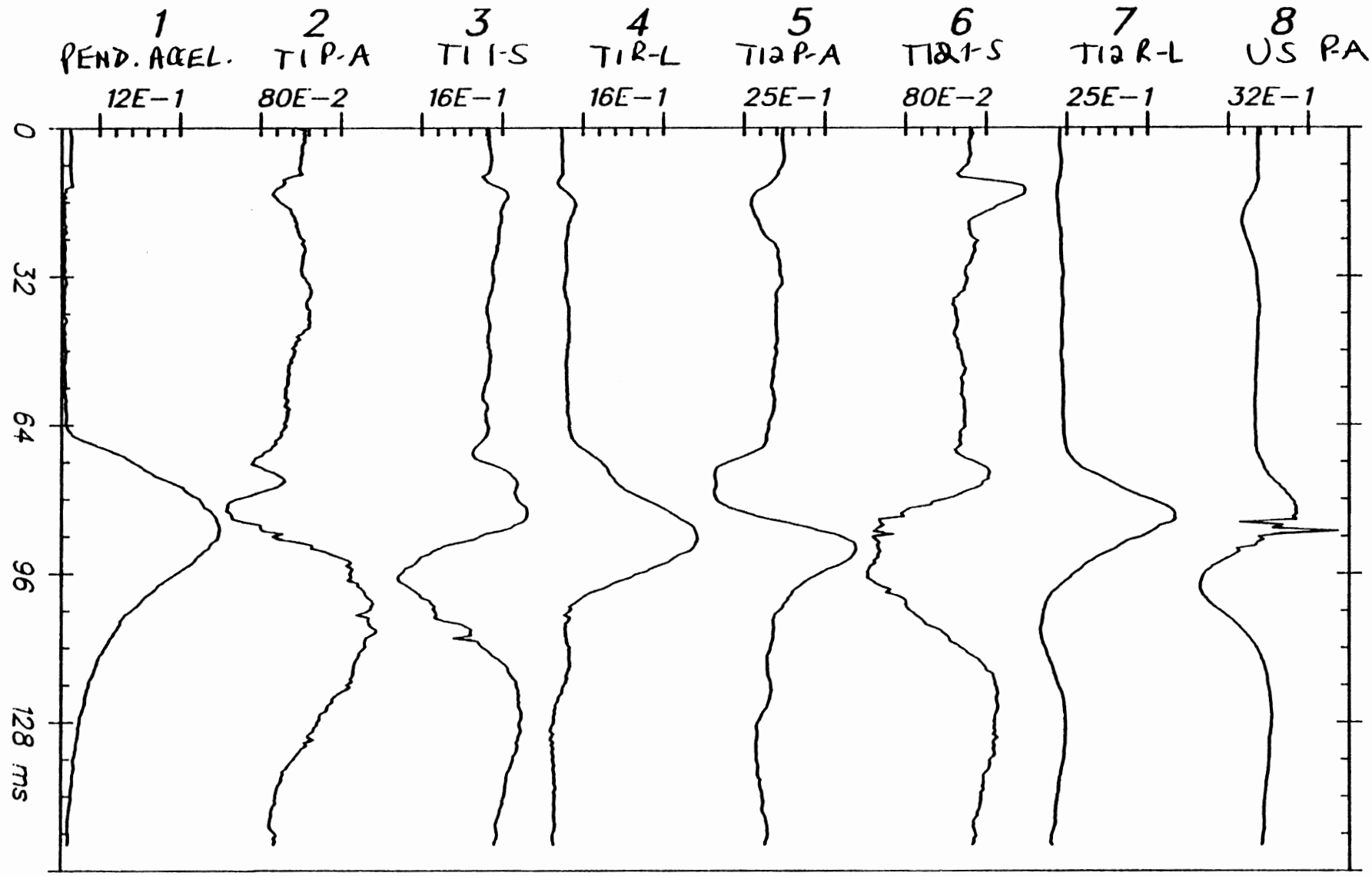

Time Histories 82E045 C3

D99

From HSRI-167 to EL-SORT, File 19: /9/10/-/11/-/12/13/14/
APR 28, 1982
14 TIME BASE 64E-2
13 GATE 50E-2
12 VEL. 50E-2
11 STROBE 25E-2
10 US R-L 64E-1
9 US I-S 20E-1
0
32
64
96
128 ms
Time Histories
82E045
C3

From HSRI-177 to EL-SORT, file 31: /1/2/3/4/5/6/7/8/ APR 30, 1982

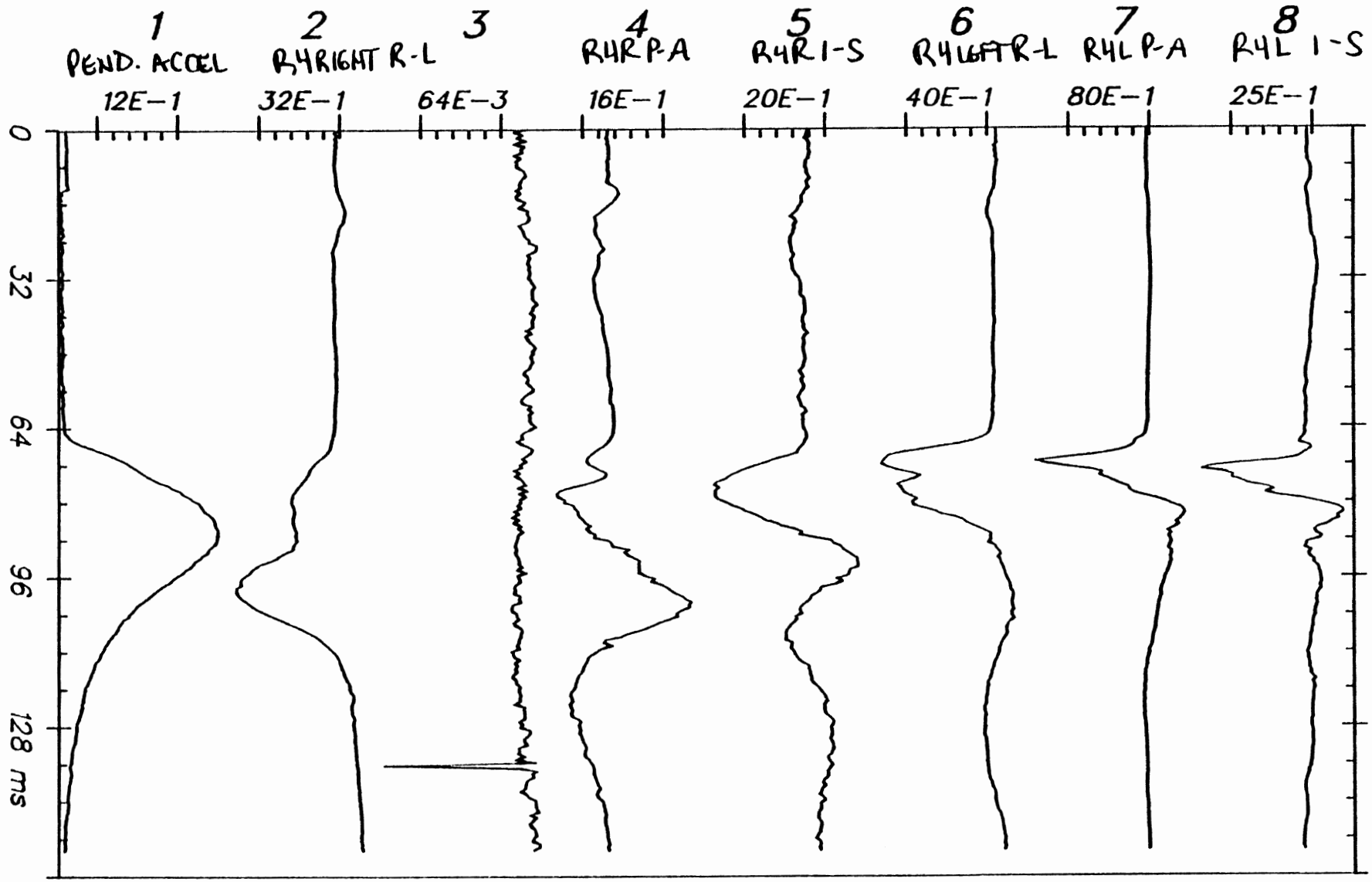

Time Histories 82E045 C4

D101

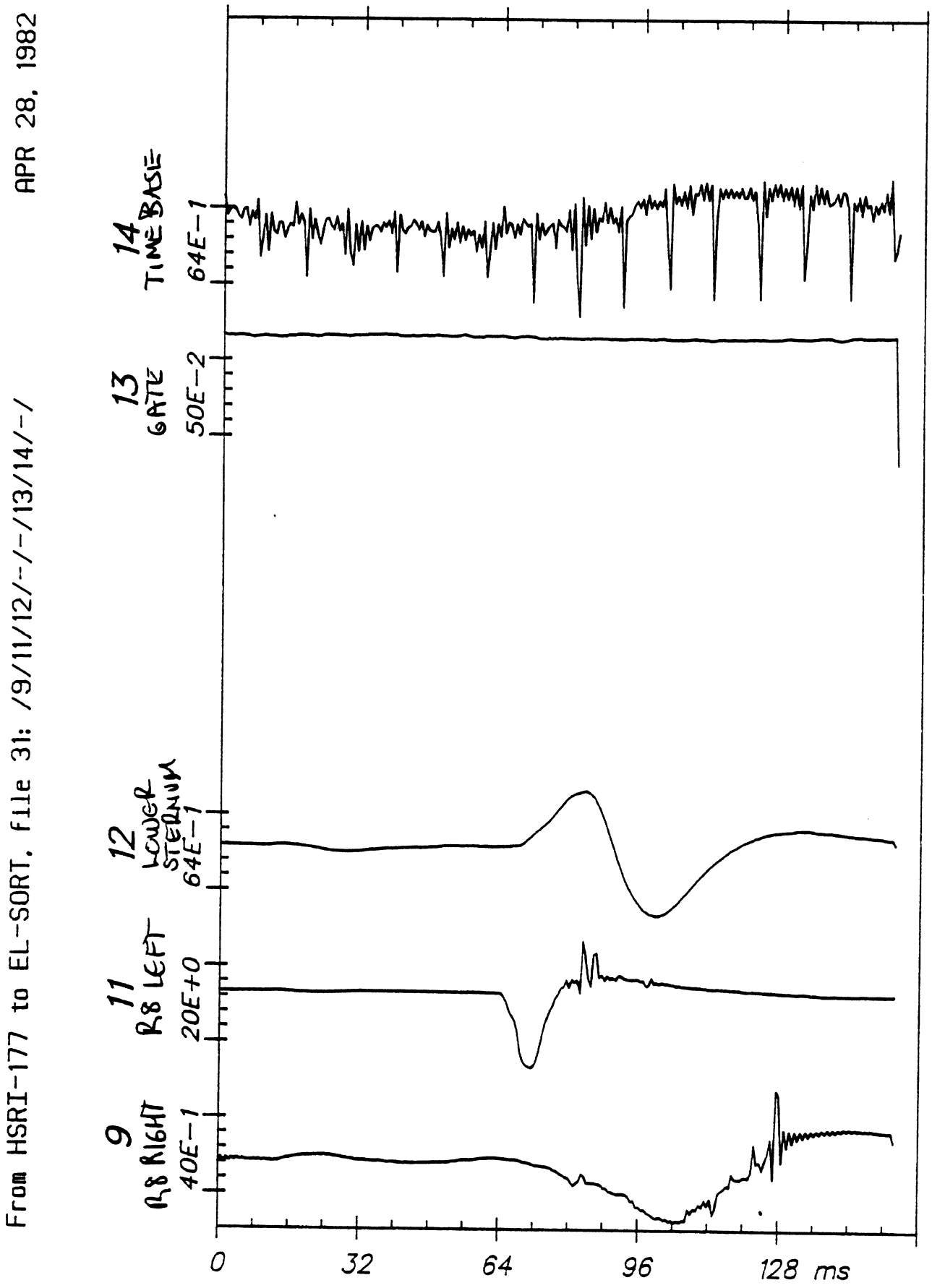
From HSRI-177 to EL-SORT, file 31: /9/11/12/-/-/13/14/-/
APR 28, 1982
14 TIME BASE 64E-1
13 GATE 50E-2
12 LOWER STERNUM 64E-1
11 R8 LEFT 20E+0
9 R8 RIGHT 40E-1
0
32
64
96
128 ms
Time Histories
82E045
C4

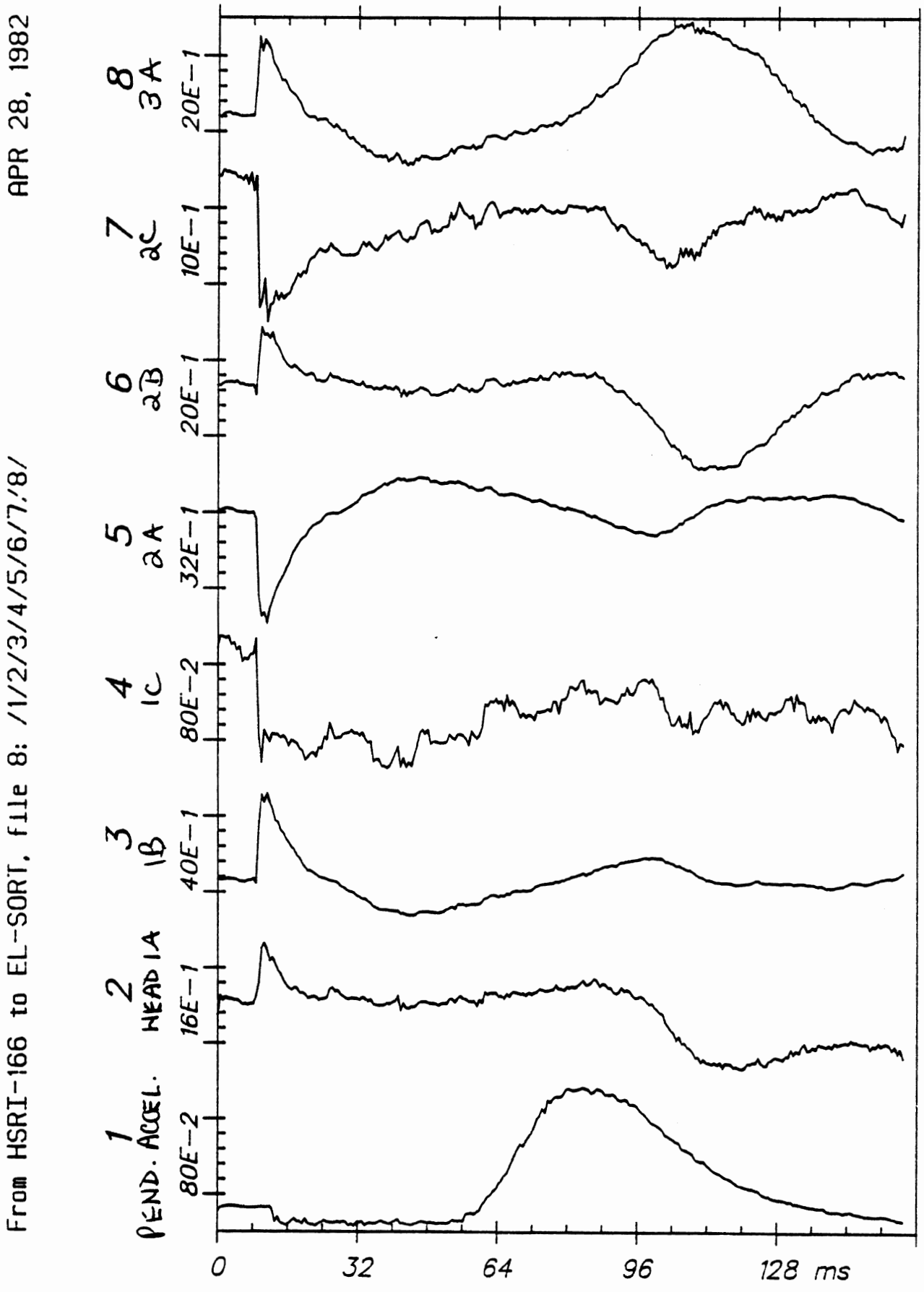

Time Histories 82E046 H7

Time Histories 82E046 H7

From HSRI-167 to EL-SORT, file 20: /1/2/3/4/5/6/7/8/ APR 28, 1982

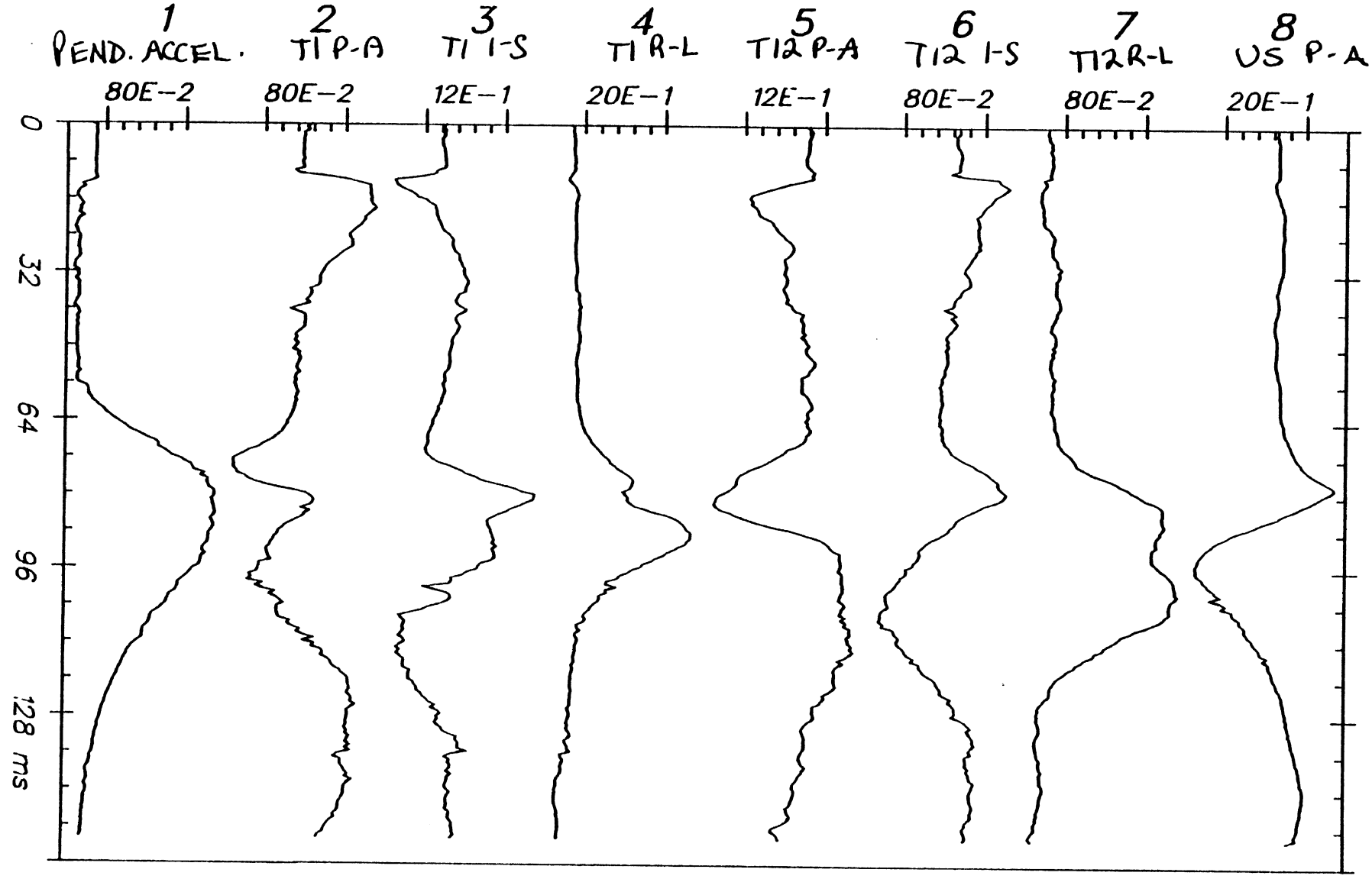

Time Histories 82E046 C3

From HSRI-167 to EL-SORT, file 20: /9/10/-/11/-/12/13/14/ APR 28, 1982

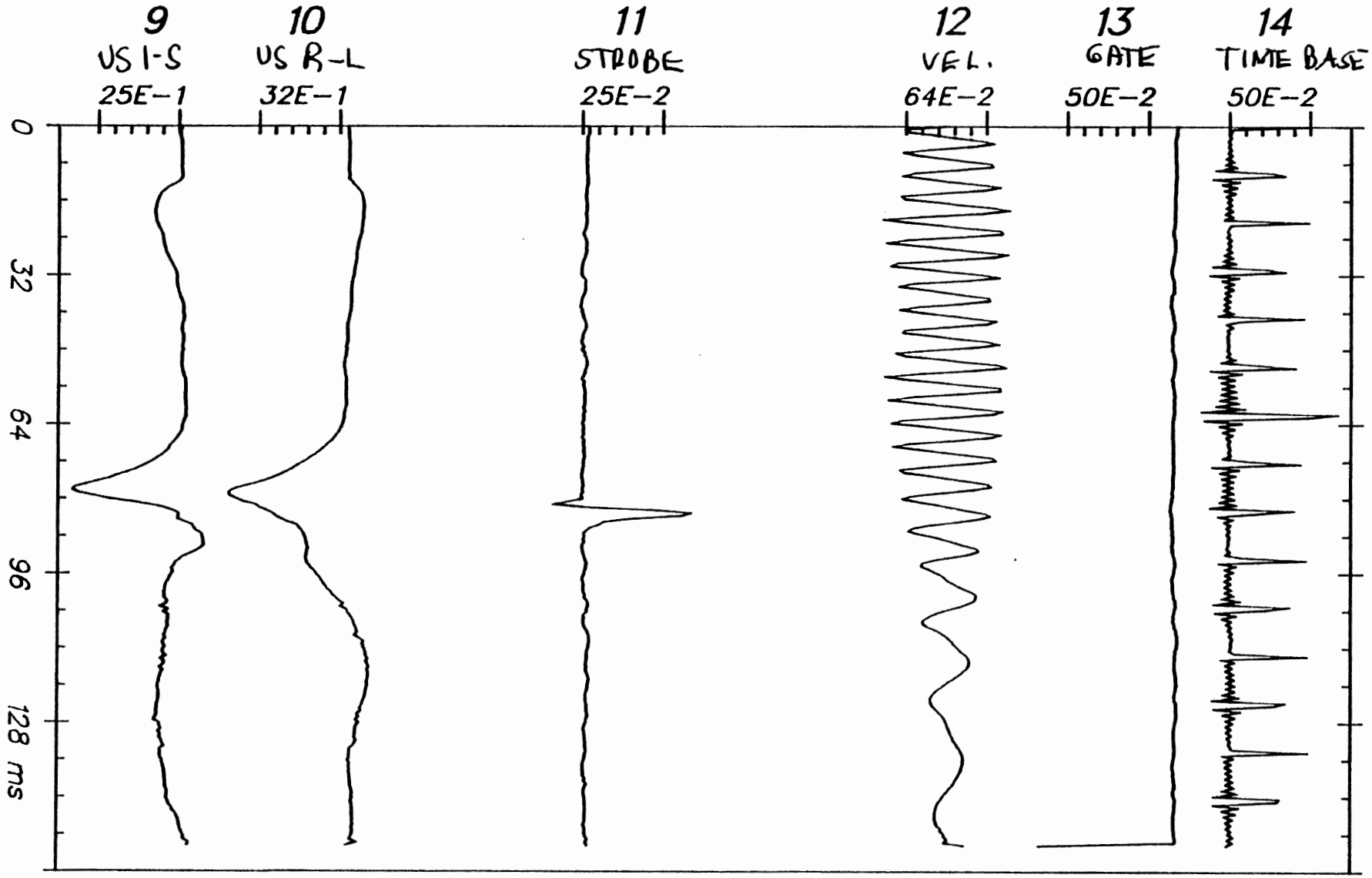

Time Histories

D106

82E046 C3

From HSRI-177 to EL-SORT, File 32: /1/2/3/4/5/6/7/8/

APR 30, 1982

Time Histories 82E046 C4

From HSRI-177 to EL-SORT, file 32: /9/11/12/-/-/13/14/-/

APR 28, 1982

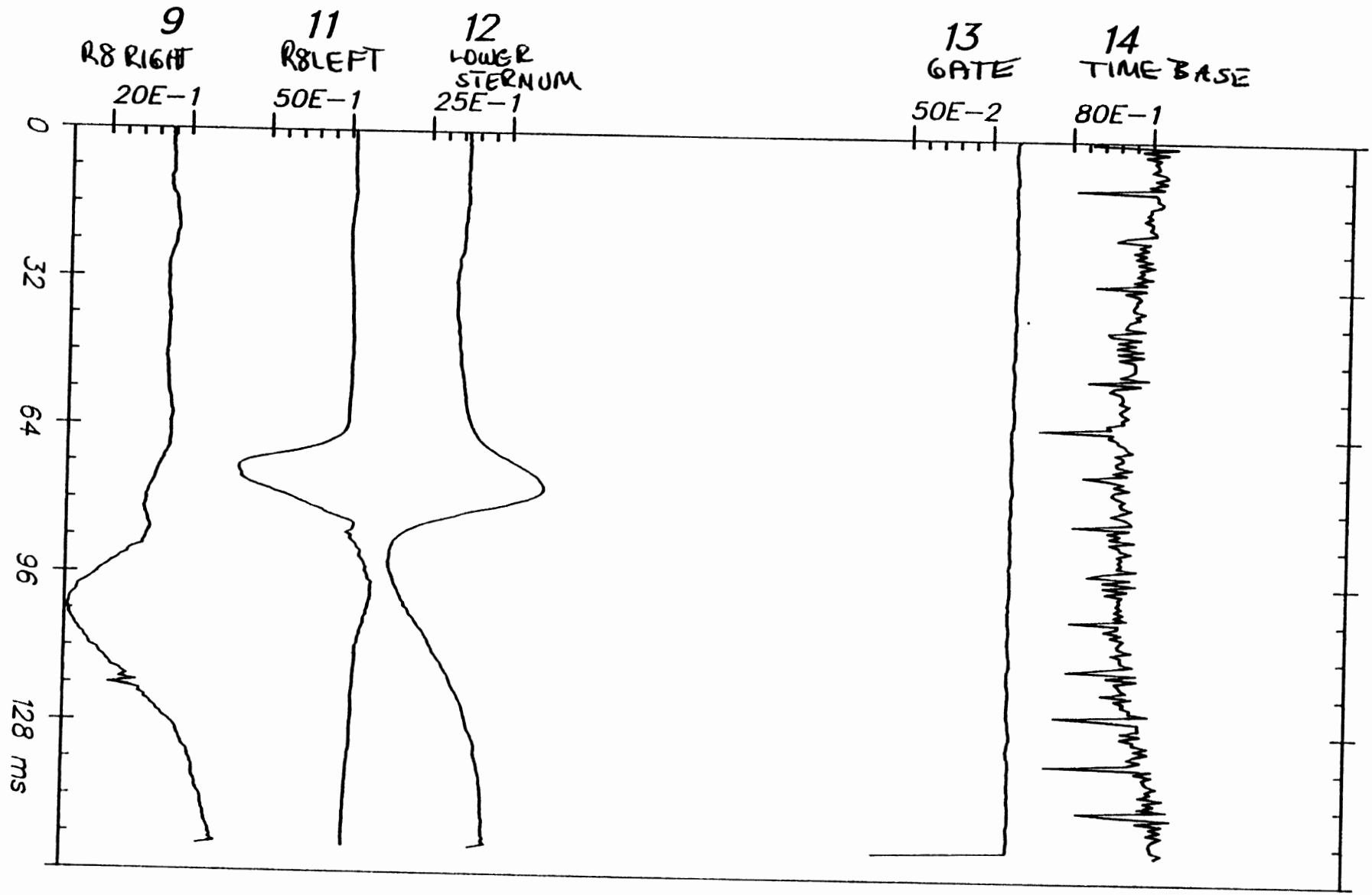

Time Histories

82E046 C4

D108

From HSRI-166 to EL--SORT, file 9: /1/2/3/4/5/6/7/8/ APR 28, 1982

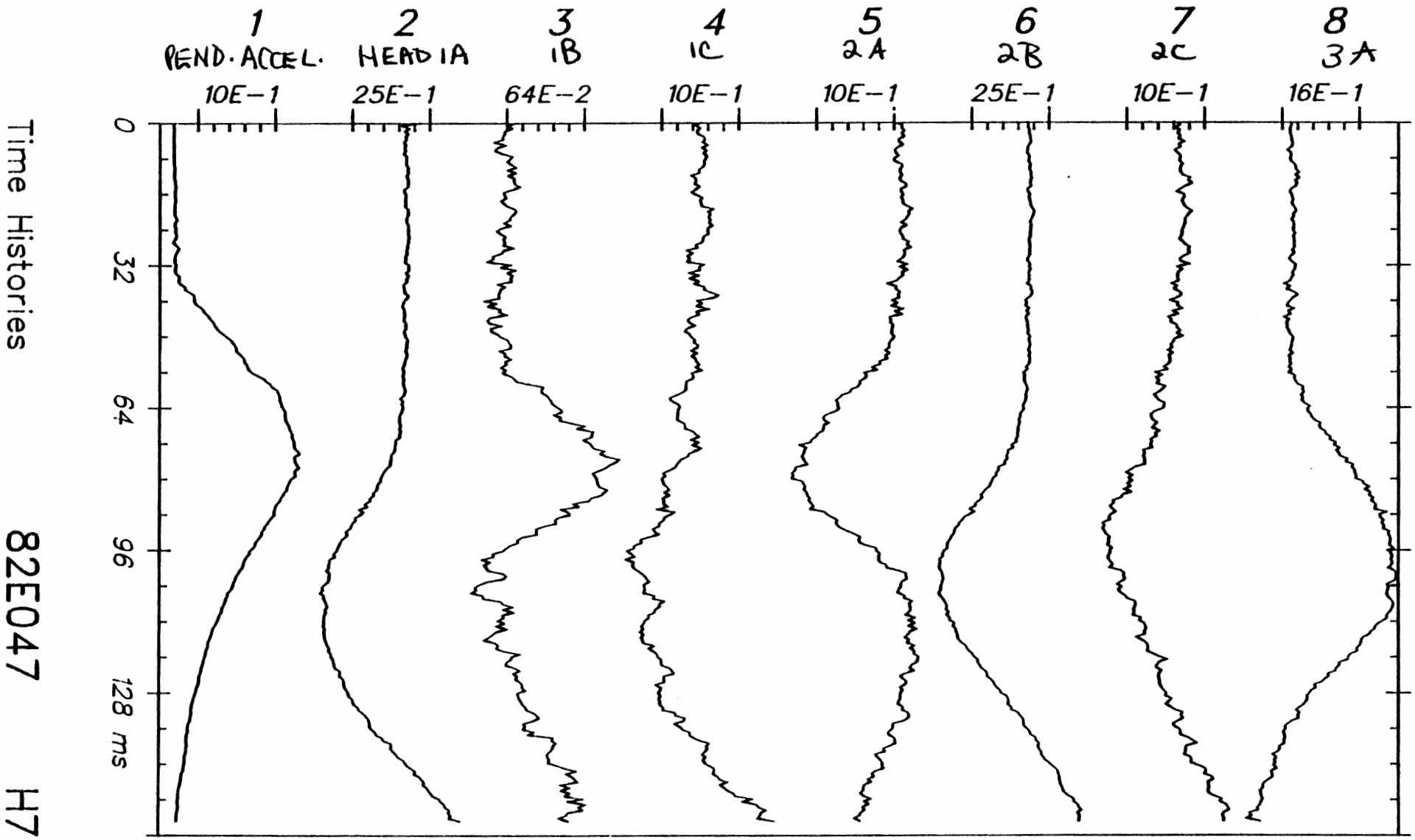

Time Histories 82E047 H7

D109

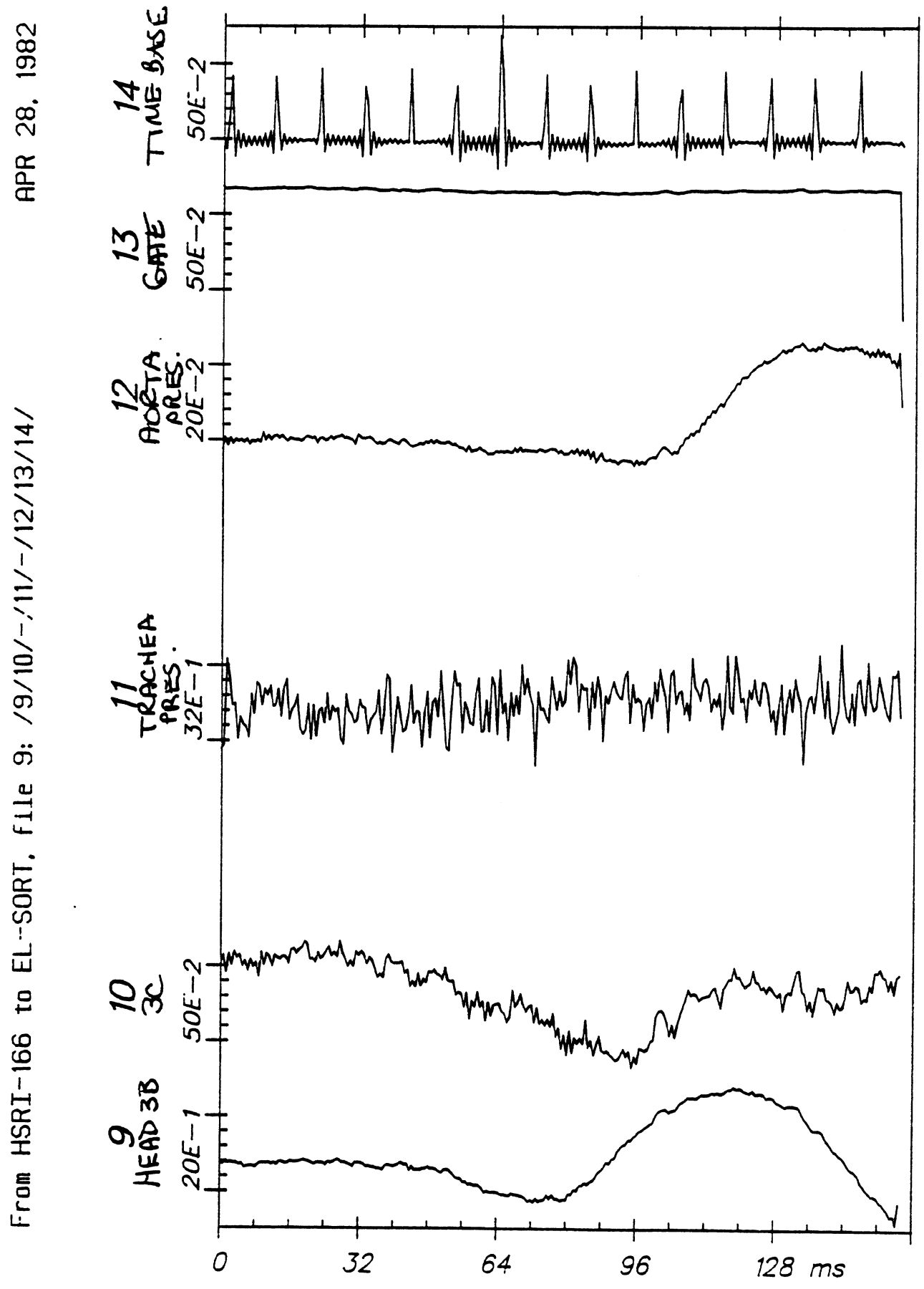

Time Histories 82E047 H7

From HSRI-167 to EL-SORT, file 21: /1/2/3/4/5/6/7/8/ APR 28, 1982

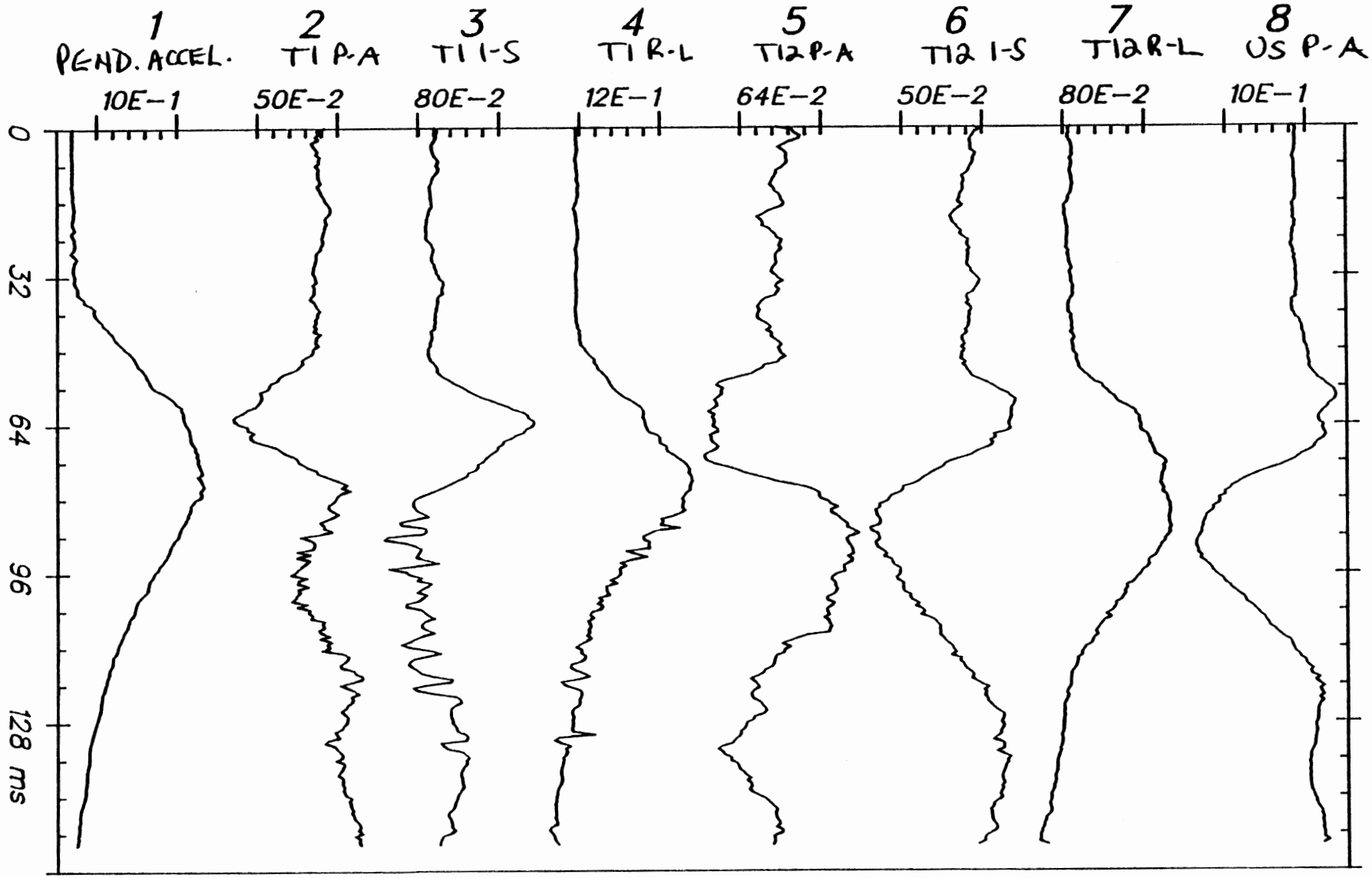

Time Histories 82E047 C3

From HSRI-167 to EL-SORT, file 21: /9/10/-/11/-/12/13/14/

APR 28, 1982

Time Histories 82E047 C3

APR 30, 1982

From HSRI-177 to EL-SORT, file 33: /1/2/3/4/5/6/7/8/

Time Histories 82E047 C4

From HSRI-177 to EL-SORT, file 33: /9/11/12/-/-/13/14/-/ APR 28, 1982

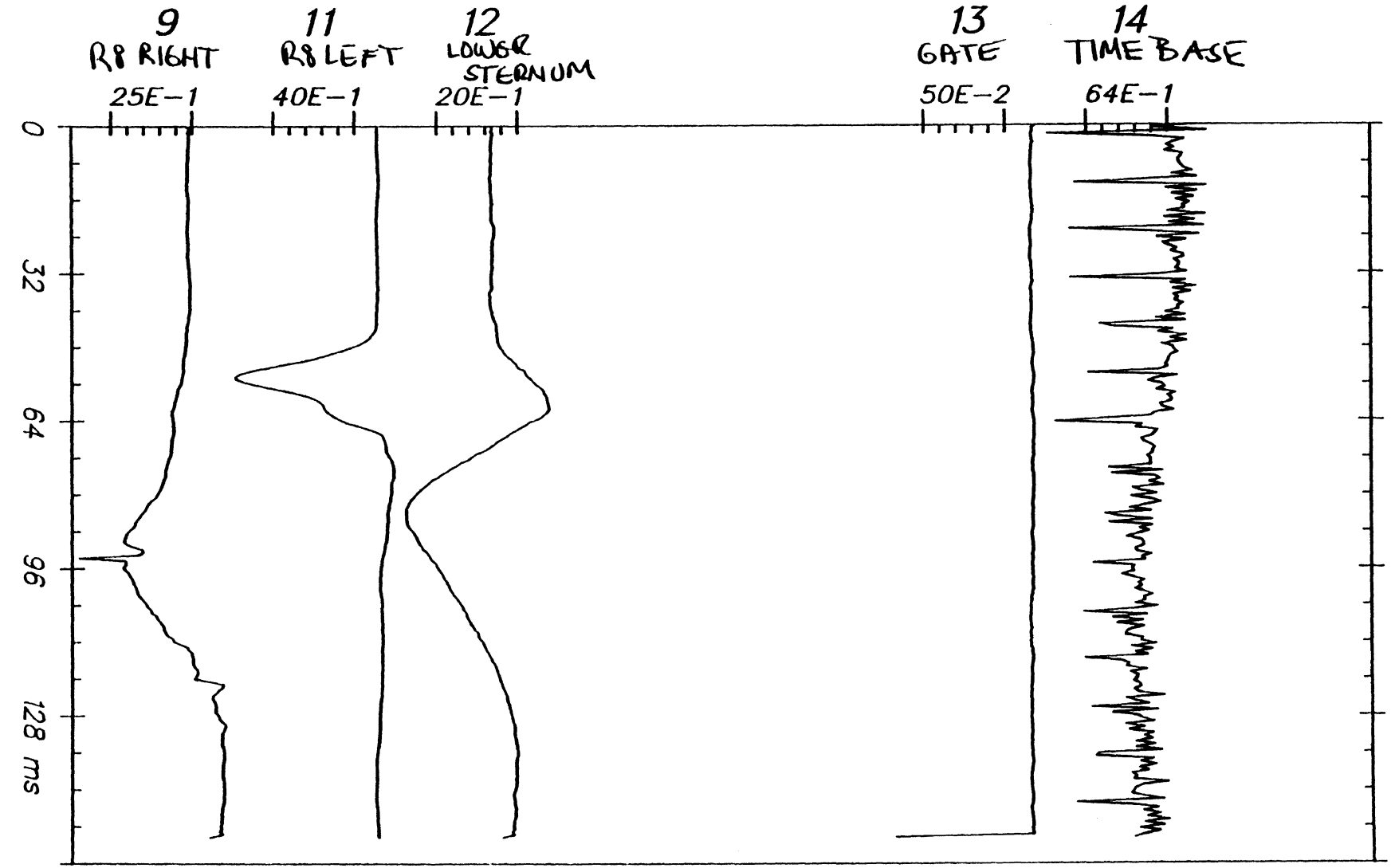

Time Histories 82E047 C4

D114

From HSRI-166 to el-sort, file 56: /1/2/3/4/5/6/7/8/

APR 27, 1982

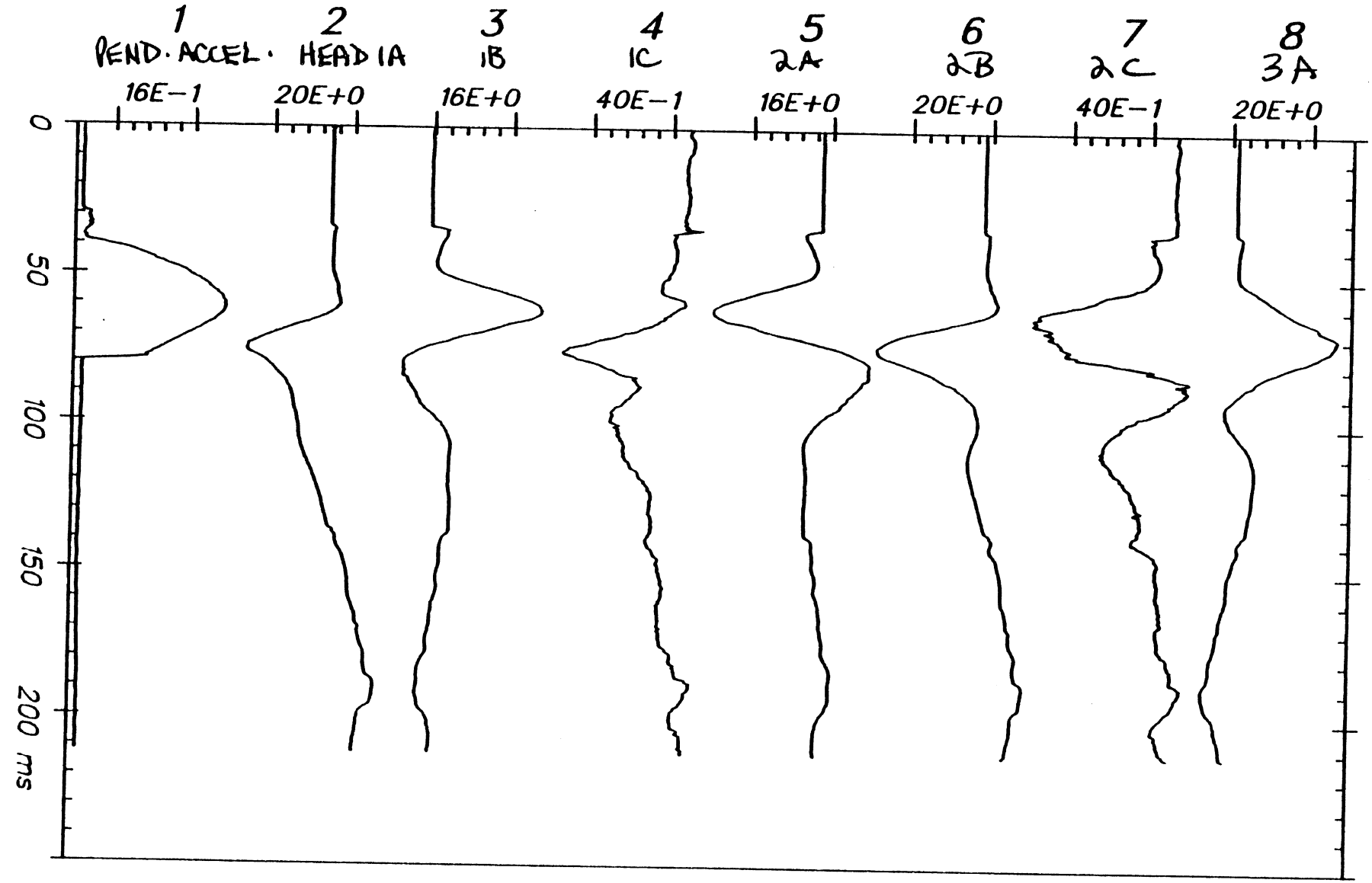

Time Histories

82E048

H7

D115

From HSRI-166 to el-sort, file 56: /9/10/-/11/12/13/14/-/

APR 27, 1982

Time Histories 82E048 H7

From HSRI-167 to el-sort, file 59: /1/2/3/4/5/6/7/8/ APR 27, 1982

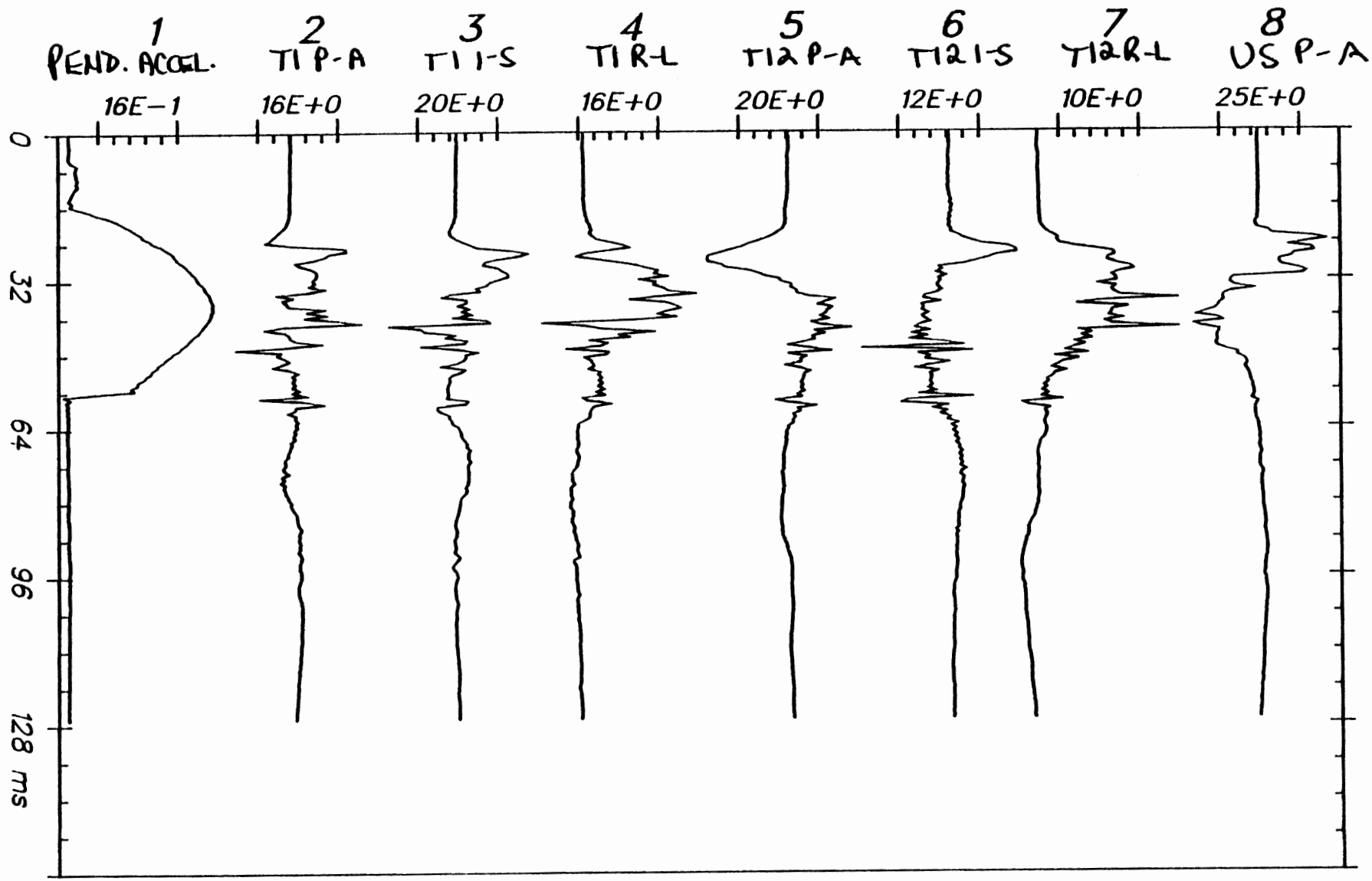

Time Histories 82E048 C3

D117

APR 27, 1982

From HSRI-167 to el-sort, file 59: /9/10/-/11/12/13/14/-/

Time Histories 82E048 C3

APR 27, 1982

From HSRI-~~167~~ 177 to el-sort, file 62: /1/2/-/4/5/6/7/8/

Time Histories 82E048 C4

From HSRI-167 to el-sort, file 62: /9/11/-/-/12/13/14/-/

APR 27, 1982

Time Histories 82E048 C4

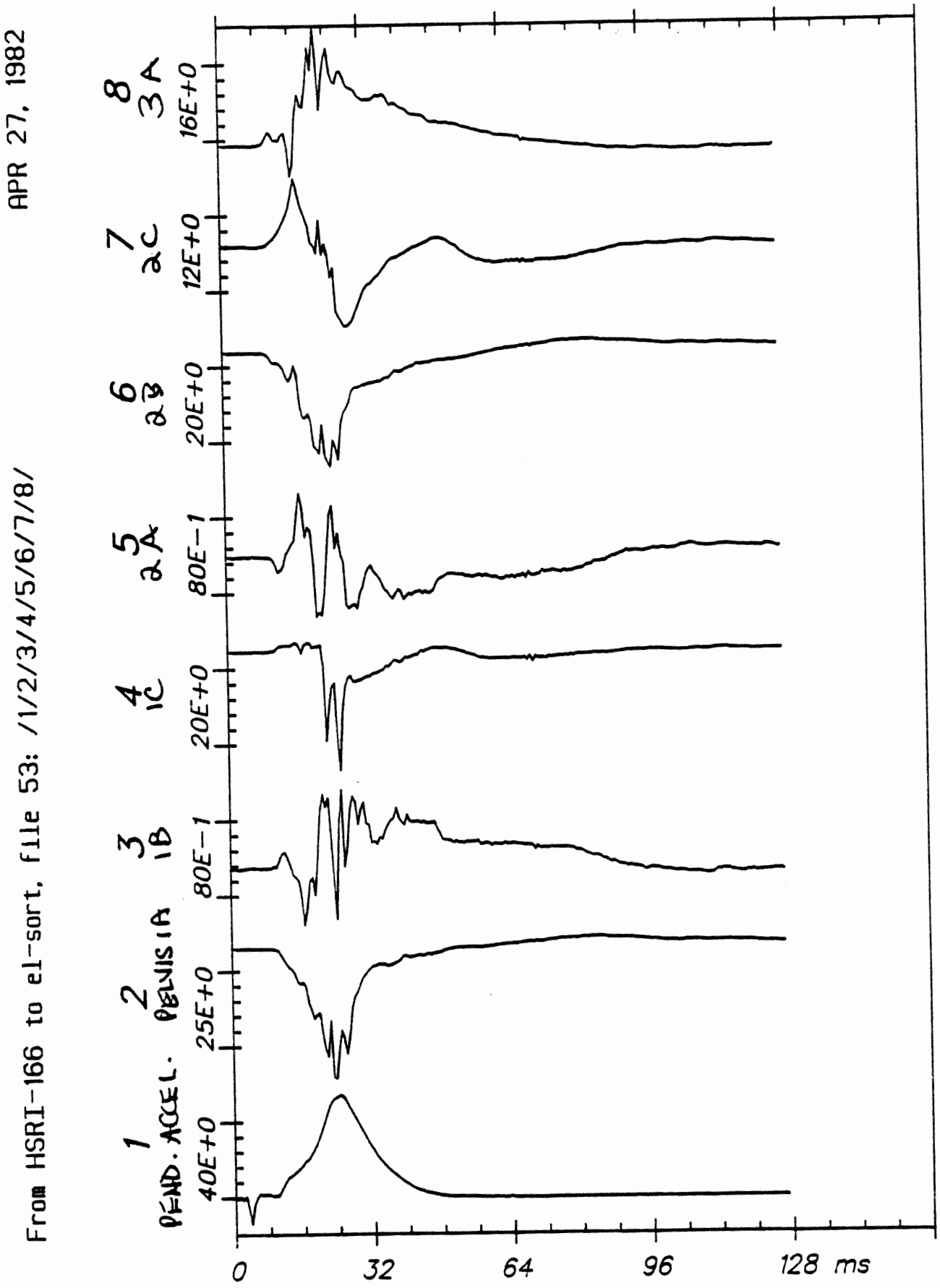
APR 27, 1982
From HSRI-166 to el-sort, file 53: /1/2/3/4/5/6/7/8/
8 3A 16E+0
7 2C 12E+0
6 2B 20E+0
5 2A 80E-1
4 1C 20E+0
3 1B 80E-1
2 PELVIS A 25E+0
1 PEND. ACCEL. 40E+0
0
32
64
96
128 ms
Time Histories
82E049
H7

From HSRI-166 to el-sort, file 53: /9/10/-/-/11/12/13/14/

APR 27, 1982

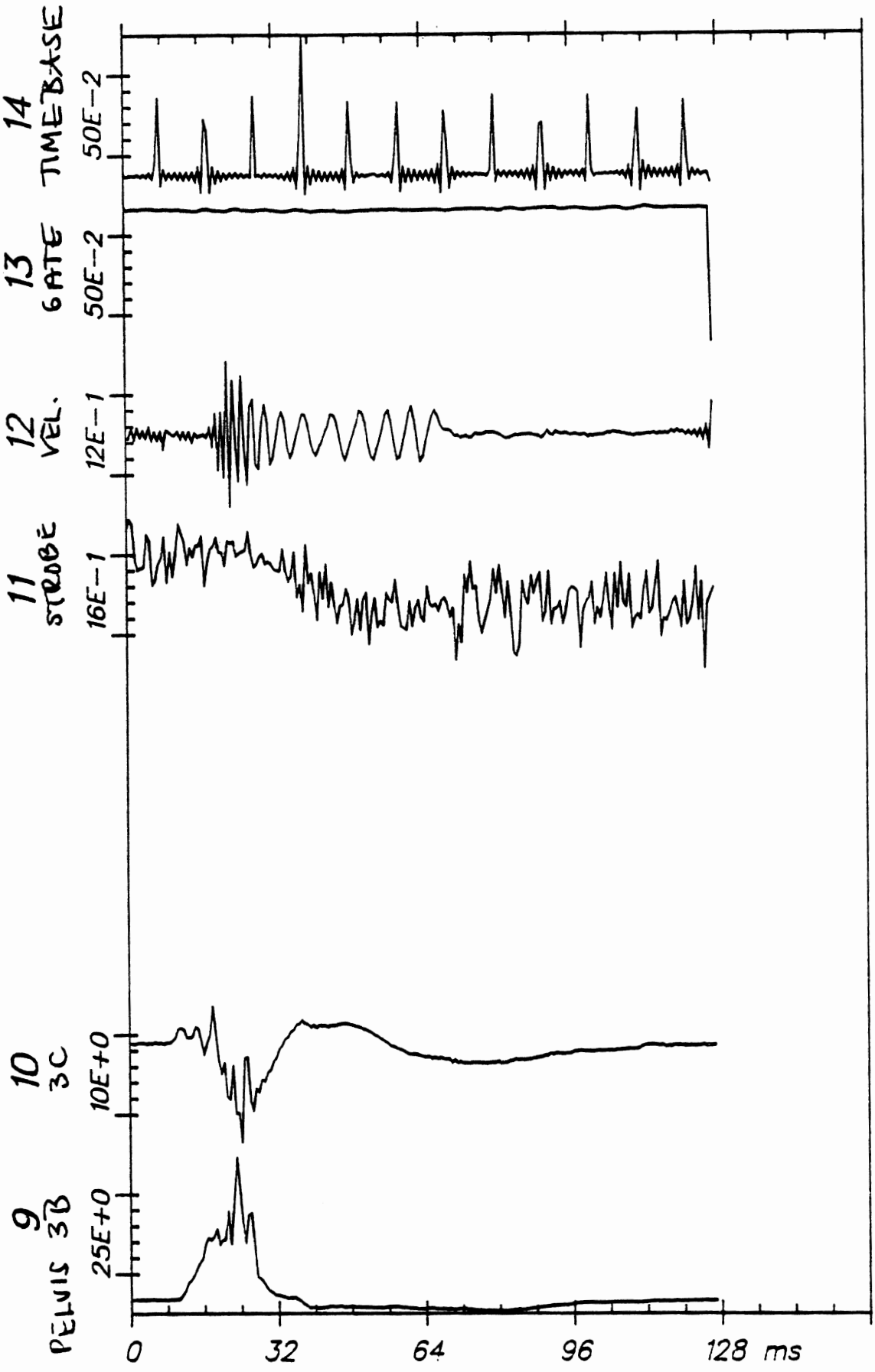

Time Histories 82E049 H7